รายงานวิจัยฉบับสมบูรณ์

โครงการ
ปฏิกิริยาการถ่ายโอนโปรตอน
และพลวัตในแนฟิออน

โดย

ศาสตราจารย์ ดร. กฤษณะ สาคริก
มหาวิทยาลัยเทคโนโลยีสุรนารี

กันยายน 2553

สัญญาเลขที่ BRG 5180022

รายงานวิจัยฉบับสมบูรณ์

โครงการ
ปฏิกิริยาการถ่ายโอนโปรตอน
และพลวัตในแนฟิออน

ผู้วิจัย

ศาสตราจารย์ ดร. กฤษณะ สาคริก

สังกัด

มหาวิทยาลัยเทคโนโลยีสุรนารี

สนับสนุนโดยสำนักงานกองทุนสนับสนุนการวิจัย
(ความเห็นในรายงานนี้เป็นของผู้วิจัย
สกว. ไม่จำเป็นต้องเห็นด้วยเสมอไป)

สารบัญ

บทคัดย่อ

ปฏิกิริยาการถ่ายโอนโปรตอน (proton transfer reaction) ในสารละลายที่เป็นน้ำ ของเหลว และของแข็ง เป็นปฏิกิริยาสำคัญในวิชาเคมีไฟฟ้า โดยเฉพาะอย่างยิ่ง ที่เกี่ยวข้องกับการพัฒนาพลังงานทดแทน เช่น เซลล์เชื้อเพลิง (fuel cell) เซลล์เชื้อเพลิงที่ใช้เมมเบรนแลกเปลี่ยนโปรตอน (proton exchange membrane fuel cell, PEMFC) ส่วนใหญ่มีน้ำเป็นตัวกลาง โดยแปลงพลังงานเคมีที่เกิดขึ้นจากปฏิกิริยาระหว่างแก๊สไฮโดรเจนและออกซิเจนไปเป็นพลังงานไฟฟ้า เมมเบรนแลกเปลี่ยนโปรตอนที่นิยมใช้ในปัจจุบันได้แก่ Nafion® ซึ่งเป็นพอลิเมอร์ประเภท perfluorinated Nafion® มีความคงทนค่อนข้างสูง เนื่องจากการทำงานพื้นฐานของเซลล์เชื้อเพลิงขึ้นอยู่กับความสามารถในการถ่ายโอนโปรตอน (H^+) จากขั้วไฟฟ้าแอโนด (anode) ผ่านเมมเบรนแลกเปลี่ยนโปรตอนไปยังแคโทด (cathode) การพัฒนาประสิทธิภาพของเซลล์เชื้อเพลิงจึงต้องศึกษาปฏิกิริยามูลฐาน (elementary reaction) และพลวัต (dynamics) ของโปรตอนในตัวกลางต่างๆ ในรายละเอียด ถึงแม้ว่าที่ผ่านมาจะมีรายงานผลการศึกษาปฏิกิริยาการถ่ายโอนโปรตอนทั้งทางทฤษฎีและการทดลองมากพอควร ปรากฏว่าในปัจจุบันยังไม่มีข้อสรุปที่ชัดเจนและเป็นที่ยอมรับ

งานวิจัยเรื่องนี้ศึกษาปฏิกิริยามูลฐาน กลไกปฏิกิริยา และพลวัตของปฏิกิริยาการถ่ายโอนโปรตอนในแบบจำลอง protonated water clusters สารเชิงซ้อน CH_3OH-H_3O^+-H_2O และ CF_3SO_3H-H_3O^+-H_2O โดยใช้วิธีเคมีควอนตัมและ Born-Oppenheimer Molecular Dynamics (BOMD) simulations ที่ 350 K การศึกษาเริ่มจากการคำนวณโครงสร้างของสารเชิงซ้อนในสภาวะสมดุลโดยวิธี density functional theory (DFT method) ที่ระดับ B3LYP/TZVP โดยเน้นโครงสร้างพันธะไฮโดรเจนที่สามารถเกิดการถ่ายโอนโปรตอนได้ง่าย ผลการวิเคราะห์ IR spectra แสดง asymmetric O-H stretching frequency ของโปรตอนที่มีศักยภาพในการถ่ายโอนที่ $\nu^{OH} \approx 1000$ cm^{-1} โดยมีความถี่ขีดเริ่มเปลี่ยน (threshold frequency) (ν^{OH*}) ในช่วง 1700 ถึง 2200 cm^{-1} ทั้งนี้ ขึ้นกับชนิดและสภาพแวดล้อมของพันธะไฮโดรเจนที่นำมาศึกษา BOMD simulations แสดง ν^{OH} เพิ่มเติมที่ความถี่สูงขึ้น โดยแถบ IR ที่ความถี่ต่ำสัมพันธ์กับ oscillatory shuttling motion และที่ความถี่สูงสัมพันธ์กับ structural diffusion motion ความถี่ทั้งสองนี้ถือเป็นอัตลักษณ์สำคัญสำหรับโปรตอนที่มีศักยภาพในการถ่ายโอนโปรตอนสูง ผลการศึกษายังแสดงด้วยว่า การที่ในพันธะไฮโดรเจนมีการสั่นหลายประเภทคู่ควบกัน (coupling) ทำให้ไม่สามารถศึกษาปฏิกิริยาการถ่ายโอนโปรตอนโดยใช้ static proton transfer potential และแบบจำลองการคำนวณที่นำมาใช้ต้องพิจารณาการกระเพื่อมของพลังงานความร้อน (thermal energy fluctuation) และพลวัตในพันธะไฮโดรเจนด้วย งานวิจัยเรื่องนี้ทำให้ทราบพฤติกรรมการสั่นของโปรตอนที่กำลังถ่ายโอนในรายละเอียด โดยเสนอทฤษฎีและแนวทางในการเปรียบเทียบความสามารถในการถ่ายโอนโปรตอนในพันธะไฮโดรเจนเมื่ออยู่ในสภาพแวดล้อมต่างๆ ตลอดจนเสนอเกณฑ์และวิธีการใช้ IR spectroscopy ในการติดตามปฏิกิริยาการถ่ายโอนโปรตอนที่ซับซ้อนขึ้น เช่น ในการทดลอง ทั้งนี้ ผลการวิจัยสามารถนำไปเป็นแนวทางในการประยุกต์ เพื่อการปรับปรุงประสิทธิภาพการถ่ายโอนโปรตอนในเมมเบรนแลกเปลี่ยนโปรตอนได้ในอนาคต

Abstract

Proton transfer reaction in condensed phase represents one of the most important problems in electrochemistry, especially in connection with the development of alternative energy sources such as fuel cells (FC). Since the basic operations in fuel cells depend upon the transportation of protons (H^+) generated at anode across proton exchange membrane (PEM) to cathode, it is vital to understand elementary reactions and dynamics of proton transfer processes in liquid, solid and aqueous solution. Although some theoretical and experimental information has been accumulated, precise mechanisms of proton transfer in PEMFC, especially in hydrogen bond (H-bond) complexes, are not completely known. In the present work, elementary reactions, energetic and dynamics of proton transfer were studied using three model systems namely, protonated water clusters, the CH_3OH-H_3O^+-H_2O and CF_3SO_3H-H_3O^+-H_2O complexes. The H-bond complexes were investigated using quantum chemical methods and Born-Oppenheimer Molecular Dynamics (BOMD) simulations. The investigations began with searching for equilibrium structures at low hydration levels using the DFT method at the B3LYP/TZVP level, from which the H-bonds susceptible to proton transfer were characterized and analyzed. The analyses of IR spectra showed characteristic asymmetric O-H stretching frequencies of the transferring proton at $\nu^{OH} \approx 1000$ cm^{-1} and the threshold frequencies for proton transfer (ν^{OH*}) in the range of 1700 and 2200 cm^{-1}. However, these cannot be definitive, due to the neglect of the thermal energy fluctuation and dynamics in B3LYP/TZVP calculations. BOMD simulations at 350 K revealed an additional ν^{OH} at higher frequency. The low- and high-frequency bands can be associated with the oscillatory shuttling and structural diffusion motions of the transferring proton in H-bond, respectively. The present results concluded that, due to coupling among various modes of vibrations, the discussions on proton transfer reactions cannot be made based on static proton transfer potentials. In order to study proton transfer reactions, thermal energy fluctuations and dynamics must be included in the model calculations, as in the case of BOMD simulations. The present work provided insights into vibrational behaviors of the transferring protons, as well as suggested theoretical methods and criteria to monitor and improve the efficiency of proton transfer in more complex systems.

Executive Summary

Proton exchange membrane fuel cells (PEMFC) have been anticipated as promising energy suppliers for the future world. The majority of commercially available PEMFC use Nafion®. Nafion® is perfluorinated polymer with hydrophobic Teflon® backbone and randomly attached hydrophilic side chains. The backbones and the side chains of Nafion® are terminated by trifluoromethanesulfonic (triflic) acid, known as one of the strongest acids in aqueous solutions. Nafion® possesses exceptional chemical and mechanical stabilities and has been known to produce high power density at low-temperature operation. Although some experimental and theoretical information on PEMFC has been accumulated, mechanisms of proton conduction in Nafion®, especially at the molecular level, seem not completely known. In order to establish important molecular scale information on transport processes in PEMFC, structures, energetic and dynamics of all active chemical components in Nafion® must be systematically studied. In the present work, elementary reactions and dynamics of proton transfer were investigated on three model systems namely, protonated water clusters, the CH_3OH-H_3O^+-H_2O and CF_3SO_3H-H_3O^+-H_2O complexes, using quantum chemical methods and Born-Oppenheimer Molecular Dynamics (BOMD) simulations. All the theoretical methods employed in the present work are summarized as follows.

Reactions and dynamics of proton transfer were studied using small model systems, with the following three basic steps; (1) searching for all important equilibrium structures and intermediate states in the proton transfer pathways using appropriate pair potentials; (2) refining of the computed structures using accurate quantum chemical method; (3) BOMD simulations starting from the refined structures. In order to discuss the tendency of proton transfer through the structural diffusion mechanism, the "asymmetric stretching coordinate" (Δd_{DA}) and a concept of the "most active" H-bond were used. Since the H-bonds susceptible to proton transfer can be characterized by low to nonexistence energy barrier along the proton transfer coordinate, manifested by a broad IR band with the asymmetric O-H stretching frequency (ν^{OH}) lower than a threshold frequency (ν^{OH*}), harmonic IR frequencies were computed from numerical second derivatives. The analyses of

normal modes in terms of internal coordinates were made and the tendencies of proton transfers in H-bonds were anticipated. Since the proton transfer reactions in H-bonds are strongly coupled with various degrees of freedom, the IR spectra of the transferring protons were also computed from BOMD simulations by Fourier transformations of the velocity autocorrelation function (VACF). The diffusion coefficients (D) of the transferring proton were computed from BOMD simulations using the Einstein relation, for which D are determined from the slope of the mean-square displacements (MSD).

For the protonated water clusters, B3LYP/TZVP calculations revealed that the active H-bond structures consist of the Zundel complex, with $\nu^{OH} < 1000$ cm^{-1}. The threshold frequencies for proton transfers in the gas phase and continuum aqueous solution are at $\nu^{OH*} = 1984$ and 1881 cm^{-1}, respectively. According to the results obtained from the static proton transfer potentials, the trends of the interaction energies with respect to the number of water molecules in the gas phase and continuum aqueous solution are quite similar. The destabilization effects caused by the continuum aqueous solvent bring about smaller variation of the interaction energies with respect to the number of water molecules compared to the gas phase. The destabilization effects also lead to shifts of the transferring protons away from the centers, especially for the H-bond complexes with the Zundel complex as the central charged species. The trend of the solvation energies revealed that, when the number of water molecules is the same, the H-bonds inside the protonated water clusters experience comparable uniform electric field. BOMD simulations at 350 K predicted $\nu^{OH,MD}$ in a quite wide range, from 940 to 1740 cm^{-1}. Most importantly, BOMD simulations suggested an additional characteristic asymmetric O-H stretching band at a higher frequency. They are in the range of 1640 and 2600 cm^{-1}. The lower-frequency band is regarded as the "oscillatory shuttling band" and the higher-frequency band the "structural diffusion band". The latter cannot not be determined from static proton transfer potentials, due to the anharmonic and dynamic behaviors of the vibrational motions of the transferring proton. The oscillatory shuttling and structural diffusion bands could be considered as the IR spectroscopic evidences for the formations of the shared-proton structure (*e.g.* the $[H_2O\text{-}H^+\text{-}OH_2]$ complex) and the $H_3O^+\text{-}H_2O$ structure, respectively. The analyses of the H-bond structures and $\nu^{OH,MD}$ yielded the threshold frequencies ($\nu^{OH,MD*}$) for the proton transfers in the gas

phase and continuum aqueous solution at $\nu^{OH,MD*}$ = 1917 and 1736 cm^{-1}, respectively. Because the quasi-dynamic equilibrium between the Zundel and Eigen complexes was suggested to be the rate-determining step, in order to achieve an "ideal" maximum efficiency, a concerted proton transfer pathway should be taken. The present results anticipated that the effective interconversion between the two proton states, the Zundel-like and hydronium-like structures, could be reflected from comparable intensities of the oscillatory shuttling and structural diffusion bands. These pieces of information provided an appropriate IR method to investigate proton transfer reactions in larger model systems, and iterated the necessity to incorporate the thermal energy fluctuations and dynamics in the model calculations.

Four H-bond complexes were identified as the intermediate states for proton transfer in the CH_3OH-H_3O^+-H_2O complexes, in which the most active unit is represented by an excess proton nearly equally shared between CH_3OH and H_2O. Linear relationships between Δd_{DA} and the H-bond distance ($R_{O\text{-}O}$) could be approximated for both internal and external H-bonds; whereas the relationship between ν^{OH} and $R_{O\text{-}O}$ could be represented by an exponential function similar to the integral rate expression for the first-order reaction. Based on the static proton transfer potentials (B3LYP/TZVP calculations), ν^{OH} for the H-bond protons in the intermediate states in the gas phase are ranging from 1778 to 2086 cm^{-1}, and in continuum aqueous solution from 1690 to 2029 cm^{-1}. These, however, cannot be definitive due to the lack of the IR spectral signatures at $\nu^{OH} \approx 1000$ cm^{-1}; using the same theoretical methods, the Zundel complex possesses ν^{OH} = 961 and 677 cm^{-1}, in the gas phase and continuum aqueous solution, respectively. More definitive results were obtained from BOMD simulations at 350 K. Based on the IR spectra obtained from the Zundel complex, the H-bond structure with incomplete water coordination at $CH_3OH_2^+$ and H_3O^+ appeared to be the most active intermediate state in continuum aqueous solution, with the characteristic ν^{OH} at 978 cm^{-1}. This is in accordance with the observation that the excess proton is preferentially taken by CH_3OH in the open chain structures, not the fully hydrated structures. According to the assumption the thermal energy fluctuations could temporarily separate or break the H-bonds connecting the intermediate states and the water molecules in the second hydration shell, and the observation that the incomplete water coordination at the charged

species could help promote structural diffusion as in the case of the Zundel and Eigen complex, two elementary reactions of proton transfer were proposed.

The B3LYP/TZVP results suggested two types of structural diffusion mechanisms for the proton transfer in the CF_3SO_3H-H_3O^+-H_2O complexes; the pass-through mechanism involves the protonation and deprotonation at the $–SO_3H$ group, whereas the pass-by mechanism, the proton transfer in the adjacent Zundel complex. The plots of ν^{OH} and Δd_{DA} anticipated the threshold frequencies (ν^{OH*}) for the proton transfers through the pass-through mechanism at 2162 and 2001 cm^{-1}, in the gas phase and continuum aqueous solution, respectively, whereas for the pass-by mechanism at 1829 and 1714 cm^{-1}, respectively. The latter are about 200 cm^{-1} lower than the protonated water clusters. These represent spectroscopic evidences for the promotion of proton transfer in the Zundel complex by the $–SO_3H$ group. For the CF_3SO_3H-H_3O^+-H_2O complexes, the inclusion of the thermal energy fluctuation and dynamics in the model calculations made it difficult to differentiate the trends of the results in the gas phase and continuum aqueous solution. For the pass-by mechanism, BOMD simulations at 350 K predicted similar characteristic asymmetric O-H stretching frequencies ($\nu_A^{OH,MD}$), with slightly lower threshold frequencies for proton transfer, $\nu_A^{OH*,MD}$ = 1733 and 1740 cm^{-1}, respectively. As in the previous cases, BOMD simulations yielded another characteristic asymmetric O-H stretching band at a higher frequency ($\nu_B^{OH,MD}$). The analyses of $\nu_A^{OH,MD}$ and $\nu_B^{OH,MD}$ yielded the vibrational energies for the proton transfer ($\Delta\nu_{BA}^{OH,MD}$) through the pass-through and pass-by mechanisms of 469 and 398 cm^{-1}, respectively. The latter is about 75 cm^{-1} lower than the protonated water clusters, indicating a decrease of the vibrational energy for the interconversion between the oscillatory shuttling and structural diffusion motions by the $–SO_3H$ group.

All the theoretical results presented in this work suggested that, due to the coupling among various vibrational modes, the discussions on proton transfer reactions cannot be made based on static proton transfer potentials. In order to study proton transfer reactions, thermal energy fluctuations and dynamics must be included in the model calculations. Although the characteristic IR frequencies of the transferring protons cannot be measured easily in experiment, due to the limitations of IR equipment and the difficulties in the assignment of absorption bands, the present theoretical results provided insights into vibrational behaviors of the transferring

protons, as well as suggested theoretical methods and criteria to monitor and improve the efficiency of proton transfer reactions in more complex systems. Together with systematic analyses of IR spectra, it has been shown that BOMD simulations are the most appropriate theoretical methods for the investigations of proton transfer reactions in H-bonds.

เนื้อหางานวิจัย

Proton transfer reactions and dynamics in CH_3OH-H_3O^+-H_2O complexes

K. Sagarik*, S. Chaiwongwattana and V. Vchirawongkwin,

Phys. Chem. Chem. Phys., **12**, 918-929 (2010). (JIF = 4.12)

Proton transfer reactions and dynamics in CH_3OH-H_3O^+-H_2O complexes

by

Kritsana Sagarik*

and

Sermsiri Chaiwongwattana

School of Chemistry

Institute of Science

Suranaree University of Technology

Nakhon Ratchasima 30000

Thailand

Viwat Vchirawongkwin

Department of Chemistry

Faculty of Science

Chulalongkorn University

Bangkok 10500

Thailand

Supakit Prueksaaroon

National Electronics and Computer Technology Center (NECTEC)

Pathumthani 12120

Thailand

*corresponding author: kritsana@sut.ac.th,

Tel./Fax: (6644) 224635

keywords: methanol, *ab initio* MD simulations, proton transfer, vibrational spectra

Abstract

Proton transfer reactions and dynamics in hydrated complexes formed from CH_3OH, H_3O^+ and H_2O were studied using theoretical methods. The investigations began with searching for equilibrium structures at low hydration levels using DFT method, from which active H-bonds in the gas phase and continuum aqueous solution were characterized and analyzed. Based on the asymmetric stretching coordinates (Δd_{DA}), four H-bond complexes were identified as potential transition states, in which the most active unit is represented by an excess proton nearly equally shared between CH_3OH and H_2O. These cannot be definitive due to the lack of asymmetric O-H stretching frequencies (ν^{OH}) which are spectral signatures of transferring protons. Born-Oppenheimer Molecular Dynamics (BOMD) simulations revealed that, when the thermal energy fluctuations and dynamics were included in the model calculations, the spectral signatures at $\nu^{OH} \approx 1000$ cm^{-1} appeared. In continuum aqueous solution, the H-bond complex with incomplete water coordination at charged species turned out to be the only active transition state. Based on the assumption that the thermal energy fluctuations and dynamics could temporarily break the H-bonds linking the transition state complex and water molecules in the second hydration shell, elementary reactions of proton transfer were proposed. The present study showed that, due to the coupling among various vibrational modes, the discussions on proton transfer reactions cannot be made based solely on static proton transfer potentials. Inclusion of thermal energy fluctuations and dynamics in the model calculations, as in the case of BOMD simulations, together with systematic IR spectral analyses, has been proved to be the most appropriate theoretical approaches.

Introduction

Proton transport in condensed phases represents one of the most important problems in electrochemistry, especially in connection with the development of alternative energy sources such as fuel cells (FC).[1,2] Since the basic operations in fuel cells depend upon the transportation of protons (H^+) generated at anode across a proton exchange membrane (PEM) - often made from Nafion® - to cathode, where they react with oxygen to produce water,[1] it is vital to understand elementary reactions and dynamics of proton transfer processes in liquids, solid and aqueous solutions. Although some theoretical and experimental information has been accumulated,[3-6] precise mechanisms of proton transfer in PEMFC, especially for those employing methanol (CH_3OH) as a direct fuel, are not completely known. Since some basic chemistry of proton transfer reactions has been discussed in details in many review articles,[4-6] only the theoretical and experimental information relevant to the present study will be briefly summarized here.

CH_3OH has been frequently selected as model compound for the investigation of proton transport in hydrogen bonds (H-bonds).[7-20] The abnormally high mobility of an excess proton in liquid methanol ($[CH_3OH]_{liq}$) has been extensively studied using *ab initio* molecular dynamics (MD) simulations, from which a structural diffusion mechanism of cationic defect was proposed.[16] Having both hydrophobic (CH_3) and hydrophilic (OH) groups in the same molecule makes the H-bond structures in $[CH_3OH]_{liq}$ different from $[H_2O]_{liq}$; one-dimensional linear H-bond chains with occasional branches seem to be the predominant species from 153 K to room temperature.[19] Due to significant roles playing by the methyloxonium ion ($CH_3OH_2^+$) in direct methanol fuel cell (DMFC),[17] delocalization of proton in the H-bond complexes formed from H_3O^+, CH_3OH and H_2O has been extensively studied.[13-16] In the presence of an excess proton, two H-bond structures dominate in the CH_3OH-H_2O clusters namely, the fully solvated and open chain structures.[13] The excess proton is preferentially taken by CH_3OH in the open chain structure.[13] A structural analogue of the Zundel complex ($C_2H_9O_2^+$) and $CH_3OH_2^+$ were suggested by density functional theory (DFT) calculations at the B3LYP/6-31+G(d) level

and vibrational predissociation spectroscopy to play important roles in proton transfer in the mixed H-bond clusters.[15]

Proton affinities in the $CH_3OH-H_3O^+-H_2O$ $1:1:n$ complexes, $1 \geq n \geq 5$, were investigated in the gas phase using DFT calculations and IR spectroscopy at 170 K.[20] DFT calculations at the B3LYP/6-31G+(d) level revealed that the excess proton can be either localized close to CH_3OH or H_2O, forming $CH_3OH_2^+$ or H_3O^+, respectively. The position of the excess proton is sensitive to the number of water molecules, as well as the geometry of the H-bond complexes. The IR spectral signatures determined from the free O-H stretching frequencies in the range of 2700 and 3900 cm^{-1} indicated that $CH_3OH_2^+$ and H_3O^+ possess comparable stability and could be concurrently detected in the gas phase.[20] Moreover, in the $CH_3OH-H_3O^+-H_2O$ $1:1:n$ complexes, the excess proton could be preferentially captured by CH_3OH when $n = 1$ and equally shared by CH_3OH and H_2O when $n = 3$. The excess proton could gradually move away from CH_3OH when $n \geq 3$. The results in ref. 20 led to the conclusion that the protonated ions in acidic $[CH_3OH]_{aq}$ are quite flexible and can fluctuate rapidly over $CH_3OH_2^+$, H_3O^+ and $CH_9O_3^+$.

Vibrational spectroscopy has been one of the most powerful techniques in H-bond research.[21] This is due to the fact that the most evident effects for the A-H..B H-bond formation are the red shift of the A-H stretching mode, accompanied by its intensity increase and band broadening.[13,18] Analyses of the A-H stretching frequencies could also lead to valuable information on proton transfer reactions in H-bonds.[17] As an example, IR experiments,[22] quantum-dynamical calculations[23-25] and Born-Oppenheimer MD (BOMD) simulations[26] suggested that the vibrational spectra of the Zundel complex ($H_5O_2^+$) in aqueous solutions can be divided into three distinct regions. The vibrational frequencies above 3000 cm^{-1} correspond to the symmetric and asymmetric stretching modes of individual water molecules, whereas those between 1000 and 2000 cm^{-1} are associated with the characteristic vibrational frequencies of the transferring protons.[25] The correlation between the O-H stretching frequency and the probability of proton

transfer in H-bond was investigated and discussed in details in ref. 13 and 17. Although the assignment of all the features of the individual spectra were not made due to the coupling and overlapping of various vibrational modes, as well as the detection limit of IR equipment,[20,21] the probability of proton transfer could be associated with the degree of the red shift, by comparison with the corresponding "free" or "non-H-bonded" O-H stretching frequency.[13]

In our previous work,[27] elementary reactions of proton transfer processes at a sulfonic acid group ($-SO_3H$) of Nafion® were studied using the H-bond complexes formed from triflic acid (CF_3SO_3H), H_3O^+ and H_2O as model systems. BOMD simulations at 298 K revealed that a quasi-dynamic equilibrium could establish between the Eigen ($H_9O_4^+$) and Zundel complexes, and is considered to be one of the most important elementary reactions. It was demonstrated that, proton transfer reactions at $-SO_3H$ are not concerted due to the thermal energy fluctuations, leading to quasi-dynamic equilibriums among precursors, transition state complexes and products. Most importantly, $-SO_3H$ could directly and indirectly mediate proton transfer reactions through the formation of proton defects, as well as the $-SO_3^-$ and $-SO_3H_2^+$ transition states.

In order to obtain information for the investigations of DMFC, elementary reactions and dynamics of proton transfer in hydrated complexes formed from CH_3OH, H_3O^+ and H_2O were studied in the present work. The H-bond complexes were systematically investigated using quantum chemical methods and BOMD simulations, both in the gas phase and continuum aqueous solution. Since proton transfer reactions could be characterized by vibrational motions of the active protons, vibrational frequencies in H-bonds were computed, categorized and analyzed. Based on the information from quantum chemical calculations and BOMD simulations, elementary reactions and dynamics of proton transfer in the model systems were discussed in comparison with available theoretical and experimental data of the same and similar systems.

Computational Methods

Since proton transfer reactions are complicated, care must be exercised in selecting appropriate model systems and theoretical methods. Our experience[27] showed that elementary reactions and dynamics of proton transfer in H-bond could be studied reasonably well by taking the following three basic steps; (1) searching for all potential precursors and transition state complexes in proton transfer pathways using pair potentials; (2) refinements of the computed structures using accurate quantum chemical method; (3) BOMD simulations starting from the refined structures. These three steps were also applied in the present work.

Our experience also showed that the inclusion of too many water molecules in the model systems could lead to difficulties in the analyses of proton transfer reactions.[27] Therefore, it was the strategy of the present work to restrict the number of water molecules in the model systems. Since the $CH_3OH_2^+ - CH_3OH$ complex contributes only 5 % to the proton transfer events[14] and the excess proton starts to move away from $CH_3OH_2^+$ when n = 3,[20] the $CH_3OH - H_3O^+ - H_2O$ $1 : 1 : n$ complexes, $1 \leq n \leq 3$, were chosen in the present study. Some basic structural and dynamic properties of the CH_3OH-H_2O and $CH_3OH - H_3O^+$ complexes were also investigated.

In order to characterize IR spectra of transferring proton, as well as their correlations with the probability of proton transfer,[28] O-H stretching frequencies in H-bond were computed and analyzed, using a quantum chemical method and BOMD simulations. Since the electric field introduced by polar solvent could determine the potential energy surface on which the active proton moves, a continuum solvent model had to be included in the model calculations. In the present work, the conductor-like screening model (COSMO), with the dielectric constant (ε) of 78, was employed to account for the effects of the extended H-bond networks of water, which were not explicitly included in the model systems. Literature survey showed that COSMO has been applied successfully in various H-bond systems.[29]

Searching for potential precursors and transition state complexes

All the H-bond complexes which could serve as precursors and transition state complexes in proton transfer pathways were searched, characterized and analyzed. In order to effectively scan the intermolecular potential energy surfaces, test-particle model (T-model) potentials[30-39] were constructed and employed in the calculations of the equilibrium structures and interaction energies of the hydrated complexes. Since the applicability of the T-model had been discussed in details in our previous studies,[30-39] only some important aspects relevant to the geometry optimizations will be briefly summarized using the $CH_3OH-H_3O^+-H_2O$ $1:1:1$ complex as an example.

Experimental geometries of CH_3OH, H_3O^+ and H_2O were employed[40] and kept constant in the geometry optimizations. For the $CH_3OH-H_3O^+-H_2O$ $1:1:1$ complex, a rigid CH_3OH was placed at the origin of the Cartesian coordinate system. The coordinates of H_3O^+ and H_2O were randomly generated in the vicinities of CH_3OH. Based on the T-model potentials, equilibrium structures of the complex were searched using a minimization technique. One hundred starting configurations were generated and employed as starting configurations in the geometry optimizations. The same procedures were applied in the calculations of equilibrium structures and interaction energies of the hydrated complexes considered here.

Structural refinements and vibrational spectra

Since the T-model potentials are based on rigid molecules, in which cooperative effects are not taken into account, structural refinements with full geometry optimizations had to be made using an appropriate quantum chemical method. Literature survey showed that DFT methods have been frequently chosen due to the ability to predict the effects of electron correlations with reasonable degree of accuracy, especially for similar H-bond systems.[41-46] Since, in the present investigations, the calculations of vibrational spectra and lengthy BOMD simulations had to be performed, it was necessary to compromise

between the accuracy of theoretical method and available computer resources. In order to achieve all the objectives, DFT calculations were performed using the B3LYP hybrid functional[47] and the triple-zeta valence basis sets augmented by polarization functions (TZVP).[48] The performance of B3LYP in the calculations of vibrational spectra of similar systems was examined and discussed in details in ref. 49 and 50. It was shown that B3LYP/TZVP calculations are sufficient for the systems with and without occupied d-states, and could be applied reasonably well in the calculations of equilibrium structures and interaction energies, as well as vibrational spectra, of such systems.[49]

The absolute and local minimum energy geometries of the H-bond complexes computed from the T-model potentials were employed as starting configurations in B3LYP/TZVP geometry optimizations. In order to ensure that the optimized geometries are at the stationary points of the potential energy surfaces, a tight SCF energy convergence criterion (less than 10^{-8} au) with the maximum norm of Cartesian gradients less than 10^{-4} au were adopted in B3LYP/TZVP geometry optimizations. In the present work, B3LYP/TZVP calculations were made using TURBOMOLE 6.0 software package.[51]

Experiment in ref. 17 showed that the H-bond distance ($R_{O\text{-}O}$) in concentrated HCl solutions could be divided into three groups namely, the internal, external and solvation groups. The H-bonds linking directly to proton belong to the internal group, with $R_{O\text{-}O}$ in the range of 2.45 – 2.57 Å, whereas $R_{O\text{-}O}$ in the external and solvation groups are in the ranges of 2.60 – 2.70 Å and longer than 2.70 Å, respectively. The H-bond protons in the internal group are considered to be active in proton transfer. In the present work, attempt was made to use similar criteria[17] to discuss the tendency of proton transfer in H-bond. A concept of the "most active" H-bond[52] was tentatively applied to describe the Grothuss mechanism.[53] Within the framework of the most active H-bond, asymmetric stretching coordinate of a donor (D) - acceptor (A) pair is defined by $\Delta d_{DA} = | d_{A\text{-}H} - d_{B..H} |$;[14] $d_{A\text{-}H}$ and $d_{B..H}$ are the A-H and B..H distances, respectively. H-bond is considered to be "active" with respect to proton transfer when $\Delta d_{DA} < 0.1$ Å, and "inactive" when $\Delta d_{DA} > 0.4$ Å.[14] Therefore, according to Δd_{DA}, the H-bond in $H_5O_2^+$ is the most active

($\Delta d_{DA} = 0$); the H-bond proton is equally shared by the two water molecules. In the present work, the internal and external H-bonds were classified using plots between Δd_{DA} and $R_{O\text{-}O}$; appropriate functions were chosen by least square method to represent the relationships in the internal and external groups.

Assuming no coupling between degrees of freedom, harmonic vibrational frequencies were computed in the present work from numerical second derivatives, from which the analyses of normal modes in terms of internal coordinates were made, using NUMFORCE and AOFORCE programs,[51] respectively. Being associated with the dynamics of proton transfer in H-bond,[54] asymmetric O-H stretching frequencies (ν^{OH}) were of primary interest. It should be noted that vibrational frequencies derived from quantum chemical calculations are generally overestimated compared to experiment, and a scaling factor which partially accounts for anharmonicities and systematic errors is required. Although the exact O-H stretching frequencies were not the main objective, a scaling factor was applied in the present study; the scaling factor of 0.9614 was proved to be appropriate for B3LYP calculations.[55]

In order to measure the activity of H-bond proton in terms of ν^{OH}, classical interpretations of IR stretching frequencies for concentrated acid solutions[56] were employed as criteria; IR stretching frequencies of H-bond proton were divided into three groups namely, the internal (1300 - 2200 cm^{-1}), external (2500 - 3200 cm^{-1}) and outer layer groups (3300 - 3400 cm^{-1}). In order to correlate the concept of the most active H-bond with the classical interpretations of IR stretching frequencies,[56] the H-bonds in the internal and external groups were distinguished based on the relationship between ν^{OH} and $R_{O\text{-}O}$; ν^{OH} and $R_{O\text{-}O}$ were plotted and appropriate functions were chosen using least square method.

Quantum MD simulations

Dynamics of rapid covalent bond formation and cleavage could be studied reasonably well using quantum MD simulations,[57] among which DFT-MD simulations have been widely used in recent years.[58,59] In the present work, proton transfers in the $CH_3OH-H_3O^+$ and $CH_3OH-H_3O^+-H_2O$ complexes were investigated using BOMD simulations[60,61] with canonical ensemble (NVT) at 350 K. Within the framework of BOMD simulations, classical equations of motions of nuclei on the BO surfaces are integrated, whereas forces on nuclei are calculated in each MD step from quantum energy gradients, with the molecular orbitals (MOs) updated by solving Schrödinger equations. BOMD simulations are therefore more accurate, as well as considerably CPU time consuming, compared to conventional classical MD simulations, in which forces on nuclei are determined from predefined empirical or quantum pair potentials. Although the high mobility of proton was initially attributed to quantum mechanical (QM) tunneling,[62,63] the results of BOMD simulations[25] and conductivity measurements[64] showed that, mechanisms of proton transfer could be explained reasonably well without assuming the proton tunneling to be the important pathways.

In order to ensure that all important dynamics of proton transfer processes in the $CH_3OH-H_3O^+-H_2O$ complexes were taken into account, the equilibrium structures computed in the previous section were used as starting configurations in BOMD simulations. Since proton transfer in aqueous solutions involves dynamic processes with different timescales,[65-67] the complexity of proton transfer reactions could be reduced using various approaches. The observation that the actual proton transfer occurs in femtosecond (fs) timescale,[67] which is in general faster than solvent structure reorganization,[66] made it possible to perform BOMD simulations by focusing on short-lived phenomena taking place before H-bond structure reorganizations. Since, in aqueous solutions, the rapid interconversion between the Zundel and Eigen complexes happens within 100 fs (10^{-13} s),[65] the timestep used in solving dynamic equations was set to about 1 fs (0.968 fs = 40 a.u.). In each BOMD simulations, 4000 timesteps were devoted to

equilibration and 10,000 timesteps to property calculations, corresponding to about 10 ps. In order to ensure that, in the course of BOMD simulations, the active proton is not trapped in a minimum, appropriate temperature fluctuations must be selected as suggested in ref. 68. This was accomplished in TURBOMOLE 6.0[51] by applying the Nose-Hoover thermostat at every 30 BOMD steps.

In order to search for spectral signatures of transferring protons, IR spectra of H-bond were computed from Fourier transformations of the velocity autocorrelation function (VACF);[69] the approach is appropriate as it allows various vibrational modes to be computed separately. Since only the H-bond protons involved in structural diffusion were of interest and the reorientation of water molecule takes about 1-2 ps,[70,71] IR spectra were calculated within a short time limit of 1 ps. This choice can be justified by the observation that the average lifetime of the H-bond in CH_3OH-H_2O solutions is approximately 1.2 ps.[14] Only symmetric and asymmetric O-H stretching frequencies (ν^{OH}) of the H-bond protons, as well as the O-O vibrations, were of interest.

Diffusion coefficient (D) of the active proton could be computed from BOMD simulations. The Einstein equation[72-74] was employed in the present work, by which the diffusion coefficient is determined from the slope of the mean square displacement (MSD). Since the calculations of diffusion coefficient of a single-particle (H^+) confined in a short H-bond distance are not straight forward,[73,74] care must be exercised especially in selecting the time interval over which MSD were computed; the time interval cannot be too large due to the limitation of the allowed displacement.[74] After several test calculations, linear relationships between MSD and simulation time could be obtained when the time intervals are not larger than 0.5 ps.

Results and discussions

Equilibrium structures and vibrational frequencies

Fig. 1 shows the refined equilibrium structures and interaction energies (ΔE) of the H-bond complexes in the gas phase and continuum aqueous solution, together with characteristic H-bond distances and asymmetric stretching coordinates (Δd_{DA}). Asymmetric O-H stretching frequencies (ν^{OH}) of H-bond protons are given in Fig. 2, together with the frequency shifts ($\Delta\nu^{OH}$) due to continuum aqueous solvent. The red shifts are designated by negative values of $\Delta\nu^{OH}$. It appeared that the equilibrium structures in the gas phase and continuum aqueous solution are the same and agree well with the theoretical results in ref. 20. Therefore, only Δd_{DA}, ν^{OH} and $\Delta\nu^{OH}$, which could be related to the tendencies of proton transfer in H-bonds, are discussed in details. In order to simplify the discussion, the H-bonds in Fig. 1 and 2 are labeled with numbers in parentheses.

For the CH_3OH-H_2O complex in the gas phase, B3LYP/TZVP calculations predicted the structure, in which water molecule acts as proton donor, to be about 1.8 kJ/mol more stable than the one as proton acceptor, structures **a** and **b** in Fig. 1, respectively. The results are in excellent agreement with microwave[75] and IR measurements.[76] The stabilities of structures **a** and **b** are considerably increased in continuum aqueous solution, with ΔE = -73.4 and -72.8 kJ/mol, respectively. Δd_{DA} and ν^{OH} do not show tendency of proton transfer in structures **a** and **b**, both in the gas phase and continuum aqueous solution.

Interesting results were obtained for the $CH_3OH-H_3O^+$ complex, structure **c** in Fig. 1. B3LYP/TZVP calculations revealed that, the H-bond proton tends to protonate at CH_3OH, forming $CH_3OH_2^+$. This is in accordance with the observation that CH_3OH in acid solution possesses higher proton affinity than water.[75] Δd_{DA} shows a slightly higher tendency of proton transfer in continuum aqueous solution compared to the gas phase,

0.24 and 0.32 Å, respectively. The trends of Δd_{DA} are supported by the asymmetric O-H stretching frequencies in Fig. 2. The strong IR absorption peaks at ν^{OH} = 2086 and 1690 cm^{-1} appeared to be the characteristics of the H-bond proton in the $CH_3OH-H_3O^+$ complex in the gas phase and continuum aqueous solution, respectively, with $\Delta\nu^{OH}$ = -369 cm^{-1}. It was reported in ref. 20 that the asymmetric O-H stretching frequencies cannot be measured easily in experiment since the energy provided by single IR photon is much lower than the minimum energy required to dissociate this complex via one-photon excitation processes.

Structures **d** and **e** in Fig. 1 are the two minimum energy geometries of the $CH_3OH-H_3O^+-H_2O$ 1 : 1 : 1 complex. For structure **d**, the H-bond between CH_3OH and H_3O^+ (H-bond **(1)**), shows higher tendency of proton transfer than H-bond **(2)**. In the gas phase and continuum aqueous solution, H-bond **(1)** possesses Δd_{DA} = 0.22 and 0.33 Å, and ν^{OH} = 1778 and 1911 cm^{-1}, respectively. The continuum aqueous solvent leads to blue shift in H-bond **(1)** and red shift in H-bond **(2)**, with $\Delta\nu^{OH}$ = 133 and -318 cm^{-1}, respectively. The results are different for structure **e**, in which $CH_3OH_2^+$ is equally stabilized by two adjacent water molecules, with Δd_{DA} in the gas phase and continuum aqueous solution of 0.49 and 0.46 Å, respectively, and ν^{OH} = 2628 and 2277 cm^{-1}, respectively. These indicated that H-bonds **(1)** and **(2)** in structure **e** are not as active as H-bond **(1)** in structure **d**.

Based on the above discussions and the results on the larger hydrated complexes in Fig. 1 and 2, the trends of proton transfer could be anticipated. It appeared that, the incomplete water coordination at the charged species, $CH_3OH_2^+$ and H_3O^+ (as in structures **c** and **d**, respectively), and the asymmetric H-bond structure at $CH_3OH_2^+$ (as in structures **g** and **h**) could help promote structural diffusion. Therefore, according to Δd_{DA} and the criteria in ref. 14, the H-bond protons in structures **c**, **d**, **g** and **h** could be active in proton transfer ($\Delta d_{DA} < 0.4$ Å), with the tendencies decreasing in the following order:

Gas phase: **d** ≥ **h** > **g** ≥ **c**.

Continuum aqueous solution: **c** > **d** ≥ **g** ≥ **h**.

Fig. 3a and 3b show the relationships between the asymmetric stretching coordinate (Δd_{DA}) and the H-bond distance ($R_{O\text{-}O}$), and between ν^{OH} and $R_{O\text{-}O}$, respectively. The trends in Fig. 3a suggest a separation between the internal and external H-bonds at $R_{O\text{-}O}$ = 2.55 Å, in good agreement with $R_{O\text{-}O}$ = 2.57 Å in ref. 17. The linear relationships for the internal and external H-bonds in the gas phase and continuum aqueous solution could be represented by equations (1) and (2), respectively.

Internal H-bonds: $\Delta d_{DA} = 2.1464 \times R_{O\text{-}O} - 4.9559$ (1)

External H-bonds: $\Delta d_{DA} = 1.2936 \times R_{O\text{-}O} - 2.7735$ (2)

Due to the asymptotic behavior at large $R_{O\text{-}O}$, the relationship between ν^{OH} and $R_{O\text{-}O}$ in Fig. 3b cannot be approximated by linear function; at large $R_{O\text{-}O}$, ν^{OH} converges to the asymmetric O-H stretching frequency of non-H-bonded proton. After several test fittings, an exponential function similar to the integrated rate expression for first order reaction was found to be the most appropriate. The fitted functions in the gas phase and continuum aqueous solution are shown in equations (3) and (4), respectively.

Gas phase: $\nu^{OH} = -1.17 \times 10^{10} e^{-R_{O\text{-}O}/0.1544} + 3526.2$ (3)

Continuum aqueous solution: $\nu^{OH} = -0.71 \times 10^{10} e^{-R_{O\text{-}O}/0.1617} + 3583.8$ (4)

The agreements between ν^{OH} derived from B3LYP/TZVP calculations and the fitted values are included in Fig. 3b.

Based on the results obtained from the static proton transfer potentials (B3LYP/TZVP calculations), one could conclude that, ν^{OH} for the H-bond protons in structures **c**, **d**, **g** and **h** in the gas phase are ranging from 1778 to 2086 cm^{-1}, and in continuum aqueous solution from 1690 to 2029 cm^{-1}. According to the classical interpretations,[56] the H-bonds

in structures **c**, **d**, **g** and **h** belong to the internal group and could be active in proton transfer reactions. However, these cannot be definitive due to the lack of the IR spectral signatures at $\nu^{OH} < 1000$ cm^{-1}, as in the case of the Zundel complex.[77]

It should be noted that, using the same approaches, ν^{OH} for the Zundel complex in the gas phase and continuum aqueous solution are 961 and 677 cm^{-1}, respectively.[77] The former is comparable with the theoretical result in ref. 78 of 983 cm^{-1}. In the gas phase, the experimental O-H stretching frequency of the transferring proton in the Zundel complex was reported to be 1085 cm^{-1}.[79] Therefore, the asymmetric O-H stretching frequencies at $\nu^{OH} \leq 1000$ cm^{-1} could be regarded as spectral signatures of proton transfer in H-bond. In this subsection, one could also conclude that the incomplete water coordination at the central charged species (H_3O^+ and $CH_3OH_2^+$), as well as the electrostatic effects introduced by continuum aqueous solvent, could directly affect the tendency of proton transfer in H-bond.

Dynamics and mechanisms of proton transfer reactions

Dynamics and mechanisms of proton transfer reactions in the $CH_3OH-H_3O^+$ and $CH_3OH-H_3O^+-H_2O$ complexes are discussed in this subsection, with the emphasis on structures **c**, **d**, **g** and **h**. The average H-bond distances ($<R_{O-O}>$) and the average asymmetric stretching coordinates ($<\Delta d_{DA}>$) obtained from BOMD simulations are listed in Table 1, together with characteristic asymmetric O-H stretching frequencies (ν^{OH}). Similar to the analyses made in the previous subsection, $<\Delta d_{DA}>$ and $<R_{O-O}>$ were plotted and shown in Fig. 3c. Power spectra of the symmetric and asymmetric O-H stretching modes of the H-bond protons in structures **c** and **d**, as well as the O-O stretching modes (ν^{OO}), are given as examples in Fig. 4. The definitions of the three vibrational modes are also included in Fig. 4.

It appeared in Fig. 3c that, linear relationships between $<\Delta d_{DA}>$ and $<R_{O-O}>$ could also be approximated for the internal and external H-bonds, with a separation at

$< R_{O-O} >$ = 2.55 Å, the same as that from B3LYP/TZVP calculations. The linear functions are shown in equations (5) and (6), respectively.

Internal H-bonds: $< \Delta d_{DA} > = 2.6440 \times < R_{O-O} > - 6.2468$ (5)

External H-bonds: $< \Delta d_{DA} > = 1.4993 \times < R_{O-O} > - 3.3128$ (6)

In order to correlate the probability of proton transfer with ν^{OH} computed from BOMD simulations, the results on the Zundel complex[77] included in Fig. 4 should be discussed. The IR spectra of the H-bond proton in the Zundel complex computed from BOMD simulations at 350 K show two asymmetric O-H stretching bands, labeled with **A** and **B** in Fig. 4a and 4b; in the gas phase at ν^{OH} = 1090 and 1809 cm^{-1} and in continuum aqueous solution at ν^{OH} = 875 and 1686 cm^{-1}, respectively. The low-frequency bands at **A** are comparable with the characteristic ν^{OH} derived from B3LYP/TZVP calculations.[77] They could be associated with the vibration modes, in which proton shuttles back and forth at the center of the O-H..O H-bond. For the higher-frequency bands at **B**, the centers of vibration are shifted towards an oxygen atom of water. Therefore, ν^{OH} at **A** and **B** could be considered as the IR spectral signatures of the transferring proton in the Zundel complex.

As the proton transfer in the Zundel complex depends strongly on the O-O stretching mode,[27] the relative probability or the extent of proton transfer in BOMD simulations could be estimated from the ratio between the intensity of the asymmetric O-H stretching mode at **A** ($\mathbf{I_A}$) and the intensity of the O-O stretching mode ($\mathbf{I_{OO}}$); high $\mathbf{I_A/I_{OO}}$ reflects a high probability of proton transfer in BOMD simulations. For the Zundel complex in the gas phase and continuum aqueous solution at 350 K, $\mathbf{I_A/I_{OO}}$ amounts to 0.33 and 0.44, respectively, indicating a higher probability of proton transfer in continuum aqueous solution. At 298 K, the diffusion coefficient of the transferring proton in the Zundel complex is 5×10^{-5} cm^2 s^{-1},[77] slightly lower than the experimental value of 7×10^{-5} cm^2 s^{-1};[66] the diffusion coefficient of a proton moving across a single water molecule was approximated from NMR hopping time (τ_p) and the Einstein relation, $D = l^2/6\,\tau_p$, where

l is the hopping length. It should be augmented that the value of D in ref. 66 was computed by subtracting the water self-diffusion coefficient, 2.3×10^{-5} cm^2 s^{-1}, from the proton diffusion coefficient, 9.3×10^{-5} cm^2 s^{-1}. The discrepancy of about 28% could be partly due to the lack of extensive H-bond networks of water in the model systems. Based on the information on the Zundel complex, one could anticipate proton transfer from the following three spectral evidences; (a) the existence of a threshold frequency at $\nu^{OH} \leq 1000$ cm^{-1}; (b) the appearance of an additional asymmetric O-H stretching frequency at ν^{OH} between 1600 - 1800 cm^{-1}, and; (c) $\mathbf{I_A/I_{OO}}$ comparable with the Zundel complex.

For structure **c**, the broadening of the asymmetric O-H stretching bands, with a coupling with the O-O stretching mode at $\nu^{OH} \approx 400$ cm^{-1}, made it difficult to analyze IR spectra. In the gas phase, the appearance of the low- and high-frequency bands at 2179 and 2559 cm^{-1}, respectively, rules out structure **c** from being an active transition state. Similarly, in continuum aqueous solution, $\mathbf{I_A/I_{OO}} = 0.15$ indicates restricted number of proton transfer events in BOMD simulations. Spectral evidences of proton transfer are clearly seen for structure **d**, especially in continuum aqueous solution. Fig. 4f reveals that, H-bond **(1)** possesses the asymmetric O-H stretching frequencies at $\nu^{OH} = 978$ and 1717 cm^{-1}, with $\mathbf{I_A/I_{OO}} = 0.41$; $\mathbf{I_A/I_{OO}}$ is slightly smaller than the Zundel complex.[77] The IR spectra of the active protons in structures **g** and **h** (not shown here) are similar to structure **d**, but with $\mathbf{I_A/I_{OO}}$ smaller than 0.1, indicating small number of proton transfer events in BOMD simulations. Thus, one could conclude that, for the $CH_3OH-H_3O^+-H_2O$ complex, structure **d** is the most active transition state in proton transfer pathways, with the proton diffusion coefficient (D) of 1.95×10^{-5} cm^2 s^{-1}. Since the time interval used in the calculations of MSD was short, the diffusion coefficient could be considered as pure structural diffusion constant. *Ab initio* MD simulations were employed in the study of proton transfer in CH_3OH-H_2O mixtures at 300 K.[14] It was reported that the diffusion coefficient of an excess proton in the mixture, with the CH_3OH mole fraction of 0.5 (16 H_2O and 16 CH_3OH), is 4.2×10^{-5} cm^2 s^{-1}. Based on the approximation in ref. 66 and the report that the self-diffusion coefficients of $[CH_3OH]_{liq}$ at 298 and 340 K are 2.4×10^{-5} and 4.9×10^{-5} cm^2 s^{-1}, respectively,[80] the proton diffusion coefficient in the

present system could be approximated as 4.35×10^{-5} and 6.85×10^{-5} cm^2 s^{-1}, respectively. The values agree well with the theoretical results in ref. 80.

The conclusion that structure **d** is the most active transition state complex is supported by the theoretical results in ref. 14, which showed that the nearest neighbors of the defect oxygen, the oxygen atom attached to an excess proton, consist of two water molecules, independent of whether the defect oxygen is in water or methanol. This corresponds to structure **d** in the present work. Based on the assumption the thermal energy fluctuations could temporarily break the H-bonds connecting the transition state complex and water molecules in the second hydration shell, two potential elementary reactions of proton transfer could be proposed in Fig. 5; Fig. 5a with the assumption that the excess proton is transferred in a linear H-bond structure, whereas Fig. 5b in a fully hydrated transition state complex. The former was suggested to be more preferential.[13] Finally, as in the case of the Zundel and Eigen complexes,[27] one could further anticipate that the rate-determining steps could be determined from the lifetimes of the quasi-dynamic equilibriums for the interconversion between the formation and cleavage of the H-bonds linking the first and second hydration shells, with structure **d** as the only active transition state complex.

Conclusions

Dynamics and mechanisms of proton transfer in hydrated complexes formed from CH_3OH, H_3O^+ and H_2O were studied using theoretical methods. The investigations began with searching for equilibrium structures at low hydration levels using DFT calculations at the B3LYP/TZVP level. Based on asymmetric stretching coordinates (Δd_{DA}) and asymmetric O-H stretching frequencies (ν^{OH}), four H-bond complexes were identified as transition states, in which the most active unit is represented by an excess proton nearly equally shared between CH_3OH and H_2O. Linear relationships between Δd_{DA} and the H-bond distance ($R_{O\text{-}O}$) could be approximated for both internal and external H-bonds, with a separation at 2.55 Å; whereas the relationship between ν^{OH} and $R_{O\text{-}O}$ could be represented by an exponential function similar to the integral rate expression for the first-order reaction. Based on the static proton transfer potentials (B3LYP/TZVP calculations), ν^{OH} for the H-bond protons in the transition state complexes in the gas phase are ranging from 1778 to 2086 cm^{-1}, and in continuum aqueous solution from 1690 to 2029 cm^{-1}. According to the classical interpretations, all the H-bonds in the transition state complexes belong to the internal group, and could be active in proton transfer. These, however, cannot be definitive due to the lack of the IR spectral signatures at $\nu^{OH} \approx 1000$ cm^{-1}; using the same theoretical methods, the Zundel complex possesses $\nu^{OH} = 961$ and 677 cm^{-1}, in the gas phase and continuum aqueous solution, respectively. Therefore, $\nu^{OH} \approx 1000$ cm^{-1} or lower could be considered as an IR spectral signature of the transferring proton in H-bond.

More definitive results were obtained from BOMD simulations. Based on the three spectral evidences obtained from the Zundel complex, the H-bond structure (structure **d**) with incomplete water coordination at $CH_3OH_2^+$ and H_3O^+ appeared to be the most active transition state in continuum aqueous solution, with characteristic ν^{OH} at 978 cm^{-1}. This is in accordance with the observation that the excess proton is preferentially taken by CH_3OH in the open chain structures, not the fully hydrated structures. According to the assumption the thermal energy fluctuations could temporarily separate or break the H-

bonds connecting the transition state complex and the water molecules in the second hydration shell, and the observation that the incomplete water coordination at the charged species could help promote structural diffusion as in the case of the Zundel and Eigen complex, two elementary reactions of proton transfer were proposed, with structure **d** as the only transition state complex.

The present theoretical results suggested that, due to the coupling among various vibrational modes, the discussions on proton transfer reactions cannot be made based solely on static proton transfer potentials. In order to study proton transfer reactions, thermal energy fluctuations and dynamics must be included in the model calculations. Although the asymmetric O-H stretching frequencies of the transferring protons cannot be measured easily in experiment, due to the limitations of IR equipment and the difficulties in the assignment of absorption bands, the present theoretical results could provide insights into vibrational behavior of transferring protons, as well as suggest theoretical methods and criteria to monitor proton transfer reactions in more complex environments. Together with systematic analyses of IR spectra, it has been shown that BOMD simulations are the most appropriate theoretical methods for the investigations of proton transfer reactions.

Acknowledgement

The authors would like to acknowledge the financial supports from the Thailand Research Fund (TRF): the Advanced Research Scholarship, Grant No. BRG5180022 to Prof. Kritsana Sagarik; the Royal Golden Jubilee (RGJ) Ph.D. Program, Grant No. PHD/0071/2547 to Sermsiri Chaiwongwattana and Prof. Kritsana Sagarik. Linux clusters provided by the following organizations are also gratefully acknowledged: School of Mathematics and School of Chemistry, SUT; National Electronics and Computer Technology Center (NECTEC), National Science and Technology Development Agency (NSTDA); the Thai National Grid Center (THAIGRID), Ministry of Information and Communication Technology.

References

1 J. Larminie and A. Dicks, *Fuel Cell Syst*., John Wiley & Sons Ltd, Chichester, 2001.

2 C. A. Vincent and B. Scrosati, *Modern Batteries: An introduction to electrochemical power sources*, John Wiley & Sons Ltd, New York, 1997.

3 M. Cappadonia, J. W. Erning, S. M. S. Niaki and U. Stimming, *Solid State Ionic,* 1995*,* **77**, 65.

4 J. A. Elliott and S. J. Paddison, *Phys. Chem. Chem. Phys*., 2007, **9**, 2602.

5 K. D. Kreuer, *Chem. Mater.*, 1996, **8**, 610.

6 K. D. Kreuer, S. J. Paddison, E. Spohr and M. Schuster, *Chem. Rev.*, 2004, **104**, 4637.

7 M. Hachiya, Y. Matsuda, K. Suhara, N. Mikami and A. Fujii, *J. Chem. Phys.*, 2008, **129**, 094306.

8 F. Huisken, S. Mohammad-Pooran and O. Werhahn, *Chem. Phys*., 1998, **239**, 11.

9 E. E. Fileti, M. A. Castro and S. Canuto, *Chem. Phys. Lett*., 2008, **452**, 54.

10 S. Urata, J. Irisawa, A. Takada and S. Tsuzuki, *J. Fluor. Chem*., 2005, **126**, 1312.

11 A. Vishnyakov and A. V. Neimark, *J. Phys. Chem. B*, 2001, **105**, 7830.

12 J. C. Jiang, C. Chaudhuri, Y. T. Lee and H. –C. Chang, *J. Phys. Chem. A*, 2002, **106**, 10937.

13 C. –C. Wu, C. Chaudhuri, J. C. Jiang, Y. T. Lee and H. –C. Chang, *J. Phys. Chem. A*, 2004, **108**, 2859.

14 J. A. Morrone, K. E. Haslinger and M. E. Tuckerman, *J. Phys. Chem. B*, 2006, **110**, 3712.

15 H. –C. Chang, J. –C. Jiang, S. H. Lin, Y. T. Lee and H. –C. Chang, *J. Phys. Chem. A*, 1999, **103**, 2941.

16 J. A. Morrone and M. E. Tuckerman, *J. Chem. Phys.,* 2002, **117**, 4403.

17 R. Buzzoni, S. Bordiga, G. Ricchiardi, G. Spoto and A. Zecchina, *J. Phys. Chem.*, 1995, **99**, 11937.

18 J. B. Asbury, T. Steinel and M. D. Fayer, *J. Lumin*., 2004, **107**, 271.

19 T. Kabeya, Y. Tamai and H. Tanaka, *J. Phys. Chem. B*, 1998, **102**, 899.

20 C. –C. Wu, J. C. Jiang, D. W. Boo, S. H. Lin, Y. T. Lee and H. –C. Chang, *J. Chem. Phys*., 2000, **112**, 176.

21 M. Okumura, L. I. Yeh, J. D. Myers and Y. T. Lee, *J. Phys. Chem*., 1990, **94,** 3416.

22 I. Natkaniec, K. Holderna-Natkaniec, I. Majerz and K. Parlinski, *Chem. Phys*., 2005, **317**, 171.

23 O. Vendrell, F. Gatti and H. –D. Meyer, *J. Chem. Phys*., 2007, **127**, 184303.

24 R. Vuilleumier and D. Borgis, *J. Chem. Phys*., 1999, **111**, 4251.

25 U. W. Schmitt and G. A. Voth, *J. Chem. Phys.*, 1999, **111**, 9361.

26 H. –P. Cheng and J. L. Krause, *J. Chem. Phys.,* 1997, **107**, 8461.

27 K. Sagarik, M. Phonyiem, C. Lao-ngam and S. Chaiwongwattana, *Phys. Chem. Chem. Phys*., 2008, **10**, 2098.

28 N. Rekik, B. Oujia and M. J. Wójcik, *Chem. Phys.*, 2008, **352**, 65.

29 J. Rejnek, M. Hanus, M. Kabeláč, F. Ryjáček and P. Hobza, *Phys. Chem. Chem. Phys.*, 2005, **7**, 2006.

30 K. P. Sagarik and B. M. Rode, *Chem. Phys*., 2000, **260**, 159.

31 K. P. Sagarik, S. Chaiwongwattana and P. Sisot, *Chem. Phys*., 2004, **306**, 1.

32 K. P. Sagarik and S. Dokmaisrijan, *J. Mol. Struct. (THEOCHEM)*, 2005, **718**, 31.

33 K. Sagarik and S. Chaiyapongs, *Biophys. Chem*., 2005, **117**, 18.

34 N. Deeying and K. Sagarik, *Biophys. Chem*., 2007, **125**, 72.

35 K. P. Sagarik and R. Ahlrichs, *J. Chem. Phys*., 1987, **86**, 5117.

36 K. P. Sagarik, V. Pongpituk, S. Chaiyapongs and P. Sisot, *Chem. Phys*., 1991, **156**, 439.

37 K. P. Sagarik, *J. Mol. Struct. (THEOCHEM)*, 1999, **465**, 141.

38 K. P. Sagarik and E. Spohr, *Chem. Phys*., 1997, **219**, 173.

39 K. P. Sagarik and P. Asawakun, *Chem. Phys*., 1997, **199**, 73.

40 *CRC Handbook of Chemistry & Physics*, 89th Edition, 2008-2009.

41 S. J. Paddison, *Annu. Rev. Mater. Res*., 2003, **33**, 289.

42 S. J. Paddison and T. Zawodzinski Jr., *Solid State Ionics*, 1998, **115**, 333.

43 S. J. Paddison, L. R. Pratt and T. A. Zawodzinski Jr., *J. New Mater. Electrochem. Syst*., 1999, **2**, 183.

44 S. J. Paddison, L. R. Pratt and T. Zawodzinski Jr., *J. Phys. Chem. A*, 2001, **105**, 6266.

45 S. J. Paddison, *J. New Mater. Electrochem. Syst.*, 2001, **4**, 197.

46 S. J. Paddison and J. A. Elliott, *J. Phys. Chem. A*, 2005, **109**, 7583.

47 R. Dreizler and E. Gross, *Density Functional Theory*, Plenum Press, New York, 1995.

48 A. Schäfer, C. Huber and R. Ahlrichs, *J. Chem. Phys*., 1994, **100**, 5829.

49 G. Santambrogio, M. Brümmer, L. Wöste, J. Döbler, M. Sierka, J. Sauer, G. Meijer and K. R. Asmis, *Phys. Chem. Chem. Phys*., 2008, **10**, 3992.

50 R. W. Larsen, P. Zielke and M. A. Suhm, *J. Chem. Phys*., 2007, **126**, 194307.

51 TURBOMOLE V6.0 2009, a development of University of Karlsruhe and Forschungszentrum Karlsruhe GmbH, 1989-2007, TURBOMOLE GmbH, since 2007; available from http://www.turbomole.com.

52 D. Marx, M. E. Tuckerman, J. Hutter and M. Parrinello, *Nature (London)*, 1999, **367**, 601.

53 C. J. D. von Grotthuss, *Annu. Chim*., 1806, **58**, 54.

54 N. B. Librovich, V. P. Sakun and N. D. Sokolov, *Chem. Phys.*, 1979, **39**, 351.

55 D. Xenides, B. R. Randolf and B. M. Rode, *J. Chem. Phys*., 2005, **122**, 174506.

56 G. C. Pimentel and A. L. McClellan, *The Hydrogen Bond*, W. H. Freeman, San Francisco, 1960.

57 P. B. Balbuena and J. M. Seminario, *Theoretical and Computational Chemistry 7, Molecular dynamics; from classical to quantum methods*, Elsevier, Amsterdam, 1999.

58 C. J. Cramer, *Essentials of Computational Chemistry: Theory and models*, John Wiley & Sons, Ltd, New York, 2002.

59 D. C. Young, *Computational Chemistry: A practical guide for applying techniques to real world problems,* Wiley Interscience, New York, 2001.

60 R. N. Barnett and U. Landman, *Phys. Rev*., 1993, **B48**, 2081.

61 X. Jing, N. Troullier, D. Dean, N. Binggeli, J. R. Chelikowsky, K. Wu and Y. Saad, *Phys. Rev*., 1994, **B50**, 122.

62 A. R. Leach, *Molecular Modelling: Principles and applications,* Longman, Edinburgh, 1996.

63 F. Fillaux, A. Cousson and M. Gutmann, *Pure Appl. Chem.*, 2007, **79**, 1023.

64 B. E. Conway, J. O. M. Bockris and H. Linton, *J. Chem. Phys*., 1956, **24**, 834.

65 K.D. Kreuer, *Solid State Ionics*, 2000, **136**, 149.

66 N. Agmon, *Chem. Phys. Lett.*, 1995**, 244**, 456.

67 P. A. Giguere, *J. Chem. Ed*., 1979, **56**, 571.

68 R. R. Sadeghi and H. –P. Cheng, *J. Chem. Phys.,* 1999, **111**, 2086.

69 P. Bopp, *Chem. Phys*., 1986, **106**, 205.

70 C. J. Montrose, J. A. Bucaro, J. Marshall-Coakley and T. A. Litovitz, *J. Chem. Phys*., 1974, **60**, 5025.

71 M. –C. Bellissent-Funel and J. Teixeira, *J. Mol. Struct*., 1991, **250**, 213.

72 M. P. Allen and D. J. Tildesley, *Computer Simulation of Liquids*, Oxford University Press, New York, 1987.

73 J. M. Haile, *Molecular Dynamics Simulations*, John Wiley & Sons Ltd, New York, 1997.

74 D. C. Rapaport, The *Art of Molecular Dynamics Simulation*, Cambridge University Press, London, 1995.

75 P. A. Stockman, G. A. Shukla, *J. Am. Chem. Soc*., 1982, **104**, 5314.

76 J. Crooks, A. J. Stace and B. J. Whitaker, *J. Phys. Chem*., 1988, **92**, 3554.

77 K. Sagarik and C. Lao-ngam, *submitted.*

78 L. Ojamäe, I. Shavitt and J. Singer, *Int. J. Quant. Chem. Quant. Chem. Symp*. 1995, **29**, 657.

79 J. M. Headrich, E. G. Diken, R. S. Walters, N. I. Hammer, R. A. Christie, J. Cui, V. M. Myshakin, M. A. Johnson and K. D. Jordan, *Science,* 2005*,* **308**, 1765.

80 G. Guevara-Carrion, C. Nieto-Draghi, J. Vrabec and H. Hasse, *J. Phys. Chem. B*, 2008, **112**, 16664.

Figure 1 Refined equilibrium structures, interaction energies (ΔE) and asymmetric stretching coordinates (Δd_{DA}) of the $CH_3OH - H_2O$, $CH_3OH - H_3O^+$ and $CH_3OH - H_3O^+ - H_2O$ complexes, obtained from B3LYP/TZVP geometry optimizations. H-bond distances are in Å and energies in kJ/mol. The values in parentheses are the results in continuum aqueous solution.

a) - b) $CH_3OH - H_2O$ complexes.

c) $CH_3OH - H_3O^+$ complex.

d) - e) $CH_3OH - H_3O^+ - H_2O$ 1 : 1 : 1 complexes.

f) - g) $CH_3OH - H_3O^+ - H_2O$ 1 : 1 : 2 complexes.

h) - j) $CH_3OH - H_3O^+ - H_2O$ 1 : 1 : 3 complexes.

Figure 2 Asymmetric O-H stretching frequencies (ν^{OH}) of the H-bond protons in the $CH_3OH - H_2O$, $CH_3OH - H_3O^+$ and $CH_3OH - H_3O^+ - H_2O$ complexes, obtained from B3LYP/TZVP calculations. The values in parentheses are the results in continuum aqueous solution. $\Delta\nu^{OH}$ are the frequency shift in continuum aqueous solution. ν^{OH} and $\Delta\nu^{OH}$ are in cm^{-1}.

a) - b) $CH_3OH - H_2O$ complexes.

c) $CH_3OH - H_3O^+$ complex.

d) - e) $CH_3OH - H_3O^+ - H_2O$ 1 : 1 : 1 complexes.

f) - g) $CH_3OH - H_3O^+ - H_2O$ 1 : 1 : 2 complexes.

h) - j) $CH_3OH - H_3O^+ - H_2O$ 1 : 1 : 3 complexes.

Figure 3 a) Plot of asymmetric stretching coordinates (Δd_{DA}) and O-H..O H-bond distances ($R_{O\text{-}O}$), obtained from B3LYP/TZVP calculations.

b) Plot of asymmetric O-H stretching frequencies (ν^{OH}) and O-H..O H-bond distances ($R_{O\text{-}O}$), obtained from B3LYP/TZVP calculations.

c) Plot of average asymmetric stretching coordinates ($< \Delta d_{DA} >$) and average O-H..O H-bond distances ($< R_{O\text{-}O} >$) obtained from BOMD simulations at 350 K.

Figure 4 Symmetric and asymmetric O-H stretching frequencies of the H-bond protons in the $H_5O_2^+$, $CH_3OH - H_3O^+$ and $CH_3OH - H_3O^+ - H_2O$ complexes, together with the O-O stretching frequencies, obtained from BOMD simulations at 350 K.

a) $H_5O_2^+$ in the gas phase.

b) $H_5O_2^+$ in continuum aqueous solution.

c) $CH_3OH - H_3O^+$ in the gas phase.

d) $CH_3OH - H_3O^+$ in continuum aqueous solution.

e) $CH_3OH - H_3O^+ - H_2O$ 1 : 1 : 1 complex in the gas phase (H-bond **(1)**).

f) $CH_3OH - H_3O^+ - H_2O$ 1 : 1 : 1 complex in continuum aqueous solution (H-bond **(1)**).

g) $CH_3OH - H_3O^+ - H_2O$ 1 : 1 : 1 complex in the gas phase (H-bond **(2)**).

h) $CH_3OH - H_3O^+ - H_2O$ 1 : 1 : 1 complex in continuum aqueous solution (H-bond **(2)**).

i) Definitions of the symmetric and asymmetric O-H stretching modes, as well as the O-O vibration.

Figure 5 Elementary reactions consisting of quasi-dynamic equilibriums for the interconversion between the formation and cleavage of the H-bonds linking the transition state complex and water molecules in the second hydration shells. The transition state complex is inside the boundary line.

a) The excess proton transferring in a linear H-bond structure.

b) The excess proton transferring in a fully hydrated transition state complex.

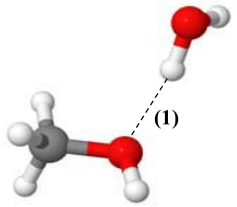

a) ΔE = -26.0 (-73.4)

(1) O..O = 2.86 (2.80)
O-H = 0.97 (0.97)
Δd_{DA} = 0.93 (0.84)

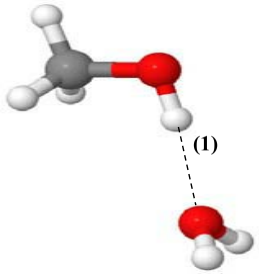

b) ΔE = -24.2 (-72.8)

(1) O..O = 2.90 (2.81)
O-H = 0.97 (0.98)
Δd_{DA} = 0.96 (0.86)

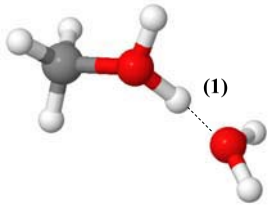

c) ΔE = -124.5 (-128.4)

(1) O..O = 2.46 (2.43)
O-H = 1.07 (1.10)
Δd_{DA} = 0.32 (0.24)

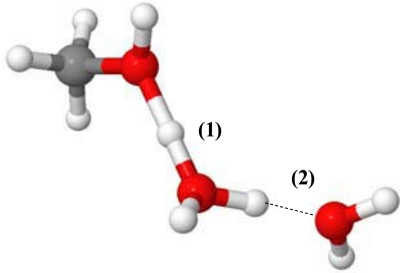

d) ΔE = -278.5 (-479.2)

(1) O..O = 2.42 (2.47)
O-H = 1.32 (1.07)
Δd_{DA} = 0.22 (0.33)

(2) O..O = 2.53 (2.51)
O-H = 1.00 (1.04)
Δd_{DA} = 0.50 (0.42)

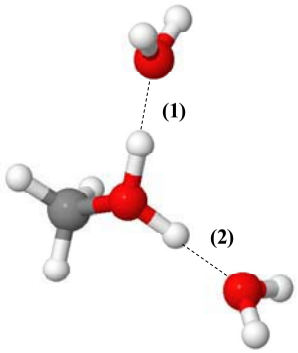

e) ΔE = -226.9 (-479.8)

(1) O..O = 2.54 (2.52)
O-H = 1.02 (1.03)
Δd_{DA} = 0.49 (0.46)

(2) O..O = 2.54 (2.51)
O-H = 1.02 (1.04)
Δd_{DA} = 0.49 (0.45)

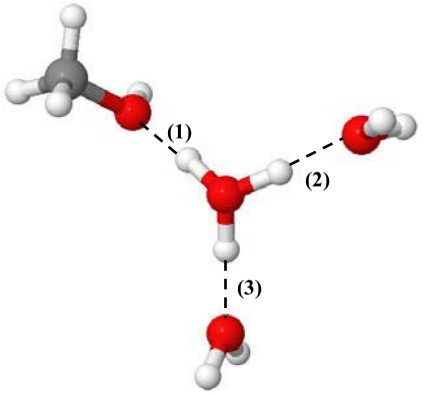

f) ΔE = -361.6 (-194.9)

(1) O..O = 2.50 (2.52)
O-H = 1.04 (1.03)
Δd_{DA} = 0.43 (0.46)

(2) O..O = 2.57 (2.55)
O-H = 1.01 (1.02)
Δd_{DA} = 0.56 (0.51)

(3) O..O = 2.57 (2.55)
O-H = 1.01 (1.03)
Δd_{DA} = 0.55 (0.50)

Figure 1/1

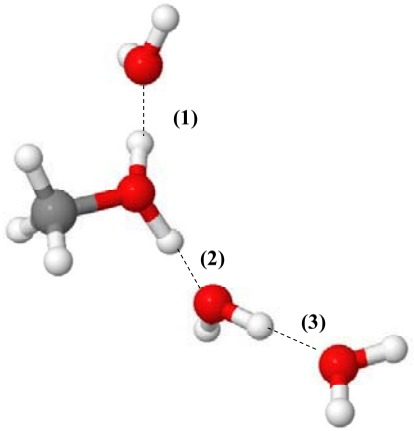

g) ΔE = -295.1 (-532.7)

(1) O..O = 2.57 (2.53)
O-H = 1.01 (1.03)
Δd_{DA} = 0.55 (0.47)

(2) O..O = 2.45 (2.46)
O-H = 1.07 (1.06)
Δd_{DA} = 0.31 (0.35)

(3) O..O = 2.65 (2.70)
O-H = 0.99 (0.99)
Δd_{DA} = 0.66 (0.74)

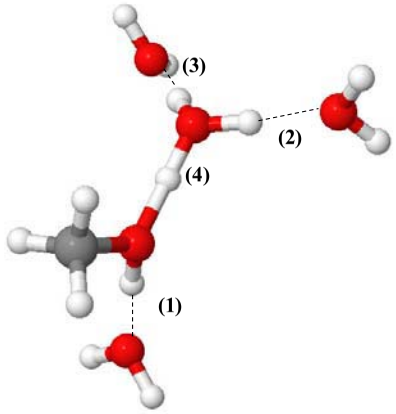

h) ΔE = -422.4 (-658.5)

(1) O..O = 2.69 (2.68)
O-H = 0.99 (0.99)
Δd_{DA} = 0.71 (0.70)

(2) O..O = 2.62 (2.57)
O-H = 1.00 (1.02)
Δd_{DA} = 0.62 (0.54)

(3) O..O = 2.62 (2.57)
O-H = 1.00 (1.02)
Δd_{DA} = 0.62 (0.53)

(4) O..O = 2.42 (2.48)
O-H = 1.10 (1.06)
Δd_{DA} = 0.23 (0.36)

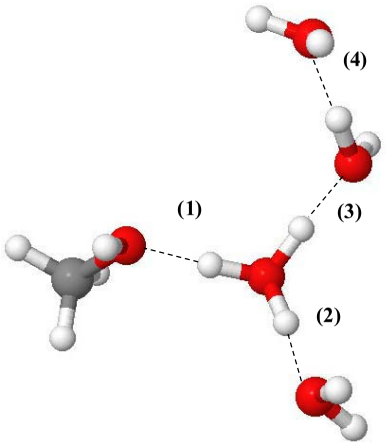

i) ΔE = -419.5 (-658.2)

(1) O..O = 2.55 (2.55)
O-H = 1.02 (1.03)
Δd_{DA} = 0.51 (0.49)

(2) O..O = 2.61 (2.57)
O-H = 1.00 (1.02)
Δd_{DA} = 0.61 (0.53)

(3) O..O = 2.50 (2.50)
O-H = 1.05 (1.05)
Δd_{DA} = 0.40 (0.41)

(4) O..O = 2.69 (2.69)
O-H = 0.99 (0.99)
Δd_{DA} = 0.71 (0.71)

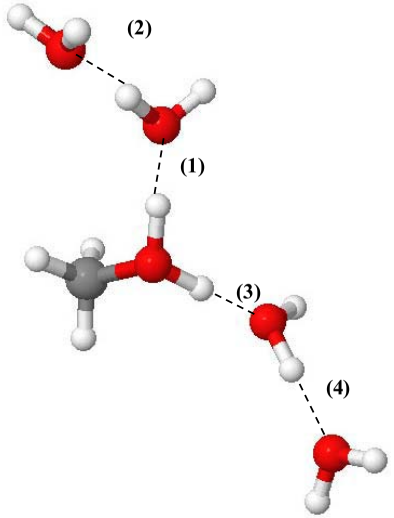

j) ΔE = -356.5 (-538.6)

(1) O..O = 2.49 (2.51)
O-H = 1.04 (1.04)
Δd_{DA} = 0.41 (0.43)

(2) O..O = 2.68 (2.76)
O-H = 0.99 (0.98)
Δd_{DA} = 0.70 (0.80)

(3) O..O = 2.49 (2.50)
O-H = 1.04 (1.04)
Δd_{DA} = 0.41 (0.43)

(4) O..O = 2.68 (2.72)
O-H = 0.99 (0.99)
Δd_{DA} = 0.70 (0.74)

Figure 1/2

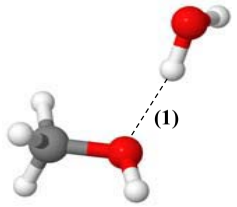

a)

(1) ν^{OH} = 3510.1 (3513.3)

$\Delta\nu^{OH}$ = 3.2

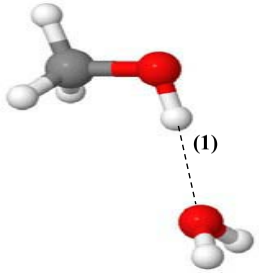

b)

(1) ν^{OH} = 3547.7 (3401.1)

$\Delta\nu^{OH}$ = -146.6

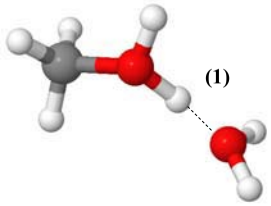

c)

(1) ν^{OH} = 2086.1 (1689.8)

$\Delta\nu^{OH}$ = -369.3

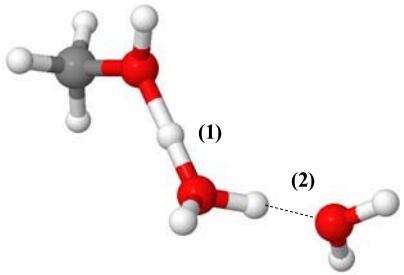

d)

(1) ν^{OH} = 1778.2 (1911.4)

$\Delta\nu^{OH}$ = 133.2

(2) ν^{OH} = 2629.9 (2311.8)

$\Delta\nu^{OH}$ = -318.1

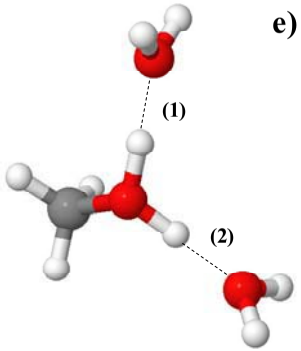

e)

(1) ν^{OH} = 2627.9 (2277.2)

$\Delta\nu^{OH}$ = -350.7

(2) ν^{OH} = 2627.9 (2277.2)

$\Delta\nu^{OH}$ = -350.7

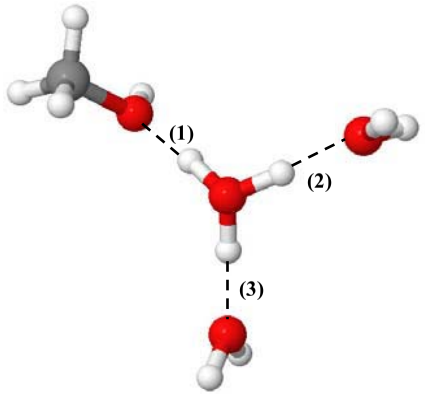

f)

(1) ν^{OH} = 2452.6 (2401.2)

$\Delta\nu^{OH}$ = -51.4

(2) ν^{OH} = 2848.3 (2528.4)

$\Delta\nu^{OH}$ = -319.9

(3) ν^{OH} = 2848.3 (2528.4)

$\Delta\nu^{OH}$ = -319.9

Figure 2/1

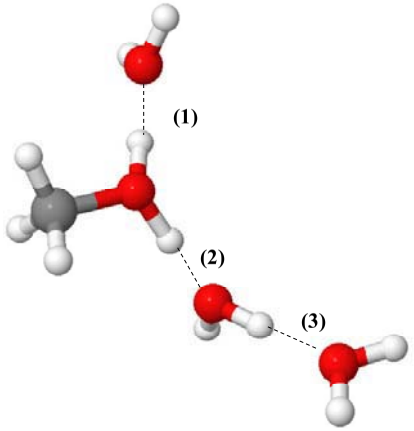

g)

(1) ν^{OH} = 2879.8 (2557.9)
$\Delta\nu^{OH}$ = -321.9

(2) ν^{OH} = 2054.3 (1831.1)
$\Delta\nu^{OH}$ = -223.2

(3) ν^{OH} = 3148.7 (3049.6)
$\Delta\nu^{OH}$ = -99.1

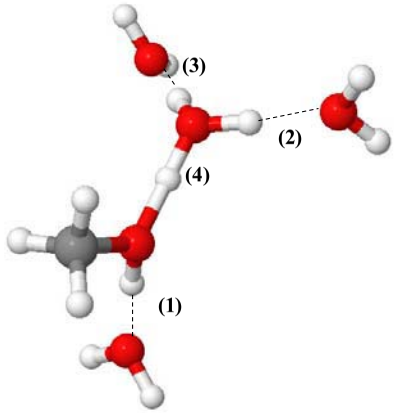

h)

(1) ν^{OH} = 3262.4 (3151.8)
$\Delta\nu^{OH}$ = -110.6

(2) ν^{OH} = 3038.9 (2643.0)
$\Delta\nu^{OH}$ = -395.9

(3) ν^{OH} = 3038.9 (2643.0)
$\Delta\nu^{OH}$ = -395.9

(4) ν^{OH} = 1793.3 (2028.6)
$\Delta\nu^{OH}$ = 235.3

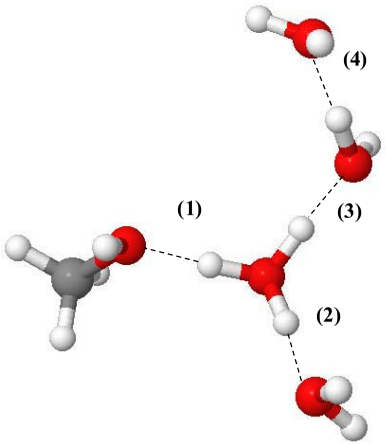

i)

(1) ν^{OH} = 2694.0 (2544.5)
$\Delta\nu^{OH}$ = -149.5

(2) ν^{OH} = 2996.9 (2544.5)
$\Delta\nu^{OH}$ = -452.4

(3) ν^{OH} = 2359.4 (2214.7)
$\Delta\nu^{OH}$ = -144.3

(4) ν^{OH} = 3258.7 (3157.3)
$\Delta\nu^{OH}$ = -101.4

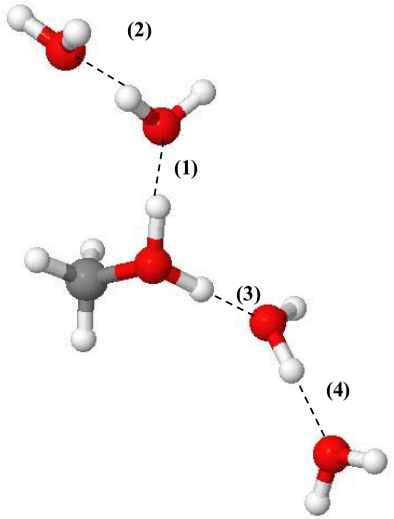

j)

(1) ν^{OH} = 2287.2 (2005.3)
$\Delta\nu^{OH}$ = -281.9

(2) ν^{OH} = 3223.8 (3230.2)
$\Delta\nu^{OH}$ = 6.4

(3) ν^{OH} = 2287.2 (2005.3)
$\Delta\nu^{OH}$ = -281.9

(4) ν^{OH} = 3223.8 (3098.5)
$\Delta\nu^{OH}$ = -125.3

Figure 2/2

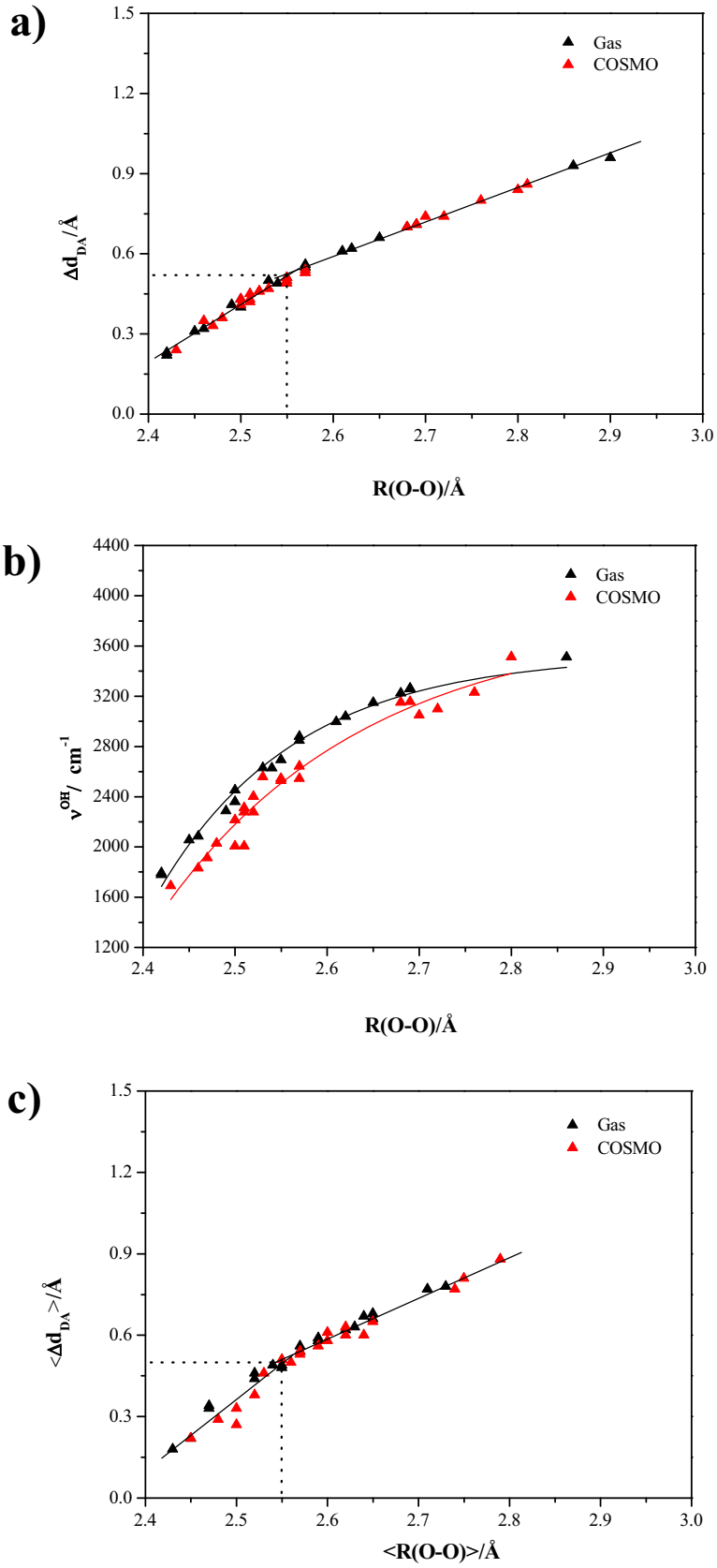
a)
Gas
COSMO
Δd_{DA}/Å
R(O-O)/Å
b)
Gas
COSMO
ν^{OH}/ cm^{-1}
R(O-O)/Å
c)
Gas
COSMO
<Δd_{DA}>/Å
<R(O-O)>/Å

Figure 3

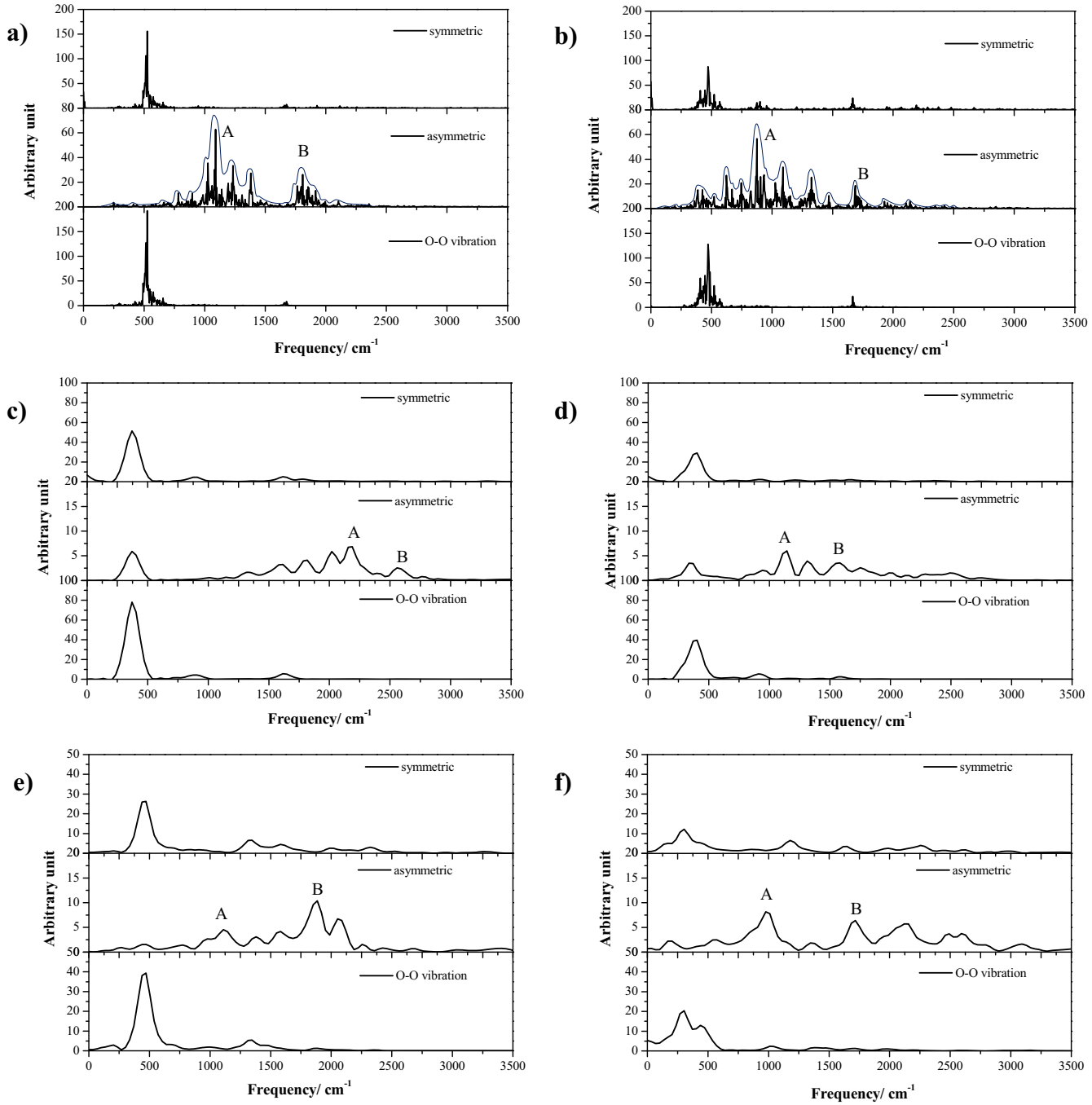
a)
b)
c)
d)
e)
f)
symmetric
asymmetric
O-O vibration
A
B
Arbitrary unit
Frequency/ cm-1

Figure 4/1

g)

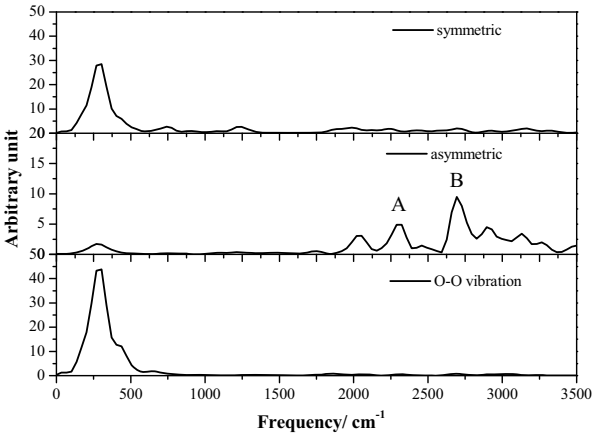

h)

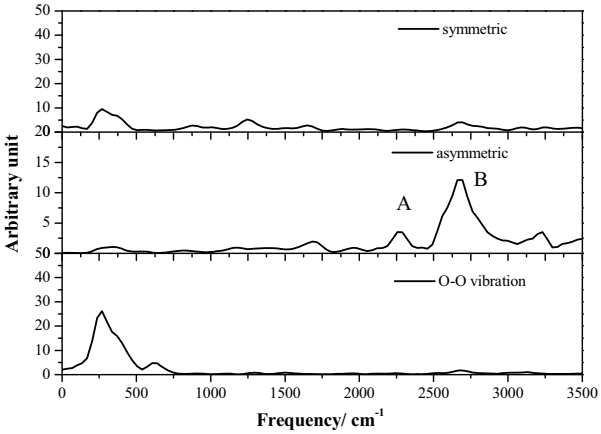

i)

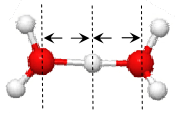

Symmetric O-H stretching

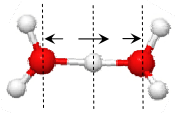

Asymmetric O-H stretching

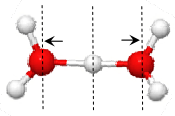

O-O vibration

Figure 4/2

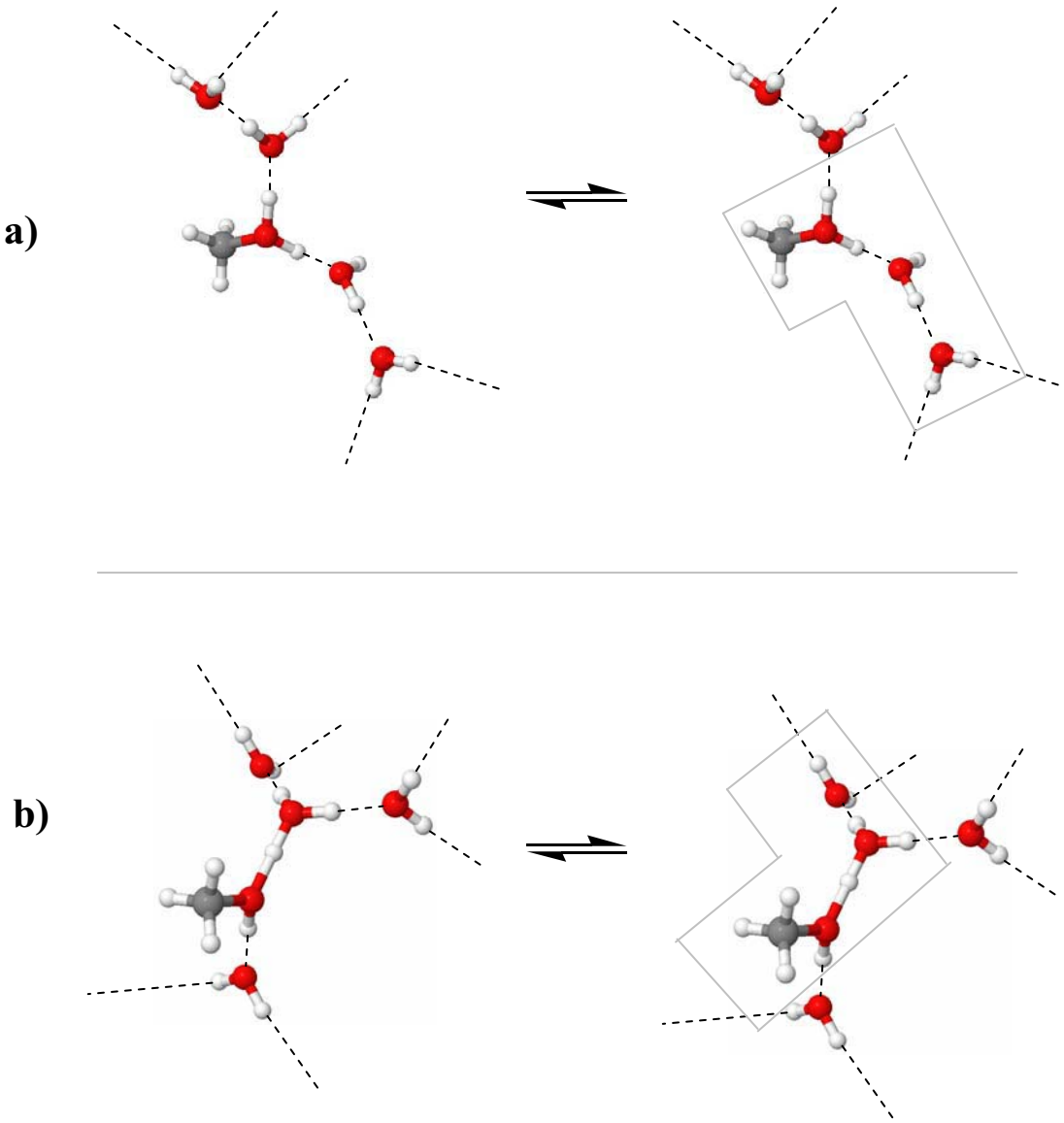

Figure 5

Table 1 Average H-bond distances ($< R_{O-O} >$), average asymmetric stretching coordinates ($< \Delta d_{DA} >$) and characteristic asymmetric O-H stretching frequencies (ν^{OH}) of the active protons in the transition state complexes. I_A/I_{O-O} are the relative probabilities of proton transfer in the course of BOMD simulations. Distances and ν^{OH} are in Å and cm^{-1}, respectively.

		$< R_{O-O} >$	$< \Delta d_{DA} >$	ν^{OH} A	ν^{OH} B	I_A/I_{O-O}
c) 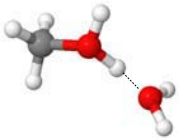	Gas	2.47	0.34	2178.9	2558.8	0.09
	COSMO	2.45	0.22	1138.9	1582.4	0.15
d) 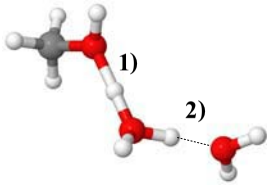	Gas	1) 2.43 2) 2.57	0.18 0.54	1115.5 2305.3	1874.5 2695.7	0.11 0.11
	COSMO	1) 2.50 2) 2.57	0.33 0.54	977.7 2265.7	1716.9 2680.1	0.41 0.13
g) 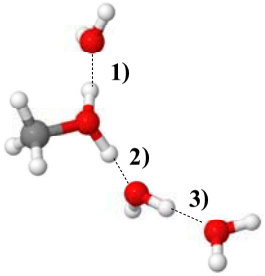	Gas	1) 2.59 2) 2.47 3) 2.71	0.59 0.33 0.77	- 1313.5 -	- 1613.2 -	- 0.03 -
	COSMO	1) 2.60 2) 2.48 3) 2.75	0.58 0.29 0.81	- 935.0 -	- 1590.8 -	- 0.08 -

		$< R_{O-O} >$	$< \Delta d_{DA} >$	ν^{OH} A	ν^{OH} B	I_A/I_{O-O}
h) 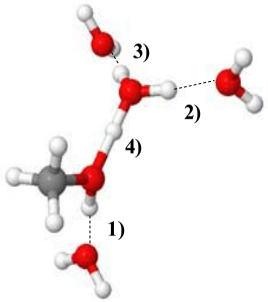	Gas	1) 2.73 2) 2.65 3) 2.65 4) 2.45	0.78 0.68 0.66 0.22	- - - 911.0	- - - 1511.3	- - - 0.08
	COSMO	1) 2.74 2) 2.65 3) 2.65 4) 2.50	0.77 0.65 0.65 0.27	- - - 979.7	- - - 1590.5	- - - 0.05

Proton transfer reactions and dynamics in protonated water clusters

K. Sagarik, C. Lao-ngam, P. Asawakun and S. Wannarat, *submitted*.

Proton transfer reactions and dynamics in protonated water clusters

by

Kritsana Sagarik*
Charoensak Lao-ngam
School of Chemistry

Prapasri Asawakun
School of Mathematics
Institute of Science
Suranaree University of Technology
Nakhon Ratchasima 30000
Thailand

and

Sornthep Wannarat
National Electronics and Computer Technology Center (NECTEC)
National Science and Technology Development Agency (NSTDA)
Pathumthani 12120
Thailand

*corresponding author: kritsana@sut.ac.th
Tel./Fax: (6644) 224635
keywords: protonated water clusters, BOMD simulations, proton transfer, vibrational spectra

Abstract

Proton transfer reactions and dynamics were theoretically studied using the hydrogen-bond (H-bond) complexes formed from H_3O^+ and nH_2O, n = 1 – 4, as model systems. The investigations began with searching for characteristics of transferring protons in the gas phase and continuum aqueous solution using DFT method at the B3LYP/TZVP level, followed by Born-Oppenheimer molecular dynamics (BOMD) simulations at 350 K. B3LYP/TZVP calculations revealed the threshold asymmetric O-H stretching frequencies (ν^{OH*}) for the proton transfers in the Zundel complex ($H_5O_2^+$) in the gas phase and continuum aqueous solution at 2004 and 1853 cm^{-1}, respectively. BOMD simulations suggested slightly higher threshold frequencies ($\nu^{OH,MD*}$= 2130 and 2053 cm^{-1}, respectively), with two characteristic $\nu^{OH,MD}$ being the IR spectral signatures of the transferring protons; the lower-frequency band could be associated with the "oscillatory shuttling motion" and the higher-frequency band with the "structural diffusion motion". These could be regarded as the spectroscopic evidences for the shared-proton complex and product (or precursor) formations, respectively. Since the quasi-dynamic equilibrium between the Zundel and Eigen complexes was suggested to be the rate-determining step, in order to achieve an "ideal" maximum efficiency of proton transfer, a concerted reaction pathway should be taken. The most effective interconversion between the two proton states, the Zundel-like and hydronium-like structures, could be reflected from comparable intensities of the oscillatory shuttling and structural diffusion bands. The present results iterated the previous conclusions that static proton transfer potentials cannot provide complete description of the structural diffusion process and it is essential to incorporate thermal energy fluctuations and dynamics in the model calculations.

Introduction

Proton transfer reactions have been of interest especially in connection with the understanding of elementary reactions in electrochemical and biological systems.[1-3] Although some theoretical and experimental information has been accumulated in the past decades,[4-7] precise mechanisms of proton transfer reactions in liquids and solids are still not completely known. Because some basic chemistry of proton transfer processes has been discussed in details in many review articles,[4-5, 7] only the theoretical and experimental information pertinent to the present work will be briefly summarized.

According to experimental and theoretical studies,[8-9] there are three basic structures involved in proton transfer reactions in aqueous solution namely, the hydronium ion (H_3O^+), the Eigen complex ($H_9O_4^+$) and the dihydrated cation known as the Zundel ($H_5O_2^+$) complex. The latter is represented by an excess proton equally shared between two neutral water molecules. Various concepts have been proposed to explain the unusually high mobility of proton in aqueous solution.[5, 8-11] Apart from the diffusion of hydrated proton through the so called "vehicle mechanism", by which protons bound with a fraction of water molecules travel through the electrolyte via mutual diffusion, Eigen and DeMaeyer[11] demonstrated that the "structural diffusion", the diffusion of the H-bond structure in which an excess proton is shuttling back and forth, represents an important elementary reaction in the proton transfer processes.

There has been a controversy as to whether the species containing an excess proton could be described as $H_9O_4^+$ or $H_5O_2^+$.[5] The controversy was partly resolved by Tuckerman *et al*.[12-13] According to the results of *ab initio* molecular dynamics (MD) simulations, a single proton in H-bond network, regarded as "proton defect", could belong to either $H_5O_2^+$ or $H_9O_4^+$, with the center of the area having the excess proton coinciding with the center of symmetry of the H-bond structure. It was demonstrated that, changes in these H-bond structures and those in the vicinities through the H-bond breaking and forming processes displace the center of symmetry in space and also the center of the excess

charge.[12-13] In this way, $H_5O_2^+$ can be converted to $H_9O_4^+$ and, therefore, regarded as structural diffusion. The proposed mechanism for the diffusion of an excess proton in water was supported by Agmon,[10] based on the interpretation of NMR data.

One of the most powerful experimental techniques in H-bond research is vibrational spectroscopy. The most evident effects of H-bond formations in aqueous solution are the red shift of the high-frequency hydroxyl (O-H) stretching mode, accompanied by its intensity increase and band broadening.[14-16] The broad and intense IR absorption bands ranging from 1000 to 3000 cm^{-1} were interpreted as spectral signatures of protonated water networks.[17] The correlation between the O-H stretching frequency and the probability of proton transfer in H-bond has been discussed in details;[16-18] the probability of proton transfer could be related to a strong red shift of the asymmetric O-H stretching frequency (ν^{OH}), compared to the corresponding "free" or "non-H-bonded" one.[16] The red shift cannot be detected easily in experiment due to the coupling and overlapping of various vibrational modes, as well as the detection limit of IR equipment;[19-21] whereas, the harmonic approximation employed in conventional *ab initio* calculations is inadequate to predict accurately the asymmetric O-H stretching frequency of the active proton in $H_5O_2^+$.[20, 22]

Theories [23] and experiments[19, 24] indicated that the IR spectra of protonated water clusters in the gas phase and aqueous solution could be divided into three distinct regions. Born-Oppenheimer molecular dynamics (BOMD) simulations at 225 and 360 K[23] suggested that the vibrational frequencies above 3000 cm^{-1} are associated with the symmetric and asymmetric O-H stretching modes of individual water molecules, whereas those between 1000 and 2000 cm^{-1} are the characteristic vibrational frequencies of the transferring protons.[25] The IR multiple photon dissociation (IRMPD) spectra of $H_5O_2^+$ were measured in the gas-phase,[22, 24] from which two different possible assignments of the observed IR bands were discussed. The IRMPD spectra showed a characteristic asymmetric O-H stretching frequency at 990 cm^{-1}, in good agreement with B3LYP/6-31+G** calculations with harmonic approximation.[24]

In our previous work, proton transfer reactions in the H-bond complexes formed from methanol (CH_3OH), H_3O^+ and H_2O,[26] as well as from triflic acid (CF_3SO_3H), H_3O^+ and H_2O,[27] were studied using theoretical methods. For the most basic unit in aqueous solution, the $H_3O^+ - H_2O$ complexes, BOMD simulations revealed that a quasi-dynamic equilibrium is established between the Eigen and Zundel complexes and considered to be the most important elementary reaction in proton transfer process.[27] It was demonstrated that proton transfer reactions are not concerted due to the thermal energy fluctuations and dynamics. The BOMD results and IR spectra of the transferring protons also revealed that, the proton transfer processes in the protonated CH_3OH-H_2O clusters involve the CH_3OH-H_3O^+-H_2O 1 : 1 : 1 complex as the most effective mediator;[26] whereas for the protonated CF_3SO_3H-H_2O clusters, the -SO_3H group could be directly and indirectly involved in proton transfer reactions, through the formation of proton defects, as well as $-SO_3^-$ and $-SO_3H_2^+$.[26] It was concluded that, due to the coupling among various modes of vibrations, the discussions on proton transfer reactions cannot be made based only on static proton transfer potentials.[26-27]

In order to obtain additional information on characteristics of proton transfers in the gas phase and aqueous solution, structures, energetic and dynamics in small protonated water clusters were studied using theoretical methods. The investigations began with searching for the equilibrium structures of the protonated water clusters which could be important in proton transfer pathways using pair potentials. The computed equilibrium structures were refined using density functional theory (DFT) method, and employed as starting configurations in BOMD simulations at 350 K. As proton transfer reactions are governed by various modes of vibrations, IR spectra of the H-bond protons susceptible to proton transfers were computed from DFT calculations and BOMD simulations. The characteristic IR frequencies and dynamics of the transferring protons, obtained from BOMD simulations, were analyzed, discussed and compared with available theoretical and experimental data.

Computational Methods

Our experience[26-27] revealed that elementary reactions and dynamics of proton transfer in H-bond could be studied reasonably well by taking the following three basic steps namely; (1) searching for the H-bond structures which could be mediators in the dynamic proton transfer pathways using pair potentials; (2) refining the computed structures using an accurate quantum chemical method; (3) BOMD simulations using the refined structures as the starting configurations. These basic steps were adopted in the present work to investigate proton transfer reactions in the protonated water clusters.

Since proton transfer reactions involve formation and cleavage of covalent bonds, inclusion of too many water molecules in the model systems could lead to difficulties in the analyses of the elementary reactions and dynamics.[20, 26-27] It was, therefore, the strategy of the previous[26-27] and present works to restrict the number of water molecules to not more than four; according to a neutron diffraction experiment with hydrogen isotope substitutions and Monte Carlo (MC) simulations,[8] the first hydration shell of H_3O^+ consists of four water molecules and only three of them strongly H-bond to the hydrogen atoms of H_3O^+. As the electric field introduced by polar solvent could determine the potential energy surface, on which the transferring proton in H-bond moves,[26, 28-31] a continuum solvent model had to be included in the model calculations. To approximate the solvent effects, a conductor-like screening model (COSMO) was proved to be applicable on similar H-bond systems.[26, 32] Therefore, to partially account for the effects of the extended H-bond networks of water, COSMO with the dielectric constant (ε) of 78 was employed in the present quantum chemical calculations and BOMD simulations.

Static calculations

Equilibrium structures and asymmetric stretching coordinates

In the present investigation, attention was focused on the H-bond structures which could be involved in proton transfer processes. The T-model potentials for H_3O^+ and H_2O were taken from ref. 26 and employed in the calculations of the equilibrium structures of the $H_3O^+ \cdot nH_2O$ complexes, n = 1- 4. Because the T-model had been discussed in details in the previous studies,[33-41] only some important aspects relevant to the geometry optimizations will be briefly summarized using the Eigen complex as an example. The experimental geometries[42] of H_3O^+ and H_2O were kept constant in the T-model geometry optimizations. For the Eigen complex, a rigid H_3O^+ was placed at the origin of the Cartesian coordinate system. The coordinates of H_2O molecules were randomly generated in the vicinities of H_3O^+. Based on the T-model potentials, equilibrium structures of the Eigen complex were searched using a minimization technique. Fifty configurations were generated randomly and employed as starting configurations in the T-model geometry optimizations.

Because the T-model is based on rigid molecules, in which the cooperative effects are neglected, further structural refinements had to be made using an appropriate quantum chemical method. Literature survey showed that, DFT methods have been frequently chosen due to the ability to treat molecules of relatively large sizes with reasonable accuracies compared to other nonempirical methods.[43-47] Especially in the present case, calculations of IR spectra and BOMD simulations with thousands of timesteps had to be made, it was necessary to compromise between the accuracy of theoretical methods and available computer resources. In order to achieve all the objectives, DFT calculations were made using the B3LYP hybrid functional,[48-49] with the triple-zeta valence basis sets augmented by polarization functions (TZVP). The TZVP basis sets were developed and tested by Ahlrichs and coworkers.[50] The applicability of the TZVP basis sets in DFT calculations on structures and IR spectra was discussed.[51] It was concluded that the TZVP

basis sets are sufficient for the systems with and without occupied d-states, and could be applied well in the calculations of equilibrium structures and interaction energies, as well as IR spectra, of such systems.[51] The applicability of B3LYP calculations on protonated water clusters was also analyzed and discussed in details.[20]

In the present work, all quantum chemical calculations were made using TURBOMOLE 6.0.[52-53] The absolute and local minimum energy geometries of the protonated water clusters obtained from the T-model potentials were employed as starting configurations in the B3LYP/TZVP geometry optimizations. In order to ensure that the optimized structures were at the stationary points and to obtain reasonable IR frequencies, a tight SCF energy convergence criterion (less than 10^{-8} au), with the maximum norm of Cartesian gradients less than 10^{-4} au, was employed in the B3LYP/TZVP geometry optimizations.

The interaction energies (ΔE) of the optimized structures were computed as $\Delta E = E(H_3O^+ - nH_2O) - [E(H_3O^+) + nE(H_2O)]$; $E(H_3O^+ - nH_2O)$ is the total energy of the optimized structures of the H_3O^+ - nH_2O complexes; $E(H_3O^+)$ and $E(H_2O)$ are the total energies of the isolated H_3O^+ and H_2O at their optimized structures, respectively. The energetic effects due to the continuum aqueous solvent (COSMO with ε = 78) were estimated from the solvation energy (ΔE^{sol}), approximated as $\Delta E^{sol} = E(H_3O^+ - nH_2O)^{COSMO} - E(H_3O^+ - nH_2O)$; $E(H_3O^+ - nH_2O)^{COSMO}$ and $E(H_3O^+ - nH_2O)$ are the total energies of the optimized structures, obtained from B3LYP/TZVP calculations with and without COSMO, respectively. The interaction energies between the central charged species and the surrounding water molecules (ΔE^X, X = H_3O^+ or $H_5O_2^+$) were computed with and without the continuum aqueous solvent as $\Delta E^X = E(X - nH_2O) - [E(X) + E(nH_2O)]$; $E(X - nH_2O)$ is the total energy of the optimized structures; $E(X)$ and $E(nH_2O)$ are the total energies obtained by removing water molecules and the central charged species from the optimized structures, respectively. In order to test the reliability of the energetic results obtained from

B3LYP/TZVP calculations, the basis set superposition errors (BSSE) were estimated for ΔE^X using the counterpoise correction.[54]

Attempt was made to anticipate the tendency of proton transfer in H-bond using the asymmetric stretching coordinate (Δd_{DA}),[26, 55] for which a concept of the "most active" H-bond[56] was employed in the discussion of the Grotthuss mechanism. Within the framework of the most active H-bond, Δd_{DA} of a H-bond donor (D) - acceptor (A) pair is defined by $\Delta d_{DA} = d_{A\text{-}H} - d_{B..H}$; where $d_{A\text{-}H}$ and $d_{B..H}$ are the A-H and B..H distances in the A-H..B H-bond, respectively. The H-bond with small Δd_{DA} is considered to be susceptible to proton transfer;[26] "active" with respect to proton transfer when $\Delta d_{DA} < 0.1$ Å, and "inactive" when $\Delta d_{DA} > 0.4$ Å.[57]

Infrared spectra and normal mode analyses

Because the theoretical results on the IR spectra of the $CH_3OH\text{-}H_3O^+ - H_2O$ complexes[26] revealed interesting correlations between the asymmetric O-H stretching frequencies (ν^{OH}) and the H-bond distances ($R_{O\text{-}O}$), ν^{OH} of the H-bond protons in the protonated water clusters were investigated in more details. Using the optimized H-bond structures obtained in the previous subsection, harmonic IR frequencies were computed from the numerical second derivatives of the B3LYP/TZVP total energies. The calculations of the second derivatives and the analyses of the normal modes in terms of internal coordinates were performed using NUMFORCE and AOFORCE programs, respectively. They were incorporated in TURBOMOLE 6.0 software package.[52-53] ν^{OH} derived from the static proton transfer potentials (B3LYP/TZVP calculations) were used to estimate the tendencies of proton transfers in the protonated water clusters.

It should be mentioned that the vibrational frequencies derived from quantum chemical calculations are in general larger than those from experiments. Therefore, a scaling factor which partially account for the anharmonicities and systematic errors is required. Although in the present study, only the changes in the O-H stretching frequencies due to

different H-bond environments were of interest, a scaling factor was used throughout; a scaling factor of 0.9614[58] was proved to be appropriate for B3LYP/TZVP calculations with comparable basis sets.[58-59]

Dynamic calculations

Born-Oppenheimer MD simulations

Dynamics of rapid covalent and H-bond formations and cleavages could be studied reasonably well using quantum MD simulations,[60] among which BOMD simulations have been widely used in recent years .[61-66] Within the framework of BOMD simulations, classical equations of motions of nuclei on the Born-Oppenheimer (BO) surfaces are integrated, whereas forces on nuclei are calculated in each MD step from quantum energy gradients, with the molecular orbitals (MO) updated by solving Schrödinger equations in the BO approximation; the nuclei thus undergo classical Newtonian dynamics on quantum potential hypersurface. BOMD simulations are therefore more accurate, as well as considerably CPU time consuming, compared to classical MD simulations, in which forces on nuclei are determined from predefined empirical or quantum pair potentials. It should be mentioned that, although the high mobility of excess proton was initially attributed to quantum mechanical (QM) tunneling,[67] the results of BOMD simulations[25] and conductivity measurements[68] indicated that mechanisms of proton transfers could be explained reasonably well without assuming the proton tunneling as an important pathway.

As proton transfers in aqueous solution involve dynamic processes with different timescales,[10, 42, 69] the complexity of proton transfer reactions could be reduced using various approaches. The observation that the actual proton transfer occurs in femtosecond (fs) timescale,[42] which is faster than solvent structure reorganization,[10] made it possible to perform BOMD simulations by focusing on short-lived phenomena taking place before the H-bond structure reorganization. The present BOMD simulations were performed with canonical (NVT) ensemble at 350 K, by applying a Nosé-Hoover chain thermostat

to each degree of freedom in the system. In order to ensure that all important dynamics in the gas phase and continuum aqueous solution (COSMO) were taken into account, the shared-proton complexes predicted in the previous subsection were used as the starting configurations. Since in aqueous solution, the rapid interconversion between the Zundel and Eigen complexes takes place within 100 fs (10^{-13} s),[69] the timestep used in solving dynamic equations was set to 0.24 fs. In each BOMD simulations, 2000 steps were devoted to equilibration, after which 10,000 steps to property calculations, corresponding to about 2.4 ps. All BOMD simulations were performed using FROG program included in TURBOMOLE 6.0[52-53]; the MD program employs the Leapfrog Verlet algorithm to turn the electronic potential energy gradients into new atomic positions and velocities.

Remarks should be made on the ensemble and simulation length chosen in the present study. The applicability and performance of NVE and NVT BOMD simulations on small H-bond chains were investigated and discussed in details.[70] For NVE BOMD simulations, it was demonstrated that the potential energy of the system decreases quite rapidly in the course of BOMD simulations. Once the proton stays at the center of the H-bond, the potential energy is at the lowest point and the proton is trapped in the minimum; no proton transfer can be observed in the later timesteps. Since NVE BOMD simulations are conducted at constant energy, a decrease in the potential energy is accompanied by an increase in the kinetic energy, as well as temperature, leading to the H-bond structure reorganization and fragmentation. For NVT BOMD simulations, the energy released during the proton transfer processes can be absorbed by the thermostat bath, allowing the H-bond structure and local temperature to be maintained for a longer time (2-5 ps), depending upon the size and the complexity of the H-bond structure. Thus, NVT BOMD simulations are more appropriate for the present investigations.

Additional comments should be made on BOMD simulations, in comparison with another theoretical method. In order to obtain a quantitative description of reaction path networks, special algorithms,[71] such as “discrete path sampling (DPS)” method, have been developed.[72] The DPS method is based on path sampling using information about

stationary points on the potential energy surface. Thermodynamics and dynamic properties (rate constants) could be computed from model density of state (*e.g.* employing classical pair potentials or databases of local minima and transition states). The method is therefore suitable for the reactions, in which the pathways consist of sequences of local minima and transition states. The DPS method can also be applied on the dynamic properties with large samples of minima, *e.g*. the rates of isomerization of water clusters.[72] One of the problems of the DPS method is the number of local minima on the potential energy surface which can grow exponentially with the system size. Since we focused attention on the motions of individual protons in small H-bond clusters, not many local energy minima and pathways had to be considered; the quasi-dynamic equilibriums between the two limiting structures, the Zundel and H_3O^+-H_2O complexes, in various H-bond environments are the most important issues, as they can determine the dynamic behaviors of proton transfers in aqueous solution. BOMD simulations are therefore the most appropriate choice in this case.

Infrared spectra and diffusion coefficients

Since proton transfer reactions in H-bonds are strongly coupled with various degrees of freedom, especially the O-O vibration ,[4, 23, 26] attention was focused on the symmetric and asymmetric O-H stretching modes, as well as the O-O vibrations. In the present work, the IR spectra of the transferring protons were computed from BOMD simulations by Fourier transformations of the velocity autocorrelation function (VACF).[73] This approach is appropriate as it allows the coupled vibrations to be distinguished, characterized and analyzed separately. Fourier transformations of VACF were made within a short time limit of 100 fs. This choice is justified by the observation that the average lifetime of the most important shared-proton complex, the Zundel complex, is about 100 fs.[12, 69] The diffusion coefficients (D) of the transferring protons were computed from BOMD simulations using the Einstein relation,[74-75] by which D were determined from the slopes of the mean-square displacements (MSD). Because the transferring proton is confined in a short H-bond distance, care must be exercised in selecting the time interval in which

MSD is computed.[76] Our previous[26] and present experience showed that, linear relationship between MSD and simulation time could be obtained when the time intervals are not larger than 0.5 ps.

Results and discussions

In this section, all important results are presented, with the emphasis on the H-bonds in the shared-proton complexes. The discussions are made primarily on the static results obtained from B3LYP/TZVP calculations, both in the gas phase and continuum aqueous solution. Then, the BOMD results are analyzed and discussed in comparison with the B3LYP/TZVP results, with special attentions on the relationships among the H-bond structures, characteristic IR frequencies and dynamics in connection with the mechanisms of proton transfer reactions.

Static results

Shared-proton complexes and infrared spectra of transferring protons

Equilibrium structures, interaction energies (ΔE and ΔE^X) and solvation energies (ΔE^{sol}) of the $H_3O^+ \cdot nH_2O$ complexes, n = 1 - 4, obtained from B3LYP/TZVP calculations are summarized in Table 1. The characteristic H-bond distances ($R_{O\text{-}O}$ and $R_{O\text{-}H}$), asymmetric stretching coordinates (Δd_{DA}) and asymmetric O-H stretching frequencies (ν^{OH}) of the transferring protons are included in Table 1. The trends of ΔE, ΔE^{sol} and ΔE^X with respect to the number of water molecules are compared in Fig. 1.

The equilibrium structures, ΔE and ΔE^X obtained from B3LYP/TZVP calculations agree in general with the results in literatures.[20, 24, 77-79] The Zundel complex with C_2 symmetry (structure **a** in Table 1) represents the absolute minimum energy geometry of the $H_3O^+ \cdot H_2O$ 1 : 1 complex, both in the gas phase and continuum aqueous solution. The equilibrium structure of the $H_3O^+ \cdot H_2O$ 1 : 2 complex (structure **b** in Table 1) consists

of two symmetric O-H..O H-bonds at H_3O^+, with R_{O-H} about 0.2 Å shorter than the Zundel complex. For the $H_3O^+ - H_2O$ 1 : 3 complex, three equilibrium structures were predicted by B3LYP/TZVP calculations (structures **c**, **d** and **e** in Table 1). With a complete water coordination at H_3O^+, ΔE of the Eigen complex (structure **c**) is about 13 kJ/mol more stable than the structures with the Zundel complex as the central charged species (structures **d** and **e**). Structures **f**, **g** and **h** are three important equilibrium structures of the $H_3O^+ - H_2O$ 1 : 4 complex. Having the Eigen complex as the central charged species, structure **g** in the gas phase is about 14 kJ/mol more stable than structures **f** and **h**, whereas in the continuum aqueous solvent (COSMO) structure **h** is about 2 kJ/mol more stable than structure **g**. The stabilization effects at the central charged species can be confirmed by the values of ΔE^X. It appeared that, for the same number of water coordinations, H_3O^+ can be more effectively stabilized by water molecules compared to the Zundel complex; as an example, ΔE^X of structure **b** in the gas phase is -290.7 kJ/mol, whereas those of structures **d** and **e** are -191.7 kJ/mol.

The environmental effects on the stabilities of charged H-bonds were investigated using *ab initio* SCRF (self-consistent reaction field) calculations at the Hartree-Fock level, from which the dependence of ΔE on a wide range of dielectric constant (ε) was established.[28] It was reported that small increases in ε from the gas-phase value ($\varepsilon = 1$) rapidly reduce the stabilities of the charged H-bonds. In the present work, although the equilibrium structures in the gas phase and continuum aqueous solution are almost the same, ΔE and ΔE^X are considerably higher (less negative) in continuum aqueous solution (see Fig. 1). The destabilization effects caused by the continuum aqueous solvent are in good agreement with ref. 28. Fig. 1 also illustrates the trends of ΔE, ΔE^X and ΔE^{sol} with respect to the number of water molecules. The trends of ΔE, as well as ΔE^X, in the gas phase and continuum aqueous solution are quite similar, with smaller variations in continuum aqueous solution. The solvent effects can be directly observed in Fig. 1a, in which ΔE^{sol} are not substantially different for structures **c** to **h**. This suggested that, when the number of water molecules is the same, the H-bonds inside the protonated water clusters experience comparable uniform electric field (COSMO), with the asymptotic ΔE

in continuum aqueous solution ≈ -149 kJ/mol and ΔE^{sol} ≈ -266 kJ/mol. Fig. 1b revealed that the trends of the interaction energies (ΔE^{X}) remain the same when the counterpoise corrections were applied; the BSSE contributes only about 3% of ΔE^{X}.

As concluded in the previous work,[26, 57] Δd_{DA} obtained from static proton transfer potentials could be used to measure the tendency of proton transfer, as well as the strength of H-bond. Based on the criteria in ref. 57 and Δd_{DA} in Table 1, The H-bonds in structures **a**, **d**, **e, f** and **h** are susceptible to proton transfers in the gas phase, with $0 \leq \Delta d_{DA} \leq 0.32$; whereas the continuum aqueous solvent (COSMO) destabilizes the protonated water clusters, resulting in shifts of the H-bond protons away from the centers, especially for structures **d**, **e** and **h**.

As reported in ref. 18, the H-bond distance ($R_{O\text{-}O}$) in concentrated HCl solution can be divided into three groups namely, the internal, external and solvation groups. The H-bonds linking directly to protons belong to the internal group, with $R_{O\text{-}O}$ in the range of 2.45 – 2.57 Å, whereas $R_{O\text{-}O}$ in the external and solvation groups are in the ranges of 2.60 – 2.70 Å and longer than 2.70 Å, respectively. Fig. 2a shows linear relationships between Δd_{DA} and $R_{O\text{-}O}$, with a separation between the internal and external H-bonds at $R_{O\text{-}O}$ ≈ 2.5 Å, in good agreement with ref. 18. The linear relationships for the internal and external H-bonds can be represented by eqn (1) and (2), respectively.

Internal H-bonds: $\Delta d_{DA} = 3.57 \times R_{O\text{-}O} - 8.50$ (1)

External H-bonds: $\Delta d_{DA} = 1.34 \times R_{O\text{-}O} - 2.90$ (2)

Theoretical and experimental results on vibrational spectra of the transferring proton in the Zundel complex were presented in the past decades,[17, 20, 22] from which the flatness of the potential energy surface was concluded by *ab initio* calculations at different levels to be the most outstanding feature of the H-bond proton.[20] For the Zundel complex in the gas phase ($\Delta d_{DA} = 0$), B3LYP/TZVP calculations predicted ν^{OH} = 961 cm^{-1}, whereas in

continuum aqueous solution ν^{OH} = 677 cm^{-1}. The former is in reasonable agreement with the theoretical results at the same levels of accuracy[24, 77] and IRMPD experiment.[24, 80]

Good agreement between theoretical and experimental data was also found for $H_7O_3^+$. In the gas phase, B3LYP/TZVP calculations predicted ν^{OH} = 2304 cm^{-1}, compared with B3LYP/T(O)DZP calculations of 2402 cm^{-1} [20] and experiment between 2200 and 2300 cm^{-1}.[81] These ν^{OH} could be associated with the H-bond protons in the $H_3O^+ - H_2O$ contact structure. For the larger protonated water clusters, the structures with the Zundel complex as the central charged species exhibit higher tendencies of proton transfers, with $1000 < \nu^{OH} < 1450$ cm^{-1}, whereas the structures with H_3O^+ as the central charged species possess $1900 < \nu^{OH} < 2760$ cm^{-1}.

Due to the asymptotic behavior at large $R_{O\text{-}O}$, the relationships between ν^{OH} and $R_{O\text{-}O}$ in Fig. 2b cannot be approximated by linear functions; at large $R_{O\text{-}O}$, ν^{OH} converges to the asymmetric O-H stretching frequency of the free or non-H-bonded proton in H_3O^+. After several trial fittings, an exponential function similar to the integrated rate expression for the first order reaction was found to be the most appropriate, with the asymptotic values in the gas phase and continuum aqueous solution fixed at ν^{OH} = 3568 and 3613 cm^{-1}, respectively. The agreements between ν^{OH} obtained from B3LYP/TZVP calculations and the fitted values are included in Fig. 2b. The fitted functions in the gas phase and continuum aqueous solution are given in eqn (3) and (4), respectively.

Gas phase: $$\nu^{OH} = -1.41\times10^{11} e^{-R_{O-O}/0.1345} + 3568 \quad (3)$$

Continuum aqueous solution: $$\nu^{OH} = -1.82\times10^{10} e^{-R_{O-O}/0.1533} + 3613 \quad (4)$$

Attempt has been made to distinguish between normal and strong H-bonds, however without a concrete result. It was found in general that, when H-bond is shorter, it becomes stronger, with the strongest attractive interaction at the shortest H-bond distance.[28, 82] According to the analyses of the H-bond energies with the H-bond distances in crystal structures, Hibbert and Emsley revealed that the experimental H-bond energies

change dramatically at the H-bond distance of 2.45 Å.[82] They concluded that 2.45 Å is the threshold distance for very strong H-bonds. Theoretical studies, on the other hand, revealed smooth linear relationships between the H-bond energies and the H-bond distances, with no dramatic change when the H-bond distance is between 2.45 and 2.80 Å, a reflection of similar electronic structures of the H-bond complexes within this range.[28] A similar linear correlation was obtained when the differences between the proton affinities of donor-acceptor pairs (ΔPA) and the H-bond energies were plotted, with no significant deviation in the H-bond energy at $\Delta PA = 0$, at which a low-barrier proton transfer potential was anticipated.[28]

Since strong H-bonds are susceptible to proton transfers, normal and strong H-bonds could be distinguished using IR frequencies of the transferring protons. In the present work, ν^{OH} and Δd_{DA} were plotted and illustrated in Fig. 2c, in which an interesting correlation was observed; the asymmetric O-H stretching frequencies (ν^{OH}) could be expressed in terms of the asymmetric stretching coordinates (Δd_{DA}) using an exponential function resembling the normal distribution function. The fitted functions for the protonated water clusters in the gas phase and continuum aqueous solution are given in eqn (5) and (6), respectively.

Gas phase: $$\nu^{OH} = 3662 - \frac{6710}{\sqrt{2\pi}} e^{-4.4\Delta d_{DA}^2} \quad (5)$$

Continuum aqueous solution: $$\nu^{OH} = 3710 - \frac{7600}{\sqrt{2\pi}} e^{-4.0\Delta d_{DA}^2} \quad (6)$$

The agreements between ν^{OH} obtained from B3LYP/TZVP calculations and the fitted values are also included in Fig. 2c. Two inflection points are seen in Fig. 2c, in the gas phase at $\Delta d_{DA} = 0.33$ and in continuum aqueous solution at $\Delta d_{DA} = 0.35$ Å. These correspond to $\nu^{OH} = 2004$ and 1853 cm^{-1}, respectively. It should be mentioned that, for the Zundel complex in the gas phase, the term "critical distance" was used to describe $R_{O\text{-}O}$ at which symmetric double-well potential with high barrier at the center is transformed into single-well potential without barrier.[55, 83] In Fig. 2a, $\Delta d_{DA} = 0.33$ and 0.35 Å correspond to $R_{O\text{-}O}$ = 2.47 and 2.48 Å, respectively, slightly longer than the

critical distance of $R_{O\text{-}O}$ = 2.43 Å.[55] Therefore, the inflection points in Fig. 2c could be associated with the "threshold" asymmetric stretching coordinates (Δd^{*}_{DA}) and frequencies ($\nu^{OH^{*}}$) for proton transfer, and could be used to distinguish between normal and strong H-bonds in the protonated water clusters.

Dynamic results

All the shared-proton complexes obtained in the previous subsection were investigated in BOMD simulations at 350 K; except structure **h**, for which the cyclic H-bonds were transformed into linear (similar to structure **f**) in the course of BOMD simulations. As pointed out in the previous subsection, the stabilities of the protonated water clusters are substantially decreased in continuum aqueous solution. This and the fact that our model systems did not take into account the H-bond networks of water in the vicinities of the protonated water clusters, especially in the presence of strong thermal energy fluctuations in BOMD simulations, made it difficult to discuss the energetic results. Therefore, the focuses are on the H-bond structures and IR spectra, from which the characteristic IR frequencies were used to explain the vibrational behaviors and dynamics of the proton transfer processes.

Average H-bond structures of shared-proton complexes

The average H-bond distances ($< R_{O-O} >$) and asymmetric stretching coordinates ($< \Delta d_{DA} >$) of the shared-proton complexes obtained from BOMD simulations are listed in Table 2. Linear relationships between $< \Delta d_{DA} >$ and $< R_{O-O} >$ were also obtained from BOMD simulations. They are illustrated in Fig. 3a. The fitted functions for the internal and external H-bonds are represented by eqn (7) and (8), respectively.

Internal H-bonds: $$< \Delta d_{DA} > = 4.93 \times < R_{O\text{-}O} > - 11.90 \qquad (7)$$

External H-bonds: $$< \Delta d_{DA} > = 1.53 \times < R_{O\text{-}O} > - 3.30 \qquad (8)$$

BOMD simulations at 350 K predicted the separation between the internal and external H-bonds at $< R_{O-O} >$ = 2.5 Å, the same as that from B3LYP/TZVP calculations.

Asymmetric O-H stretching frequencies and proton transfer pathways

The characteristic asymmetric O-H stretching frequencies ($\nu^{OH,MD}$) of the protons in the shared-proton complexes are included in Table 2. Examples of symmetric and asymmetric O-H stretching bands, as well as the O-O vibration band, are shown in Fig. 4.

In order to discuss the dynamics of the structural diffusion mechanism, the IR spectra of the transferring protons were analyzed in details, using the Zundel complex as an example. The IR spectra of the transferring protons are broad in general, especially in continuum aqueous solution. The BOMD results in Fig. 4 show two characteristic asymmetric O-H stretching bands, labeled with **A** and **B**; for the Zundel complex in the gas phase (in Fig. 4a) at $\nu^{OH,MD}$ = 1128 and 1852 cm^{-1}, respectively, and in continuum aqueous solution (in Fig. 4b) at $\nu^{OH,MD}$ = 943 and 1751 cm^{-1}, respectively. The low-frequency bands at **A**, appearing at $\nu^{OH,MD}$ slightly higher than those from B3LYP/TZVP calculations, are associated with the asymmetric O-H stretching mode, for which proton shuttles back and forth at the center of the H-bond. $\nu^{OH,MD}$ at **A** agree well with the IRMPD experiment[24] and BOMD simulations at 80 and 270 K.[20] The higher-frequency bands at **B**, not obtainable from single-well static proton transfer potentials with harmonic approximation, represent the vibrational mode with the center of vibration slightly shifted towards an oxygen atom.[26] Both characteristic IR bands could be regarded as spectral signatures of proton transfer reactions;[26-27] the former reflects the extent of the shared-proton complex formation and the latter the product formation. They are comparable with the "oscillatory shuttling motion" and the "Grotthuss shuttling motion" (or "structural diffusion motion"), respectively.[79]

A review on state-of-the-art methods for the calculations of vibrational energies of polyatomic molecules using quantum mechanical, variationally-based approaches was presented,[84] in which accurate IR spectra of ionic species in the gas phase were discussed in comparison with experiment.[80] One of the emphases was on the analyses of the middle spectral region (800 – 2000 cm^{-1}) which can be directly related to the proton transfer in the Zundel complex; the experiment[80] showed a doublet centered at 1000 cm^{-1} as the most characteristic feature, with the low-energy component at 928 cm^{-1} and the high-energy component at 1047 cm^{-1}. Based on the multiconfiguration time-dependent Hartree (MCTDH) method, the most intense band was concluded to be the proton transfer fundamental band (asymmetric O-H stretching mode) and the doublet was attributed to the coupling among the low-frequency water-wagging modes, water-water stretching motion and the proton transfer motion. Additionally, the MCTDH method predicted a water bending state which couples strongly with the proton transfer motion at 1741 cm^{-1}, compared with the experiment at 1763 cm^{-1}.[80] The present BOMD simulations predicted the proton transfer fundamental frequency in the gas phase close to the MCTDH method and the experiment[80] (1128 cm^{-1} at 350 K, compared with 1047 cm^{-1} at 275 K). Since one of the main objectives of the present work is to search for an appropriate theoretical method to monitor proton transfer processes in BOMD simulations on larger H-bond systems and it is sufficient to employ the fundamental asymmetric O-H stretching frequencies, the low-frequency band of the doublet was not investigated in details.

As the proton transfer in H-bond depends strongly on the O-O vibration,[27] the relative probability or the extent of the shared-proton complex formation in BOMD simulations could be approximated from the ratio between the intensity of $\nu^{OH,MD}$ at **A** ($\mathbf{I_A}$) and the intensity of the O-O vibration ($\mathbf{I_{O\text{-}O}}$).[26] In Table 2, $\mathbf{I_A/I_{O\text{-}O}}$ for the Zundel complex in the gas phase and continuum aqueous solution are 0.6 and 0.7, respectively, indicating that, in BOMD simulations in the gas phase, about 60 % of the H_3O^+ - H_2O 1 : 1 complex are in the form of the Zundel complex, whereas in continuum aqueous solution about 70 %. The values of $\mathbf{I_A/I_{O\text{-}O}}$ in Table 2 also suggest that the extent of the oscillatory shuttling

motion is decreased when the number of water molecule increased; indicating a higher efficiency of proton transfer in extended H-bond network.

The observation that the proton transfer process in the H_3O^+-H_2O 1 : 1 complex consists of two consecutive steps namely, a quasi-dynamic equilibrium between the precursor (the H_3O^+-H_2O 1 : 1 complex) and the shared-proton complex (the Zundel complex), followed by the actual proton transfer,[27] made it possible to establish a criterion to measure the extent or the efficiency of proton transfer from IR spectra; the quasi-dynamic equilibrium prevents proton transfer reaction from being concerted and is considered to be the rate-determining step.[26-27] Hence, an effective proton transfer process should take the reaction path with the shortest lifetime of the quasi-dynamic equilibrium. Therefore, in order to achieve an "ideal" maximum efficiency, according to the transition-state theory, the populations of the shared-proton complex and the product must be the same. In other words, for maximum efficiency, every shared-proton complex formation should lead to the actual proton transfer. This is possible only when the O-O distance undergoes large-amplitude vibration, for which the O-H and O-O vibrations are coherent.[27] It should be emphasized that, since the present model systems involved only the O..H^+..O H-bonds, the product becomes precursor for the successive proton transfer event.

As the populations of the shared-proton complex and the precursor in BOMD simulations could be approximated from the intensities of the oscillatory shuttling band (**A**) and the structural diffusion band (**B**), the efficiency of proton transfer could be approximated from the ratio between $\mathbf{I_B/I_A}$ ($\mathbf{I_B/I_A}$ = 1 for the ideal maximum efficiency). Table 2 reveals that, for the Zundel complex in the gas phase, $\mathbf{I_B/I_A}$ is about 0.5 (half of the ideal maximum efficiency), whereas in continuum aqueous solution $\mathbf{I_B/I_A} < 0.1$, a dominance of the oscillatory shuttling vibration (shared-proton complex). It turned out that, based on this criterion, the most extended H-bond structure with incomplete hydration at H_3O^+ (structure **f**) possesses the highest efficiency for proton transfer.

Fig. 3b shows the relationships between $\nu^{OH,MD}$ at **A** (the oscillatory shuttling frequencies) and $< R_{O-O} >$. Similar to B3LYP/TZVP calculations, the exponential functions in eqn (9) and (10) can well represent $\nu^{OH,MD}$ in the gas phase and continuum aqueous solution, respectively.

Gas phase: $$\nu^{OH,MD} = -3.21\times10^{10}\, e^{-<R_{O-O}>/0.1478} + 3686 \qquad (9)$$

Continuum aqueous solution: $$\nu^{OH,MD} = -1.72\times10^{11}\, e^{-<R_{O-O}>/0.1356} + 3771 \qquad (10)$$

As in the case of B3LYP/TZVP calculations, the relationships between $\nu^{OH,MD}$ and $< \Delta d_{DA} >$ in Fig. 3c were used to approximate the threshold frequencies for proton transfers in BOMD simulations. They are represented by eqn (11) and (12), in the gas phase and continuum aqueous solution, respectively.

Gas phase: $$\nu^{OH,MD} = 3662 - \frac{6220}{\sqrt{2\pi}} e^{-3.5<\Delta d_{DA}>^2} \qquad (11)$$

Continuum aqueous solution: $$\nu^{OH,MD} = 3710 - \frac{6800}{\sqrt{2\pi}} e^{-3.6<\Delta d_{DA}>^2} \qquad (12)$$

The calculations of the second derivatives of the functions in eqn (11) and (12) yielded two inflection points at $< \Delta d_{DA} >$ = 0.37 Å, corresponding to the threshold frequencies at $\nu^{OH,MD*}$ = 2130 and 2053 cm^{-1}, in the gas phase and continuum aqueous solution, respectively. The values are slightly higher than those obtained from B3LYP/TZVP calculations, due to the inclusions of the thermal energy fluctuations and dynamics in the model calculations.

Dynamics of structural diffusions

The diffusion coefficients (D) of the transferring protons in the shared-proton complexes are listed in Table 2. The diffusion coefficients of the Zundel complex in the gas phase and continuum aqueous solution, obtained from BOMD simulations at 350 K, are 10.3×10^{-5} and 9.2×10^{-5} $cm^2\ s^{-1}$, respectively. Based on the same approach, BOMD simulations predicted the diffusion coefficient at 298 K to be 5.0×10^{-5} $cm^2\ s^{-1}$,[26] slightly

lower than the NMR result;[10] in NMR experiment, the diffusion coefficient of a proton moving across a single water molecule was estimated from the NMR hopping time (τ_p) and the Einstein relation ($D = l^2/6\tau_p$) to be 7.0×10^{-5} cm^2 s^{-1}; where l is the hopping length or the H-bond distance (2.5 Å) and τ_p = 1.5 ps. It should be added that, the diffusion coefficient reported in ref. 10 was derived by subtracting the water self-diffusion coefficient (2.3×10^{-5} cm^2 s^{-1}) from the proton diffusion coefficient (9.3×10^{-5} cm^2 s^{-1}). The deviation of about 28% from the experimental value[10] could be attributed to the neglect of the H-bond networks connecting the hydration shells of the Zundel complex.[26] For larger protonated water clusters in Table 2, the shared-proton complex with an extended H-bond network, structure **f**, possess D = 8.9×10^{-5} and 8.2×10^{-5} cm^2 s^{-1}, in the gas phase and continuum aqueous solution, respectively. The values are lower than those of the Zundel complex. These support the conclusion that the oscillatory shuttling motion is slightly more important in the H_3O^+ - H_2O 1 : 1 complex, compared to the extended H-bond structures.

Finally, in order to ensure that the dynamics and IR results discussed above are reliable, attempt was made to perform NVT BOMD simulations with longer simulation time. This was successful only for the Zundel complex in the gas phase, and not longer than 5 ps; all the other shared-proton complexes became fragmented after 2.5 ps. It appeared that, for the IR spectra, the oscillatory shuttling and structural diffusion frequencies remain the same (see Fig. 4a), with slight decreases of the intensities, $\mathbf{I_B/I_A}$ = 0.49 compared with 0.51. The diffusion coefficient in the gas phase is slightly decreased, from 10.3×10^{-5} to 9.5×10^{-5} cm^2 s^{-1}. This leads to a conclusion that, although for small H-bond complexes, the IR spectra obtained from short BOMD simulations show some fine structures, meaningful and reasonable interpretations could be made, especially for all the H-bond complexes investigated here; a similar conclusion was presented by Termath and Sauer [20] based on a series of BOMD simulations on $H_5O_2^+$ and $H_7O_3^+$, from which insights into fast dynamic processes in H-bonds (*e.g.* H-bond structures and IR spectra) were obtained from relatively short BOMD trajectories (about 2 ps).

Conclusion

Proton transfer reactions and dynamics in protonated water clusters were systematically studied using the H-bond complexes formed from H_3O^+ and nH_2O, n = 1 – 4, as model systems. The theoretical investigations began with searching for the H-bond complexes which could be important in the dynamic proton transfer pathways, as well as characteristic H-bond structures and IR spectra of the transferring protons, both in the gas phase and continuum aqueous solution. DFT calculations at the B3LYP/TZVP level revealed that the potential H-bond structures consist of the Zundel complex, with the characteristic asymmetric O-H stretching frequencies (ν^{OH}) < 1000 cm^{-1} and the threshold frequencies for proton transfers in the gas phase and continuum aqueous solution at ν^{OH*} = 2004 and 1853 cm^{-1}, respectively. According to the results obtained from the static proton transfer potentials, the trends of the interaction energies with respect to the number of water molecules in the gas phase and continuum aqueous solution are quite similar. The destabilization effects caused by the continuum aqueous solvent bring about smaller variation of the interaction energies with respect to the number of water molecules compared to the gas phase. The destabilization effects also lead to shifts of the transferring protons away from the centers, especially for the H-bond complexes with the Zundel complex as the central charged species. The trend of the solvation energies revealed that, when the number of water molecules is the same, the H-bonds inside the protonated water clusters experience comparable uniform electric field.

BOMD simulations at 350 K predicted the characteristic asymmetric O-H stretching frequencies in a quite wide range, from 940 to 1740 cm^{-1}. Most importantly, BOMD simulations suggested additional characteristic asymmetric O-H stretching bands at higher frequencies. They are in the range of 1640 and 2600 cm^{-1}. The lower-frequency bands are regarded as the “oscillatory shuttling band” and the higher-frequency bands the “structural diffusion band”. The latter cannot not be determined easily from static proton transfer potentials, due to the anharmonic and dynamic behaviors of the vibrational motions of the transferring protons. The oscillatory shuttling and structural diffusion

bands could be considered as the spectroscopic evidences for the shared-proton complex and product (or precursor) formations, respectively.

The analyses of the H-bond structures and $\nu^{OH,MD}$ yielded the threshold frequencies ($\nu^{OH,MD*}$) for the proton transfers in the gas phase and continuum aqueous solution at $\nu^{OH,MD*}$ = 2130 and 2053 cm^{-1}, respectively. Because the quasi-dynamic equilibrium between the Zundel and Eigen complexes was suggested to be the rate-determining step, in order to achieve an "ideal" maximum efficiency, a concerted proton transfer pathway should be taken. The present results anticipated that the effective interconversion between the two proton states, the Zundel-like and hydronium-like structures, could be reflected from comparable intensities of the oscillatory shuttling and structural diffusion bands. These pieces of information could provide an appropriate IR spectroscopic method to investigate proton transfer reactions in larger model systems, and iterated the necessity to incorporate the thermal energy fluctuations and dynamics in the model calculations.

Acknowledgement

The authors would like to acknowledge the financial supports from the Thailand Research Fund (TRF): the Advanced Research Scholarship, Grant No. BRG5180022 to Prof. Kritsana Sagarik; the Royal Golden Jubilee (RGJ) Ph.D. Program, Grant No. PHD/0121/2549 to Charoensak Lao-ngam and Prof. Kritsana Sagarik. Linux clusters provided by the following organizations are also gratefully acknowledged: School of Mathematics and School of Chemistry, SUT; National Electronics and Computer Technology Center (NECTEC), National Science and Technology Development Agency (NSTDA); the Thai National Grid Center (THAIGRID), Ministry of Information and Communication Technology.

References

1 T. Koppel, *Powering the Future: The ballard fuel cell and the race to change the world*, John Wiley & Sons Ltd., New York, 1999.

2 J. Larminie and A. Dicks, *Fuel Cell Systems*, John Wiley & Sons Ltd., Chichester, 2001.

3 C. A. Vincent and B. Scrosati, *Modern Batteries: An introduction to electrochemical power sources*, John Wiley & Sons Ltd., New York, 1997.

4 K. D. Kreuer, *Chem. Mater.*, 1996, **8**, 610.

5 K. D. Kreuer, S. J. Paddison, E. Spohr and M. Schuster, *Chem. Rev.*, 2004, **104**, 4637.

6 K. A. Mauritz and R. B. Moore, *Chem. Rev.*, 2004, **104**, 4535.

7 S. J. Paddison, *Annu. Rev. Mater. Res.*, 2003, **33**, 289.

8 A. Botti, F. Bruni, S. Imberti, M. A. Ricci and A. K. Soper, *J. Mol. Liquid*, **in press**.

9 J. M. Hermida-Ramon and G. Karlstroem, *J. Mol. Struct. (Theochem)*, 2004, **712**, 167.

10 N. Agmon, *Chem. Phys. Letters*, 1995, **244**, 456.

11 M. Eigen and L. D. Maeyer, *Proc. Roy. Soc.*, 1958, **A247**, 505.

12 M. E. Tuckerman, K. Laasonen, M. Sprik and M. Parrinello, *J. Chem. Phys.*, 1995, **103**, 150.

13 M. E. Tuckerman, D. Marx, M. L. Klein and M. Parrinello, *Science*, 1997, **275**, 817.

14 J. B. Asbury, T. Steinel and M. D. Fayer, *J. Luminescence*, 2004, **107**, 271.

15 J. C. Jiang, C. Chaudhuri, Y. T. Lee and H. C. Chang, *J. Phys. Chem. A*, 2002, **106**, 10937.

16 C. C. Wu, C. Chaudhuri, J. C. Jiang, Y. T. Lee and H.C. Chang, *J. Phys. Chem. A*, 2004, **108**, 2859.

17 R. Iftimie, V. Thomas, S. Plessis, P. Marchand and P. Ayotte, *J. Am. Chem. Soc.*, 2008, **130**, 5901.

18 R. Buzzoni, S. Bordiga, G. Ricchiardi, G. Spoto and A. Zecchina, *J. Phys. Chem.*, 1995, **99**, 11937.

19 M. Okumura, L. I. Yeh, J. D. Myers and Y. T. Lee, *J. Phys. Chem.*, 1990, **94**, 3416.

20 V. Termath and J. Sauer, *Mol. Phys.*, 1977, **91**, 963.

21 C.-C. Wu, J. C. Jiang, D. W. Boo, S. H. Lin, Y. T. Lee and H.-C. Chang, *J. Chem. Phys.*, 2000, **112**, 176.

22 K. R. Asmis, N. L. Pivonka, G. Santambrogio, M. Bruemmer, C. Kaposta, D. M. Neumark and L. Woeste, *Science*, 2003, **299**, 1375.

23 H.-P. Cheng and J. L. Krause, *J. Chem. Phys.*, 1997, **107**, 8461.

24 T. D. Fridgen, T. B. McMahon, L. MacAleese, J. Lemaire and M. Maitre, *J. Phys. Chem. A*, 2004, **108**, 9008.

25 U. W. Schmitt and G. A. Voth, *J. Chem. Phys.*, 1999, **111**, 9361.

26 K. Sagarik, S. Chaiwongwattana, V. Vchirawongkwin and S. Prueksaaroon, *Phys. Chem. Chem. Phys.*, 2010, **12**, 918.

27 K. Sagarik, M. Phonyiem, C. Lao-Ngam and S. Chaiwongwattana, *Phys. Chem. Chem. Phys.*, 2008, **10**, 2098.

28 J. Chen, M. A. McAllister, J. K. Lee and K. N. Houk, *J. Org. Chem.*, 1998, **63**, 4611.

29 J. Fritsch and G. Zundel, *J. Phys. Chem.*, 1981, **85**, 556.

30 M. Rospenk, J. Fritsch and G. Zundel, *J. Phys. Chem.*, 1984, **88**, 321.

31 G. Zundel and J. Fritsch, *J. Phys. Chem.*, 1984, **88**, 6295.

32 J. Rejnek, M. Hanus, M. Kabelá, F. Ryjáek and P. Hobza, *Phys. Chem. Chem. Phys.*, 2005, **7**, 2006.

33 K. Sagarik and S. Chaiyapongs, *Biophys. Chem.*, 2005, **117**, 18.

34 K. P. Sagarik, *J. Mol. Struct. (Theochem)*, 1999, **465**, 141.

35 K. P. Sagarik and R. Ahlrichs, *J. Chem. Phys.*, 1987, **86**, 5117.

36 K. P. Sagarik and P. Asawakun, *Chem. Phys.*, 1997, **219**, 173.

37 K. P. Sagarik, S. Chaiwongwattana and P. Sisot, *Chem. Phys.*, 2004, 1.

38 K. P. Sagarik and S. Dokmaisrijan, *J. Mol. Struct. (Theochem)*, 2005, **718**, 31.

39 K. P. Sagarik, V. Pongpituk, S. Chiyapongs and P. Sisot, *Chem. Phys.*, 1991, **156**, 439.

40 K. P. Sagarik and B. M. Rode, *Chem. Phys.*, 2000, **260**, 159.

41 K. P. Sagarik and E. Spohr, *Chem. Phys.*, 1995, **199**, 73.

42 P. A. Giguere, *J. Chem. Ed.*, 1979, **56**, 571.

43 S. J. Paddison, *J. New Mater. Electrochem. Syst.*, 2001, **4**, 197.

44 S. J. Paddison and J. A. Elliott, *J. Phys. Chem. A*, 2005, **109**, 7583.

45 S. J. Paddison, L. R. Pratt and T. Zawodzinski, *J. New Mater. Electrochem. Syst.*, 1999, **2**, 183.

46 S. J. Paddison, L. R. Pratt and T. Zawodzinski, *J. Phys. Chem. A*, 2001, **105**, 6266.

47 S. J. Paddison and T. Zawodzinski, *Solid State Ionics,*, 1998, **115**, 333.

48 A. D. Becke, *J. Chem. Phys.*, 1993, **98**, 5648.

49 C. Lee, W. Yang and R. G. Parr, *Phys. Rev. B,*, 1988, **37**, 785.

50 A. Schaefer, C. Huber and R. Ahlrichs, *J. Chem. Phys.*, 1994, **100**, 5829.

51 G. Santambrogio, M. Bruemmer, L. Woeste, J. Doebler, M. Sierka, J. Sauer, G. Meijer and K. R. Asmis, *Phys. Chem. Chem. Phys.*, 2008, **10**, 3992.

52 R. Ahlrichs, M. Baer, M. Haeser, H. Horn and C. Koelmel, *Chem. Phys. Lett.*, 1989, **162**, 165.

53 O. Treutler and R. Ahlrichs, *J. Chem. Phys.*, 1995, **102**, 346.

54 S. F. Boys and F. Bernardi, *Mol. Phys.*, 1970, **19**, 553.

55 M. Benoit and D. Marx, *ChemPhysChem*, 2005, **6**, 1738.

56 D. Marx, M. E. Tuckerman, J. Hutter and M. Parrinello, *Nature*, 1999, **367**, 101.

57 J. A. Morrone, K. E. Haslinger and M. E. Tuckerman, *J. Phys. Chem. B*, 2006, **110**, 3712.

58 A. P. Scott and L. Radom, *J. Phys. Chem.*, 1996, **100**, 16502.

59 D. Xenides, B. R. Randolf and B. M. Rode, *J. Chem. Phys.*, 2005, **122**, 174506.

60 P. B. Balbuena and J. M. Seminario, *Theoretical and Computational Chemistry 7*, Elsevier, Amsterdam, 1999.

61 R. N. Barnett and U. Landman, *Phys. Rev.*, 1993, **B48**, 2081.

62 C. J. Cramer, *Essentials of Computational Chemistry: Theory and models*, John Wiley & Sons, Ltd., 2002.

63 F. Huisken, S. Mohammad-Pooran and O. Werhahn, *Chem. Phys.*, 1998, **239**, 11.

64 E. P. L. Hunter and S. G. Lias, *J. Phys. Chem. Ref. Data*, 1998, **27**, 413.

65 X. Jing, N. Troullier, D. Dean, N. Binggeli, J. R. Chelikowsky, K. Wu and Y. Saad, *Phys. Rev.*, 1994, **B50**, 122.

66 J. Lobaugh and G. A. Voth, *J. Chem. Phys.*, 1996, **104**, 2056.

67 A. R. Leach, *Molecular Modelling: Principles and applications*, Longman, Edinburgh, 1996.

68 B. E. Conway, J. O. M. Bockris and H. Linton, *J. Chem. Phys.*, 1956, **24**, 834.

69 K. D. Kreuer, *Solid State Ionics*, 2000, **136**, 149.

70 R.R. Sadeghi and H-P. Cheng, *J. Chem. Phys.*, 1999, **111**, 2086.

71 D. Sheppard, R. Terrell and G. Henkelman, *J. Chem. Phys.*, 2008, **128**, 134106.

72 D. J. Wales, *Mol. Phys.*, 2002, **100**, 3285-3305.

73 P. Bopp, *Chem. Phys.*, 1986, **106**, 205.

74 M. P. Allen and D. J. Tildesley, *Computer Simulation of Liquids*, Oxford University Press, New York, 1987.

75 J. M. Haile, *Molecular Dynamics Simulations*, John Wiley & Sons Ltd, New York, 1997.

76 D. C. Rapaport, *The Art of Molecular Dynamics Simulation*, Cambridge University Press, London, 1995.

77 M. Park, I. Shin, N. J. Singh and K. S. Kim, *J. Phys. Chem. A*, 2007, **111**, 10692.

78 R. Parthasarathi, V. Subramanian and N. Sathyamurthy, *J. Phys. Chem. A, Lett.*, 2007, **111**, 13287.

79 Y. Wu, H. Chen, F. Wang, F. Paesani and G.A. Voth, *J. Phys. Chem. B*, 2008, **112**, 467.

80 N. I. Hammer, E. G. Diken, J. R. Roscioli, M. A. Johnson, Evgeniy M. Myshakin, K. D. Jordan, A. B. McCoy, X. Huang, J. M. Bowman and S. Carter, *J. Chem. Phys.*, 2005, **122**, 244301

81 H. A. Schwarz, *J. Chem. Phys.*, 1977, **67**, 5525.

82 F. Hibbert and J. Emsley, *Adv. Phys. Org. Chem.*, 1990, **26**, 255.

83 T. Komatsuzaki and I. Ohmine, *Chem. Phys.*, 1994, **180**, 239.

84 J. M. Bowman, T. Carrington and H. Meyer, *Mol. Phys.*, 2008, **106**, 2145-2182.

Figure 1 a) Trends of the interaction (ΔE) and solvation energies (ΔE^{sol}) with respect to the number of water molecules, obtained from B3LYP/TZVP calculations: -▲- = ΔE in the gas phase; -Δ- = ΔE in continuum aqueous solution; -■- = ΔE^{sol}.

b) Trends of the interaction energies between the central charged species and water molecules (ΔE^{X}, X = H_3O^+ or $H_5O_2^+$) with respect to the number of water molecules, obtained from B3LYP/TZVP calculations: -▲- = H_3O^+ in the gas phase; -Δ- = H_3O^+ in the continuum aqueous solution; -■- = $H_5O_2^+$ in the gas phase; -□- = $H_5O_2^+$ in continuum aqueous solution.

____ = calculations without the counterpoise correction.

------ = calculations with the counterpoise correction.

Figure 2 a) Plot of the asymmetric stretching coordinates (Δd_{DA}) and the O-H..O H-bond distances ($R_{O\text{-}O}$), obtained from B3LYP/TZVP calculations.

b) Plot of the asymmetric O-H stretching frequencies (ν^{OH}) and the O-H..O H-bond distances ($R_{O\text{-}O}$), obtained from B3LYP/TZVP calculations.

c) Plot of the asymmetric O-H stretching frequencies (ν^{OH}) and the asymmetric stretching coordinates (Δd_{DA}), obtained from B3LYP/TZVP calculations.

Figure 3 a) Plot of the average asymmetric stretching coordinates ($<\Delta d_{DA}>$) and the average O-H..O H-bond distances ($<R_{O\text{-}O}>$), obtained from BOMD simulations at 350 K.

b) Plot of the asymmetric O-H stretching frequencies ($\nu^{OH,MD}$) and the average O-H..O H-bond distances ($<R_{O\text{-}O}>$), obtained from BOMD simulations at 350 K.

c) Plot of the asymmetric O-H stretching frequencies ($\nu^{OH,MD}$) and the asymmetric stretching coordinates ($<\Delta d_{DA}>$), obtained from BOMD simulations at 350 K.

Figure 4 Symmetric and asymmetric O-H stretching bands of the transferring protons in the shared-proton complexes, together with the O-O vibration band, obtained from BOMD simulations at 350 K.

a) The Zundel complex (structure **a**) in the gas phase;
_____ = BOMD simulations with the simulation length of 5 ps.

b) The Zundel complex (structure **a**) in continuum aqueous solution.

c) The H_3O^+-H_2O 1 : 4 complex (structure **f**) in the gas phase.

d) The H_3O^+-H_2O 1 : 4 complex (structure **f**) in continuum aqueous solution.

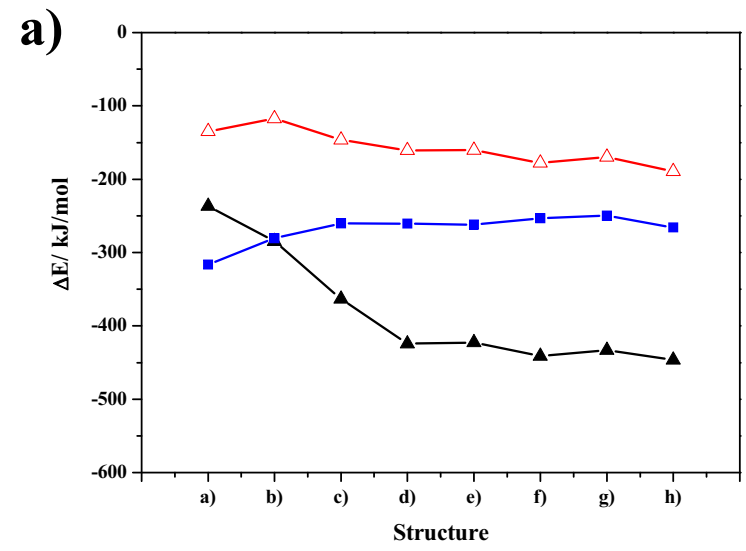
a)
0
-100
-200
-300
-400
-500
-600
ΔE/ kJ/mol
a)
b)
c)
d)
e)
f)
g)
h)
Structure

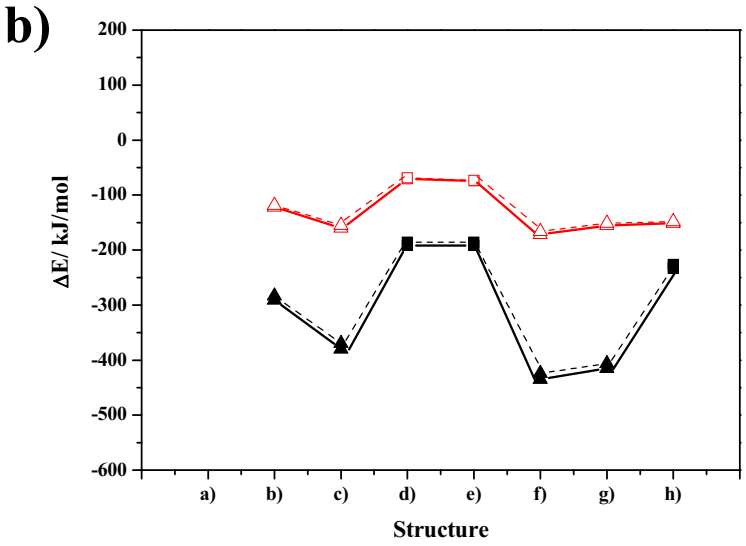
b)
200
100
0
-100
-200
-300
-400
-500
-600
ΔE/ kJ/mol
a)
b)
c)
d)
e)
f)
g)
h)
Structure

Figure 1

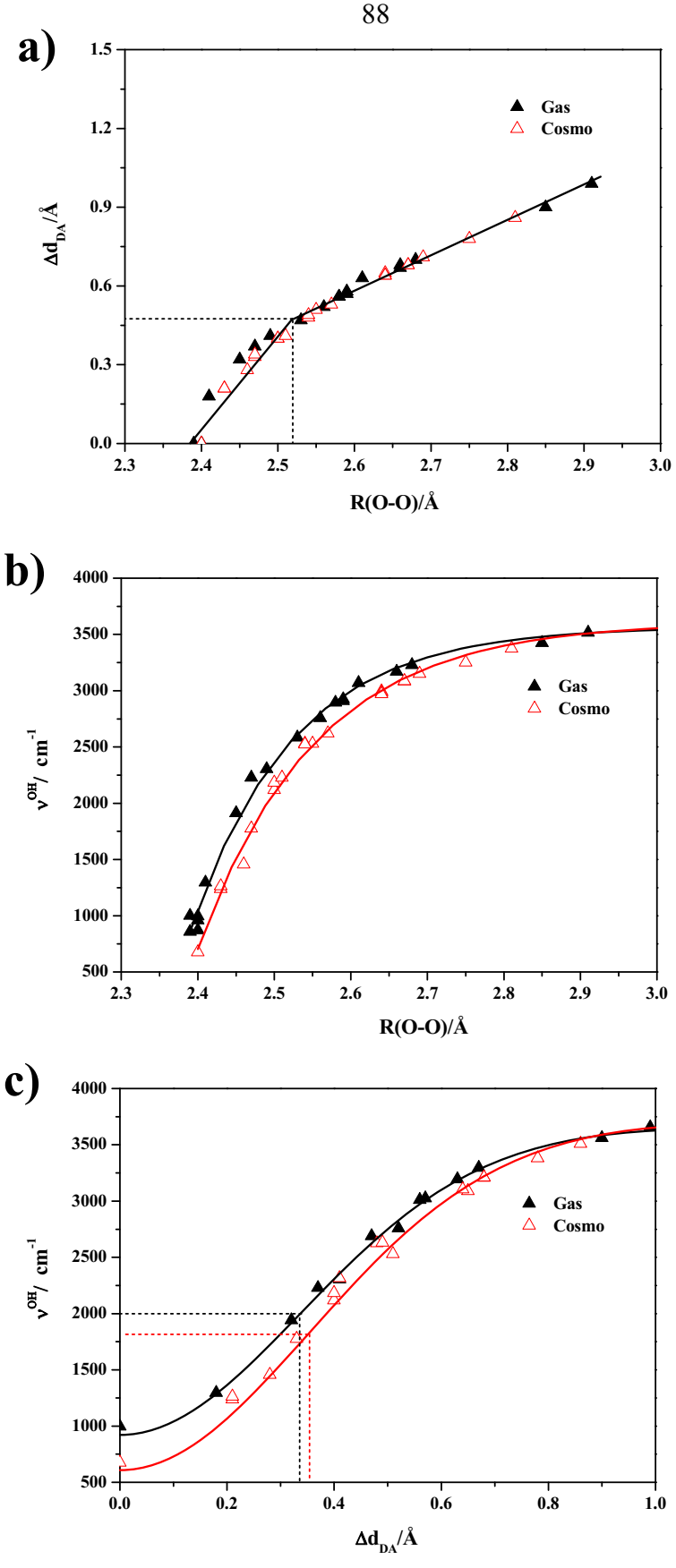
a)
Gas
Cosmo
Δd_{DA}/Å
R(O-O)/Å
b)
Gas
Cosmo
ν^{OH}/ cm^{-1}
R(O-O)/Å
c)
Gas
Cosmo
ν^{OH}/ cm^{-1}
Δd_{DA}/Å

Figure 2

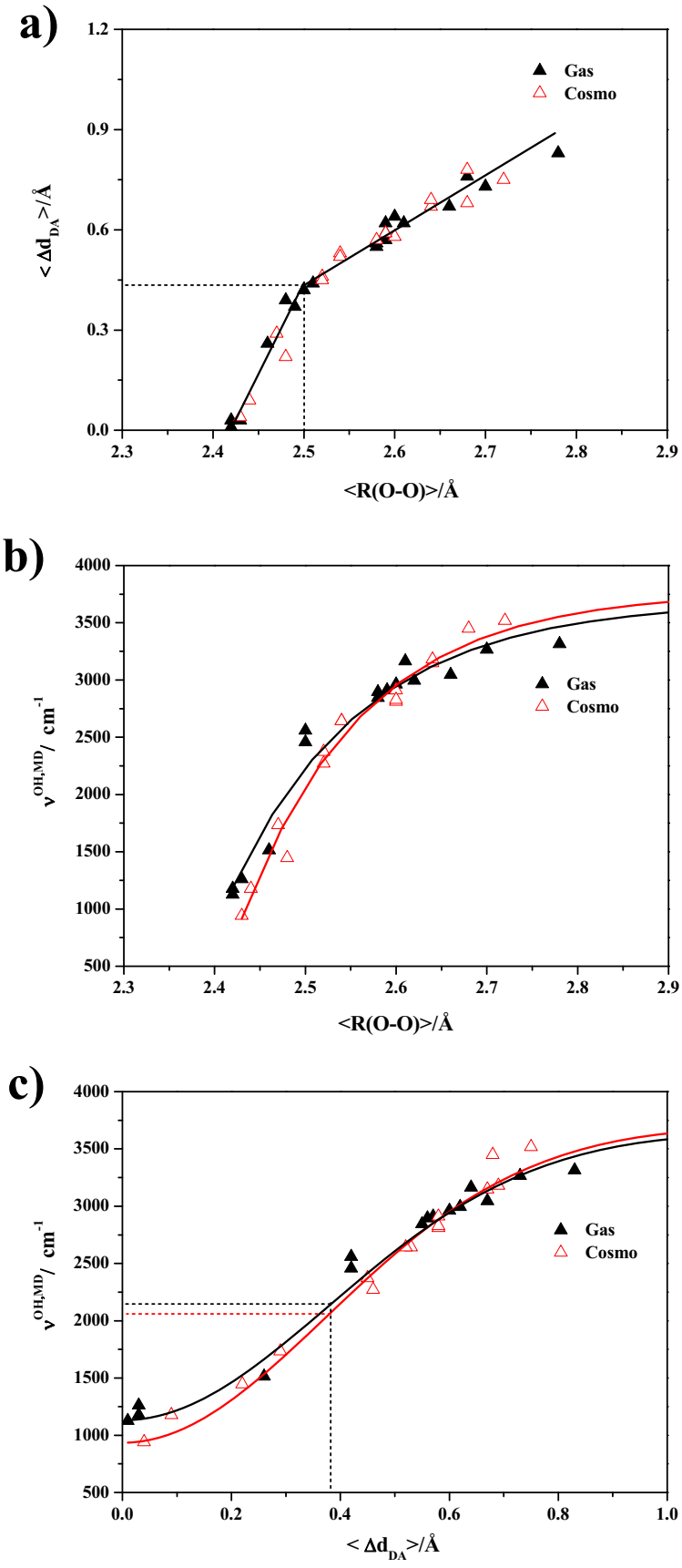
a)
Gas
Cosmo
< Δd_DA >/Å
<R(O-O)>/Å
b)
Gas
Cosmo
ν^OH,MD / cm^-1
<R(O-O)>/Å
c)
Gas
Cosmo
ν^OH,MD / cm^-1
< Δd_DA >/Å

Figure 3

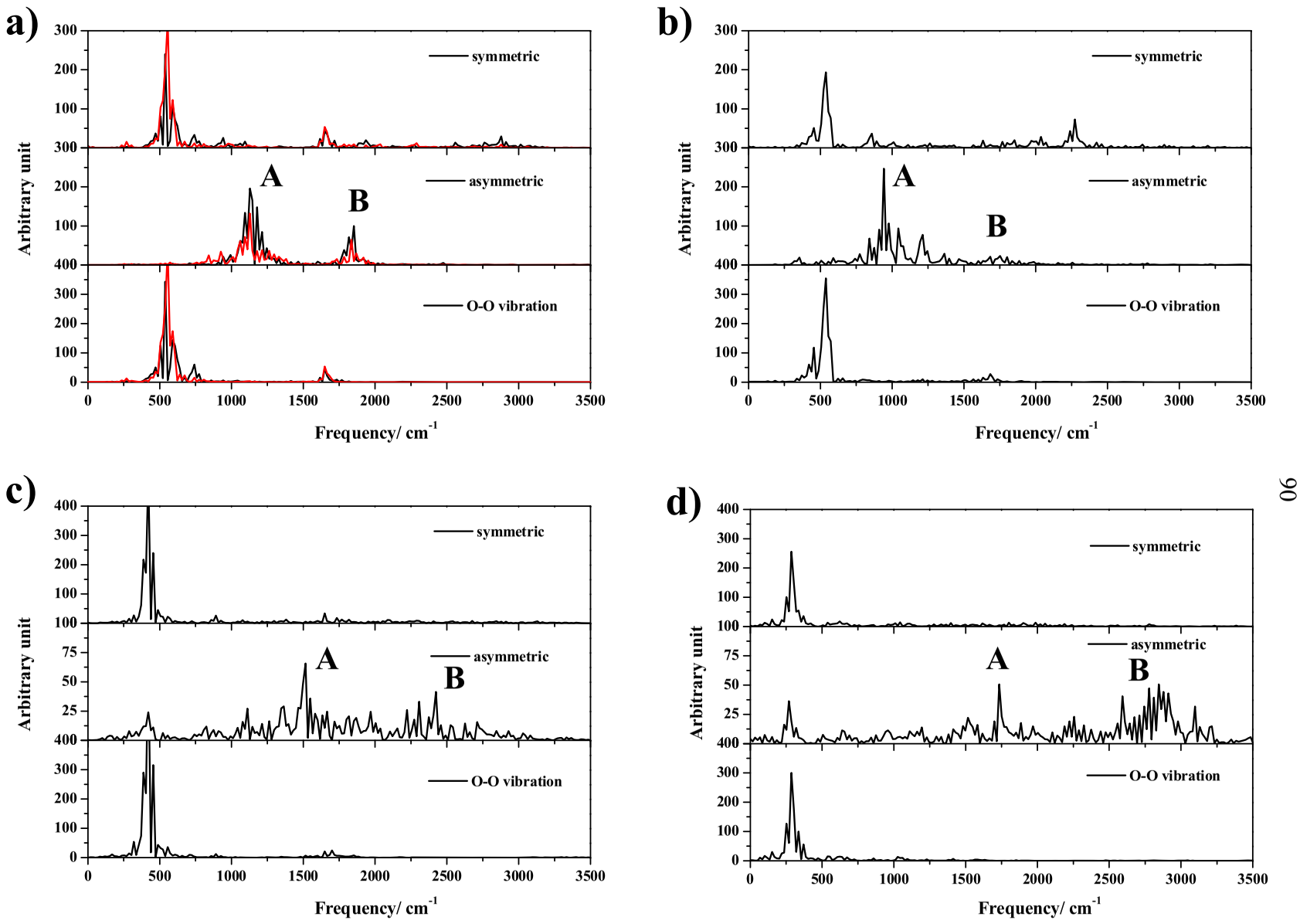
a)
b)
c)
d)
symmetric
asymmetric
O-O vibration
A
B
Arbitrary unit
Frequency/ cm-1

90

Figure 4

Table 1 Static results of the protonated water clusters obtained from B3LYP/TZVP calculations. Distances, energies and IR frequencies are in Å, kJ/mol and cm^{-1}, respectively.

Structure		R_{O-O}	R_{O-H}	Δd_{DA}	ΔE	ΔE^{sol}	ΔE^{X}	ν^{O-H}
a 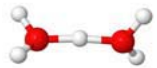	Gas	2.40	1.20	0.00	-158.8	-316.4		961.3
	Cosmo	2.40	1.20	0.00	-58.2			676.8
b 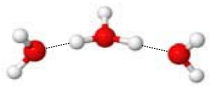	Gas	2.49	1.04	0.41	-265.7	-280.3	-290.7 (-283.2) -121.7 (-118.3)	2304.5
	Cosmo	2.50	1.05	0.40	-95.2			2120.1
c 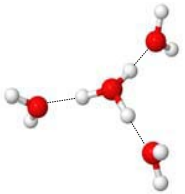	Gas	2.56	1.02	0.52	-353.7	-260.2	-379.7 (-369.7) -159.8 (-154.7)	2759.7
	Cosmo	2.55	1.02	0.51	-129.3			2531.4
d 	Gas	2.40	1.20	0.00	-340.6	-260.6	-191.7 (-185.4) -70.3 (-68.5)	997.9
	Cosmo	2.43	1.11	0.21	-116.7			1240.4

R_{O-O} and R_{O-H} = H-bond distances; Δd_{DA} = asymmetric stretching coordinate; ΔE = interaction energy in the protonated water clusters; ΔE^{sol} = solution energy; ΔE^{X} = interaction energy between the central charged species (X = H_3O^+ or $H_5O_2^+$) and water molecules (the values in parentheses computed with the counterpoise corrections; ν^{OH} = asymmetric O-H stretching frequency.

Table 1 ***(Cont.)***

Structure		R_{O-O}	R_{O-H}	Δd_{DA}	ΔE	ΔE^{sol}	ΔE^{X}	ν^{O-H}
e 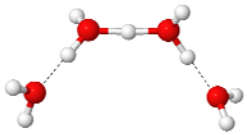	Gas	2.39	1.20	0.00	-340.5	-261.8	-191.7 (-185.3)	1001.9
	Cosmo	2.43	1.11	0.21	-117.7		-74.5 (-73.2)	1263.6
f 	Gas	2.45	1.07	0.32	-403.2	-253.2	-434.9 (-424.2)	1914.7
	Cosmo	2.47	1.07	0.33	-138.0		-171.5 (-166.1)	1778.0
g 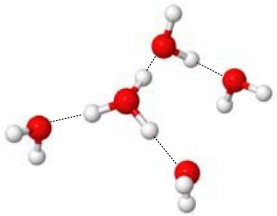	Gas	2.47	1.05	0.37	-416.5	-249.7	-415.3 (-406.4)	2229.6
	Cosmo	2.50	1.05	0.40	-147.9		-155.2 (-150.9)	2185.8
h 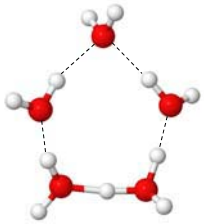	Gas	2.41	1.12	0.18	-402.0	-265.9	-233.1 (-226.1)	1296.8
	Cosmo	2.46	1.09	0.28	-149.5		-151.0 (-148.4)	1457.7

Table 2 Dynamic results of the shared-proton complexes obtained from BOMD simulations at 350 K. Distances, energies and IR frequencies are in Å, kJ/mol and cm^{-1}, respectively. Proton diffusion coefficient (D) is in $cm^2\ s^{-1}$.

Structure		$<R_{O-O}>$	$<\Delta d_{DA}>$	$\nu^{OH,MD}$ A	$\nu^{OH,MD}$ B	I_A/I_{O-O}	I_B/I_A	D (10^{-5})
a 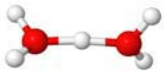	Gas	2.42	0.01	1127.8	1851.7	0.57	0.51	10.26
	Cosmo	2.43	0.04	942.7	1750.7	0.69	0.09	9.16
d 	Gas	2.42	0.03	1178.3	1767.5	0.48	0.19	10.89
	Cosmo	2.48	0.22	1447.7	2003.3	0.14	0.55	10.54
e 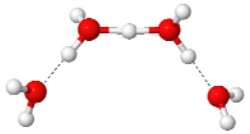	Gas	2.43	0.03	1262.5	1784.4	-*	0.45	11.09
	Cosmo	2.44	0.09	1178.3	1649.7	0.29	0.23	12.95
f 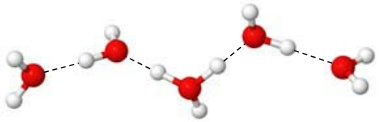	Gas	2.46	0.26	1515.0	2424.1	0.28	0.63	8.89
	Cosmo	2.47	0.29	1733.9	2592.4	0.17	0.79	8.20

$<R_{O-O}>$ = average H-bond distance; $<\Delta d_{DA}>$ = average asymmetric stretching coordinate; $\nu^{OH,MD}$ = asymmetric O-H stretching frequency;
I_A = intensity of the oscillatory shuttling band; I_B = intensity of the structural diffusion band I_{O-O} = intensity of the O-O stretching band;
D = proton diffusion coefficient. * not obtainable due to H-bond structure reorganization in the course of BOMD simulations.

Proton transfer reactions and dynamics at sulfonic acid group of Nafion®

M. Phonyiem and **K. Sagarik**, *submitted*

Proton transfer reactions and dynamics at sulfonic acid group of Nafion®

by

Mayuree Phonyiem

Chareonsak Lao-Ngam

and

Kritsana Sagarik*

School of Chemistry
Institute of Science
Suranaree University of Technology
Nakhon Ratchasima 30000
Thailand

*corresponding author
E-mail: kritsana@sut.ac.th
Tel./Fax: (6644) 224635

keywords: Nafion®, triflic acid, proton transfer, BOMD simulations, continuum aqueous solution

Abstract

Proton transfer reactions and dynamics at a hydrophilic group (-SO_3H) of Nafion® were studied at low hydration levels, using the complexes formed from CF_3SO_3H, H_3O^+ and nH_2O, $1 \leq n \leq 3$, as model systems. The equilibrium structures obtained from DFT calculations suggested at least two structural diffusion mechanisms at the –SO_3H group namely, the "pass-through" and "pass-by" mechanisms. The former involves the protonation and deprotonation at the -SO_3H group, whereas the latter the proton transfer in the adjacent Zundel complex. Analyses of the asymmetric O-H stretching frequencies (ν^{OH}) of the hydrogen bond (H-bond) protons showed the threshold frequencies (ν^{OH*}) of proton transfer in the range of 1700 to 2200 cm^{-1}. Born-Oppenheimer Molecular Dynamics (BOMD) simulations at 350 K anticipated slightly lower threshold frequencies ($\nu_A^{OH*,MD}$), with two characteristic asymmetric O-H stretching frequencies being the spectral signatures of proton transfer in the H-bond complexes. The lower frequency ($\nu_A^{OH,MD}$) is associated with the oscillatory shuttling motion and the higher frequency ($\nu_B^{OH,MD}$) the structural diffusion motion. Analyses of the BOMD results indicated that the -SO_3H group promotes proton transfer by reducing the vibrational energy for the interconversion between the two dynamic states ($\nu_{BA}^{OH,MD}$), resulting in a higher population of the H-bond with the structural diffusion motion. The present theoretical results showed the possibility to discuss quantitatively the tendency of proton transfer using $\nu_{BA}^{OH,MD}$, and the necessity to include the thermal energy fluctuations and dynamics in the model calculations.

1. Introduction

Polymer electrolyte membrane widely used in proton exchange membrane fuel cells (PEMFC) is Nafion®.[1-2] Nafion® consists of Teflon® backbone and randomly attached hydrophilic side chains. The backbone and side chains of Nafion® are terminated by trifluoromethanesulfonic (triflic) acid groups. Experiments have shown that the triflic acid groups ($-CF_2SO_3H$) are preferentially hydrated, resulting in large interconnected hydrophilic domains which play important roles in proton transfer reactions.[3] Although some basic information has been accumulated in the past decades, mechanisms of proton transfer reactions in Nafion®, especially at the molecular level, are not well understood.[4-7]

Proton transfer reactions in minimally hydrated PEM were studied by molecular dynamic (MD) simulations of triflic acid monohydrate solid ($(CF_3SO_3H_3O^+)_4$).[8] The MD results showed a relay-type mechanism with a proton defect representing an intermediate state in the proton transfer pathway. The proton defect involves formation of the Zundel complex ($H_5O_2^+$) and the reorganization of the neighboring $-SO_3^-$ groups which share a proton between the oxygen atoms of the anionic sites. The proposed mechanism revealed a possibility for proton transfer along the hydrophilic head groups, $-SO_3H$ and $-SO_3^-$.

Similar theoretical study was reported on short-side-chain perfluorosulfonic acids, in which large scale density functional theory (DFT) calculations were performed on fragments of Nafion®, with and without water molecules and with distinct pendant chain separations.[9-11] The B3LYP/6-311G(d,p) results revealed a possibility for proton transfer between two adjacent hydrophilic groups, along the hydrogen bond (H-bond) networks of water connecting them. The proposed proton transfer pathway is mediated by formation of the -S-O..H..O-H H-bond and $H_5O_2^+$.[9] It was concluded that,[10-11] the number of water molecules required to promote proton dissociation could be reduced when the $-SO_3H$ groups are brought closer to each other, through conformational changes in the backbone.

The number of water molecules required to promote proton dissociation at the $-SO_3H$ group was also investigated in ref. 12, using on the H-bond complexes formed from $CF_3CF_2SO_3H$ and nH_2O, $1 \le n \le 4$. *Ab initio* calculations and MD simulations revealed that, for n = 3, the neutral and ion-pair complexes are close in energy and are accessible in the fluctuation dynamics of proton transport. Whereas for $n \le 2$, the only relevant complex is the neutral form. Most importantly, it was reported based on the free energy surfaces of proton exchange that, the $CF_3CF_2SO_3H_2^+ - H_2O$ and $CF_3CF_2SO_3H - H_3O^+$ complexes are nearly isoenergetic and $CF_3CF_2SO_3H_2^+$ could play important roles in proton transfer reactions at low hydration levels.[12]

Proton transfer reactions at the –SO_3H group of Nafion® were investigated at low hydration levels, using the complexes formed from CF_3SO_3H, H_3O^+ and nH_2O, $1 \le n \le 3$, as the model systems.[13] With the emphasis on how $-SO_3H$ facilitates or mediates transportation of an excess proton, a series of BOMD simulations was conducted at 298 K, from which the intermediate states in the proton transfer pathways were identified, analyzed and categorized. It was found that the proton transfer reactions at -SO_3H are not concerted due to the thermal energy fluctuation and the existence of quasi-dynamic equilibriums between the Zundel and Eigen complexes, and the -SO_3H group could directly and indirectly mediate the proton transfer reactions through the formation of proton defects, as well as the $-SO_3^-$ and $-SO_3H_2^+$.

Since one of the most important evidence of H-bond formation in aqueous solution is the red shift of the high-frequency hydroxyl (O-H) stretching mode, accompanied by its intensity increase and band broadening,[14-16] attempt was made to correlate the O-H stretching frequency with the tendency of proton transfer in H-bond;[16-18] the broad and intense IR absorption bands ranging from 1000 to 3000 cm^{-1} were interpreted as spectral signatures of protonated water networks,[18] whereas the tendency of proton transfer was measured from strong red shift of the asymmetric O-H stretching frequency (ν^{OH}), compared with the corresponding “free” or “non-H-bonded” one.[16] However, the red shift cannot be detected easily in experiments due to the coupling and overlapping of various vibrational modes, as well as the detection limit of IR

equipment.[19-21] In order to estimate the tendency of proton transfer in term of ν^{OH}, the classical interpretations of IR stretching frequencies for concentrated acid solutions were employed as criteria;[22] the IR stretching frequencies for the H-bond proton are divided into three groups namely, the internal (1300 - 2200 cm^{-1}), external (2500 - 3200 cm^{-1}), and outerlayer groups (3300 - 3400 cm^{-1}). The H-bond proton in the internal group is considered to be susceptible to proton transfer.

For protonated water clusters,[23] DFT calculations revealed that the intermediate states in proton transfer pathways consist of the Zundel complex, with the threshold asymmetric O-H stretching frequencies (ν^{OH*}) in the gas phase and aqueous solution at ν^{OH*} = 1984 and 1881 cm^{-1}, respectively. Born-Oppenheimer MD (BOMD) simulations predicted slightly lower threshold frequencies, $\nu^{OH*,MD}$ = 1917 and 1736 cm^{-1}, respectively, with two characteristic asymmetric O-H stretching frequencies ($\nu^{OH,MD}$) being the IR spectral signatures of proton transfer. The lower-frequency band ($\nu_A^{OH,MD}$) could be associated with the "oscillatory shuttling motion", whereas the higher-frequency bands ($\nu_B^{OH,MD}$) with the "structural diffusion motion". [23]

In the present work, proton transfer reactions at the -SO_3H group of Nafion® were further investigated, using the complexes formed from CF_3SO_3H, H_3O^+ and nH_2O, $1 \le n \le 3$, as the model systems.[13] Since the dynamics of proton transfer can be characterized by vibrational behavior of the transferring proton, attempt was made to correlate the tendency of proton transfer with characteristic IR frequencies of H-bond,[24-25] Based on the theoretical results in the gas phase and continuum aqueous solution, dynamics and mechanisms, as well as the IR spectral signatures, of proton transfer in the model systems were analyzed and discussed, in comparison with available theoretical and experimental data of the same and similar systems.

2. Computational methods

Since proton transfer reactions are complex, care must be exercised in selecting model systems and theoretical methods. Our previous experience showed that reactions and dynamics of proton transfer reactions can be studied reasonably well using small model systems, with the following three basic steps;[13] (1) searching for all important

equilibrium structures and intermediate states in the proton transfer pathways using appropriate pair potentials; (2) refining of the computed structures using accurate quantum chemical method; (3) BOMD simulations starting from the refined structures. These three basic steps were also adopted in the present investigations,

Since including many water molecules in the model systems could lead to difficulties in the analyses of proton transfer reactions, it was the strategy of the previous and present work to restrict the number of water molecules to $1 \leq n \leq 3$. This is justified by B3LYP/6-31G(d,p) calculations which showed that no proton transfer took place until three water molecules were included in the model systems.[26-27] In the present work, to account for the effects of the extended H-bond networks of water, a conductor-like screening model (COSMO) with the dielectric constant (ε) of 78 was included in the model calculations.

Static properties

Equilibrium structures and IR spectra

The equilibrium structures of the H-bond complexes formed from CF_3SO_3H, H_3O^+ and H_2O [13] were reoptimized using the DFT method, both in the gas phase and continuum aqueous solution. In order to obtain reliable spectroscopic results, a tight SCF energy convergence criterion (less than 10^{-8} au), with the maximum norm of Cartesian gradients less than 10^{-4} au, was adopted in the DFT geometry optimizations. DFT calculations were performed using the B3LYP hybrid functional,[28-29] with the triple-zeta valence basis sets augmented by polarization functions (TZVP).[30] The performance of B3LYP calculations and the TZVP basis sets on similar systems was discussed in details.[20, 31] In the present work, B3LYP/TZVP calculations were conducted using TURBOMOLE 6.0 software package.[32-33]

The interaction energies (ΔE) of the H-bond complexes were computed from $\Delta E = E(CF_3SO_3H - H_3O^+ - nH_2O) - [E(CF_3SO_3H) + E(H_3O^+) + nE(H_2O)]$;[23]where $E(CF_3SO_3H - H_3O^+ - nH_2O)$ are the total energies of the H-bond complexes; $E(CF_3SO_3H)$, $E(H_3O^+)$ and $E(H_2O)$ the total energies of the isolated molecules at

their optimized structures. The energetic effects of the continuum aqueous solvent (COSMO with ε = 78) were estimated from the solvation energy (ΔE^{sol}); $\Delta E^{sol} = E(CF_3SO_3H - H_3O^+ - nH_2O)^{COSMO} - E(CF_3SO_3H - H_3O^+ - nH_2O)$; where $E(CF_3SO_3H - H_3O^+ - nH_2O)^{COSMO}$ and $E(CF_3SO_3H - H_3O^+ - nH_2O)$ are the total energies of the H-bond complexes, obtained from B3LYP/TZVP calculations with and without COSMO, respectively.

In order to discuss the tendency of proton transfer through the structural diffusion mechanism, the "asymmetric stretching coordinate"[24-25] and a concept of the "most active" H-bond were used.[34] Within the framework of the most active H-bond, the asymmetric stretching coordinate of a donor (D) - acceptor (A) pair in the A-H..B H-bond is defined by $\Delta d_{DA} = | d_{A-H} - d_{B..H} |$, where d_{A-H} and $d_{B..H}$ are the A-H and B..H distances, respectively. The H-bond with small Δd_{DA} is considered to be active and susceptible to proton transfer. According to Δd_{DA}, the H-bond proton in $H_5O_2^+$ is the most active, since the H-bond proton is equally shared by two water molecules. Δd_{DA} obtained from B3LYP/TZVP calculations were plotted as a function of the H-bond distances (R_{O-O}).

The H-bond susceptible to proton transfer can also be characterized by low to nonexistence energy barrier along the proton transfer coordinate. This is manifested by a broad IR band with the asymmetric O-H stretching frequency (ν^{OH}) lower than a threshold frequency (ν^{OH*}).[23] In the present work, based on the well-optimized H-bond structures, harmonic IR frequencies were computed from numerical second derivatives, from which the analyses of normal modes in terms of internal coordinates were made. NUMFORCE and AOFORCE programs, included in TURBOMOLE 6.0 software package, were employed in the second derivative calculations and normal mode analyses, respectively. Since the vibrational frequencies obtained from quantum chemical calculations are generally overestimated compared to experiments, a scaling factor, which partially accounts for anharmonicities and systematic errors, had to be applied; the scaling factor of 0.9614[35] was shown to be appropriate for B3LYP/TZVP calculations.[23, 25] In order to alternatively discuss the tendency of proton transfer in H-bond, ν^{OH} were plotted as a function of R_{O-O}, and ν^{OH*} were determined from the plot of ν^{OH} and Δd_{DA}.[23]

Dynamic properties

Quantum MD simulations

Elementary reactions and dynamics of rapid covalent bond formation and cleavage can be studied reasonably well using theoretical approaches that incorporate quantum chemical methods into MD simulations,[36] among which BOMD simulations have been widely used.[13, 23, 25, 37-38] Within the framework of BOMD simulations, classical equations of motions of nuclei on the Born-Oppenheimer (BO) surfaces are integrated, whereas forces on nuclei are calculated in each MD step from quantum energy gradients, with the molecular orbitals (MOs) updated by solving Schroedinger equations in the BO approximation; the nuclei thus undergo classical Newtonian dynamics on quantum potential hypersurface. BOMD simulations are therefore more accurate, as well as considerably CPU time consuming, compared to classical MD simulations, in which forces on nuclei are determined from predefined empirical or quantum pair potentials. Our experience showed that BOMD simulations with the DFT method represent an appropriate combination, due to the optimal accuracy versus CPU times.[13, 23, 25] Therefore, BOMD simulations with the B3LYP/TZVP calculations were adopted in the present investigations.

Since proton transfer reactions especially in aqueous solution involve dynamic processes with different timescales,[39-41] the complexity of proton transfer processes could be reduced by selecting an appropriate timestep, from which the classical dynamic equations are solved. The observation that the actual proton transfer takes place in femtosecond (fs) timescale,[40] which is generally faster than solvent structure reorganization,[39] makes it reasonable to perform MD simulations by focusing only on short-lived phenomena. Our previous BOMD results showed that, for small H-bond clusters, only few structure reorganization took place within the simulation length of 1-2 ps.[13, 25]

All the equilibrium structures, including potential intermediate states, obtained from the B3LYP/TZVP geometry optimizations were employed as starting configurations in BOMD simulations at 350 K, using canonical ensemble (NVT) with a Nosé-

Hoover chain thermostat applied to each degree of freedom in the model system. Since, in aqueous solution, rapid interconversion between the Zundel and Eigen complexes takes place within 100 fs,[41] the timestep used in solving dynamic equations was set to 1.0 fs. In each BOMD simulations, 500 fs was spent on equilibration, after which 4000 fs was devoted to property calculations. These choices are justified by BOMD simulations on $H_5O_2^+$ and $H_7O_3^+$,[20] from which insights into fast dynamic processes in H-bonds (*e.g.* H-bond structures and IR spectra) could be obtained from relatively short BOMD trajectories (about 2 ps). All BOMD simulations were performed using FROG program included in TURBOMOLE 6.0;[32-33] FROG program employs the Leapfrog Verlet algorithm to turn the electronic potential energy gradients into new atomic positions and velocities.

Remarks should be made on the ensemble and simulation length chosen in the present study. The applicability and performance of NVE and NVT BOMD simulations on small H-bond chains were investigated and discussed in details.[42] For NVE BOMD simulations, it was demonstrated that the potential energy of the system decreases quite rapidly in the course of BOMD simulations. Once the proton stays at the center of the H-bond, the potential energy is at the lowest point and the proton is trapped in the minimum; no proton transfer can be observed in the later timesteps. Since NVE BOMD simulations are conducted at constant energy, a decrease in the potential energy is accompanied by an increase in the kinetic energy, as well as temperature, leading to the H-bond structure reorganization and fragmentation. For NVT BOMD simulations, the energy released during the proton transfer processes can be absorbed by the thermostat bath, allowing the H-bond structure and local temperature to be maintained for a longer time (2-5 ps), depending upon the size and the complexity of the H-bond structure. Thus, NVT BOMD simulations are more appropriate for the present investigations.

IR spectra and diffusion coefficients

Since proton transfer reactions in H-bond are strongly coupled with various degrees of freedom,[4, 25, 43] attention was focused on the symmetric and asymmetric O-H stretching modes, as well as the O-O vibrations. In the present work, the IR spectra of

the transferring protons were computed from BOMD simulations by Fourier transformations of the velocity autocorrelation function (VACF).[44] This approach is appropriate as it allows the coupled vibrations to be distinguished, characterized and analyzed separately. Fourier transformations of VACF were made within a short time limit of 100 fs.[25] This is supported by the observation that the average lifetime of the most important intermediate state, the Zundel complex, is about 100 fs.[41]

The diffusion coefficients (D) of the transferring proton were computed from BOMD simulations using the Einstein relation,[45-46] for which D are determined from the slope of the mean-square displacements (MSD). Because the transferring proton is confined in a short H-bond distance, care must be exercised in selecting the time interval in which MSD and D are computed.[46] Our experience showed that linear relationship between MSD and simulation time could be obtained when the time intervals are not larger than 0.5 ps.[23, 25]

3. Results and discussion

In this section, all important theoretical results are discussed in comparison with available theoretical and experimental data. The static results obtained from B3LYP/TZVP calculations are analyzed and used as guidelines for the interpretations of the BOMD results. The emphases are on the effects of the -SO_3H group on the H-bond structures, IR spectra and dynamics of proton transfer in the Zundel complex, as well as the protonation and deprotonation at the -SO_3H group.

Static results

Equilibrium structures, energetic and IR spectra

The equilibrium structures, ΔE, ΔE^{sol} and $R_{O\text{-}O}$ of the $CF_3SO_3H\text{-}H_3O^+ - nH_2O$ complexes, $1 \le n \le 3$, in the gas phase and continuum aqueous solution are shown in Table 1, together with Δd_{DA} and ν^{OH}. The trends of ΔE and ΔE^{sol} with respect to the number of water molecules are presented in Fig. 1.

The environmental effects on the stabilities of charged H-bonds were investigated using *ab initio* SCRF (self-consistent reaction field) calculations at the Hartree-Fock level, from which the dependence of ΔE on a wide range of dielectric constant (ε) was established.[47] It was demonstrated that small increases in ε from the gas-phase value ($\varepsilon=1$) rapidly reduce the stabilities of the charged H-bonds. The trends of ΔE with respect to the number of water molecules in the gas phase and continuum aqueous solutions are similar, with smaller variations in continuum aqueous solution. The destabilization effects caused by the continuum aqueous solvent are quite large, ranging from 120 kJ/mol in the $CF_3SO_3H-H_3O^+$ complex to 235 kJ/mol in the $CF_3SO_3H-H_3O^+-3H_2O$ complex. Fig. 1 reveals that ΔE^{sol} are not substantially different for the H-bond complexes with the same number of water molecules; when the number of water molecules is the same, the H-bonds inside the clusters experience comparable uniform electric field (COSMO).

The results in Table 1 anticipated three $CF_3SO_3H-H_3O^+-H_2O$ complexes as the most basic intermediate states in proton transfer pathways.

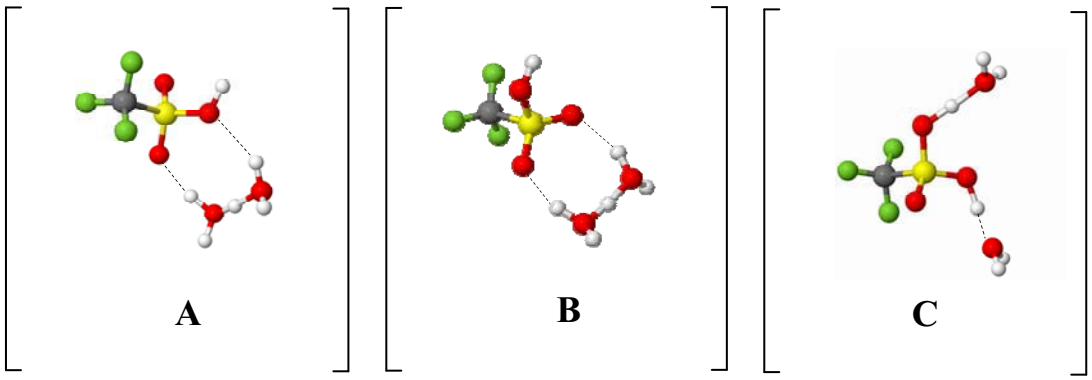

Structures **A** and **B** are represented by the Zundel complex H-bonding at two oxygen atoms of the $-SO_3H$ group. In structure **C**, $-SO_3H$ separates H_3O^+ and H_2O. The H-bonding features in structures **A**, **B** and **C** suggested two important structural diffusion mechanisms at the $-SO_3H$ group. Since the $-SO_3H$ group in structure **C** could be protonated or deprotonated and directly involved in proton transfer, one could regard the structural diffusion through structure **C** as the "pass-through" mechanism. Likewise, since the energetic and dynamics of the proton in the Zundel complex can be affected by the $-SO_3H$ group, one could consider the proton transfer through structures **A** and **B** as the "pass-by" mechanism.

In order to simplify the discussion, the H-bond structures in Table 1 are labeled with three or four-character code; according to the basic intermediate states (**A**, **B** or **C**); the number of water molecules (***n***) in the gas phase (**G**) or continuum aqueous solution (**C**); different H-bond structures with the same basic intermediate states and number of water molecule are distinguished by **[*m*]**. As examples, based on the four-character code, **A2G-[1]** and **A2G-[2]** represent different H-bond structures with the same number of water molecules in the gas phase, whereas **A2G-[1]** and **A2C-[1]**, the same H-bond structures with two water molecules in the gas phase and continuum aqueous solution, respectively.

Attempt was made to distinguish between normal and strong H-bonds in the protonated water clusters.[23] B3LYP/TZVP calculations showed that the "critical distance" (R^{*}_{O-O}), the H-bond distance at which symmetric double-well potential with a barrier at the center is transformed into single-well potential without barrier, and the threshold asymmetric O-H stretching frequencies for proton transfers (ν^{OH*}) could be approximated from the plots of Δd_{DA} and R_{O-O}, ν^{OH} and R_{O-O}, and ν^{OH} and Δd_{DA}. The relationship between Δd_{DA} and R_{O-O} could be represented by a linear function, ν^{OH} and R_{O-O} by an exponential function similar to the integrated rate expression for the first order reaction, and ν^{OH} and Δd_{DA} by an exponential function resembling the normal distribution function. For the protonated water clusters,[23] calculations of the second derivatives of the plots of ν^{OH} and Δd_{DA} yielded two inflection points, in the gas phase at Δd^{*}_{DA} = 0.33 Å and in continuum aqueous solution at Δd^{*}_{DA} = 0.36 Å. The values correspond to ν^{OH*} = 1984 and 1881 cm^{-1}, respectively.

In the present study, to estimate ν^{OH*}, Δd_{DA} and R_{O-O}, ν^{OH} and R_{O-O} and ν^{OH} and Δd_{DA} for the pass-through mechanism were plotted and shown in Fig. 2a to 2c, respectively, whereas for the pass-by mechanism in Fig. 2d to 2f, respectively. The corresponding fitted functions are given in Table 2. For the pass-through mechanism in the gas phase, the inflection point is seen in Fig. 2c at ν^{OH*} = 2162 cm^{-1} and Δd^{*}_{DA} = 0.36 Å, and in continuum aqueous solution at ν^{OH*} = 2001 cm^{-1} and Δd^{*}_{DA} = 0.36 Å. For the pass-by mechanism, Fig. 2f shows the inflection points in the gas phase at ν^{OH*} = 1829 cm^{-1} and Δd^{*}_{DA} = 0.29 Å, and in continuum aqueous solution at ν^{OH*} =

1714 cm^{-1} and Δd^{*}_{DA} = 0.30 Å. Comparison ν^{OH*} of the transferring protons in the pass-by mechanism and those of the protonated water clusters[23] suggested red-shifts of about 200 cm^{-1} due to the presence of the -SO_3H group.

Although the H-bond structures in the gas phase and continuum aqueous solution are approximately the same, the trends of proton transfers are quite different. Δd_{DA} and ν^{OH} in Table 1 reveals that the -SO_3H group is not preferentially dissociated in the gas phase, whereas in continuum aqueous solution, -SO_3H deprotonates, resulting in -SO_3^- in close contact with H_3O^+, with the highest tendency of proton dissociation in structure **A2C-[1]** (Δd_{DA} = 0.06 Å and ν^{OH} = 905 cm^{-1}). Δd_{DA} and ν^{OH} obtained from B3LYP/TZVP calculations indicates that, in continuum aqueous solution, structure **A2C-[2]** possesses the highest tendency of proton transfer through the pass-by mechanism (Δd_{DA} = 0.07 Å and ν^{OH} = 823 cm^{-1}).

As in the case of IR experiments,[14-16] Table I showed that ν^{OH} vary in a quite wide range; in the gas phase from 1100 to 3500 cm^{-1}, in continuum aqueous solution from 820 to 3600 cm^{-1}. In order to resolve these broad IR frequencies, the H-bonds in Table 1 were divided into two groups; the ones connecting directly to the -SO_3H or -SO_3^- group belong to **Group 1** (potentially involved in the pass-through mechanism) and those in the adjacent Zundel complex to **Group 2** (potentially involved in the pass-by mechanism). Investigation of the protonic states, reflected from the H-bond structures and ν^{OH} in Table 1, allowed the H-bonds in **Group 1** and **2** to be further divided into six subgroups. The definitions of the groups and subgroups are summarized as follows:

Group 1 H-bonds connecting directly to the -SO_3H or -SO_3^- group. (potentially involved in the pass-through mechanism)

Subgroup (I) Cyclic H-bonds between the Zundel complex and two oxygen atoms of -SO_3H or -SO_3^-, *e.g.* H-bonds **(1)** and **(3)** in structures **A1C** and **B1C**.

Subgroup (II) Linear H-bond between an oxygen atom of the -SO_3H or -SO_3^- group and H_3O^+, $H_5O_2^+$ or H_2O, *e.g.* H-bonds **(1)** and **(2)** in structure **C1C**.

Subgroup (III) Subgroup (II) with the H-bond proton nearly equally shared between the donor and acceptor, *e.g.* H-bond **(4)** in structure **A2C-[1]** and H-bond **(2)** in structure **C2C**.

Group 2 H-bonds in the adjacent Zundel complex. (potentially involved in the pass-by mechanism)

Subgroup (IV) H-bond in the H_3O^+- H_2O complex, *e.g.* H-bond **(3)** in structure **C2G** and **C3G**.

Subgroup (V) H-bond in the Zundel complex in the structure with Subgroup (II) *e.g.* H-bond **(3)** in structures **C2C** and **C3C**.

Subgroup (VI) H-bond of the Zundel complex in the structure with Subgroup (I), *e.g.* H-bond **(2)** in structures **A1C** and **B1C**.

The ranges of ν^{OH} for the H-bond protons in **Group 1** and **2**, as well as Subgroup (I) to (VI), are compared in Fig. 3a and 3b, in the gas phase and continuum aqueous solution, respectively.

Dynamic results

In the present work, the neglect of extensive H-bond networks in the vicinities of the solute (CF_3SO_3H), as well as the thermal energy fluctuations and dynamics in BOMD simulations, made it difficult to analyze all the dynamics in the CF_3SO_3H-H_3O^+-H_2O complexes. Therefore, attention was focused on the H-bond protons in the intermediate states.

Average H-bond structures and IR spectra

Before the dynamics in the CF_3SO_3H-H_3O^+-H_2O complexes are discussed, the characteristic vibrations in the protonated water clusters have to be analyzed.[23] The IR spectra of the H-bond proton in the Zundel complex obtained from BOMD simulations at 350 K are illustrated as examples in Fig. 4a and 4b, in the gas phase and continuum aqueous solution, respectively. For the transferring proton (ν^{OH} lower than ν^{OH*}), the static proton transfer potential (B3LYP/TZVP calculations) yielded

only one asymmetric O-H stretching band, whereas BOMD simulations predicted in addition a higher frequency band. The two bands are labeled with **A** and **B** in Fig. 4a and 4b. Since the lower frequency ($\nu_A^{OH,MD}$) could be associated with the oscillatory shuttling motion and the higher frequency ($\nu_B^{OH,MD}$) with the structural diffusion motion,[23] the vibrational energy for the interconversion between the two dynamic states can be estimated from the difference between $\nu_B^{OH,MD}$ and $\nu_A^{OH,MD}$, denoted by $\Delta\nu_{BA}^{OH,MD}$, and the relative probability of finding these characteristic motions in the course of BOMD simulations can be approximated in principle from the ratio of the IR intensities at **B** ($\mathbf{I_B}$) and **A** ($\mathbf{I_A}$);[23] the lower $\mathbf{I_B/I_A}$ the higher the probability of finding the oscillatory shuttling motion. It should be mentioned that the discussion on $\Delta\nu_{BA}^{OH,MD}$ and $\mathbf{I_B/I_A}$ is meaningful only when the H-bond considered is susceptible to proton transfer, $\nu_A^{OH,MD}$ lower than $\nu_A^{OH,MD*}$.

The intensities of the IR bands at **A** and **B** in Fig. 4a and 4b showed that the oscillatory shuttling motion dominates in the Zundel complex, especially in continuum aqueous solution; in the gas phase, $\mathbf{I_B/I_A}$ = 0.5, whereas in continuum aqueous solution $\mathbf{I_B/I_A}$ = 0.1. The trend of $\mathbf{I_B/I_A}$ in the gas phase and continuum aqueous solution can be explained using $\Delta\nu_{BA}^{OH,MD}$; in the gas phase, $\Delta\nu_{BA}^{OH,MD}$ = 724 cm^{-1} and in continuum aqueous solution, $\Delta\nu_{BA}^{OH,MD}$ = 808 cm^{-1}. The latter reflects a higher vibrational energy for the interconversion between the oscillatory shuttling and structural diffusion motions, resulting in higher population of the oscillatory shuttling motion for the Zundel complex in continuum aqueous solution. It should be noted that, due to short BOMD simulation length, $\mathbf{I_B/I_A}$ cannot be determined precisely. Therefore, attempt was made to alternatively estimate the relative population of the oscillatory shuttling and structural diffusion motions from $\Delta\nu_{BA}^{OH,MD}$. For the protonated water clusters, an interesting relationship was observed from the plot of $\Delta\nu_{BA}^{OH,MD}$ and $<\Delta d_{DA}>$. Together with the plot of the standard deviations of the O-H distances ($\sigma_{R_{O-H}}$) and $<\Delta d_{DA}>$, energetic aspects of the two characteristic vibrations in the protonated water cluster could be studied as follows.

The plots of $\sigma_{R_{O-H}}$ and $<\Delta d_{DA}>$ and $\Delta\nu_{BA}^{OH,MD}$ and $<\Delta d_{DA}>$ are shown in Fig. 4c and 4d, respectively. Due to the thermal energy fluctuations and dynamics, $\sigma_{R_{O-H}}$ and $\Delta\nu_{BA}^{OH,MD}$ in the gas phase and continuum aqueous solution are not well separated.

Therefore, the discussion on the relative population of the oscillatory shuttling and structural diffusion was made based on the combined data sets. It appeared that, for the protonated water clusters, $\sigma_{R_{O-H}}$ decreases exponentially with $<\Delta d_{DA}>$, confirming that the oscillatory shuttling motion dominates in the H-bond with small $<\Delta d_{DA}>$, whereas $\Delta\nu_{BA}^{OH,MD}$ decreases exponentially with $<\Delta d_{DA}>$ and reaches a minimum at $<\Delta d_{DA}>$ = 0.28 Å ($<R_{O-O}>$ = 2.46.Å), corresponding to the lowest vibrational energy for the interconversion between the oscillatory shuttling and the structural diffusion motions, $\Delta\nu_{BA}^{OH,MD}$ = 473 cm^{-1} or 5.7 kJ/mol. Since the probability of finding a physical system being in a certain energy state is proportional to the Boltzmann factor, the probability of finding the structural diffusion motion relative to the oscillatory shuttling motion ($\mathbf{P_B/P_A}$) is proportional to $e^{-\Delta\nu_{BA}^{OH,MD}/RT}$. For the protonated water clusters, the plot of $\mathbf{P_B/P_A}$ and $<\Delta d_{DA}>$, shown in Fig. 4e, suggested the maximum probability of finding the structural diffusion vibration, relative to the oscillatory shuttling vibration, $\mathbf{P_B/P_A}$ = 0.17 at $<\Delta d_{DA}>$ = 0.27 Å. At larger $<\Delta d_{DA}>$, the H-bond becomes weaker and $\mathbf{P_B/P_A}$ decreases, especially when $\nu_A^{OH,MD}$ larger than $\nu_A^{OH,MD*}$.

For the CF_3SO_3H-H_3O^+-H_2O complexes, the average H-bond structures, $<R_{O-O}>$ and $<\Delta d_{DA}>$ obtained from BOMD simulations at 350 K are summarized in Table 2, together with $\nu_B^{OH,MD}$, $\nu_A^{OH,MD}$ and the proton diffusion coefficients (D). The H-bonds susceptible to proton transfers are designated by asterisk. The plots between $<\Delta d_{DA}>$ and $<R_{O-O}>$, $\nu_A^{OH,MD}$ and $<R_{O-O}>$ and $\nu_A^{OH,MD}$ and $<\Delta d_{DA}>$ for the pass-through mechanism are shown in Fig. 5a to 5c, respectively, and for the pass-by mechanism in Fig. 5d to 5f, respectively. All the fitted functions can be sent on request.

Since BOMD simulations were conducted in a short period of time, the average H-bond structures are not substantially different from the B3LYP/TZVP results. Comparison of $\nu_A^{OH,MD}$ in Table 2 with ν^{OH} in Table 1 showed a general trend. The inclusion of the thermal energy fluctuations and dynamics in the model calculations brought about red shifts of the oscillatory shuttling bands both in the gas phase and continuum aqueous solution, except for structures **A2C-[1]**, **A2C-[2]** and **A3C-[2]** in continuum aqueous solutions; B3LYP/TZVP calculations predicted the H-bonds **(4)** and **(2)** in structures **A2C-[1]** and **A2C-[2]** to possess the highest tendencies of proton

transfer through the pass-through and pass-by mechanisms, respectively, whereas coupling among various modes of vibrations in BOMD simulations led to blue shifts of only 43 and 52 cm^{-1}, respectively.

Similar trends were observed when Fig. 5 is compared with Fig. 2. According to the thermal energy fluctuations and dynamics, as well as coupling among various modes of vibrations, the results in the gas phase and continuum aqueous solution are not well separated. For the pass-through mechanism in Fig. 5c, the inflection points are seen at $\nu_A^{OH^*,MD}$ = 1656 and 1684 cm^{-1}, respectively, whereas for the pass-by mechanism in Fig. 5f at $\nu_A^{OH^*,MD}$ = 1733 and 1741 cm^{-1}, respectively. The latter are 290 and 104 cm^{-1} lower than the corresponding values for the protonated water clusters. [23] These are the energetic evidences for the promotion of proton transfer by the -SO_3H group.

$\Delta\nu_{BA}^{OH,MD}$ and $\mathbf{P_B/P_A}$ for the H-bond protons in the CF_3SO_3H-H_3O^+-H_2O complexes are included in Table 2. Examples of the characteristic asymmetric O-H stretching bands for the H-bond protons in the pass-through and pass-by mechanisms obtained from BOMD simulations at 350 K are shown in Fig. 6a and 6e, respectively. For the pass-through mechanism, the plots of $\sigma_{R_{O-H}}$ and $<\Delta d_{DA}>$, $\Delta\nu_{BA}^{OH,MD}$ and $<\Delta d_{DA}>$, and $\mathbf{P_B/P_A}$ and $<\Delta d_{DA}>$ are illustrated in Fig. 6b to 6d, respectively, and for the pass-by mechanism in Fig. 6f to 6h respectively. The fitted functions for the pass-through and pass-by mechanisms can be obtained on request.

All the outstanding features discussed in the protonated water clusters were observed in the CF_3SO_3H-H_3O^+-H_2O complexes. For the pass-through mechanism, $\Delta\nu_{BA}^{OH,MD}$ in Fig. 6c decreases exponentially with $<\Delta d_{DA}>$ and reaches a minimum at $\Delta\nu_{BA}^{OH,MD}$ = 469 cm^{-1}, corresponding to the maximum value of $\mathbf{P_B/P_A}$ of 0.17. For the pass-by mechanism, due to the presence of the -SO_3H group, the vibrational energy for the interconversion between the oscillatory shuttling and the structural diffusion motions are decreased, from $\Delta\nu_{BA}^{OH,MD}$ = 473 cm^{-1} in the protonated water clusters to $\Delta\nu_{BA}^{OH,MD}$ = 398 cm^{-1} in the CF_3SO_3H-H_3O^+-H_2O complexes. This is accompanied by an increase in the population of the structural diffusion motion in the CF_3SO_3H-H_3O^+-H_2O complexes, from $\mathbf{P_B/P_A}$ = 0.17 to 0.21, respectively.

Dynamics of proton transfer and diffusion coefficients

In order to discuss the rate of proton transfer at and in the vicinities of the -SO_3H group, distributions of the proton diffusion coefficients (D) in the $CF_3SO_3H - H_3O^+ - H_2O$ complexes in the gas phase and continuum aqueous solution were computed and shown in Fig. 7, with the emphasis on the H-bonds susceptible to proton transfer ($<\Delta d_{DA}>$ lower than $<\Delta d^*_{DA}>$). It appeared that D can vary in a quite wide range, with the maxima at 2.5×10^{-5} and 3.2×10^{-5} cm^2 s^{-1}, in the gas phase and continuum aqueous solution, respectively, indicating a slightly higher mobility of proton in the gas phase. The H-bond structures and the values of D in Table 2 revealed only the pass-by mechanism for D $=2.5\times10^{-5}$ cm^2 s^{-1}. Whereas, in continuum aqueous solution the contribution of the pass-through and pass-by mechanisms.

4. Conclusion

Proton transfer reactions and dynamics at a hydrophilic group of Nafion® were investigated at low hydration levels using the complexes formed from CF_3SO_3H, H_3O^+ and nH_2O, $1 \leq n \leq 3$, as model systems. The theoretical investigations began with calculations of the equilibrium structures and interaction energies of the model molecules in the gas phase and continuum aqueous solution, using the DFT method at B3LYP/TZVP level of accuracy. The H-bond structures, asymmetric stretching coordinates (Δd_{DA}) and asymmetric O-H stretching frequencies (ν^{OH}) obtained from B3LYP/TZVP calculations were analyzed and categorized. The B3LYP/TZVP results suggested two types of structural diffusion mechanisms namely, the pass-through mechanism, involving the protonation and deprotonation at the $-SO_3H$ group, and the pass-by mechanism, the proton transfer in the adjacent Zundel complex. The plots of ν^{OH} and Δd_{DA} predicted the threshold frequencies (ν^{OH*}) for the proton transfers through the pass-through mechanism at 2162 and 2001 cm^{-1}, in the gas phase and continuum aqueous solution, respectively, whereas for the pass-by mechanism at 1829 and 1714 cm^{-1}, respectively. The latter are about 200 cm^{-1} lower than the protonated water clusters, a spectroscopic evidence for the promotion of proton transfer in the Zundel complex by the $-SO_3H$ group.

Inclusion of the thermal energy fluctuations and dynamics in the model calculations made it difficult to differentiate the trends of the results in the gas phase and continuum aqueous solution. For the pass-by mechanism, BOMD simulations at 350 K predicted similar characteristic asymmetric O-H stretching frequencies ($\nu_A^{OH,MD}$), with slightly lower threshold frequencies for proton transfer, $\nu_A^{OH*,MD}$ = 1733 and 1740 cm^{-1}, respectively. In addition, BOMD simulations yielded another asymmetric O-H stretching band at higher frequency ($\nu_B^{OH,MD}$). As in the case of the protonated water clusters, $\nu_A^{OH,MD}$ and $\nu_B^{OH,MD}$ are associated with the oscillatory shuttling and structural diffusion motions, respectively, the characteristic motions of proton transfers in H-bonds. The analyses of $\nu_A^{OH,MD}$ and $\nu_B^{OH,MD}$ yielded the vibrational energies for the proton transfer ($\Delta\nu_{BA}^{OH,MD}$) through the pass-through and pass-by mechanisms of 469 and 398 cm^{-1}, respectively. The latter is about 75 cm^{-1} lower than the protonated water clusters, a decrease of the vibrational energy for the

interconversion between the oscillatory shuttling and structural diffusion motions by the $–SO_3H$ group.

The present study confirmed again that, due to the coupling among various vibrational modes, the discussions on proton transfer reactions cannot be made based solely on static proton transfer potentials. Inclusion of thermal energy fluctuations and dynamics in the model calculations, as in the case of BOMD simulations, together with systematic IR spectral analyses, has been proved to be the most appropriate theoretical approaches.

Acknowledgement

The authors would like to acknowledge the financial supports from the Thailand Research Fund (TRF); the Advanced Research Scholarship (BRG-5180022) for Prof. Kritsana Sagarik; the Royal Golden Jubilee (RGJ) Ph.D. Program, Grant No. PHD/0110/2548 for Prof. Kritsana Sagarik and Mayuree Phonyiem; RGJ-Ph.D. Program, Grant No. PHD/0121/2549 for Prof. Kritsana Sagarik and Chareonsak Lao-Ngam. High- performance computer facilities provided by the following organizations are gratefully acknowledged: School of Mathematics and School of Chemistry, SUT; National Electronics and Computer Technology Center (NECTEC) and National Nanotechnology Center (NANOTEC), National Science and Technology Development Agency (NSTDA); the Thai National Grid Center (THAIGRID), Ministry of Information and Communication Technology (MICT).

References

1 J. Larminie and A. Dicks, *Fuel Cell Systems*, John Wiley & Sons Ltd., Chichester, 2001.

2 C. A. Vincent and B. Scrosati, *Modern batteries: an introduction to electrochemical power sources* John Wiley & Sons Ltd., New York, 1997.

3 J. T. Hinatsu, M. Mizuhata and H. Takenaka, *Journal of The Electrochemical Society*, 1994, **141**, 1493-1498.

4 K.-D. Kreuer, *Chemistry of Materials*, 1996, **8**, 610-641.

5 K.-D. Kreuer, S. J. Paddison, E. Spohr and M. Schuster, *Chemical Reviews*, 2004, **104**, 4637-4678.

6 S. J. Paddison, *Annual Review of Materials Research*, 2003, **33**, 289-319.

7 S. J. Paddison and T. A. Zawodzinski Jr, *Solid State Ionics*, 1998, **113-115**, 333-340.

8 M. Eikerling, S. J. Paddison, L. R. Pratt and T. A. Zawodzinski, *Chemical Physics Letters*, 2003, **368**, 108-114.

9 S. J. Paddison and J. A. Elliott, *The Journal of Physical Chemistry A*, 2005, **109**, 7583-7593.

10 S. J. Paddison and J. A. Elliott, *Solid State Ionics*, 2006, **177**, 2385-2390.

11 S. J. Paddison, K.-D. Kreuer and J. Maier, *Physical Chemistry Chemical Physics*, 2006, **8**, 4530 - 4542.

12 V. A. Glezakou, M. Dupuis and C. J. Mundy, *Physical Chemistry Chemical Physics*, 2007, **9**, 5752 - 5760.

13 K. Sagarik, M. Phonyiem, C. Lao-Ngam and S. Chaiwongwattana, *Phys. Chem. Chem. Phys.*, 2008, **10**, 2098.

14 J. B. Asbury, T. Steinel and M. D. Fayer, *Journal of Luminescence*, 2004, **107**, 271-286.

15 J. C. Jiang, C. Chaudhuri, Y. T. Lee and H. C. Chang, *J. Phys. Chem. A*, 2002, **106**, 10937.

16 C. C. Wu, C. Chaudhuri, J. C. Jiang, Y. T. Lee and H.C. Chang, *J. Phys. Chem. A*, 2004, **108**, 2859.

17 R. Buzzoni, S. Bordiga, G. Ricchiardi, G. Spoto and A. Zecchina, *Journal of Physical Chemistry*, 1995, **99**, 11937-11951.

18 R. Iftimie, V. Thomas, S. Plessis, P. Marchand and P. Ayotte, *J. Am. Chem. Soc.*, 2008, **130**, 5901.

19 M. Okumura, L. I. Yeh, J. D. Myers and Y. T. Lee, *J. Phys. Chem.*, 1990, **94**, 3416.

20 V. Termath and J. Sauer, *Mol. Phys.*, 1977, **91**, 963.

21 C.-C. Wu, J. C. Jiang, D. W. Boo, S. H. Lin, Y. T. Lee and H.-C. Chang, *J. Chem. Phys.*, 2000, **112**, 176.

22 G. C. Pimentel and A. L. McClellan, *The Hydrogen Bond*, W. H. Freeman, San Francisco, 1960

23 K. Sagarik, C. Lao-ngam, P. Asawakun and S. Wannarat, submitted.

24 M. Benoit and D. Marx, *ChemPhysChem*, 2005, **6**, 1738-1741.

25 K. Sagarik, S. Chaiwongwattana, V. Vchirawongkwin and S. Prueksaaroon, *Phys. Chem. Chem. Phys.*, 2010, **12**, 918.

26 S. J. Paddison, *Journal of New Materials for Electrochemical Systems*, 2001, **4**, 197-207

27 S. J. Paddison, L. R. Pratt and T. A. Zawodzinski, *Journal of Physical Chemistry A*, 2001, **105**, 6266-6268.

28 A. D. Becke, *The Journal of Chemical Physics*, 1993, **98**, 5648-5652.
29 C. Lee, W. Yang and R. G. Parr, *Phys. Rev. B,*, 1988, **37**, 785.
30 A. Schaefer, C. Huber and R. Ahlrichs, *J. Chem. Phys.*, 1994, **100**, 5829.
31 G. Santambrogio, M. Bruemmer, L. Woeste, J. Doebler, M. Sierka, J. Sauer, G. Meijer and K. R. Asmis, *Phys. Chem. Chem. Phys.*, 2008, **10**, 3992.
32 R. Ahlrichs, M. Bär, M. Häser, H. Horn and C. Kölmel, *Chemical Physics Letters*, 1989, **162**, 165-169.
33 O. Treutler and R. Ahlrichs, *J. Chem. Phys.*, 1995, **102**, 346.
34 D. Marx, M. E. Tuckerman, J. Hutter and M. Parrinello, *Nature*, 1999, **367**, 101.
35 A. P. Scott and L. Radom, *J. Phys. Chem.*, 1996, **100**, 16502.
36 P. B. Balbuena and J. M. Seminario, *Theoretical and Computational Chemistry 7*, Elsevier, Amsterdam, 1999.
37 R. N. Barnett and U. Landman, *Physical Review B*, 1993, **48**, 2081.
38 X. Jing, N. Troullier, D. Dean, N. Binggeli, J. R. Chelikowsky, K. Wu and Y. Saad, *Physical Review B*, 1994, **50**, 12234.
39 N. Agmon, *Chemical Physics Letters*, 1995, **244**, 456-462.
40 P. A. Giguere, *Journal of Chemical Education*, 1979, **56**, 571.
41 K. D. Kreuer, *Solid State Ionics*, 2000, **136-137**, 149-160.
42 R. R. Sadeghi and H. Cheng, *J. Chem. Phys.*, 1999, **111**, 2086.
43 H.-P. Cheng and J. L. Krause, *The Journal of Chemical Physics*, 1997, **107**, 8461-8468.
44 P. Bopp, *Chemical Physics*, 1986, **106**, 205-212.
45 J. M. Haile, *Molecular Dynamics Simulations*, John Wiley & Sons Ltd., New York, 1997.
46 D. C. Rapaport, *The Art of Molecular Dynamics Simulation*, Cambridge University Press, London, 1995.
47 J. Chen, M. A. McAllister, J. K. Lee and K. N. Houk, *J. Org. Chem.*, 1998, **63**, 4611.

Figure 1 The trends of the interaction (ΔE) and solvation energies (ΔE^{sol}) with respect to the number of water molecules, obtained from B3LYP/TZVP calculations: -▲- = ΔE in the gas phase; -Δ- = ΔE in continuum aqueous solution; -■- = ΔE^{sol}.

Figure 2 Static results of the $CF_3SO_3H - H_3O^+ - H_2O$ complexes obtained from B3LYP/TZVP calculations in the gas phase and continuum aqueous solution.

a) Plot of Δd_{DA} and $R_{O\text{-}O}$ for the pass-through mechanism.
b) Plot of ν^{OH} and $R_{O\text{-}O}$ for the pass-through mechanism.
c) Plot of ν^{OH} and Δd_{DA} for the pass-through mechanism.
d) Plot of Δd_{DA} and $R_{O\text{-}O}$ for the pass-by mechanism.
e) Plot of ν^{OH} and $R_{O\text{-}O}$ for the pass-by mechanism.
f) Plot of ν^{OH} and Δd_{DA} for the pass-by mechanism.
(Δd_{DA} = asymmetric stretching coordinate;
$R_{O\text{-}O}$ = O-H..O H-bond distance;
ν^{OH} = asymmetric O-H stretching frequency)

Figure 3 The ranges of ν^{OH} for the H-bond protons in **Group 1** and **2**, as well as Subgroup (I) to (VI).
a) in the gas phase. b) in continuum aqueous solution.

Figure 4 BOMD results on the Zundel complex at 350 K.

a) – b) IR spectra of the transferring proton in the gas phase and continuum aqueous solution, respectively.
c) Plot of $\sigma_{R_{O-H}}$ and $<\Delta d_{DA}>$.
d) Plot of $\Delta\nu_{BA}^{OH,MD}$ and $<\Delta d_{DA}>$.
e) Plot of $\mathbf{P_B/P_A}$ and $<\Delta d_{DA}>$.

$\sigma_{R_{O-H}}$ = standard deviations of the O-H distances;
$<\Delta d_{DA}>$ = average asymmetric stretching coordinate;
$\mathbf{P_B/P_A}$ = probability of finding the structural diffusion motion relative to the oscillatory shuttling motion.

Figure 5 The BOMD results on the $CF_3SO_3H - H_3O^+ - H_2O$ complexes at 350 K.

a) Plot of $<\Delta d_{DA}>$ and $<R_{O\text{-}O}>$ for the pass-through mechanism.
b) Plot of ν^{OH} and $<R_{O\text{-}O}>$ for the pass-through mechanism.
c) Plot of ν^{OH} and $<\Delta d_{DA}>$ for the pass-through mechanism.
d) Plot of $<\Delta d_{DA}>$ and $<R_{O\text{-}O}>$ for the pass-by mechanism.
e) Plot of ν^{OH} and $<R_{O\text{-}O}>$ for the pass-by mechanism.
f) Plot of ν^{OH} and $<\Delta d_{DA}>$ for the pass-by mechanism.

$<\Delta d_{DA}>$ = average asymmetric stretching coordinate;
$<R_{O\text{-}O}>$ = average O-H..O H-bond distance;
ν^{OH} = asymmetric O-H stretching frequency.

Figure 6 BOMD results of the $CF_3SO_3H - H_3O^+ - H_2O$ complexes at 350 K.

a) Example of the IR spectra of the transferring proton in the pass-through mechanism.
b) Plot of $\sigma_{R_{O-H}}$ and $<\Delta d_{DA}>$ for the pass-through mechanism.
c) Plot of $\Delta\nu_{BA}^{OH,MD}$ and $<\Delta d_{DA}>$ for the pass-through mechanism..
d) Plot of $\mathbf{P_B/P_A}$ and $<\Delta d_{DA}>$ for the pass-through mechanism.
e) Example of the IR spectra of the transferring proton in the pass-by mechanism.
f) Plot of $\sigma_{R_{O-H}}$ and $<\Delta d_{DA}>$ for the pass-by mechanism.
g) Plot of $\Delta\nu_{BA}^{OH,MD}$ and $<\Delta d_{DA}>$ for the pass-by mechanism..
h) Plot of $\mathbf{P_B/P_A}$ and $<\Delta d_{DA}>$ for the pass-by mechanism

$\sigma_{R_{O-H}}$ = standard deviations of the O-H distances;
$<\Delta d_{DA}>$ = average asymmetric stretching coordinate;
$\mathbf{P_B/P_A}$ = probability of finding the structural diffusion motion relative to the oscillatory shuttling motion**.**

Figure 7 Distributions of the diffusion coefficients (D) of the transferring proton in the $CF_3SO_3H - H_3O^+ - H_2O$ complexes, obtained from BOMD simulations at 350 K.

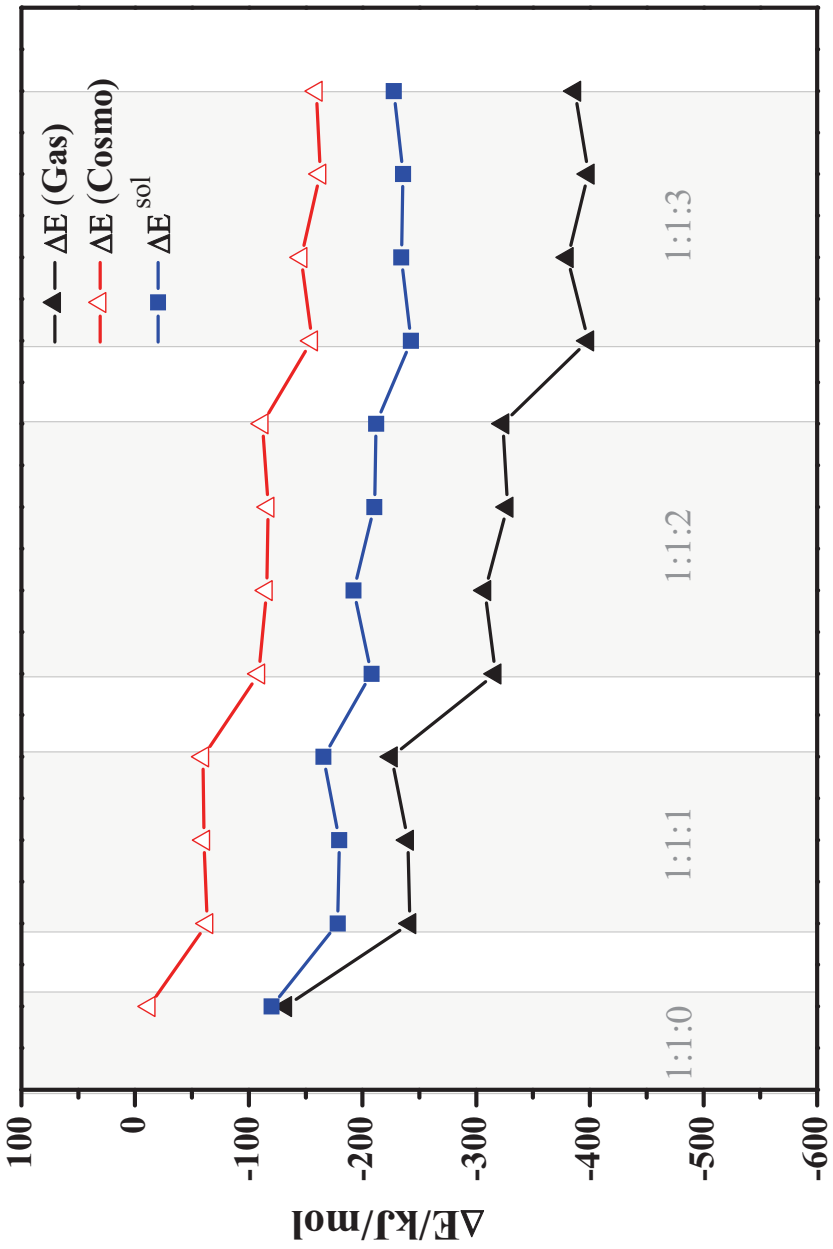
ΔE (Gas)
ΔE (Cosmo)
ΔE sol
ΔE/kJ/mol
100
0
-100
-200
-300
-400
-500
-600
1:1:0
1:1:1
1:1:2
1:1:3

Figure 1

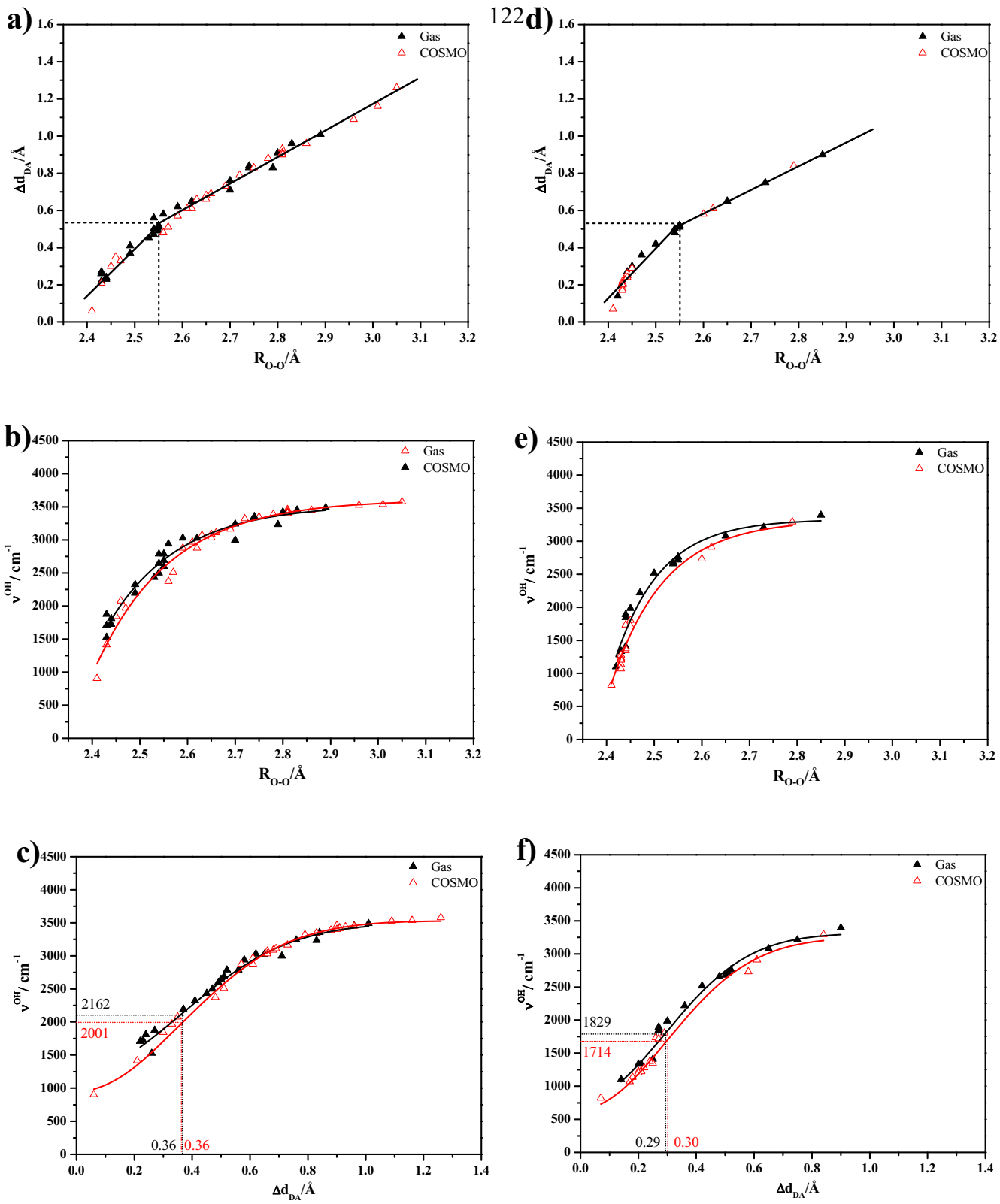
a)
d)
b)
e)
c)
f)
Gas
COSMO
Δd_{DA}/Å
$R_{O\text{-}O}$/Å
ν^{OH}/ cm^{-1}
Δd_{DA}/Å
2162
2001
0.36
0.36
1829
1714
0.29
0.30

Figure 2

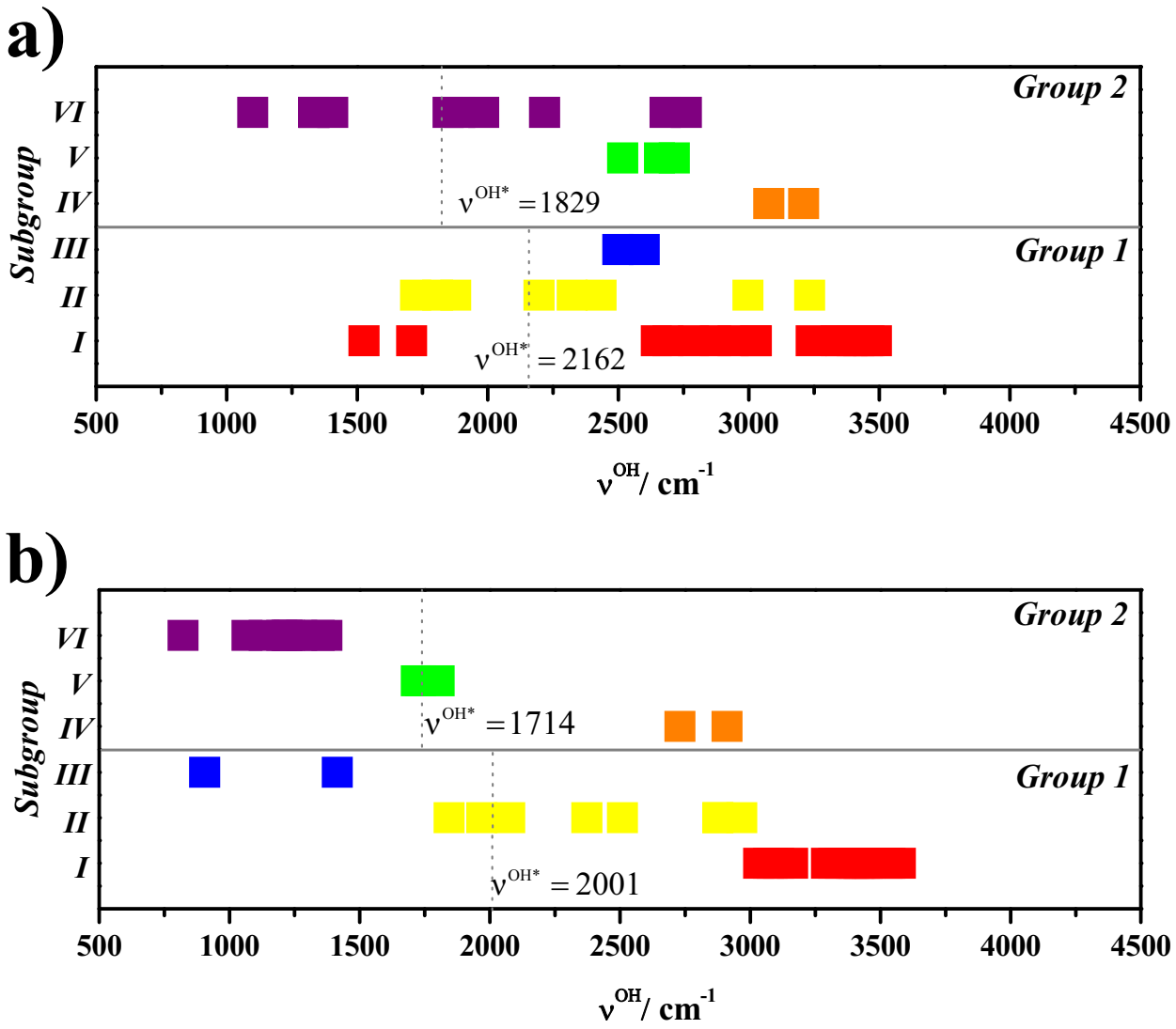
a)
Group 2
Group 1
Subgroup
VI
V
IV
III
II
I
ν^{OH*} =1829
ν^{OH*} =2162
500
1000
1500
2000
2500
3000
3500
4000
4500
ν^{OH}/ cm^{-1}
b)
Group 2
Group 1
Subgroup
VI
V
IV
III
II
I
ν^{OH*} =1714
ν^{OH*} =2001
500
1000
1500
2000
2500
3000
3500
4000
4500
ν^{OH}/ cm^{-1}

Figure 3

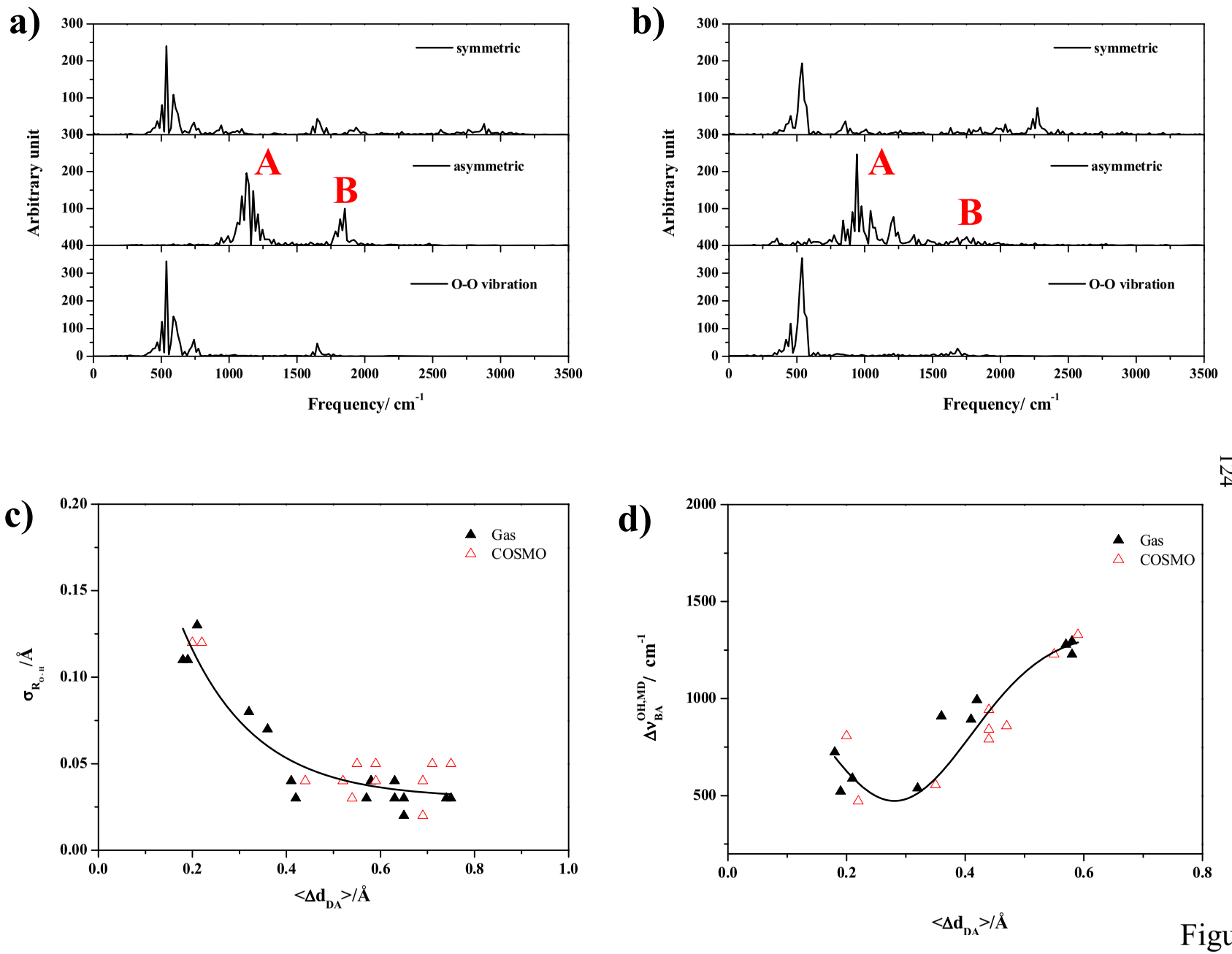
a)
b)
c)
d)
symmetric
asymmetric
O-O vibration
A
B
Arbitrary unit
Frequency/ cm-1
Gas
COSMO
<ΔdDA>/Å
σRO-H /Å
Δν OH,MD BA / cm-1

Figure 4

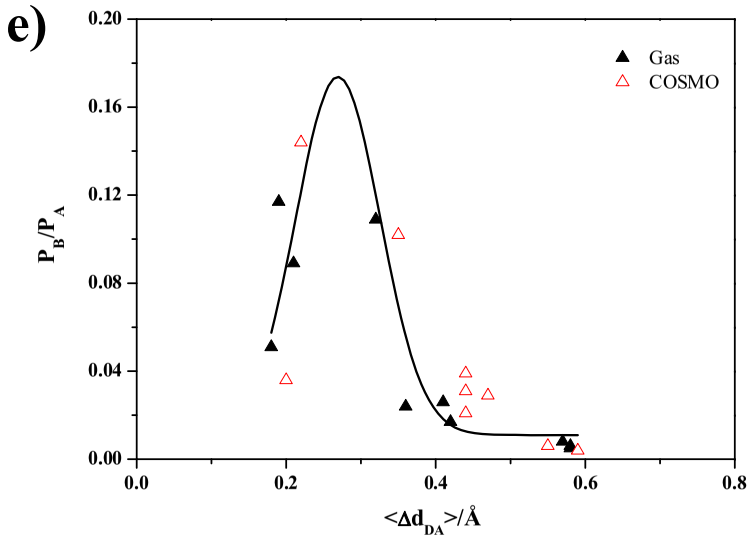

Figure 4 (cont.)

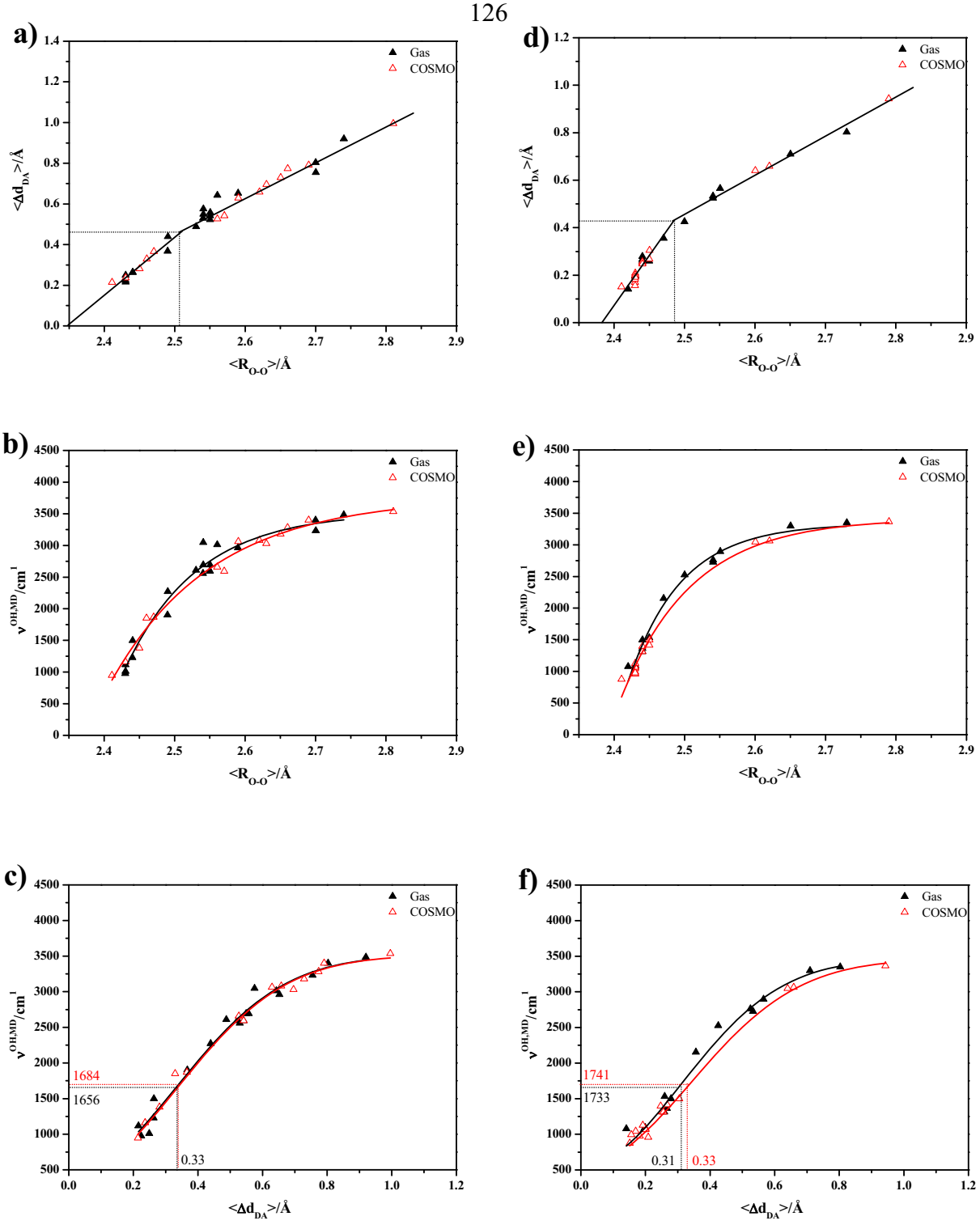
a)
d)
b)
e)
c)
f)
Gas
COSMO
<ΔdDA>/Å
<RO-O>/Å
νOHMD/cm-1
1684
1656
1741
1733
0.33
0.31

Figure 5

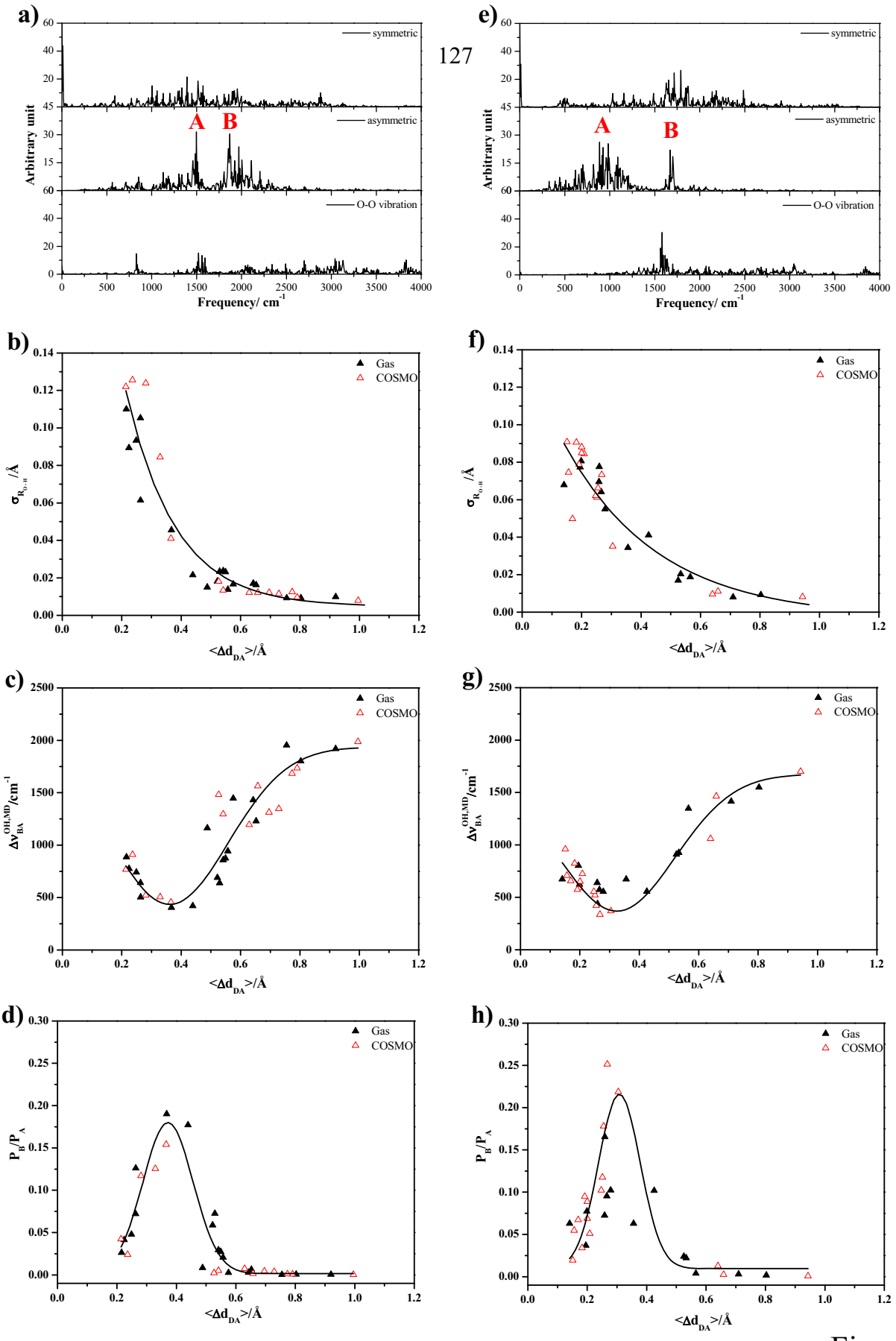
a)
e)
symmetric
asymmetric
O-O vibration
A
B
Arbitrary unit
Frequency/ cm-1
b)
f)
Gas
COSMO
σ R...H /Å
<ΔdDA>/Å
c)
g)
Δν OH,MD BA /cm-1
d)
h)
PB/PA

Figure 6

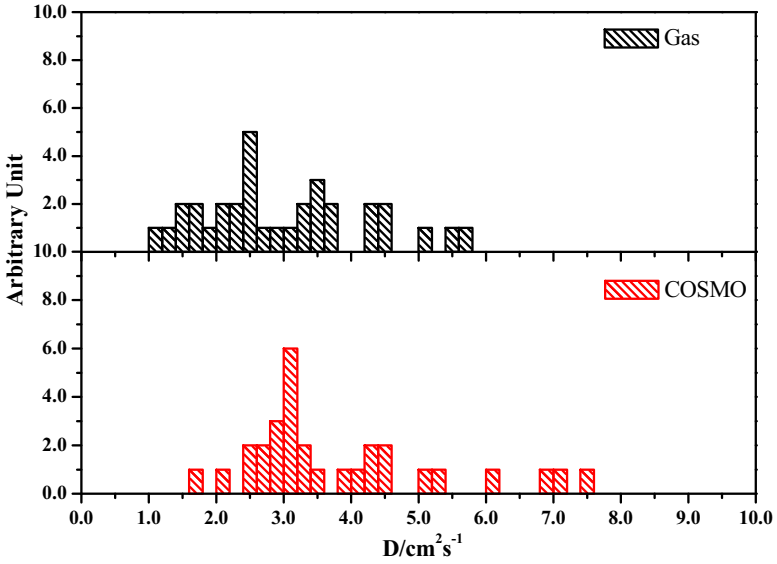
Gas
COSMO
Arbitrary Unit
D/cm^{2}s^{-1}
10.0
8.0
6.0
4.0
2.0
0.0
1.0
2.0
3.0
4.0
5.0
6.0
7.0
8.0
9.0
10.0

Figure 7

Table 1 Static results of the CF_3SO_3H, H_3O^+ and nH_2O, $n = 1 – 3$, complexes, obtained from B3LYP/TZVP calculations. Energies, distances and IR frequencies are in Å, kJ mol^{-1} and cm^{-1}, respectively.

Gas	COSMO	ΔE	ΔE^{Sol}	H-bond	R_{O-O}	Δd_{DA}	ν^{OH}
A1G	A1C	-241.7 (-63.5)	-178.1	(1)	2.55 (2.75)	0.52 (0.83)	2788 (3347)
				(2)	2.47 (2.43)	0.36 (0.20)*	2218 (1223)*
				(3)	- (3.05)	- (1.26)	- (3577)
A2G-[1]	A2C-[1]	-316.9 (-109.0)	-207.9	(1)	2.59 (2.72)	0.62 (0.79)	3029 (3320)
				(2)	2.44 (2.43)	0.27* (0.21)*	1893* (1230)*
				(3)	2.89 (2.96)	1.01 (1.09)	3490 (3525)
				(4)	2.54 (2.41)	0.47 (0.06)*	2498 (905)*
A2G-[2]	A2C-[2]	-308.0 (-115.6)	-192.3	(1)	2.54 (2.69)	0.56 (0.84)	2873 (3422)
				(2)	2.45 (2.41)	0.30 (0.07)*	1985 (823)*
				(3)	2.85 (2.79)	0.90 (0.84)	3396 (3292)
				(4)	2.79 (2.57)	0.83 (0.51)	3233 (2509)
A3G-[1]	A3C-[1]	-398.3 (-155.6)	-242.7	(1)	2.54 (2.63)	0.50 (0.66)	2645 (3071)
				(2)	2.44 (2.44)	0.27* (0.25)*	1848* (1345)*
				(3)	2.74 (2.86)	0.84 (0.96)	3353 (3449)
				(4)	2.43 (2.62)	0.27* (0.61)	1877* (2876)
				(5)	2.54 (2.44)	0.48 (0.26)*	2659 (1735)*
A3G-[2]	A3C-[2]	-380.3 (-146.1)	-234.2	(1)	2.56 (2.81)	0.58 (0.90)	2940 (3460)
				(2)	2.43 (2.44)	0.21* (0.24)*	1335* (1374)*
				(3)	2.73 (2.62)	0.75 (0.61)	3211 (2910)
				(4)	2.70 (2.56)	0.71 (0.48)	2997 (2373)
				(5)	2.65 (2.60)	0.65 (0.58)	3077 (2731)

ΔE = interaction energy; ΔE^{sol} = solution energy; R_{O-O} = H-bond distance; Δd_{DA} = asymmetric stretching coordinate; ν^{OH} = asymmetric O-H stretching frequency; (..) = continuum aqueous solution (COSMO); * = susceptible to proton transfer.

Table 1 (*cont.*)

Gas		COSMO		ΔE	ΔE^{Sol}	H-bond	$R_{O\text{-}O}$	Δd_{DA}	ν^{OH}
B1G	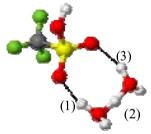	**B1C**	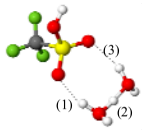	-239.8 (-60.4)	-179.4	(1)	2.70 (2.81)	0.76 (0.93)	3239 (3439)
						(2)	2.42 (2.43)	0.14* (0.18)*	1100* (1134)*
						(3)	2.83 (3.01)	0.96 (1.16)	3454 (3537)
B2G	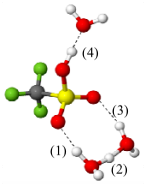	**B2C**	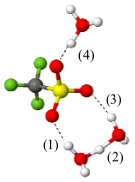	-327.6 (-117.0)	-210.6	(1)	2.62 (2.69)	0.65 (0.73)	3026 (3163)
						(2)	2.43 (2.43)	0.20* (0.17)*	1333* (1068)*
						(3)	2.80 (2.81)	0.91 (0.91)	3422 (3417)
						(4)	2.53 (2.45)	0.45 (0.30)*	2434 (1843)*
B3G	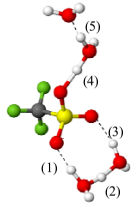	**B3C**	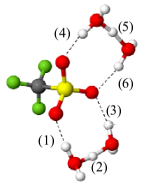	-398.7 (-162.9)	-235.8	(1)	2.55 (2.65)	0.51 (0.68)	2691 (3085)
						(2)	2.44 (2.43)	0.25* (0.22)*	1407* (1276)*
						(3)	2.74 (2.81)	0.83 (0.91)	3334 (3416)
						(4)	2.43 (2.66)	0.26* (0.69)	1526* (3109)
						(5)	2.54 (2.43)	0.50 (0.21)*	2679 (1221)*
						(6)	- (2.81)	- (0.90)	- (3399)
C1G	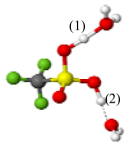	**C1C**	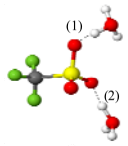	-225.5 (-59.7)	-165.8	(1)	2.44 (2.47)	0.23* (0.33)	1724* (1970)
						(2)	2.49 (2.46)	0.37 (0.35)	2196 (2076)
C2G	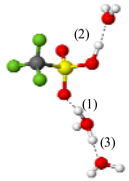	**C2C**	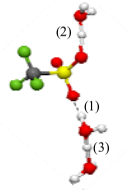	-323.8 (-111.7)	-212.1	(1)	2.49 (2.61)	0.41 (0.61)	2324 (2967)
						(2)	2.55 (2.43)	0.49 (0.21)*	2599 (1413)*
						(3)	2.50 (2.45)	0.42 (0.27)*	2516 (1717)*
C3G	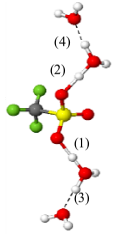	**C3C**	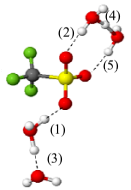	-387.1 (-159.7)	-227.4	(1)	2.44 (2.59)	0.24* (0.57)	1809* (2876)
						(2)	2.43 (2.65)	0.22* (0.66)	1708* (3032)
						(3)	2.55 (2.45)	0.51 (0.29)*	2715 (1805)*
						(4)	2.55 (2.43)	0.52 (0.20)*	2760 (1201)*
						(5)	- (2.78)	- (0.88)	- (3390)

Table 2 Dynamic results of the CF_3SO_3H, H_3O^+ and nH_2O, $n = 1 – 3$, complexes, obtained from BOMD simulations at 350 K. Distances, IR frequencies and proton diffusion coefficients are in Å, cm^{-1} and $cm^2\ s^{-1}$ respectively.

Gas		COSMO		H-bond	$<R_{O-O}>$		$\sigma_{R_{O-H}}$		$<\Delta d_{DA}>$		$\nu_A^{OH,MD}$		$\nu_B^{OH,MD}$		$\Delta\nu_{BA}^{OH,MD}$		P_B/P_A		D	
A1G	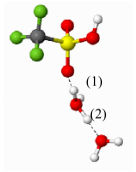	A1C	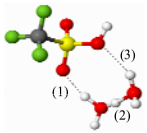	(1)	2.6	-	0.01	-	0.56	-	1750	-	2693	-	943	-	0.02	-	4.58	-
				(2)	2.5	(2.4)	0.03	(0.05)	0.36	(0.17)*	1515	(1043)*	2154	(1700)	673	(657)	0.06	(0.07)	2.48	(1.69)
				(3)	-	-	-	-	-	-	-	-	-	-	-	-	-	-	-	-
A2G-[1]	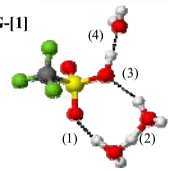	A2C-[1]	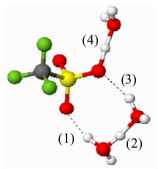	(1)	2.6	(2.7)	0.02	(0.01)	0.65	(0.91)	1733	(1683)	2962	(3501)	1229	(1818)	0.01	(0.00)	5.06	(5.02)
				(2)	2.4	(2.4)	0.05	(0.08)	0.28*	(0.21)*	1498*	(959)*	2053	(1683)	555	(724)	0.10	(0.05)	2.45	(2.56)
				(3)	-	-	-	-	-	-	-	-	-	-	-	-	-	-	-	-
				(4)	2.5	(2.4)	0.02	(0.12)	0.55	(0.21)*	1818	(948)*	2693	(1717)	875	(769)	0.03	(0.04)	2.46	(2.67)
A2G-[2]	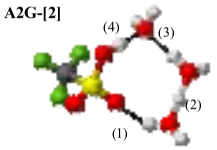	A2C-[2]	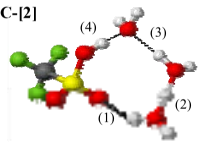	(1)	2.5	-	0.02	-	0.58	-	1599	-	3046	-	1447	-	0.00	-	1.52	-
				(2)	2.5	(2.4)	0.08	(0.09)	0.26*	(0.15)*	1531*	(875)*	1969	(1834)	438	(959)	0.17	(0.02)	1.77	(2.91)
				(3)	-	(2.8)	-	(0.01)	-	(0.94)	-	(1666)	-	(3366)	-	(1700)	-	(0.00)	-	(7.42)
				(4)	-	(2.6)	-	(0.01)	-	(0.54)	-	(1296)	-	(2592)	-	(1296)	-	(0.00)	-	(2.91)
A3G-[1]	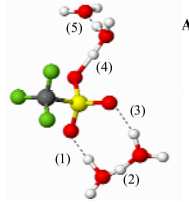	A3C-[1]	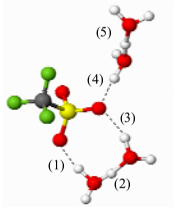	(1)	2.5	(2.6)	0.02	(0.01)	0.53	(0.70)	1919	(1717)	2558	(3030)	639	(1313)	0.07	(0.00)	2.98	(3.01)
				(2)	2.4	(2.4)	0.06	(0.06)	0.27*	(0.25)*	1363*	(1313)*	1935	(1834)	572	(521)	0.10	(0.12)	1.65	(4.43)
				(3)	2.7	-	0.01	-	0.90	-	1548	-	3450	-	1902	-	0.00	-	2.51	-
				(4)	2.4	(2.6)	0.09	(0.01)	0.25*	(0.66)	1010*	(1515)	1750	(3080)	740	(1565)	0.05	(0.00)	4.38	(5.20)
				(5)	2.5	(2.4)	0.02	(0.07)	0.53	(0.26)*	1801	(1313)*	2727	(1733)	926	(420)	0.02	(0.18)	4.51	(3.29)
A3G-[2]	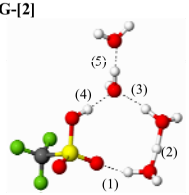	A3C-[2]	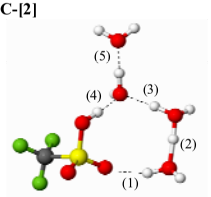	(1)	2.6	-	0.02	-	0.64	-	1582	-	3013	-	1431	-	0.00	-	5.74	-
				(2)	2.4	(2.4)	0.08	(0.06)	0.20*	(0.25)*	1094*	(1397)*	1717	(1952)	623	(555)	0.08	(0.10)	2.00	(5.03)
				(3)	2.7	(2.6)	0.01	(0.01)	0.80	(0.66)	1801	(1599)	3349	(3063)	1548	(1464)	0.00	(0.00)	3.79	(6.17)
				(4)	2.7	(2.7)	0.01	(0.02)	0.75	(0.53)	1279	(1178)	3232	(2659)	1953	(1481)	0.00	(0.00)	3.59	(2.81)
				(5)	2.7	(2.6)	0.01	(0.01)	0.71	(0.64)	1885	(2323)	3299	(3046)	1414	(1060)	0.00	(0.01)	3.55	(4.10)

$< R_{O-O} >$ = average H-bond distance; $\sigma_{R_{O-H}}$ = standard diviation of the O-H distance; $< \Delta d_{DA} >$ = average asymmetric stretching coordinate; $\nu_A^{OH,MD}$ and $\nu_B^{OH,MD}$ = asymmetric O-H stretching frequency; $\Delta\nu_{BA}^{OH,MD}$ = vibarational energy for the interconversion between the oscillatory shuttling and structural diffusion motions; P_B/P_A = relative probability of finding the oscillatory shuttling motion; D = proton diffusion coefficient; (..) = continuum aqueous solution (COSMO); * = susceptible to proton transfer.

Table 2 (*cont.*)

	Gas	COSMO	H-bond	$<R_{O\text{-}O}>$	$\sigma_{R_{O-H}}$	$<\Delta d_{DA}>$	$\nu_A^{OH,MD}$	$\nu_B^{OH,MD}$	$\Delta\nu_{BA}^{OH,MD}$	P_B/P_A	D
B1G	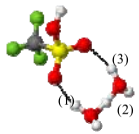	**B1C** 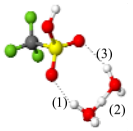	(1)	2.7 -	0.01 -	0.80 -	1599 -	3400 -	1801 -	0.00 -	3.48 -
			(2)	2.4 (2.4)	0.07 (0.07)	0.14* (0.16)*	1077* (993)*	1750 (1700)	673 (707)	0.06 (0.05)	2.18 (2.52)
			(3)	- -	- -	- -	- -	- -	- -	- -	- -
B2G	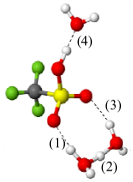	**B2C** 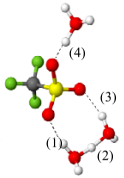	(1)	- (2.7)	- (0.01)	- (0.79)	- (1666)	- (3400)	- (1734)	- (0.00)	- (3.32)
			(2)	2.4 (2.4)	0.08 (0.09)	0.20* (0.18)*	1066* (976)*	1868 (1700)	802 (724)	0.04 (0.03)	2.57 (2.12)
			(3)	- -	- -	- -	- -	- -	- -	- -	- -
			(4)	2.5 (2.5)	0.01 (0.12)	0.49 (0.28)*	1447 (1380)*	2609 (1902)	1162 (522)	0.01 (0.12)	1.17 (3.91)
B3G	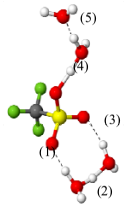	**B3C** 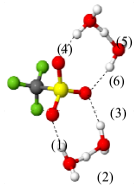	(1)	2.6 (2.7)	0.02 (0.01)	0.54 (0.77)	1733 (1666)	2592 (3501)	859 (1835)	0.03 (0.00)	3.36 (4.32)
			(2)	2.4 (2.4)	0.07 (0.09)	0.26* (0.20)*	1313* (1077)*	1952 (1666)	639 (589)	0.07 (0.09)	3.27 (3.07)
			(3)	2.7 (2.8)	0.01 (0.01)	0.92 (1.00)	1565 (1548)	3484 (3535)	1919 (1987)	0.00 (0.00)	5.56 (2.64)
			(4)	2.4 (2.7)	0.09 (0.01)	0.22* (0.77)	976* (1599)	1751 (3282)	775 (1683)	0.04 (0.00)	2.20 (7.09)
			(5)	2.5 (2.4)	0.02 (0.08)	0.52 (0.20)*	1851 (1066)*	2760 (1717)	909 (651)*	0.02 (0.07)	2.46 (4.58)
			(6)	- -	- -	- -	- -	- -	- -	- -	- -
C1G	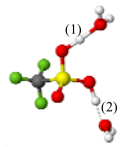	**C1C** 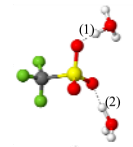	(1)	2.4 (2.5)	0.06 (0.04)	0.26* (0.37)	1499* (1767)	2003 (2323)	504 (556)	0.13 (0.15)	1.33 (3.46)
			(2)	2.5 (2.5)	0.05 (0.08)	0.37 (0.33)	1902 (1851)	2306 (2356)	404 (505)	0.19 (0.13)	1.46 (3.15)
C2G	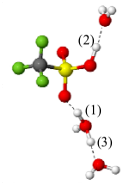	**C2C** 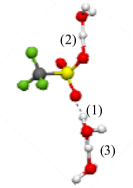	(1)	2.5 -	0.02 -	0.44 -	2272 -	2592 -	320 -	0.18 -	1.91 -
			(2)	2.6 (2.4)	0.02 (0.13)	0.52 (0.24)*	1582 (1161)*	2592 (2070)	1010 (909)	0.06 (0.02)	2.27 (3.15)
			(3)	2.5 (2.5)	0.04 (0.07)	0.43 (0.27)*	2171 (1414)*	2525 (1750)	556 (336)	0.10 (0.25)	3.65 (3.01)
C3G	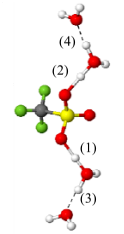	**C3C** 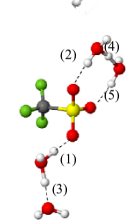	(1)	2.4 (2.6)	0.11 (0.01)	0.26* (0.63)	1228* (1868)	1868 (3063)	640 (1195)	0.07 (0.01)	2.74 (4.39)
			(2)	2.4 (2.7)	0.11 (0.01)	0.22* (0.73)	1117* (1834)	2003 (3181)	886 (1347)	0.03 (0.00)	3.05 (6.82)
			(3)	- (2.5)	- (0.04)	- (0.30)*	- (1498)*	- (1868)	- (370)	- (0.22)	- (3.07)
			(4)	2.6 (2.4)	0.02 (0.08)	0.57 (0.19)*	1548 (1127)*	2895 (1700)	1347 (573)	0.00 (0.09)	4.25 (4.24)
			(5)	- -	- -	- -	- -	- -	- -	- -	- -

Structures and Dynamics of Phenol Clusters in Benzene Solutions

S. Chaiwongwattana and **K. Sagarik**,
Chem. Phys., **355**, 103-117 (2009). (JIF = 2.28)
(Paper acknowledged BRG 5180022)

Structures and dynamics of phenol clusters in benzene solutions

by

Sermsiri Chaiwongwattana

and

Kritsana Sagarik*

School of Chemistry
Institute of Science
Suranaree University of Technology
Nakhon-Ratchasima 30000
Thailand

and

National Nanotechnology Center (NANOTEC)
National Science and Technology Development Agency (NSTDA)
Pathumthani 12120
Thailand

*corresponding author: kritsana@sut.ac.th
Tel./Fax: (6644) 224635

Keywords: phenol clusters, benzene solutions, T-model, molecular dynamics.

Abstract

Structures and dynamics of phenol clusters ($(PhOH)_n$, n = 1 – 3) in benzene (Benz) solutions ($[(PhOH)_n]_{Benz}$) at 298 K were studied using intermolecular potentials derived from the Test-particle model (T-model) and Molecular Dynamics (MD) simulations. Although Benz molecules interact weakly among themselves and with PhOH, the average three-dimensional structures and interaction energy distributions obtained from MD simulations showed that, they could form well-defined solvent cages in $[(PhOH)_n]_{Benz}$. At infinite dilution, some solvent-separated structures, in which a Benz molecule linked between two PhOH molecules, were observed in $[(PhOH)_2]_{Benz}$, whereas hydrogen bond (H-bond) structures dominated in $[(PhOH)_3]_{Benz}$. Based on the observation that, under thermal equilibrium conditions and at short time, the exchange dynamics between the associated and dissociated forms involved periodic motions of the O-H.. π H-bond, the lifetimes of the PhOH-Benz 1 : 1 complex were estimated and in reasonable agreement with 2D-IR vibrational echo experiment. Due to high potential energy barriers on the average potential energy landscapes, solvent exchanges in $[(PhOH)_n]_{Benz}$ could take place through large-amplitude intermolecular vibrations of molecules in the first solvation shell. In order to provide insights into structures and dynamics in $[(PhOH)_n]_{Benz}$, it was shown that, explicit solvent molecules have to be included in the theoretical models.

1. Introduction

Structures and stability of clusters of aromatic compounds in aqueous and non-aqueous solutions are examples of classical problems in the area of molecular associations [1-9]. Molecular clusters formed from aromatic compounds have been of interest, since they represent interactions between π-systems, which are found in DNA and side chains of proteins [10]. Therefore, various experimental and theoretical investigations have been performed in the past two decades to obtain basic information concerning with the driving forces responsible for interactions in aromatic systems, especially among biomolecules [11]. For example, the so-called "π-hydrogen bond" (π-H-bond) has been put forward due to its importance in biological systems, *e.g.* the ability to stabilize α–helix in proteins [12-14].

The presence of π-electrons enables clusters of aromatic compounds, generated in continuous or pulsed supersonic beams, to be examined effectively using modern spectroscopic techniques, such as resonance two photon ionization [15-17], disperse fluorescence [18], cluster ion dip spectroscopy [19,20] and ionization-detected stimulated Raman spectroscopy [21]. Significant advancement in computational chemistry software packages and parallel computer technology [22] has also allowed *ab initio* calculations that include the effects of electron correlations to study large clusters of aromatic compounds with higher accuracy [23]. It has, therefore, become a general practice to apply structural models obtained from *ab initio* calculations for the fitting of spectroscopic observations [24]. Since a large number of review articles on molecular associations have been published, only some important information relevant to the present work will be briefly summarized.

Clusters of benzene ($(Benz)_n$) are considered as prototypes for the π-π and C-H.. π interactions. They have been extensively studied by theoretical and experimental methods [25-31]. Theoretical methods [23,32] predicted at least four equilibrium structures of $(Benz)_2$ in the gas phase namely, parallel displaced, T-shaped, parallel staggered and herringbone structures. The parallel displaced structure is stabilized solely by the π-π interaction, whereas the T-shaped structure mainly by the C-H.. π interaction. The former was suggested by *ab initio* calculations at the highest level of

accuracy [32] to possess the lowest interaction energy and in good agreement with experiment [31], whereas the latter was pointed out to represent a low-energy saddle point for the interconversion between parallel displaced structures.

Fast dynamics of single Benz molecule in the liquid phase ($[Benz]_{liquid}$) was studied in femtosecond heterodyne detected optical Kerr effect (HD-OKE) experiments in a wide temperature range [25]. The results at short times were interpreted by assuming that the basic microscopic system consists of a Benz molecule librating and oscillating in a local confinement or solvent "cage". The instantaneous cage structures and dynamics in $[Benz]_{liquid}$ and $[Benz]_{crystal}$ were studied in details by spectroscopic measurements [26], as well as molecular dynamics (MD) [29] and lattice dynamics simulations [28]. It was reported in Ref. [29] that, a reminiscence of crystalline structure was evident in $[Benz]_{liquid}$, although no preferential orientation was observed in the first coordination shell. Moreover, the cages in $[Benz]_{liquid}$ are similar in composition to those in $[Benz]_{crystal}$, and the majority of the cages in $[Benz]_{liquid}$ could live several hundred femtoseconds (fs) or picoseconds (ps), depending upon the radius used to define the cage [29]. Similar solvent cages were observed in our previous theoretical studies [33] to accommodate benzoic acid dimer ($(BA)_2$), as well as BA-H_2O m : n complexes, m and n = 1 - 2, in Benz solutions.

As the simplest aromatic compound which can form O-H.. π and O-H..O H-bonds, and a prototype for structurally related subunits in larger biomolecules, such as tyrosine (Tyr) residue in proteins, phenol (PhOH) has been frequently selected as a model molecule in both experimental and theoretical investigations [23,34]. For example, theoretical methods at MP2/6-31G(d) and B3LYP/6-31G(d) levels were employed in the study of structures and stabilities of the O-H..O H-bond in $(PhOH)_n$ and $(H_2O)_n$, n = 1 – 4, as well as the PhOH-H_2O m : n complexes, m and n = 1 – 3, and m + n ≤ 4 [35]. MP2/6-31G(d) results showed that $(PhOH)_n$ and $(H_2O)_n$ possess similar H-bond patterns, and $(PhOH)_n$ are slightly more stable due to the effects of electron correlations. Moreover, it was shown that, the H-bonds in the PhOH-H_2O m : n complexes are similar to $(H_2O)_n$.

The interplay between electrostatic and dispersion interactions has been frequently studied through the weak interaction between the O-H group in PhOH and the polarizable π-electron clouds in Benz [36,37]. For example, in the gas phase, B3LYP/6-31G(d,p) calculations revealed that, the PhOH-Benz 1 : 1 complex is stabilized mainly by the O-H.. π H-bond, whereas in the 1 : 2 complex, the O-H group of PhOH acts simultaneously as proton donor and acceptor towards Benz molecules [37]. It should be noted that, although the density functional theory (DFT) and MP2 have been frequently employed in the calculations of molecular clusters, there have been examples in which both methods could not describe accurately the long-range electron correlation effects; $(Benz)_2$ was predicted to be unstable by almost all standard DFT functionals [32,38], whereas the interaction energy of the PhOH-Benz 1 : 1 complex was pointed out to be overestimated at the MP2 level [39].

Molecular associations of PhOH in Benz solutions were examined in classical partition experiments, in which distributions of PhOH between Benz and water were studied at 298 K [40]. The measurements of partition coefficients revealed that, in Benz, equilibrium could establish between PhOH and $(PhOH)_3$, whereas in water, PhOH is monomolecular up to at least 0.15 M. It was emphasized in Ref. [40] that, PhOH associates itself in triple molecules and not in double molecules. The existence of the monomer-trimer equilibrium was also suggested from NMR experiment [41], in which the equilibrium constant was determined in CCl_4 by measuring the hydroxyl NMR frequencies as functions of concentrations. However, Philbrick [4] proposed the existence of $(PhOH)_2$ in Benz solutions, by measuring the partition coefficients of PhOH between Benz and water at the concentrations in the water layer below 0.1 M. The results were confirmed by isopiestic experiments in anhydrous solutions [42].

Two-dimensional IR (2D-IR) vibrational echo spectroscopy [39,43-49], an ultrafast vibrational analog of two-dimensional NMR [45], has been developed to study fast chemical exchange in the ground electronic state under thermal equilibrium conditions. For small H-bonded systems, Hochstrasser *et al.* [48] investigated the H-bond exchange between CH_3OH and the CN of CH_3CN, using 2D-IR heterodyne echo spectroscopy. The activation energy for the exchange from the H-bonded state to the free state was reported to be 6.2 kJ/mol. With the enthalpy of formation of about 17

kJ/mol [12], the association and dissociation of the PhOH-Benz complex in solutions seem too rapid to measure using conventional spectroscopic methods. In Ref. [43], equilibrium dynamics in the PhOH-Benz complex was studied in a mixed solvent of Benz, by measuring in real time the appearance of off-diagonal peaks in the 2D-IR vibrational echo spectra of the PhOH hydroxyl stretching. The high-frequency hydroxyl stretching was assigned to the free PhOH, whereas the low-frequency to the PhOH-Benz complex. According to the analysis of the 2D-IR spectra, the dissociation time of the PhOH-Benz 1 : 1 complex was estimated to be about 8 ps.

In our previous work, $[PhOH]_{aq}$ [50], $[BA]_{aq}$ and $[(BA)_2]_{aq}$ [51], as well as $[(BA)_2]_{Benz}$ and small microhydrates of BA in Benz [33], were studied using intermolecular potentials derived from the Test-particle model (T-model) and MD simulations at 298 K. It was shown that, in the gas phase and dilute aqueous solutions, the strong cyclic H-bonds in $(BA)_2$ could be disrupted by H-bonding with water. Whereas in Benz, some microhydrates, not particularly associated in the gas phase and dilute aqueous solutions, become quite stable in the course of MD simulations. This reflects the impact of weak but complicated C-H.. π, O-H.. π and π..π interactions on structures and stability of H-bond clusters.

In the present study, the effects of weak C-H.. π, O-H.. π and π..π interactions on structures, energetic and dynamics of H-bond clusters in non-aqueous environment were further examined using $[(PhOH)_n]_{Benz}$, n = 1 – 3 as model systems. In order to acquire some basic information, equilibrium structures and interaction energies of the PhOH-Benz m : n complexes, m and n = 1 – 2, in the gas phase, were investigated using the T-model potentials. Then, NVE-MD simulations were performed on $[(PhOH)_n]_{Benz}$ at 298 K. The average three-dimensional structures and interaction energy distributions in $[(PhOH)_n]_{Benz}$ were visualized and analyzed based on solvent probability distribution (PD) maps and average solute-solvent and solvent-solvent interaction energy PD maps, respectively [52-54]. The dynamics in the first solvation shell of $[(PhOH)_n]_{Benz}$ was analyzed and discussed using the average interaction energy PD maps and their cross section plots [52-54], as well as the H-bond and solvent exchange diagrams. The results were discussed in comparison with available theoretical and experimental results of the same and similar systems.

2. Theoretical methods

The theoretical methods employed in the studies of solutions fall into two categories [55]. Microscopic methods consider solvent molecules with solute explicitly, whereas macroscopic methods take into account solvent as a continuum medium characterized by a dielectric constant. Although in principle, *ab initio* calculations, such as the Self-Consistent Reaction Field (SCRF) method [56], could provide insights into the stability of clusters of molecules in a continuum solvent, it is inappropriate in the present case, since the average three-dimensional structures and dynamics of solvent molecules were of primary interest.

2.1 The T-model potentials

Intermolecular potentials employed in the present work were constructed based on the T-model. Since the T-model has been explained in details in our previous investigations [33,50-53], only some important aspects will be briefly summarized here. Within the framework of the T-model, the interaction energy ($\Delta E_{T\text{-model}}$) between molecules A and B is written as a sum of the first-order SCF interaction energy (ΔE^{1}_{SCF}) and a higher-order energy (ΔE^{r}) [57].

$$\Delta E_{T-model} = \Delta E^{1}_{SCF} + \Delta E^{r} \qquad (1)$$

ΔE^{1}_{SCF} accounts for the exchange repulsion and electrostatic energies, and takes the following form:

$$\Delta E^{1}_{SCF} = \sum_{i\in A}\sum_{j\in B}\left[\exp\left[\frac{-R_{ij}+\sigma_i+\sigma_j}{\rho_i+\rho_j}\right]+\frac{q_i q_j}{R_{ij}}\right]. \qquad (2)$$

i and j in Eq. (2) label the sites of molecules A and B, respectively. σ_i, ρ_i and q_i are the site parameters. R_{ij} is the site-site distance. The exponential term in Eq. (2) takes into account the sizes and shapes of the interacting molecules A and B. The point charges q_i and q_j are determined to reproduce the electrostatic potentials of the molecules. The

higher-order energy, ΔE^r in Eq. (1), represents the dispersion and polarization contributions of the T-model potential. ΔE^r could be determined from both theoretical and experimental data, and takes the following form:

$$\Delta E^r = -\sum_{i\in A}\sum_{j\in B} C_{ij}^6 F_{ij}(R_{ij}) R_{ij}^{-6} \tag{3}$$

where

$$F_{ij}(R_{ij}) = \exp\left[-\left(1.28\, R_{ij}^0/R_{ij} - 1\right)^2\right],\ R_{ij} < 1.28\, R_{ij}^0 \tag{4}$$
$$= 1, \quad \text{elsewhere}$$

and

$$C_{ij}^6 = C_6 \frac{3}{2} \frac{\alpha_i \alpha_j}{(\alpha_i/N_i)^{1/2} + (\alpha_j/N_j)^{1/2}} \tag{5}$$

R_{ij}^0 in Eq. (4) is the sum of the van der Waals radii of the interacting atoms. Eq. (5) is the Slater-Kirkwood relation; α_i and N_i denote the atomic polarizability and the number of valence electrons of the corresponding atom, respectively. $F_{ij}(R_{ij})$ in Eq. (4) is a damping function, introduced to correct the behavior of R_{ij}^{-6} at short R_{ij} distance. Only C_6 in Eq. (5) is unknown. C_6 could be determined by a fit of the incomplete potential, including ΔE_{SCF}^1, to the experimental second-virial coefficients (B(T)) [58]. In the present study, σ_i, ρ_i, q_i and C_6 for PhOH and Benz were taken from Refs. [33] and [50]. They were applied successfully in MD simulations of H-bond and aromatic systems, both in aqueous [50] and non-aqueous solutions [33].

2.2 Equilibrium structures in the gas phase

In this subsection, some important aspects of geometry optimization will be briefly summarized, using the PhOH-Benz 1 : 1 complex as an example. The geometries of PhOH and Benz were taken from Refs. [33] and [50], respectively. They were kept constant throughout the calculations. The equilibrium structures and interaction energies of the PhOH-Benz 1 : 1 complex were computed by placing PhOH at the origin of the Cartesian coordinate system. The coordinates of Benz were randomly generated in the vicinities of PhOH. Based on the T-model potentials [33,50], the absolute and local minimum energy geometries of the PhOH-Benz 1 : 1 complex

were searched using a minimization technique [59]. One hundred starting configurations were employed in each geometry optimization. Similar approaches were applied in the calculations of equilibrium structures and interaction energies of the PhOH-Benz m : n complexes, m and n = 1 – 2. Some characteristic H-bond distances in the PhOH-Benz complexes were computed and used in the discussion of $[(PhOH)_n]_{Benz}$.

2.3 Molecular dynamics simulations

In order to obtain insights into structures, energetic and dynamics in $[(PhOH)_n]_{Benz}$, n = 1 - 3, NVE-MD simulations were performed at 298 K. MD-$[(PhOH)_n]_{Benz}^{frozen}$ and MD-$[(PhOH)_n]_{Benz}^{free}$ represent two scenarios in $[(PhOH)_n]_{Benz}$. In MD-$[(PhOH)_n]_{Benz}^{frozen}$, the structures of $(PhOH)_n$ were frozen at the T-model equilibrium geometries [50] and only Benz molecules were allowed to move. MD-$[(PhOH)_n]_{Benz}^{frozen}$ was aimed primarily at the average three-dimensional structures and interaction energy distributions of Benz molecules in $[(PhOH)_n]_{Benz}$. MD-$[(PhOH)_n]_{Benz}^{free}$ represents the situation, in which all PhOH and Benz molecules were free to move, starting from the equilibrium configurations of MD-$[(PhOH)_n]_{Benz}^{frozen}$. MD-$[(PhOH)_n]_{Benz}^{free}$ was aimed at the structures and stabilities of solutes, as well as the dynamics in $[(PhOH)_n]_{Benz}$.

In both MD-$[(PhOH)_n]_{Benz}^{frozen}$ and MD-$[(PhOH)_n]_{Benz}^{free}$, $(PhOH)_n$ and five hundred Benz molecules were put in a cubic box subject to periodic boundary conditions. The center of mass of $(PhOH)_n$ was coincide with the center of the simulation box. The density of $[(PhOH)_n]_{Benz}$ was maintained at the liquid density of 0.87 g cm^{-3} [60], corresponding to the box length of about 42 Å. The cut-off radius was half of the box length. The long-range Coulomb interaction was taken into account by means of the Ewald summations. Fifty thousand MD steps of 0.5 fs were devoted to equilibration and one hundred thousand steps to property calculations. The primary energetic results of interest were the average solute-solute ($< E_{Benz}^{solu-solu} >$) and solute-solvent ($< E_{Benz}^{solu-solv} >$) interaction energies, as well as the average potential energies of $[(PhOH)_n]_{Benz}$ ($< E_{Benz}^{pot} >$). $< E_{Benz}^{solu-solu} >$ resulted from the average over the number of MD steps, whereas $< E_{Benz}^{solu-solv} >$ over the number of MD steps and solute molecules.

In order to visualize the average three-dimensional structures of solvent molecules in $[(PhOH)_n]_{Benz}$, solvent probability distribution (π-PD) maps were constructed from MD-$[(PhOH)_n]_{Benz}^{frozen}$; the center of mass of Benz is denoted by π and that of PhOH by π_{Ph}. In the calculations of the π-PD maps, molecular plane of a PhOH molecule was assumed to coincide with the XY plane of the simulation box (Z = 0 Å). The volumes above and below the plane were divided into layers, with the thickness of 1 Å. In each layer, a π-PD map was constructed from 61x61 grid intersections, by following the trajectories of the center of mass of Benz in the course of MD simulations. The π-PD maps were represented by contour lines, computed and displayed using SURFER program [61]. Therefore, the densities of the contour lines could reflect the probability of finding Benz in $[(PhOH)_n]_{Benz}$. For simplicity, the minimum and maximum values of the contour lines, as well as the contour intervals, were chosen to be the same for all π-PD maps. Since the solvent cages in $[(PhOH)_2]_{Benz}$ and $[(PhOH)_3]_{Benz}$ were rather complicated, additional π-PD maps were constructed with respect to XZ and YZ planes.

Based on similar approaches, the average solute-solvent and solvent-solvent interaction energy PD maps, denoted by the PB-PD and BB-PD maps, respectively, were constructed from MD-$[(PhOH)_n]_{Benz}^{frozen}$. The PB-PD maps were computed from the interaction energies between Benz at the grid intersections and $(PhOH)_n$, whereas BB-PD maps from the interaction energies between Benz at the grid intersections and all other Benz molecules. The average potential energy landscapes in $[(PhOH)_n]_{Benz}$ were represented by the PB-BB-PD maps, computed by combinations of the PB-PD and BB-PD maps. Because the solvent cages tend to bring about stabilization effects in $[(PhOH)_n]_{Benz}$, only negative-energy contour lines were displayed on the PB-PD, BB-PD and PB-BB-PD maps. It should be noted that, since the solvent-solvent interaction energies dominate in $[(PhOH)_n]_{Benz}$, the minimum and maximum values of the contours, as well as the contour intervals, must be assigned differently for the PB-PD, BB-PD and PB-BB-PD maps.

Since the dynamics of PhOH and Benz in the first solvation shell was one of the main objectives, additional MD analyses had to be made. Our experience in aqueous solutions [52-54] showed that, although not straightforward, the dynamics of specific

solvent molecules in the first solvation shell could be anticipated at least qualitatively from the structures of the average potential energy landscapes. Therefore, the PB-PD, BB-PD and PB-BB-PD maps computed from MD-$[(PhOH)_n]^{frozen}_{Benz}$ were further analyzed in details. Several cross section plots were generated by taking vertical slices along the predefined profile lines, through the surfaces of the PB-BB-PD maps, as well as the PB-PD and BB-PD maps, using the methods described in Ref. [53]. The cross section plots derived from the longitudinal profile lines could be associated with the average potential energy barriers to solvent exchanges within, as well as between, the first solvation shells $(< E^{L}_{Benz} >)$. Whereas those computed from the transverse profile lines are connected to the average potential energy barriers to the solvent exchanges between Benz molecules in the first solvation shell and the outside $(< E^{T}_{Benz} >)$.

Solvation structures, stability and dynamics in $[(PhOH)_n]_{Benz}$ were further analyzed based on MD-$[(PhOH)_n]^{free}_{Benz}$. Some atom-atom pair correlation functions (g(R)) and the corresponding average running coordination numbers (n(R)) related to the π..π interactions, the C-H.. π, O-H.. π and O-H..O H-bonds were computed and employed in the discussion. g(R) represents basic one-dimensional views on the structures in solutions. Because large-amplitude intermolecular motions, which could lead to solvent structure reorganization, were pointed out to be one of the main reasons for the non-rigidity in aromatic van der Waal clusters [27], they were also investigated in the present study. Since under thermal equilibrium conditions, the PhOH-Benz complexes are repeatedly dissociating and forming, and the O-H.. π and O-H..O H-bonds, as well as π..π interactions are responsible for the molecular associations in $[(PhOH)_n]_{Benz}$, their periodic motions at short time could be related to the lifetimes of the complexes. In the present case, fast Fourier transformations (FFT) [62] were performed on the O-H.. π and π..π distances, from which the large-amplitude intermolecular vibrational frequencies and the lifetimes of the complexes were approximated. Additionally, in the present case, the H-bond exchange diagrams, showing the distance between the oxygen atom of PhOH and the center of mass of a specific Benz molecule as a function of MD simulation time, were constructed.

3. Results and discussion

3.1 The PhOH-Benz m : n complexes

The absolute and some low-lying minimum energy geometries of the PhOH-Benz complexes, obtained from the T-model potentials, are displayed in Figs. 1 and 2. In Fig. 1, the absolute minimum energy geometry of the PhOH-Benz 1 : 1 complex is represented by structure **a**, in which the O-H group of PhOH acts as proton donor towards the π-electron cloud of Benz, with the interaction energy ($\Delta E_{T-model}$) of -19.5 kJ/mol and the O-H..π and π_{Ph}-π distances of 3.4 and 5.4 Å, respectively. The structure and interaction energy of structure **a** are in good agreement with the T-shaped structure obtained from *ab initio* calculations [37,39] and the picosecond photofragment spectroscopy [12]. Structures **b** and **c** are two local minimum energy geometries, with $\Delta E_{T-model}$ of -13.5 and -9.3 kJ/mol, respectively. Structure **b** shows a possibility for the oxygen atom and the π-electron cloud of PhOH to act as proton acceptor towards the C-H groups of Benz, with the C-H..O and C-H..π_{Ph} H-bond distances of 3.4 and 4.0 Å, respectively. Structure **c** is stabilized solely by the C-H..π H-bonds, with the C-H..π and π_{Ph}-π distances of 3.8 and 4.9 Å, respectively.

A compact H-bond cluster formed from the O-H..π, C-H..O, C-H..π and C-H..π_{ph} H-bonds represents the absolute minimum energy geometry of the PhOH-Benz 1 : 2 complex, structure **a** in Fig. 2. Structure **a** possesses $\Delta E_{T-model}$ of -41.6 kJ/mol, with the H-bond distances similar to the PhOH-Benz 1 : 1 complexes. Structure **a** has more C-H.. π H-bonds compared to that suggested from supersonic jet spectroscopy [36]. Structure **b** is about 11 kJ/mol less stable than structure **a**. In structure **b**, the oxygen atom of PhOH acts as proton acceptor towards two C-H groups of Benz, with the C-H..O H-bond distances of 3.3 Å. The stability of structure **c** is comparable to structure **b**, with $\Delta E_{T-model}$ of -28.8 kJ/mol and the O-H.. π and C-H..π H-bond distances of 3.4 and 3.8 Å, respectively. The O-H.. π H-bond in structure **c** is similar to structure **a** of the PhOH-Benz 1 : 1 complex, whereas the C-H..π H-bond resembles the T-shaped structure in $(Benz)_2$ [23].

Since H-bonds in the PhOH-Benz 2 : 1 and 2 : 2 complexes are not substantially different from the PhOH-Benz 1 : 1 and 1 : 2 complexes, in which all characteristic H-bond structures were explained, they are not presented here. Comparison of the results obtained in this subsection with those from experiments [12,36] and *ab initio* calculations [31,45] showed that the T-model potentials [33,50] are accurate enough for further application in MD simulations.

3.2 MD simulations on $[(PhOH)_n]_{Benz}$

The T-model potentials applied in the previous subsection were employed in MD simulations of $[(PhOH)_n]_{Benz}$, n = 1 – 3, at 298 K. $< E^{pot}_{Benz} >$, $< E^{solu-solu}_{Benz} >$ and $< E^{solu-solv}_{Benz} >$ obtained from MD-$[(PhOH)_n]^{frozen}_{Benz}$ and MD-$[(PhOH)_n]^{free}_{Benz}$ are summarized in Table 1. In order to limit the number of figures, only selected g(R), π-PD, PB-PD and PB-BB-PD maps are displayed. High-density contours on the PD maps are labeled with capital letters.

The average interaction energies in Table 1 show both expected and unexpected trends in $[(PhOH)_n]_{Benz}$. Due to large number of Benz molecules, $< E^{pot}_{Benz} >$ are nearly the same for all MD simulations, and since the degree of freedom in MD-$[PhOH]^{free}_{Benz}$ is higher than MD-$[PhOH]^{frozen}_{Benz}$, $< E^{solu-solv}_{Benz} >$ is about a factor two higher, -58.1 and -106.0 kJ/mol, respectively. As only one O-H group could act as proton donor towards Benz molecules in both MD-$[(PhOH)_2]^{frozen}_{Benz}$ and MD-$[PhOH]^{frozen}_{Benz}$, $< E^{solu-solv}_{Benz} >$ are not substantially different, the former is about 5 kJ/mol higher than the latter. The energetic results seem to be more complicated in MD-$[(PhOH)_2]^{free}_{Benz}$, in which $< E^{solu-solv}_{Benz} >$ is about 21 kJ/mol lower than MD-$[(PhOH)_2]^{frozen}_{Benz}$, and $< E^{solu-solu}_{Benz} >$ = -2.3 kJ/mol. These represent direct evidences for substantial changes in H-bond structures in MD-$[(PhOH)_2]^{free}_{Benz}$; an increase in solute-solvent interaction is accompanied by a decrease in solute-solute interaction, leading to some solvent-separated structures. The situations seem to be less complicated in MD-$[(PhOH)_3]^{free}_{Benz}$, in which $< E^{solu-solu}_{Benz} >$ is about 64 % of $\Delta E_{T-model}$ of $(PhOH)_3$ in the gas phase [50], and $< E^{solu-solv}_{Benz} >$ = -98.0 kJ/mol. These indicate that, on average, the three H-bonds in $(PhOH)_3$ did not change substantially in the course of MD-$[(PhOH)_3]^{free}_{Benz}$. The formations of solvent-separated structures in $[(PhOH)_2]_{Benz}$ and

close-contact trimers in $[(PhOH)_3]_{Benz}$ will be discussed in detail in the forth coming subsections.

$[PhOH]_{Benz}$

The average three-dimensional structures and interaction energy distributions of solvent molecules obtained from MD-$[PhOH]^{frozen}_{Benz}$ are shown in Fig. 3. The values of the highest probabilities at the labeled contours on the π-PD maps ($< P^{\pi-PD} >_{max}$), together with the corresponding lowest-average interaction energies on the PB-PD, BB-PB and PB-BB-PD maps, denoted by $< \Delta E^{PB-PD}_{Benz} >_{min}$, $< \Delta E^{BB-PD}_{Benz} >_{min}$ and $< \Delta E^{PB-BB-PD}_{Benz} >_{min}$, respectively, are summarized in Table 2.

The π-PD maps in Figs. 3a and 3b reveal that, at least three Benz molecules stay in the vicinity the O-H group of PhOH, labeled with **A** (Z = -0.5 – 0.5 Å), **B** (Z = 2.0 – 3.0 Å) and **C** (Z = 2.0 – 3.0 Å). It is obvious that, the π-electron clouds of Benz molecules at **A** and **B** act as proton acceptor towards the O-H and C-H groups of PhOH, respectively, whereas a C-H group of Benz at **C** acts as proton donor towards the oxygen atom of PhOH. Table 2 shows that, Benz molecules at **A**, **B** and **C** possess $< \Delta E^{PB-PD}_{Benz} >_{min}$ of -17.3, -11.7 and -9.8 kJ/mol, respectively. Comparison of $\Delta E_{T-model}$ in Fig. 1 and $< \Delta E^{PB-PD}_{Benz} >_{min}$ suggests a possibility for a C-H group of Benz at **B** to act as proton donor towards the oxygen atom of PhOH.

The preferential solvation order according to $<P^{\pi-PD}>_{max}$ and the average interaction energy orders based on the absolute values of $< \Delta E^{PB-PD}_{Benz} >_{min}$, $< \Delta E^{BB-PD}_{Benz} >_{min}$ and $< \Delta E^{PB-BB-PD}_{Benz} >_{min}$ in Table 2 can be written as:

$<P^{\pi-PD}>_{max}$: **B** > **A** > **C**

$< \Delta E^{PB-PD}_{Benz} >_{min}$: **A** > **B** > **C**

$< \Delta E^{BB-PD}_{Benz} >_{min}$: **C** > **A** > **B**

$< \Delta E^{PB-BB-PD}_{Benz} >_{min}$: **A** > **C** > **B**.

It should be noted that, the preferential solvation order and the average interaction energy orders in the present case, as well as in many cases [52-54], are different. This

is due to the fact that, the π-PD maps show relative probabilities that, a specific "position" in the first solvation shell of PhOH is occupied by Benz molecules, whereas the minima on the average potential energy landscapes, such as $<\Delta E_{Benz}^{PB\text{-}BB\text{-}PD}>_{min}$, represent "low-lying interaction energy states", probed in the course of MD simulations. In other words, Benz molecules at the position with the highest $<P^{\pi\text{-}PD}>_{max}$ need not possess the lowest $<\Delta E_{Benz}^{PB\text{-}BB\text{-}PD}>_{min}$. Since the occupancies of the interaction energy states depend upon dynamics of individual solvent molecules, which could be described by structures of the average potential energy landscapes, it is necessary to include the cross section plots in the discussion of $[(PhOH)_n]_{Benz}$ [52-54]. They show both the average potential energy barriers interconnecting interaction the energy states and the average potential energy wells, in which solvent molecules are confined. The latter could be related to the "average cage potentials" [26].

Figs. 3c and 3d are examples of the average potential energy landscapes and the cross section plots obtained from MD-$[PhOH]_{Benz}^{frozen}$. The cross section plots indicate that, the average potential energy barriers at **A**, **B** and **C** are quite high, in both longitudinal and transverse directions, *e.g.* about 120 kJ/mol at **A** in Fig. 3d (I) and (II). On the PB-PD and PB-BB-PD maps in Fig. 3b (Z = 2.0 – 3.0 Å), a possibility for the solvent exchange within the first solvation shell is evident from an interaction energy channel connecting **B** and **C**. All the cross section plots in Figs. 3c and 3d reveal that, the size and shape of the average potential energy wells are determined nearly exclusively by the average solvent-solvent interactions. These could restrict translational motion of Benz in the first solvation shell of PhOH, especially in the transverse direction. One could, therefore, conclude that, Benz molecules at **A**, **B** and **C** form a part of a quite well-defined local solvent cage at the O-H group of PhOH. Our qualitative interpretation of dynamics of individual solvent molecules in connection to the average potential energy landscapes is similar to Rabani *et al.* [63]; molecular translation in the liquid phase is characterized by average potential energy landscapes and occurs through jumps between basins separated by high-energy barriers, and the identity of the solvent cage should be more related to the multi-minimum basin itself, rather than to single actual configuration.

It appeared in general that, all structural information obtained from MD-$[PhOH]^{free}_{Benz}$ could be interpreted reasonably well based on the results of the PhOH-Benz 1 : 1 and 1 : 2 complexes in Figs. 1 and 2. $g(R_{O\text{-}H..\pi})$ in Fig. 4a shows the main peak at $R_{O\text{-}H..\pi}$ = 4.4 Å, with a small shoulder at $R_{O\text{-}H..\pi}$ = 3.5 Å, and according to $n(R_{O\text{-}H..\pi})$ at the first minimum ($R_{O\text{-}H..\pi}$ = 5.5 Å), about five Benz molecules are in the first solvation shell of the O-H group. Since the main peak of $g(R_{C\text{-}H..O_{ph}})$ in Fig. 4b is seen at $R_{C\text{-}H..O_{ph}}$ = 3.3 Å, one could conclude that, the main peak and small shoulder of $g(R_{O\text{-}H..\pi})$ correspond to structures **b** and **a** in Fig. 1, respectively. The predominance of the C-H..O_{ph} H-bond in $[PhOH]_{Benz}$ was also suggested based on experiments in Ref. [4]. Additionally in Fig. 4a, $n(R_{O\text{-}H..\pi})$ = 2.1 at the first maximum ($R_{O\text{-}H..\pi}$ = 4.4 Å) indicates that, in $[PhOH]_{Benz}$, two Benz molecules are in close contact with the O-H group, with the H-bond structures similar to structures **b** and **a** in Fig. 2. These support the three-dimensional structures of solvent obtained from the π-PD maps and the preferential solvation order according to $<P^{\pi\text{-}PD}>_{max}$.

Due to deep average potential energy wells, Benz molecules in the inner and outer shells of the O-H group seem not exchange as fast as water solvent [53,54,64]. The H-bond exchange diagram in Fig. 4c demonstrates the exchange of Benz 65 and Benz 423 in the course of MD-$[PhOH]^{free}_{Benz}$. At t_1 = 18.2 ps, Benz 423 entered and shared the first solvation shell with Benz 65, until Benz 65 left at t_2 = 28.3 ps. Therefore, the exchange process, taking place in panel **P1** in Fig. 4c, took about 10 ps. The residence time of Benz 423 could be approximated from the widths of panel **P1** and **P2** to be about 23 ps. The same exchange process repeated again in panel **P3**; at t_3 = 41.6 ps, Benz 65 reentered and shared the first solvation shell with Benz 423 *etc*.

Although the solvent exchange rates and residence times are extremely sensitive to the methods employed, some comparisons could be made using the results on liquid water. Based on MD simulations with the T-model potentials [52], the longest H-bond lifetime at the H atom of water was predicted to be 8.7 ps, whereas that at the O atom was 3.2 ps. These are compared well with the H-bond residence times of water obtained from NMR experiment of about 8 ps [65] and MD simulations of 4.5 ps [66]. Literature survey showed that the mean residence times of water within the first hydration shell of a single water molecule are ranging from 2.5 to 10 ps [67].

Therefore, the residence time of Benz in the first solvation shell of PhOH obtained in the present work is in reasonable agreement with the previous investigations.

Investigations of the H-bond exchange diagrams in details revealed that, Benz molecules at the O-H group of PhOH exchange through large-amplitude intermolecular vibrational motions, which involve periodic displacement of the O-H.. π H-bond as discussed in Ref. [27]. According to the five-exchange mechanisms proposed by Langford and Gray [68], the exchanges seem to favor the associative-interchange ($\mathbf{I_a}$) scheme, in which a solvent molecule enters and spends sometime in the first solvation shell before the other leaves.

Analyses of the time evolutions of the cage structures in $[Benz]_{liquid}$ [69,70] showed two relaxation components, which could affect the exchange of Benz molecules constituting the solvent cage; the slow relaxing component is associated with the cage lifetime, whereas the fast relaxing component with the structural rearrangements due to molecular vibrations. Since the average cage potentials or the average potential energy wells are quite low in $[PhOH]_{Benz}$, it was reasonable and possible to investigate the fast component. Based on the assumption that, at short time, the dynamic equilibrium between the associated and dissociated forms could be studied from characteristic intermolecular vibrational frequency [41], the lifetime of the PhOH-Benz 1 : 1 complex could be approximated. FFT [62] was performed on the O-H..π H-bond distance curve, from which the lifetime of the PhOH-Benz 1 : 1 complex ($\tau_{O-H..\pi}^{PhOH-Benz}$) was approximated from the characteristic intermolecular vibrational frequency, as half of the association-dissociation dynamic equilibrium cycle time. Examples of FFT obtained from MD-$[PhOH]_{Benz}^{free}$ are shown in Fig. 4d, together with $\tau_{O-H..\pi}^{PhOH-Benz}$. Due to lower degree of freedom, MD-$[PhOH]_{Benz}^{frozen}$ yielded the upper limit of $\tau_{O-H..\pi}^{PhOH-Benz}$ to be 9.2 ps (not shown here), whereas MD-$[PhOH]_{Benz}^{free}$ predicted the lower limit to be 3.1 ps. The values are in reasonable agreement with the 2D-IR vibrational echo spectroscopy of 8 ps [43].

It should be noted that, the present MD simulations estimated $\tau_{O-H..\pi}^{PhOH-Benz}$ directly from the intermolecular vibrational frequencies, whereas the 2D-IR vibrational echo experiment [43] compared the O-H stretching frequencies in the free PhOH with those

in the PhOH-Benz 1 : 1 complex. Although efficient coupling of the O-H stretching with the low-frequency O-H.. π H-bond vibrations could be presumed, the excited O-H stretching could live longer than 4 ps [21]. It should be augmented that, MD-$[PhOH]^{free}_{Benz}$ was based on pair-wise additive intermolecular potentials, in which many-body contributions were not taken into account. One could, however, expect that the inclusion of the cooperative effects will lead to slightly more associated PhOH-Benz 1 : 1 complex and longer $\tau^{PhOH-Benz}_{O-H..\pi}$. In order to obtain a rough estimate of the cooperative effects, *ab initio* geometry optimizations were performed on the PhOH-Benz 1 : 1 complexes. For this weak O-H.. π H-bond, MP2/6-311G(d,p) predicted the upper limit of the cooperative effects to be only about 0.6 kJ/mol, corresponding to the red shift of about 50 cm^{-1}. Therefore, the discrepancy between MD-$[PhOH]^{free}_{Benz}$ and the 2D-IR vibrational echo experiment is reasonable and explainable.

$[(PhOH)_2]_{Benz}$

In order to distinguish H-bonds in $[(PhOH)_2]_{Benz}$, the oxygen atoms were numbered as follow:

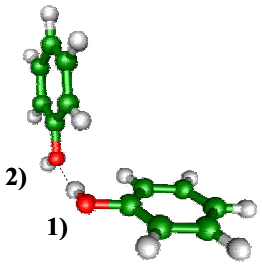

Since the O1-H..O2 H-bond was fixed in MD-$[(PhOH)_2]^{frozen}_{Benz}$, only the O2-H group could act as proton donor towards the π-electron cloud of Benz. Structural and energetic results obtained from MD-$[(PhOH)_2]^{frozen}_{Benz}$ demonstrated that, the solvent cages in $[(PhOH)_2]_{Benz}$ are stronger and more complicated than in $[PhOH]_{Benz}$. The π-PD maps in Figs. 5a to 5c, show well-defined solvent structures in the vicinities of $(PhOH)_2$; the preferential solvation positions are labeled with **A** to **E**. It is obvious that, Benz molecules prefer to stay at the O2-H group, with the highest probability at **A** (Z = -2.0 – 1.0 Å) in Fig. 5c and $< \Delta E^{PB-BB-PD}_{Benz} >_{min}$ in Table 3 of -86.5 kJ/mol. It appeared that, the C-H.. π H-bonds between PhOH and Benz become stronger upon dimer formation. They are labeled with **B**, **C** and **D** on the π-PD maps. The PB-PD

and PB-BB-PD maps in Fig. 5b show a larger and more well-defined energy channel in $[(PhOH)_2]_{Benz}$, compared to $[PhOH]_{Benz}$. Therefore, a possibility for the solvent exchange within the first solvation shell of frozen $(PhOH)_2$ could be anticipated at **E**, **D** and **C**.

In $[(PhOH)_2]_{Benz}$, the preferential solvation order according to $<P^{\pi\text{-PD}}>_{max}$ and the average interaction energy orders based on the absolute values of $<\Delta E_{Benz}^{PB\text{-}PD}>_{min}$, $<\Delta E_{Benz}^{BB\text{-}PD}>_{min}$ and $<\Delta E_{Benz}^{PB\text{-}BB\text{-}PD}>_{min}$ in Table 3 can be written as:

$<P^{\pi\text{-PD}}>_{max}$: **A** > **C** > **D** > **E** > **B**

$<\Delta E_{Benz}^{PB\text{-}PD}>_{min}$: **D** > **E** ≥ **B** > **A** > **C**

$<\Delta E_{Benz}^{BB\text{-}PD}>_{min}$: **C** > **E** > **A** > **B** > **D**

$<\Delta E_{Benz}^{PB\text{-}BB\text{-}PD}>_{min}$: **A** > **E** > **B** > **D** > **C**.

The cross section plots in Figs. 5d and 5e show high average potential energy barriers for solvent exchanges between the fist solvation shell and the outside, up to about 138 kJ/mol at **A** in Fig. 5d (IV). Since the π-PD, PB-PD and PB-BB-PD maps show high-density contours in the vicinity of the O1-H..O2 H-bond, one could anticipate its easy access by Benz molecules, and due to additional entropic effects when $(PhOH)_2$ are free to move, the H-bond dissociation could be expected, as in the cases of $(BA)_2$ [51] and the guanidinium-formate (Gdm^+-FmO^-) complexes in aqueous solutions [52].

Structures and dynamics in $[(PhOH)_2]_{Benz}$ were further examined in MD-$[(PhOH)_2]_{Benz}^{free}$, in which both PhOH and all Benz molecules were free to move. As expected, due to weak solute-solute interaction and the thermal energy fluctuation at 298 K, the O1-H..O2 H-bond was dissociated in MD-$[(PhOH)_2]_{Benz}^{free}$. $g(R_{O1\text{-}O2})$ in Fig. 6a shows three well-defined peaks at $R_{O1\text{-}O2}$ = 5.7, 8.1 and 9.4 Å, and for $g(R_{\pi_{Ph1}\text{-}\pi_{Ph2}})$, two main peaks are seen at $R_{\pi_{Ph1}\text{-}\pi_{Ph2}}$ = 6.5 and 9.2 Å. Since the latter is more structured, with two well-defined shoulders at $R_{\pi_{Ph1}\text{-}\pi_{Ph2}}$ = 8.1 and 9.8 Å, one could conclude that, the majority of $(PhOH)_2$ in MD-$[(PhOH)_2]_{Benz}^{free}$ took solvent-separated structures. Comparison of $g(R_{O\text{-}H..\pi})$ and $g(R_{\pi_{Ph}..\pi})$ in Figs. 6b and 6c with those obtained from MD-$[PhOH]_{Benz}^{free}$ in Fig. 4a confirms the dissociation of the O1-H..O2 H-bond and the existence of solvent-separated structures in MD-$[(PhOH)_2]_{Benz}^{free}$.

Investigation of structures of $(PhOH)_2$ in the course of MD-$[(PhOH)_2]^{free}_{Benz}$ revealed four examples of close-contact and solvent-separated structures, with $R_{\pi_{Ph1}\text{-}\pi_{Ph2}}$ comparable to the positions of the main peaks and shoulders of $g(R_{\pi_{Ph1}\text{-}\pi_{Ph2}})$. They are shown in Fig. 6d, and will be used in the discussion of the exchange diagrams in Figs. 6e and 6f. In structure (**I**), both PhOH molecules are in close contact, with $R_{\pi_{Ph1}\text{-}\pi_{Ph2}}$ = 6.7 Å. In structures (**II**), (**III**) and (**IV**), Benz 496 separates both PhOH molecules, with $R_{\pi_{Ph1}\text{-}\pi_{Ph2}}$ of 8.1, 9.0 and 9.7 Å, respectively.

Figs. 6e and 6f show examples of solvent exchange diagrams. In Fig. 6e, the distances between the center of mass of Benz 496 ($\pi_{Benz\,496}$) and those of PhOH molecules ($R_{\pi_{Ph1}\text{-}\pi_{Benz\,496}}$ and $R_{\pi_{Ph2}\text{-}\pi_{Benz\,496}}$) were plotted as functions of MD simulation time. Instantaneous solvent-separated structures could be recognized in panels **P1** and **P$_3$**, in which Benz 496 stayed between both PhOH molecules, with comparable $R_{\pi_{Ph1}\text{-}\pi_{Benz\,496}}$ and $R_{\pi_{Ph2}\text{-}\pi_{Benz\,496}}$. PhOH 2 and PhOH 1 could be temporarily separated from Benz 496 in panel **P$_2$** and **P$_4$**, respectively. Finally, at t_5 = 43.6 ps, Benz 496 moved away from PhOH 1, resulting in close-contact structures similar to structure (**I**) in Fig. 6d. Fig. 6f reveals further that, Benz 502 stayed closer to PhOH 2 from t = 15 to 33 ps. A similar solvent separated structure was proposed from experiment, in which the association of $(PhOH)_2$ in water saturated CCl_4 was studied [5]; spectroscopic evidence revealed that, the hydrogen atoms of water are not involved in H-bond. It was presumed that, the dimer owes its stability to weak interaction between the hydrogen atoms of the O-H groups of both PhOH molecules and the oxygen atom of water. The so called “hemihydrate dimer” was used to describe this dimer.

$[(PhOH)_3]_{Benz}$

Structures and dynamics of $(PhOH)_3$ in Benz solution are discussed based on MD-$[(PhOH)_3]^{free}_{Benz}$. It appeared that, the cyclic O-H..O H-bonds, similar to the water trimer, could be partially opened in the course of MD-$[(PhOH)_3]^{free}_{Benz}$, as follow:

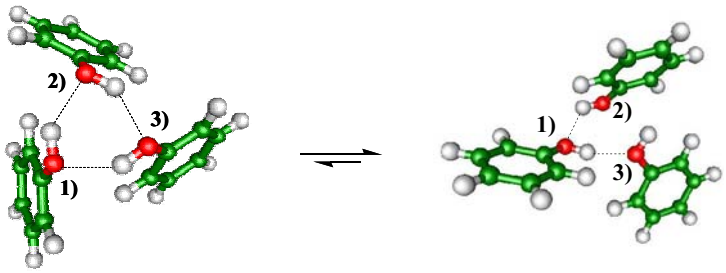

This is evident from $g(R_{O..O})$ in Fig. 7a; $g(R_{O_1..O_2})$ and $g(R_{O_1..O_3})$ are quite similar, with the main peak positions at the average O-H..O H-bond distance of 2.8 Å [50], whereas $g(R_{O_2..O_3})$ possesses different structure, a broad peak with maximum at 4 Å. In Figs. 7b and 7c, similar trends were observed for $g(R_{O1.\pi_{Ph2}})$, $g(R_{O1.\pi_{Ph3}})$ and $g(R_{O2.\pi_{Ph3}})$, as well as for $g(R_{\pi_{Ph1}.\pi_{Ph2}})$, $g(R_{\pi_{Ph1}.\pi_{Ph3}})$ and $g(R_{\pi_{Ph2}.\pi_{Ph3}})$, respectively. Although the average structure is not as compact as in the gas phase, one could conclude that, $(PhOH)_3$ forms H-bond clusters in $[(PhOH)_3]_{Benz}$. Comparison of the solute structures in the course of MD-$[(PhOH)_2]^{free}_{Benz}$ and MD-$[(PhOH)_3]^{free}_{Benz}$ revealed that, the O-H..O H-bonds in $(PhOH)_3$ are more sterically hindered by the three PhOH molecules, therefore not easily accessible by Benz molecules. Similar steric effects were observed in our previous MD-$[(BA)_2]^{free}_{Benz}$ in Ref. [33], in which cyclic H-bonds in $(BA)_2$ were sterically hindered from Benz molecules, but could be partially opened by small polar molecule such as water.

As mentioned earlier that, molecular associations of aromatic compounds in non-aqueous solvents, such as Benz and CCl_4, represent classical problems in the area of molecular associations, in which partition experiments and various spectroscopic methods have been generally employed in the investigations. For some H-bonded solutes, the associated forms are sufficiently stable to be detected in experiments. However, for PhOH, there have been disagreements as to the most important species in solutions. The majority of the partition experiments seem to point to the existence of the PhOH-$(PhOH)_3$ equilibrium in CCl_4, whereas several spectroscopic results were interpreted in terms of the PhOH-$(PhOH)_2$ equilibrium. At infinite dilution and within ps time scale, the present MD simulations seem to favor instantaneous solvent-separated structures in $[(PhOH)_2]_{Benz}$ and H-bond clusters in $[(PhOH)_3]_{Benz}$. Since it is well accepted that, different experiments could lead to different results, and the advancement of femtosecond laser technology has allowed experiments to probe instantaneous molecular structures and dynamics in weakly associated systems in smaller time scales, it seems unrealistic to rule out possibilities of finding various

forms of dimers and trimers, as well as larger clusters in Benz or CCl_4 solutions. Therefore, we anticipate that, no single associated form could be representative in solutions, except in very restricted experimental conditions, such as temperature, concentration and time scale.

4. Conclusions

Structures and dynamics of aromatic clusters have been frequently and extensively studied to demonstrate that, cluster non-rigidity is a general phenomenon in weakly bound systems. In the present study, the effects of weak C-H.. π, O-H.. π H-bond and π..π interactions on structures and dynamics of H-bond clusters in non-aqueous environment, were studied using $[(PhOH)_n]_{Benz}$, n = 1 – 3 as model systems. In order to acquire some basic information on equilibrium structures and interaction energies in the gas phase, the PhOH-Benz m : n complexes, m = 1 – 2, n = 1 – 2, were investigated using the T-model potentials. It appeared that, the H-bond structure, in which the O-H group of PhOH acts as proton donor towards the π–electrons of Benz, represents the absolute minimum energy geometry of the PhOH-Benz 1 : 1 complex. Although the C-H group is not an effective proton donor, various possibilities for the C-H..O and C-H.. π H-bond formations were observed from the T-model results on larger PhOH-Benz complexes.

Based on the T-model potentials, a series of NVE-MD simulations was performed on $[(PhOH)_n]_{Benz}$, n = 1 – 3, at 298 K. Insights on the solvent cage structures and energetic were obtained from $[PhOH]_{Benz}$ and $[(PhOH)_2]_{Benz}$. It was observed from the average three-dimensional structures in $[PhOH]_{Benz}$ that, at least three Benz molecules solvate at the O-H group, and PhOH could act both as proton donor and acceptor towards Benz molecules. The average potential energy landscapes and cross section plots obtained from MD simulations indicated that, the size and shape of the average potential energy wells are determined nearly exclusively by the average solvent-solvent interactions, and the average potential energy barriers to solvent exchanges at the O-H group are quite high. Therefore, Benz molecules at the O-H group could from part of a quite strong local solvent cage. Our interpretation of dynamics of solvent molecules in connection to the average potential energy landscapes is similar to

Rabani *et al*., by which molecular translation in liquid was proposed to occur through jumps between potential energy wells, separated by high-energy barriers. Investigation on the H-bond exchange diagrams revealed that, Benz molecules at the O-H group could exchange through large-amplitude intermolecular vibrational motions, which involve the periodic displacement of the O-H.. π H-bond, and the solvent exchanges seem to favor the associative-interchange scheme, in which a solvent molecule enters and spends sometime in the first solvation shell before the other leaves. From the characteristic intermolecular vibrational frequencies of the O-H.. π H-bond, the lifetimes of the PhOH-Benz 1 : 1 complex were approximated and in reasonable agreement with 2D-IR vibrational echo experiment.

Due to weak interaction and the thermal energy fluctuation at 298 K, the O-H..O H-bond in $(PhOH)_2$ was disrupted in MD simulations. Instantaneous solvent-separated structures, in which a Benz molecule separates both PhOH molecules, were observed in $[(PhOH)_2]_{Benz}$, whereas the cyclic H-bonds in $(PhOH)_3$ were partially opened in $[(PhOH)_3]_{Benz}$. A similar water separated dimer was suggested from experiment, in which spectroscopic evidence revealed that the hemihydrate $(PhOH)_2$ owes its stability to weak interaction between the hydrogen atoms of the O-H groups of both PhOH molecules and the oxygen atom of water. Comparisons of the π-PD maps and the dimer and trimer structures in the course of MD simulations revealed that, the O-H..O H-bonds in $(PhOH)_3$ were quite well protected by the three PhOH molecules, therefore not easily accessible by Benz molecules as in the case of $(PhOH)_2$. This suggests that, the competition between solute-solute and solute-solvent interactions could be studied only when explicit solvent molecules are taken into account in the model calculations.

It should be noted finally that, the MD results reported here were based on pair-wise additive scheme, in which many-body effects were not taken into account. Since the interactions among aromatic compounds are not particularly strong, the inclusion of the cooperative effects in our model calculations should not lead to significant change in structures and stability of the complexes considered here; only slightly more associated complexes with longer association times could be anticipated. For organic and biological systems, weak intermolecular interactions could produce complexes

that are short-lived. Although short-lived and cannot be detected easily by conventional experimental techniques, the dissociation and association of such complexes can influence chemical processes, especially reactivity and mechanisms in biochemical reactions. Therefore, progress is being made in our laboratory to apply similar theoretical approaches to investigate short-lived phenomena in some biological systems.

Acknowledgements

The authors would like to acknowledge the financial supports from the Thailand Research Fund (TRF): the Royal Golden Jubilee (RGJ) Ph.D. Program, Grant No. PHD/0071/2547 to Sermsiri Chaiwongwattana and Prof. Kritsana Sagarik: the Advanced Research Scholarship, Grant No. BRG-4880008 to Prof. Kritsana Sagarik. Linux clusters provided by the following organizations are also gratefully acknowledged: School of Mathematics and School of Chemistry, SUT; National Electronics and Computer Technology Center (NECTEC) and National Nanotechnology Center (NANOTEC), National Science and Technology Development Agency (NSTDA); the Thai National Grid Center (THAIGRID), Ministry of Information and Communication Technology.

LIST OF ABBREVIATIONS AND SYMBOLS

T-model = The test-particle model.

π-H-bond = π-hydrogen bond.

PD map = Probability distribution map.

π-PD maps = Solvent probability distribution map.

$< P^{\pi-PD} >_{max}$ = Highest probability at the labeled contour on the π-PD maps.

$MD\text{-}[(PhOH)_n]^{frozen}_{Benz}$ = MD simulations with the structure of $(PhOH)_n$ frozen at the T-model equilibrium geometries.

$MD\text{-}[(PhOH)_n]^{free}_{Benz}$ = MD simulations with all molecules allowed to move, starting from the equilibrated configurations of $MD\text{-}[(PhOH)_n]^{frozen}_{Benz}$.

$< E^{solu-solu}_{Benz} >$ = Average solute-solute interaction energy.

$< E^{solu-solv}_{Benz} >$ = Average solute-solvent interaction energy.

$< E^{pot}_{Benz} >$ = Average potential energies of $[(PhOH)_n]_{Benz}$.

$< E^{L}_{Benz} >$ = The average potential energy barriers to the solvent exchange within, as well as between, the first solvation shells.

$< E^{T}_{Benz} >$ = The average potential energy barriers to the solvent exchange between Benz molecules in the first solvation shell and the outside.

g(R) = Atom-atom pair correlation functions.

n(R) = Average running coordination numbers.

FFT = Fast Fourier transformations.

I_a = Associative-interchange scheme.

$\tau^{PhOH-Benz}_{O-H..\pi}$ = Lifetime of the PhOH-Benz 1 : 1 complex.

PB-PD = The average solute-solvent interaction energy PD maps.

BB-PD = The average solvent-solvent interaction energy PD maps.

PB-BB-PD = The average potential energy PD maps.

$< \Delta E^{PB\text{-}PD}_{Benz} >_{min}$ = Lowest-average interaction energies on the PB-PD map

$< \Delta E^{BB\text{-}PD}_{Benz} >_{min}$ = Lowest-average interaction energies on the BB-PD map

$< \Delta E^{PB\text{-}BB\text{-}PD}_{Benz} >_{min}$ = Lowest-average interaction energies on the PB-BB-PD map

References

[1] E.M. Woolley, L.G. Hepler, J. Phys. Chem. 76 (1972) 3058.

[2] S.H. Weidman, L.E. Swearingen, J. Am. Chem. Soc. 35 (1931) 836.

[3] J.N. Spencer, J.C. Andrefsky, A. Grushow, J. Naghdi, L.M. Patti, J.F. Trader, J. Phys. Chem. 91 (1987) 1673.

[4] F.A. Philbrick, J. Am. Chem. Soc. 56 (1934) 2581.

[5] R.M. Badger, R.C. Greenough, J. Phys. Chem. 65 (1961) 2088.

[6] F.T. Wall, J. Am. Chem. Soc. 64 (1942) 472.

[7] F.T. Wall, P.E. Rouse Jr., J. Am. Chem. Soc. 63 (1941) 3002.

[8] A.K.M. Shamsul Huq, S.A.K. Lodhi, J. Phys. Chem. 70 (1966) 1354.

[9] R. Van Duyne, S.A. Taylor, S.D. Christian, H.E. Affsprung, J. Phys. Chem. 71 (1967) 3427.

[10] K.E. Van Holde, W.C. Johnson, P.S. Ho, Principles of Physical Biochemistry, Prentice Hall, New Jersey, 1998.

[11] B. Brutschy, Chem. Rev. 100 (2000) 3891.

[12] J.L. Knee, L.R. Khundkar, A.H. Zewail, J. Chem. Phys. 87 (1987) 115.

[13] M.F. Perutz, Philos. Trans. Roy. Soc. London Ser. A 345 (1993) 105.

[14] E.A. Meyer, R.K. Castellano, F. Diederich, Angew. Chem. Int. Ed. Engl. 42 (2003) 1210.

[15] W. Roth, M. Schmitt, C. Jacoby, D. Spangenberg, C. Janzen, K. Kleinerman, Chem. Phys. 239 (1998) 1.

[16] N. Mikami, Bull. Chem. Soc. Jpn. 68 (1995) 683.

[17] R.J. Lipert, S.D. Colson, J. Chem. Phys. 89 (1988) 4579.

[18] Ch. Jacoby, W. Roth, M. Schmitt, Ch. Janzen, D. Spangenberg, K. Kleinermanns, J. Phys. Chem. A 102 (1998) 4471.

[19] T. Sawamura, A. Fujii, S. Sato, T. Ebata, N. Mikami, J. Phys. Chem. 100 (1996) 8131.

[20] K. Ohashi, Y. Inokuchi, N. Nishi, Chem. Phys. Lett. 257 (1996) 137.

[21] G.V. Hartland, B.F. Henson, V.A. Venturo, P.M. Felker, J. Phys. Chem. 96 (1992) 1164.

[22] D.C. Young, Computational Chemistry: A practical guide for applying techniques to real-world problems, Wiley Interscience, New York, 2001.

[23] M.O. Sinnokrot, C.D. Sherrill, J. Am. Chem. Soc. 126 (2004) 7690.

[24] B.M. Rode, C.F. Schwenk, T.S. Hofer, B.R. Randolf, Coord. Chem. Rev. 249 (2005) 2993.

[25] M. Ricci, P. Bartolini, R. Chelli, G. Cardini, S. Califano, R. Righini, Phys. Chem. Chem. Phys. 3 (2001) 2795.

[26] A. Magro, D. Frezzato, A. Polimeno, G.J. Moro, R. Chelli, R. Righini, J. Chem. Phys. 123 (2005) 124511.

[27] S. Sun, E.R Bernstein, J. Phys. Chem. 100 (1996) 13348.

[28] G.J. Kearley, M.R. Johnson, J. Tomkinson, J. Chem. Phys. 124 (2006) 044514.

[29] R. Chelli, G. Cardini, P. Procacci, R. Righini, S. Califano, A. Albrecht, J. Chem. Phys. 113 (2000) 6851.

[30] L.S Bartell, F.J. Dulles, J. Phys. Chem. 99 (1995) 17107.

[31] J.R. Grover, E.A. Walters, E.T. Hui, J. Phys. Chem. 91 (1987) 3233.

[32] M.O. Sinnokrot, E.F. Valeev, C.D. Sherrill, J. Am. Chem. Soc. 124 (2002) 10887.

[33] K. Sagarik, S. Chaiwongwattana, P. Sisot, Chem. Phys. 306 (2004) 1.

[34] C.A. Hunter, J. Singh, J.M. Thornton, J. Mol. Biol. 218 (1991) 837.

[35] R. Parthasarathi, V. Subramanian, N. Sathyamurthy, J. Phys. Chem. A 109 (2005) 843.

[36] A. Olkawa, H. Abe, N. Mikami, M. Ito, J. Phys. Chem. 87 (1983) 5083.

[37] R.C. Guedes, K. Coutinho, B.J. Costa Cabral, S. Canuto, C.F. Correia, R.M. Borges dos Santos, J.A. Martinho Simões, J. Phys. Chem. A 107 (2003) 9197.

[38] S. Tsuzuki, K. Honda, T. Uchimaru, M. Mikami, K. Tanabe, J. Am. Chem. Soc. 124 (2002) 104.

[39] K. Kwac, C. Lee, Y. Jung, J. Han, K. Kwak, J. Zheng, M.D. Fayer, M. Cho, J. Chem. Phys. 125 (2006) 244508.

[40] K. Endo, Bull. Chem. Soc. Jpn. 1 (1926) 25.

[41] M. Saunders, J.B. Hyne, J. Chem. Phys. 29 (1958) 1319.

[42] E.N. Lassettre, R.G. Dickinson, J. Am. Chem. Soc. 61 (1939) 54.

[43] J. Zheng, K. Kwak, J. Asbury, X. Chen, I.R. Piletic, M.D. Fayer, Science 309 (2005) 1338.

[44] J. Zheng, K. Kwak, M.D. Fayer, Acc. Chem. Res. 40 (2007) 75.

[45] K. Kwak, J. Zheng, H. Cang, M.D. Fayer, J. Phys. Chem. B 110 (2006) 19998.

[46] J. Zheng, K. Kwak, X. Chen, J.B. Asbury, M.D. Fayer, J. Am. Chem. Soc. 128 (2006) 2977.

[47] I.J. Finkelstein, J. Zheng, H. Ishikawa, S. Kim, K. Kwak, M.D. Fayer, Phys. Chem. Chem. Phys. 9 (2007) 1533.

[48] Y.S. Kim, R.M. Hochstrasser, Proc. Natl. Acad. Sci. 102 (2005) 11185.

[49] R.M. Hochstrasser, Proc. Natl. Acad. Sci. 104 (2007) 14190.

[50] K. Sagarik, P. Asawakun, Chem. Phys. 219 (1997) 173.

[51] K. Sagarik, B.M. Rode, Chem. Phys. 260 (2000) 159.

[52] K. Sagarik, S. Chaiyapongs, Biophys. Chem. 117 (2005) 18.

[53] K. Sagarik, S. Dokmaisrijan, J. Mol. Struct. (THEOCHEM) 718 (2005) 31.

[54] N. Deeying, K. Sagarik, Biophys. Chem. 125 (2006) 14.

[55] M. Orozco, F.J. Luque, Chem. Rev. 100 (2000) 4187.

[56] B.J. Costa Cabral, R.G. Bakker Fonseca, J.A. Martinho Simões, Chem. Phys. Lett. 258 (1996) 436.

[57] H.J, Böhm, R.J. Ahlrichs, J. Chem. Phys. 77 (1982) 2028.

[58] J.H, Dymond, E.B. Smith, The Virial Coefficients of Pure Gases and Mixtures, Clarendon Press, Oxford, 1980.

[59] H.B. Schlegel, J. Comput. Chem. 3 (1982) 214.

[60] Selected Values of Physical and Thermodynamics Properties of Hydrocarbons and Related Compounds, American Petroleum Institute Research Project 44, Carnegie Press, Pittsburg, 1953.

[61] SURFER for Window, V. 6.04, Golden Software Inc., USA, 1997.

[62] G.J. Borse, Numerical Methods with MATLAB: A resources for scientists and engineers, PWS Publishing, Boston, 1997.

[63] J.D. Gezelter, E. Rabani, B.J. Berne, J. Chem. Phys. 107 (1997) 4618.

[64] S. Chaiwongwattana, K. Sagarik, in preparation.

[65] H.G. Hertz, in: F. Franks (Ed). Water, A Comprehensive Treatise, V. 3, Plenum Press, New York, 1973.

[66] R.W. Impey, P.A. Madden, I.R. McDonald, J. Phys. Chem. 87 (1983) 5071.

[67] F. Brugé, E. Parisi, S.L. Fornili, Chem. Phys. Lett. 250 (1996) 443.

[68] C.H. Langford, H.B. Gray, Ligand Substitution Processes, W.A. Benjain, New York, 1966.

[69] E. Rabani, J.D. Gezelter, B.J. Berne, J. Chem. Phys. 107 (1997) 6867.

[70] J.D. Gezelter, E. Rabani, B.J. Berne, J. Chem. Phys. 110 (1999) 3444.

Figure 1 Equilibrium structures and interaction energies of the PhOH-Benz 1 : 1 complexes in the gas phase, computed from the T-model potentials.

Figure 2 Equilibrium structures and interaction energies of the PhOH-Benz 1 : 2 complexes in the gas phase, computed from the T-model potentials.

Figure 3 Structural and energetic results obtained from MD-$[PhOH]^{frozen}_{Benz}$.
X-, Y- and Z-axes are in Å, energies in kJ/mol.
a) – b) The π-PD, PB-PD and PB-BB-PD maps.
c) – d) Average potential energy landscapes and the cross section plots computed from longitudinal and transverse profile lines.
_____ PB-BB-PD cross section plot.
- - - - - PB-PD cross section plot.
- - - - - BB-PD cross section plot.

Note: π-PD contour: min = 0.0 : max = 0.13: interval = 0.01.
PB-PD contour: min = -18.0 : max = -3.0: interval = 2.5.
PB-BB-PD contour: min = -96.0 : max = -75.0: interval = 7.0.

Figure 4 Structural and dynamic results obtained from MD-$[PhOH]^{free}_{Benz}$.
a) – b) g(R); characteristic distances given with n(R) in parentheses.
c) Example of H-bond exchange diagram.
d) Fourier transformations of the O-H.. π H-bond and π_{ph}..π distances.

Note: $\tau^{PhOH-Benz}_{O-H..\pi}$ = the lifetime of the PhOH-Benz complex computed from FFT of the O-H.. π H-bond distance.
$\tau^{PhOH-Benz}_{\pi_{Ph}..\pi}$ = the lifetime of the PhOH-Benz complex computed from FFT of the π_{ph}.. π distance.

Figure 5 Structural and energetic results obtained from MD-$[(PhOH)_2]^{frozen}_{Benz}$.
X-, Y- and Z-axes are in Å, energies in kJ/mol.
a) – c) The π-PD, PB-PD and PB-BB-PD maps.
d) – e) Average potential energy landscapes and the cross section plots computed from longitudinal and transverse profile lines.
_____ PB-BB-PD cross section plot.
- - - - - PB-PD cross section plot.
- - - - - BB-PD cross section plot.

Note: π-PD contour: min = 0.0 : max = 0.13: interval = 0.01.
PB-PD contour: min = -30.0 : max = -1.0: interval = 4.5.
PB-BB-PD contour: min = -99.0 : max = -70.0: interval = 7.2.

Figure 6 Structural and dynamic results obtained from MD-$[(PhOH)_2]^{free}_{Benz}$.
a) – c) g(R); characteristic distances given with n(R) in parentheses.
d) Snapshots of the PhOH-Benz clusters in $[(PhOH)_2]_{Benz}$.
e) – f) Example of H-bond exchange diagram.

Figure 7 g(R) obtained from MD-$[(PhOH)_3]^{free}_{Benz}$, together with characteristic distances.

Figure-1

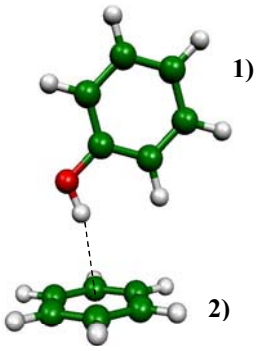

a) $\Delta E_{T\text{-model}}$ = -19.5 kJ/mol

O-H..π (1-2) = 3.4 Å
H..π (1-2) = 2.5 Å
π_{Ph}..π (1-2) = 5.4 Å

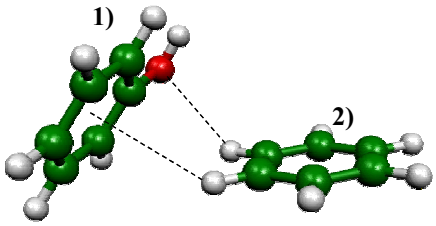

b) $\Delta E_{T\text{-model}}$ = -13.5 kJ/mol

C-H..O (2-1) = 3.4 Å
H..O (2-1) = 2.6 Å
C-H..π_{Ph} (2-1) = 4.0 Å
H..π_{Ph} (2-1) = 3.2 Å
π..π_{Ph} (2-1) = 5.1 Å

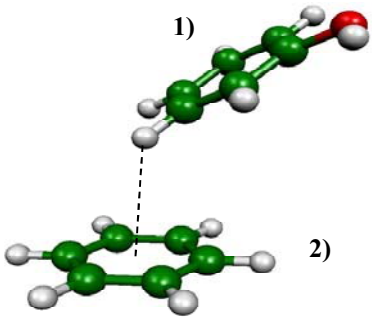

c) $\Delta E_{T\text{-model}}$ = -9.3 kJ/mol

C-H..π (1-2) = 3.8 Å
H..π (1-2) = 3.0 Å
π_{Ph}..π (1-2) = 4.9 Å

Fig. 1

Figure-2

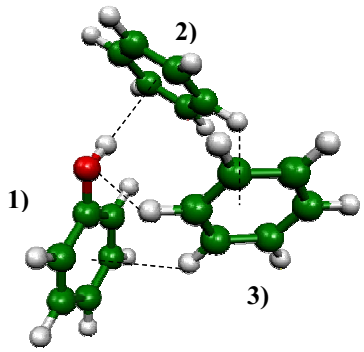

a) $\Delta E_{T\text{-model}}$ = -41.6 kJ/mol

O-H..π (1-2) = 3.4 Å
H..π (1-2) = 2.5 Å
π_{Ph}..π (1-2) = 5.2 Å

C-H..π (2-3) = 3.8 Å
H..π (2-3) = 3.0 Å
π..π (2-3) = 4.9 Å

C-H..O (3-1) = 3.3 Å
H..O (3-1) = 2.7 Å
C-H..π_{Ph} (3-1) = 4.0 Å
H..π_{Ph} (3-1) = 3.2 Å
π..π_{Ph} (3-1) = 5.0 Å

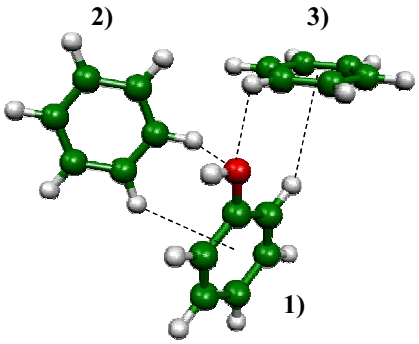

b) $\Delta E_{T\text{-model}}$ = -30.6 kJ/mol

C-H..π (1-3) = 4.4 Å
H..π (1-3) = 3.4 Å

C-H..O (3-1) = 3.3 Å
H..O (3-1) = 2.6 Å

C-H..O (2-1) = 3.3 Å
H..O (2-1) = 2.8 Å
C-H..π_{Ph} (2-1) = 4.0 Å
H..π_{Ph} (2-1) = 3.2 Å
π..π_{Ph} (2-1) = 5.0 Å

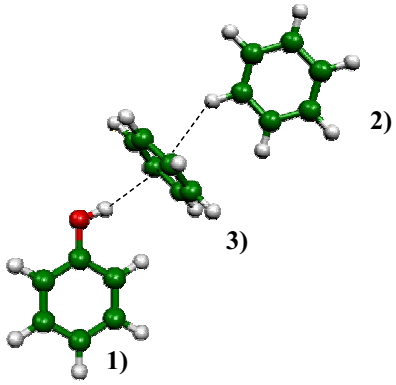

c) $\Delta E_{T\text{-model}}$ = -28.8 kJ/mol

O-H..π (1-3) = 3.4 Å
H..π (1-3) = 2.5 Å
π_{Ph}..π (1-3) = 5.4 Å

C-H..π (2-3) = 3.8 Å
H..π (2-3) = 2.9 Å
π..π (2-3) = 5.0 Å

Fig. 2

Figure-3

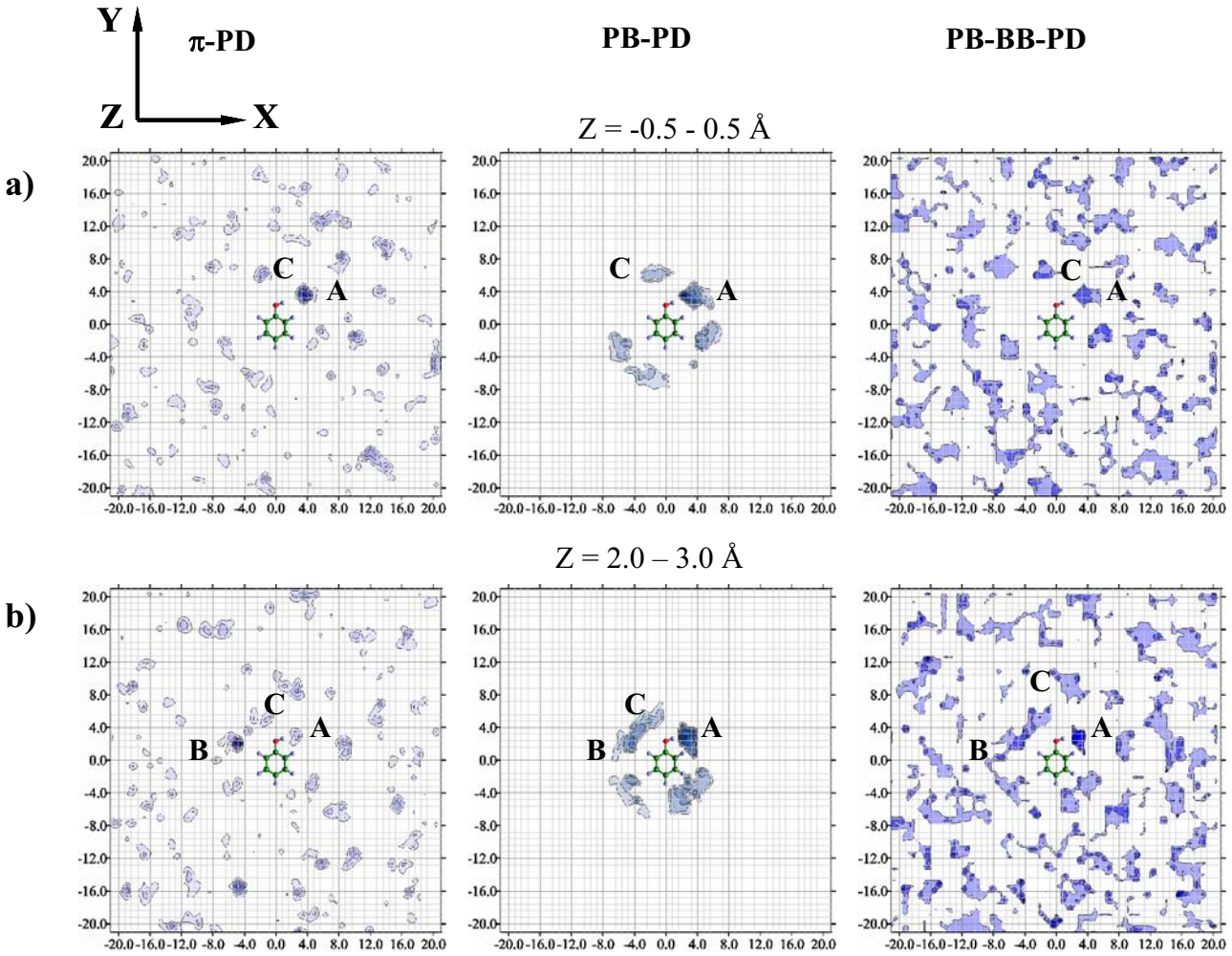

Fig. 3

c) Z = -0.5 – 0.5 Å

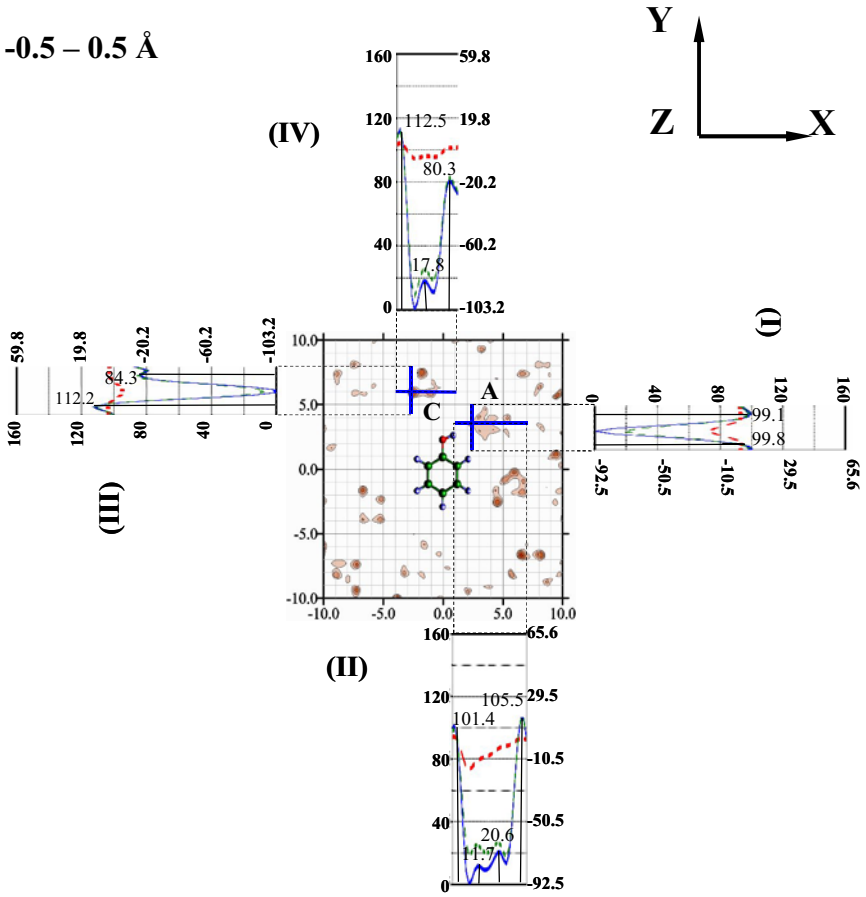

d) Z = 2.0 – 3.0 Å

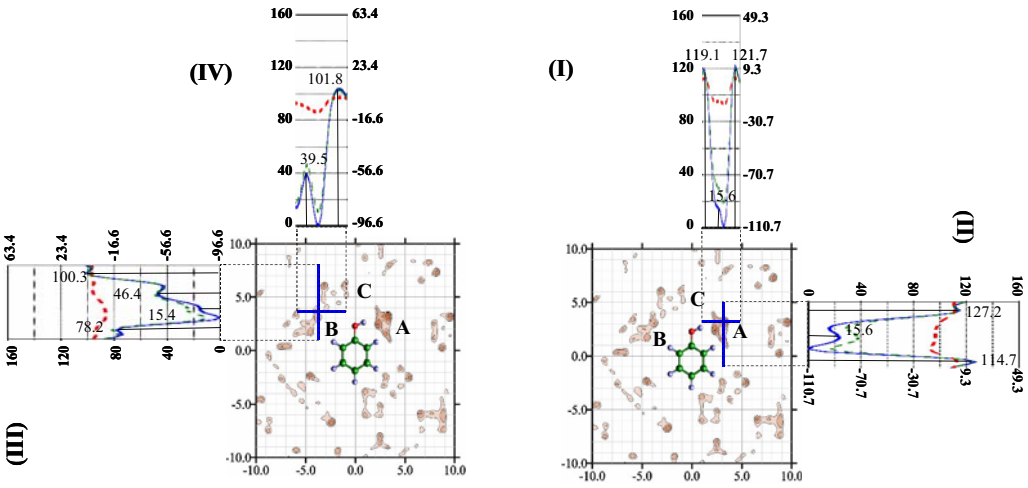

Fig. 3 (continued)

Figure-4

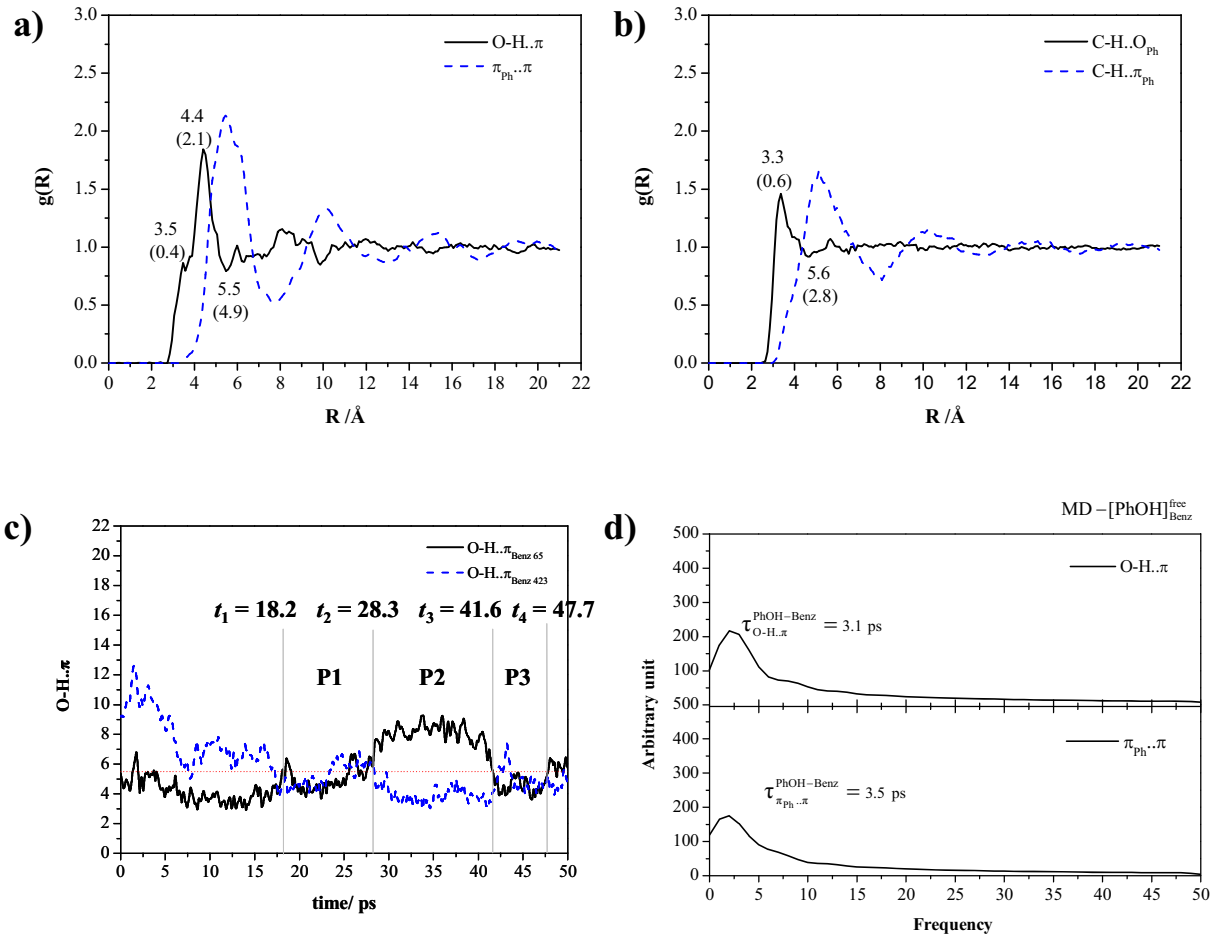

Fig. 4

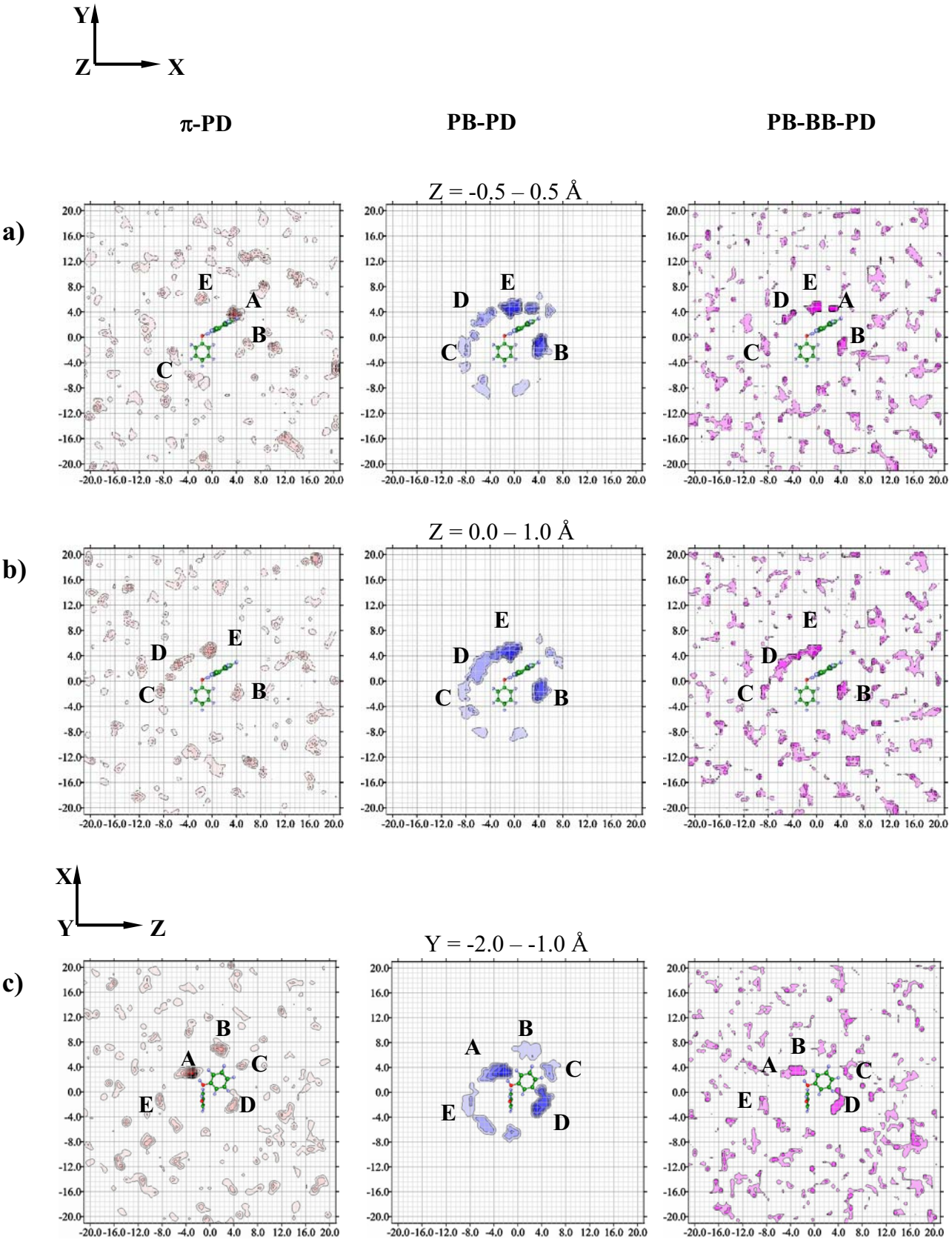

Fig. 5

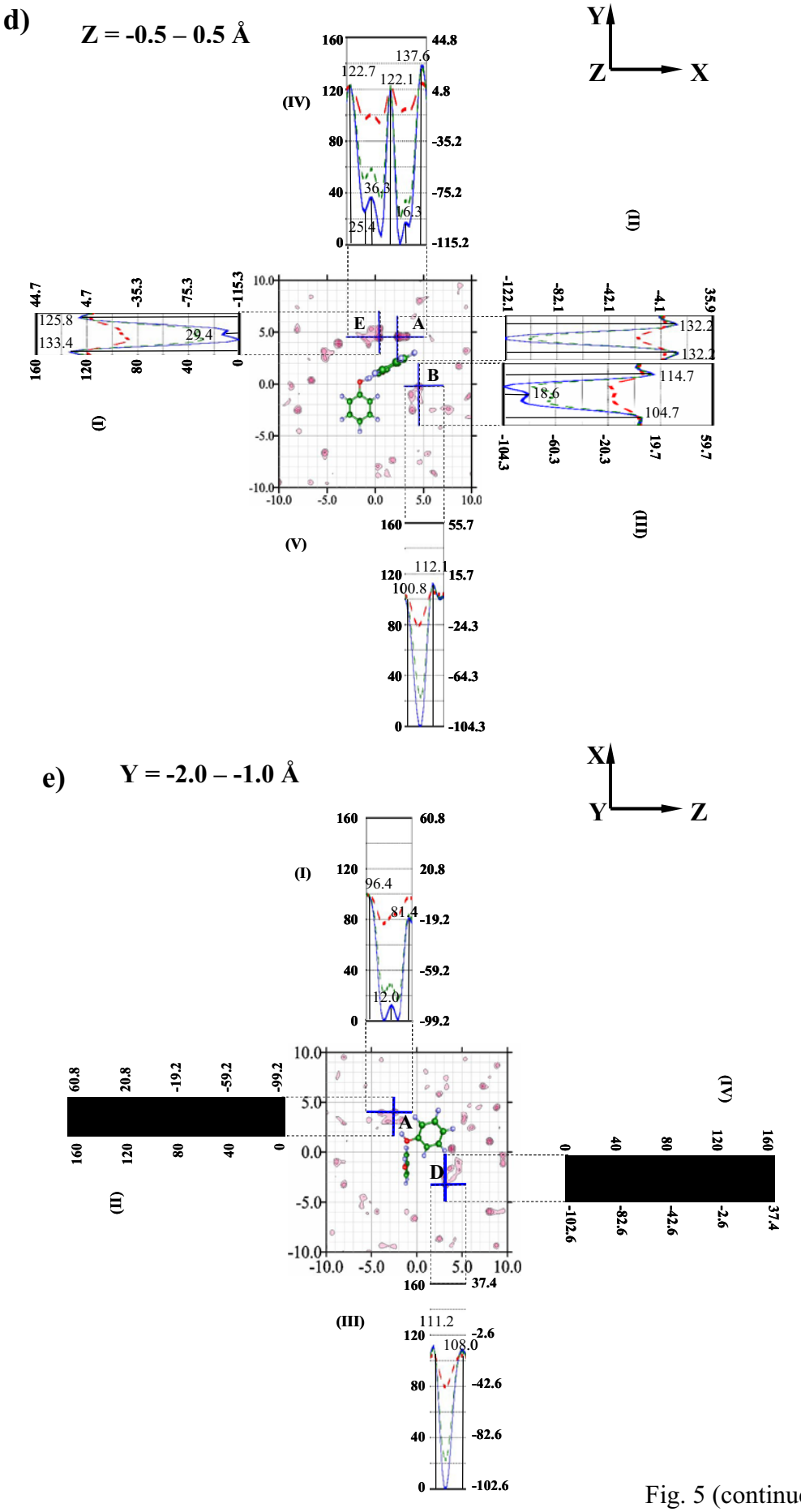

Fig. 5 (continued)

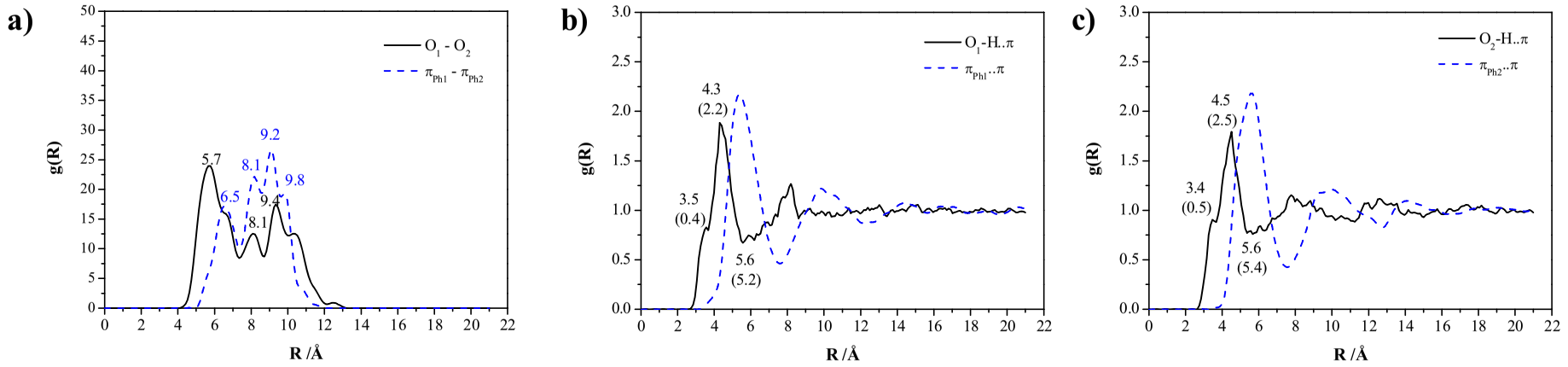

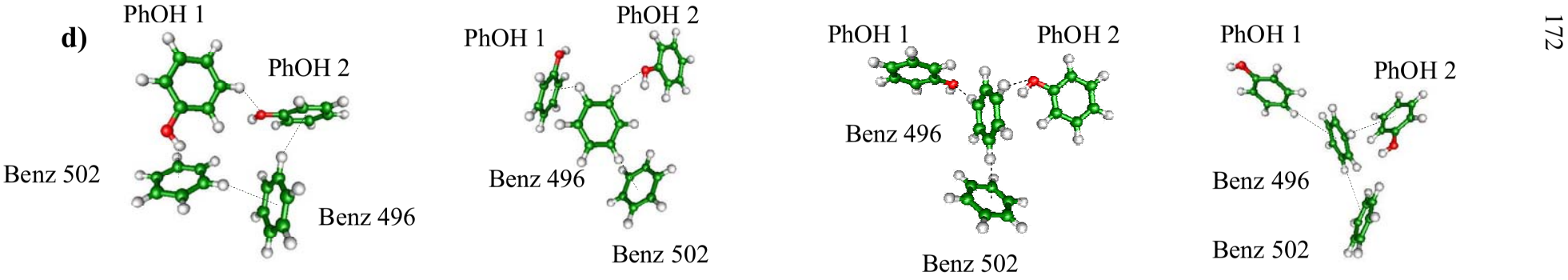

(I) $R_{\pi_{Ph1-Ph2}} = 6.7$ Å

(II) $R_{\pi_{Ph1-Ph2}} = 8.1$ Å

(III) $R_{\pi_{Ph1-Ph2}} = 9.0$ Å

(IV) $R_{\pi_{Ph1-Ph2}} = 9.7$ Å

Fig. 6

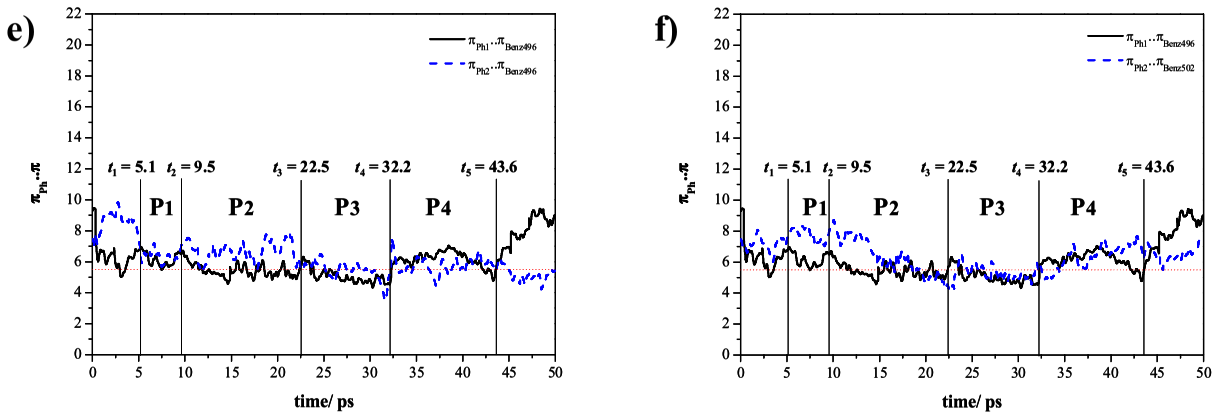

Fig. 6 (continued)

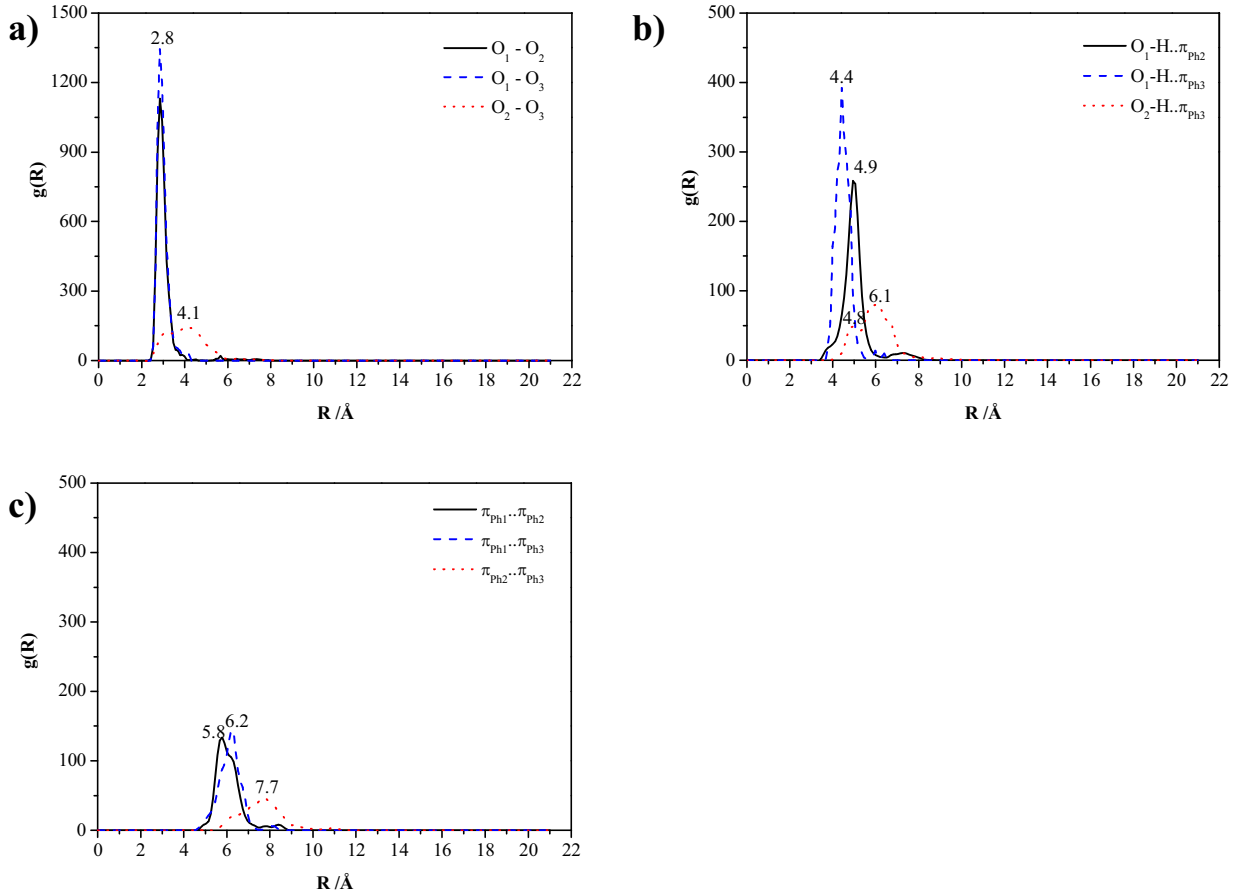
a)
2.8
4.1
O_1 - O_2
O_1 - O_3
O_2 - O_3
g(R)
R /Å
b)
4.4
4.9
6.1
4.8
O_1-H..π_{Ph2}
O_1-H..π_{Ph3}
O_2-H..π_{Ph3}
g(R)
R /Å
c)
5.8
6.2
7.7
π_{Ph1}..π_{Ph2}
π_{Ph1}..π_{Ph3}
π_{Ph2}..π_{Ph3}
g(R)
R /Å

Fig. 7

Table-1

Table 1 Energetic results obtained from MD-$[(PhOH)_n]^{frozen}_{Benz}$ and MD-$[(PhOH)_n]^{free}_{Benz}$, n = 1 – 3. Energies are in kJ/mol.

	$< E^{pot}_{Benz} >$	$< E^{solu-solu}_{Benz} >$	$< E^{solu-solv}_{Benz} >$
MD-$[PhOH]^{frozen}_{Benz}$	-35.4	-	-106.0
MD-$[PhOH]^{free}_{Benz}$	-35.3	-	-58.1
MD-$[(PhOH)_2]^{frozen}_{Benz}$	-35.5	-	-101.0
MD-$[(PhOH)_2]^{free}_{Benz}$	-35.5	-2.3	-123.4
MD-$[(PhOH)_3]^{free}_{Benz}$	-35.4	-51.8	-98.0

$< E^{pot}_{Benz} >$ = average potential energy.

$< E^{solu-solu}_{Benz} >$ = average solute-solute interaction energy.

$< E^{solu-solv}_{Benz} >$ = average solute-solvent interaction energy.

Table-2

Table 2 The highest probabilities at the labeled contours on the π-PD maps ($<P^{\pi\text{-PD}}>_{max}$) in Fig. 3, together with the corresponding lowest average interaction energies ($< \Delta E^{X}_{Benz} >_{min}$) obtained from MD-$[PhOH]^{frozen}_{Benz}$. Energies are in kJ/mol and X = PB-PD, BB-PD or PB-BB-PD.

	$<P^{\pi\text{-PD}}>_{max}$	$< \Delta E^{PB\text{-}PD}_{Benz} >_{min}$	$< \Delta E^{BB\text{-}PD}_{Benz} >_{min}$	$< \Delta E^{PB\text{-}BB\text{-}PD}_{Benz} >_{min}$
Z = -0.5 – 0.5 Å				
A	0.104	-17.28	-74.23	-83.65
C	0.042	-7.29	-79.74	-81.41
Z = 0.0 – 1.0 Å				
A	0.080	-16.10	-78.33	-94.43
C	0.034	-7.53	-77.17	-82.12
Z = 1.0 – 2.0 Å				
A	0.033	-16.10	-72.97	-83.14
B	0.031	-10.84	-72.94	-82.91
C	0.024	-7.91	-76.35	-88.18
Z = 2.0 – 3.0 Å				
A	0.036	-9.48	-76.87	-91.47
B	0.114	-11.71	-75.00	-86.06
C	0.027	-9.78	-74.77	-82.46

Table 3 The highest probabilities at the labeled contours on the π-PD maps ($<P^{\pi\text{-PD}}>_{max}$) in Fig. 5, together with the corresponding lowest average interaction energies ($<\Delta E^{X}_{Benz}>_{min}$) obtained from MD-$[(PhOH)_2]^{frozen}_{Benz}$. Energies are in kJ/mol and X = PB-PD, BB-PD or PB-BB-PD.

	$<P^{\pi\text{-PD}}>_{max}$	$<\Delta E^{PB\text{-}PD}_{Benz}>_{min}$	$<\Delta E^{BB\text{-}PD}_{Benz}>_{min}$	$<\Delta E^{PB\text{-}BB\text{-}PD}_{Benz}>_{min}$
Z = -0.5 – 0.5 Å				
A	0.083	-15.11	-79.86	-94.14
B	0.048	-23.67	-65.44	-79.34
C	0.054	-11.66	-76.19	-79.58
E	0.023	-23.89	-71.31	-93.26
Z = 0.0 – 1.0 Å				
B	0.038	-20.32	-70.17	-89.78
C	0.047	-9.06	-79.95	-82.23
D	0.053	-11.79	-73.16	-84.73
E	0.062	-23.91	-71.35	-91.18
Y = -2.0 – -1.0 Å				
A	0.133	-22.14	-73.05	-86.50
B	0.056	-7.10	-74.90	-80.76
C	0.035	-10.94	-81.60	-81.30
D	0.037	-20.85	-70.79	-86.51
E	0.039	-8.33	-80.29	-84.28
X = -1.0 – 0.0 Å				
A	0.047	-13.68	-74.05	-85.53
B	0.043	-18.03	-74.05	-92.08
C	0.106	-9.08	-75.12	-79.62
D	0.091	-26.68	-67.89	-87.73
E	0.040	-15.16	-78.05	-91.64

ผลผลิต

Publications

1. *Proton transfer reactions and dynamics in the CH_3OH-H_3O^+-H_2O Complexes*,
   K. Sagarik*, S. Chaiwongwattana and V. Vchirawongkwin,
   Phys. Chem. Chem. Phys., **12**, 918-929 (2010). (JIF = 4.12)
2. *Proton transfer reactions and dynamics in protonated water clusters*,
   K. Sagarik*, C. Lao-ngam, P. Asawakun and S. Wannarat, *submitted*.
3. *Proton transfer reactions and dynamics at sulfonic acid group of Nafion®,*
   M. Phonyiem and K. Sagarik, *submitted.*
4. *Structures and Dynamics of Phenol Clusters in Benzene Solutions*,
   S. Chaiwongwattana and **K. Sagarik**, *Chem. Phys*., **355**, 103-117 (2009). (JIF = 2.28)
   (Paper acknowledged BRG 5180022)

Presentations

1. *Structures and Dynamics of Proton Transfer at Sulfonate Group of Nafion®,*
   K. Sagarik, 7th International Conference of Computational Methods
   in Sciences and Engineering 2009 (ICCMSE 2009), Rhodes, Greece 2009.
2. *Proton transfer reactions and dynamics at hydrophilic group of Nafion®:*
   Born-Oppenheimer MD simulations on model systems,
   K. Sagarik, 43rd IUPAC world polymer congress, The Royal Society
   of Chemistry (RSC), Glasgow, United Kingdom 2010.

บทความสำหรับเผยแพร่

ปฏิกิริยาการถ่ายโอนโปรตอนและพลวัตในแนฟิออน

กฤษณะ สาคริก
สาขาวิชาเคมี สำนักวิชาวิทยาศาสตร์
มหาวิทยาลัยเทคโนโลยีสุรนารี นครราสีมา 30000

ปฏิกิริยาการถ่ายโอนโปรตอน (proton transfer reaction) ในสารละลายที่เป็นน้ำ ของเหลว และของแข็ง เป็นปฏิกิริยาสำคัญในวิชาเคมีไฟฟ้า โดยเฉพาะอย่างยิ่ง ที่เกี่ยวข้องกับการพัฒนาพลังงานทดแทน เช่น เซลล์เชื้อเพลิง (fuel cell) เซลล์เชื้อเพลิงที่ใช้เมมเบรนแลกเปลี่ยนโปรตอน (proton exchange membrane fuel cell, PEMFC) ส่วนใหญ่มีน้ำเป็นตัวกลาง โดยแปลงพลังงานเคมีที่เกิดขึ้นจากปฏิกิริยาระหว่างแก๊สไฮโดรเจนและออกซิเจนไปเป็นพลังงานไฟฟ้า เมมเบรนแลกเปลี่ยนโปรตอนที่นิยมใช้ในปัจจุบัน ได้แก่ Nafion® ซึ่งเป็นพอลิเมอร์ประเภท perfluorinated Nafion® มีความคงทนค่อนข้างสูง เนื่องจากการทำงานพื้นฐานของเซลล์เชื้อเพลิงขึ้นอยู่กับความสามารถในการถ่ายโอนโปรตอน (H^+) จากขั้วไฟฟ้าแอโนด (anode) ผ่านเมมเบรนแลกเปลี่ยนโปรตอนไปยังแคโทด (cathode) การพัฒนาประสิทธิภาพของเซลล์เชื้อเพลิงจึงต้องศึกษาปฏิกิริยามูลฐาน (elementary reaction) และพลวัต (dynamics) ของโปรตอนในตัวกลางต่างๆ ในรายละเอียด ถึงแม้ว่าที่ผ่านมาจะมีรายงานผลการศึกษาปฏิกิริยาการถ่ายโอนโปรตอนทั้งทางทฤษฎีและการทดลองมากพอควร ปรากฏว่าในปัจจุบันยังไม่มีข้อสรุปที่ชัดเจนและเป็นที่ยอมรับ

งานวิจัยเรื่องนี้ศึกษาปฏิกิริยามูลฐาน กลไกปฏิกิริยา และพลวัตของปฏิกิริยาการถ่ายโอนโปรตอนในแบบจำลอง protonated water clusters สารเชิงซ้อน CH_3OH-H_3O^+-H_2O และ CF_3SO_3H-H_3O^+-H_2O โดยใช้วิธีเคมีควอนตัมและ Born-Oppenheimer Molecular Dynamics (BOMD) simulations ที่ 350 K การศึกษาเริ่มจากการคำนวณโครงสร้างของสารเชิงซ้อนในสภาวะสมดุลโดยวิธี density functional theory (DFT method) ที่ระดับ B3LYP/TZVP โดยเน้นโครงสร้างพันธะไฮโดรเจนที่สามารถเกิดการถ่ายโอนโปรตอนได้ง่าย ผลการวิเคราะห์ IR spectra แสดง asymmetric O-H stretching frequency ของโปรตอนที่มีศักยภาพในการถ่ายโอนที่ $\nu^{OH} \approx 1000$ cm^{-1} โดยมีความถี่ขีดเริ่มเปลี่ยน (threshold frequency) (ν^{OH*}) ในช่วง 1700 ถึง 2200 cm^{-1} ทั้งนี้ ขึ้นกับชนิดและสภาพแวดล้อมของพันธะไฮโดรเจนที่นำมาศึกษา BOMD simulations แสดง ν^{OH} เพิ่มเติมที่ความถี่สูงขึ้น โดยแถบ IR ที่ความถี่ต่ำสัมพันธ์กับ oscillatory shuttling motion และที่ความถี่สูงสัมพันธ์กับ structural diffusion motion ความถี่ทั้งสองนี้ถือเป็นอัตลักษณ์สำคัญสำหรับโปรตอนที่มีศักยภาพในการถ่ายโอนโปรตอนสูง ผลการศึกษายังแสดงด้วยว่า การที่ในพันธะไฮโดรเจนมีการสั่นหลายประเภทคู่ควบกัน (coupling) ทำให้ไม่สามารถศึกษาปฏิกิริยาการถ่ายโอนโปรตอนโดยใช้ static proton transfer potential และแบบจำลองการคำนวณที่นำมาใช้ต้องพิจารณาการกระเพื่อมของพลังงานความร้อน (thermal energy fluctuation) และพลวัตในพันธะไฮโดรเจนด้วย

งานวิจัยเรื่องนี้ทำให้ทราบพฤติกรรมการสั่นของโปรตอนที่กำลังถ่ายโอนในรายละเอียด โดยได้เสนอทฤษฎีและแนวทางในการเปรียบเทียบความสามารถในการถ่ายโอนโปรตอนในพันธะไฮโดรเจนเมื่ออยู่ในสภาพแวดล้อมต่าง ๆ ตลอดจนเสนอเกณฑ์และวิธีการใช้ IR spectroscopy ในการติดตามปฏิกิริยาการถ่ายโอนโปรตอนที่ซับซ้อนขึ้น เช่น ในการทดลอง ทั้งนี้ ผลการวิจัยสามารถนำไปเป็นแนวทางในการประยุกต์ เพื่อการปรับปรุงประสิทธิภาพการถ่ายโอนโปรตอนในเมมเบรนแลกเปลี่ยนโปรตอนได้ในอนาคต

Proton transfer reactions and dynamics in Nafion®

Kritsana Sagarik
School of Chemistry, Institute of Science, Suranaree University of Technology
Nakhon Ratchasima 30000, THAILAND

Proton transfer reaction in condensed phase represents one of the most important problems in electrochemistry, especially in connection with the development of alternative energy sources such as fuel cells (FC). Since the basic operations in fuel cells depend upon the transportation of protons (H^+) generated at anode across proton exchange membrane (PEM) to cathode, it is vital to understand elementary reactions and dynamics of proton transfer processes in liquid, solid and aqueous solution. Although some theoretical and experimental information has been accumulated, precise mechanisms of proton transfer in PEMFC, especially in hydrogen bond (H-bond) complexes, are not completely known. In the present work, elementary reactions, energetic and dynamics of proton transfer were studied using three model systems namely, protonated water clusters, CH_3OH-H_3O^+-H_2O and CF_3SO_3H-H_3O^+-H_2O complexes. The H-bond complexes were investigated using quantum chemical methods and Born-Oppenheimer Molecular Dynamics (BOMD) simulations. The investigations began with searching for equilibrium structures at low hydration levels using the DFT method at the B3LYP/TZVP level, from which the H-bonds susceptible to proton transfer were characterized and analyzed. The analyses of IR spectra showed characteristic asymmetric O-H stretching frequencies of the transferring proton at $\nu^{OH} \approx 1000$ cm^{-1} and the threshold frequencies for proton transfer (ν^{OH*}) in the range of 1700 and 2200 cm^{-1}. However, these cannot be definitive, due to the neglect of the thermal energy fluctuation and dynamics in B3LYP/TZVP calculations. BOMD simulations at 350 K revealed an additional ν^{OH} at a higher frequency. The low- and high-frequency bands can be associated with the oscillatory shuttling and structural diffusion motions of the transferring proton in H-bond, respectively. The present results concluded that, due to coupling among various modes of vibrations, the discussions on proton transfer reactions cannot be made based on static proton transfer potentials. In order to study proton transfer reactions, thermal energy fluctuations and dynamics must be included in the model calculations, as in the case of BOMD simulations. The present work provided insights into vibrational behaviors of the transferring protons, as well as suggested theoretical methods and criteria to monitor and improve the efficiency of proton transfer in more complex systems.

กิตติกรรมประกาศ

The authors would like to acknowledge the financial supports from the Thailand Research Fund (TRF); the Advanced Research Scholarship (BRG-5180022) for Prof. Kritsana Sagarik; the Royal Golden Jubilee (RGJ) Ph.D. Program, Grant No. PHD/0110/2548 for Prof. Kritsana Sagarik and Mayuree Phonyiem; RGJ-Ph.D. Program, Grant No. PHD/0121/2549 for Prof. Kritsana Sagarik and Chareonsak Lao-Ngam. High- performance computer facilities provided by the following organizations are gratefully acknowledged: School of Mathematics and School of Chemistry, SUT; National Electronics and Computer Technology Center (NECTEC) and National Nanotechnology Center (NANOTEC), National Science and Technology Development Agency (NSTDA); the Thai National Grid Center (THAIGRID), Ministry of Information and Communication Technology (MICT).

ภาคผนวก

Proton transfer reactions and dynamics in CH_3OH–H_3O^+–H_2O complexes

Kritsana Sagarik,*[a] Sermsiri Chaiwongwattana,[a] Viwat Vchirawongkwin[b] and Supakit Prueksaaroon[c]

Received 7th July 2009, Accepted 26th October 2009
First published as an Advance Article on the web 4th December 2009
DOI: 10.1039/b913385b

Proton transfer reactions and dynamics in hydrated complexes formed from CH_3OH, H_3O^+ and H_2O were studied using theoretical methods. The investigations began with searching for equilibrium structures at low hydration levels using the DFT method, from which active H-bonds in the gas phase and continuum aqueous solution were characterized and analyzed. Based on the asymmetric stretching coordinates (Δd_{DA}), four H-bond complexes were identified as potential transition states, in which the most active unit is represented by an excess proton nearly equally shared between CH_3OH and H_2O. These cannot be definitive due to the lack of asymmetric O–H stretching frequencies (ν^{OH}) which are spectral signatures of transferring protons. Born–Oppenheimer molecular dynamics (BOMD) simulations revealed that, when the thermal energy fluctuations and dynamics were included in the model calculations, the spectral signatures at $\nu^{OH} \approx 1000\ cm^{-1}$ appeared. In continuum aqueous solution, the H-bond complex with incomplete water coordination at charged species turned out to be the only active transition state. Based on the assumption that the thermal energy fluctuations and dynamics could temporarily break the H-bonds linking the transition state complex and water molecules in the second hydration shell, elementary reactions of proton transfer were proposed. The present study showed that, due to the coupling among various vibrational modes, the discussions on proton transfer reactions cannot be made based solely on static proton transfer potentials. Inclusion of thermal energy fluctuations and dynamics in the model calculations, as in the case of BOMD simulations, together with systematic IR spectral analyses, have been proved to be the most appropriate theoretical approaches.

Introduction

Proton transport in condensed phases represents one of the most important problems in electrochemistry, especially in connection with the development of alternative energy sources such as fuel cells (FC).[1,2] Since the basic operations in fuel cells depend upon the transportation of protons (H^+) generated at the anode across a proton exchange membrane (PEM)—often made from Nafion®—to the cathode, where they react with oxygen to produce water,[1] it is vital to understand elementary reactions and dynamics of proton transfer processes in liquids, solid and aqueous solutions. Although some theoretical and experimental information has been accumulated,[3–6] precise mechanisms of proton transfer in PEMFC, especially for those employing methanol (CH_3OH) as a direct fuel, are not completely known. Since some basic chemistry of proton transfer reactions has been discussed in details in many review articles,[4–6] only the theoretical and experimental information relevant to the present study will be briefly summarized here.

CH_3OH has been frequently selected as a model compound for the investigation of proton transport in hydrogen bonds (H-bonds).[7–20] The abnormally high mobility of an excess proton in liquid methanol ($[CH_3OH]_{liq}$) has been extensively studied using *ab initio* molecular dynamics (MD) simulations, from which a structural diffusion mechanism of cationic defects was proposed.[16] Having both hydrophobic (CH_3) and hydrophilic (OH) groups in the same molecule makes the H-bond structures in $[CH_3OH]_{liq}$ different from $[H_2O]_{liq}$; one-dimensional linear H-bond chains with occasional branches seem to be the predominant species from 153 K to room temperature.[19] Due to significant roles played by the methyloxonium ion ($CH_3OH_2^+$) in direct methanol fuel cells (DMFC),[17] delocalization of proton in the H-bond complexes formed from H_3O^+, CH_3OH and H_2O has been extensively studied.[13–16] In the presence of an excess proton, two H-bond structures dominate in the CH_3OH–H_2O clusters, namely the fully solvated and open chain structures.[13] The excess proton is preferentially taken by CH_3OH in the open chain structure.[13] A structural analogue of the Zundel complex ($C_2H_9O_2^+$) and $CH_3OH_2^+$ were suggested by density functional theory (DFT) calculations at the B3LYP/6-31 + G(d) level and

[a] *School of Chemistry, Institute of Science, Suranaree University of Technology, Nakhon Ratchasima 30000, Thailand. E-mail: kritsana@sut.ac.th; Fax: (6644) 224635; Tel: (6644) 224635*
[b] *Department of Chemistry, Faculty of Science, Chulalongkorn University, Bangkok 10500, Thailand*
[c] *National Electronics and Computer Technology Center (NECTEC), Pathumthani 12120, Thailand*

vibrational predissociation spectroscopy to play important roles in proton transfer in the mixed H-bond clusters.[15]

Proton affinities in the CH_3OH–H_3O^+–H_2O $1:1:n$ complexes, $1 \leqslant n \leqslant 5$, were investigated in the gas phase using DFT calculations and IR spectroscopy at 170 K.[20] DFT calculations at the B3LYP/6-31G + (d) level revealed that the excess proton can be either localized close to CH_3OH or H_2O, forming $CH_3OH_2^+$ or H_3O^+, respectively. The position of the excess proton is sensitive to the number of water molecules, as well as the geometry of the H-bond complexes. The IR spectral signatures determined from the free O–H stretching frequencies in the range of 2700 and 3900 cm^{-1} indicated that $CH_3OH_2^+$ and H_3O^+ possess comparable stability and could be concurrently detected in the gas phase.[20] Moreover, in the CH_3OH–H_3O^+–H_2O $1:1:n$ complexes, the excess proton could be preferentially captured by CH_3OH when $n = 1$ and equally shared by CH_3OH and H_2O when $n = 3$. The excess proton could gradually move away from CH_3OH when $n \geq 3$. The results in ref. 20 led to the conclusion that the protonated ions in acidic $[CH_3OH]_{aq}$ are quite flexible and can fluctuate rapidly over $CH_3OH_2^+$, H_3O^+ and $CH_9O_3^+$.

Vibrational spectroscopy has been one of the most powerful techniques in H-bond research.[21] This is due to the fact that the most evident effects of the A–H$\cdots$B H-bond formation are the red shifts of the A–H stretching mode, accompanied by its intensity increase and band broadening.[13,18] Analyses of the A–H stretching frequencies could also lead to valuable information on proton transfer reactions in H-bonds.[17] As an example, IR experiments,[22] quantum-dynamical calculations[23–25] and Born–Oppenheimer MD (BOMD) simulations[26] suggested that the vibrational spectra of the Zundel complex ($H_5O_2^+$) in aqueous solutions can be divided into three distinct regions. The vibrational frequencies above 3000 cm^{-1} correspond to the symmetric and asymmetric stretching modes of individual water molecules, whereas those between 1000 and 2000 cm^{-1} are associated with the characteristic vibrational frequencies of the transferring protons.[25] The correlation between the O–H stretching frequency and the probability of proton transfer in H-bond was investigated and discussed in detail in ref. 13 and 17. Although the assignments of all the features of the individual spectra were not made due to the coupling and overlapping of various vibrational modes, as well as the detection limit of the IR equipment,[20,21] the probability of proton transfer could be associated with the degree of the red shift, by comparison with the corresponding "free" or "non-H-bonded" O–H stretching frequency.[13]

In our previous work,[27] elementary reactions of proton transfer processes at a sulfonic acid group (–SO_3H) of Nafion® were studied using the H-bond complexes formed from triflic acid (CF_3SO_3H), H_3O^+ and H_2O as model systems. BOMD simulations at 298 K revealed that a quasi-dynamic equilibrium could establish between the Eigen ($H_9O_4^+$) and Zundel complexes, and is considered to be one of the most important elementary reactions. It was demonstrated that proton transfer reactions at –SO_3H are not concerted due to the thermal energy fluctuations, leading to quasi-dynamic equilibriums among precursors, transition state complexes and products. Most importantly, –SO_3H could directly and indirectly mediate proton transfer reactions through the formation of proton defects, as well as the –SO_3^- and –$SO_3H_2^+$ transition states.

In order to obtain information for the investigations of DMFC, elementary reactions and dynamics of proton transfer in hydrated complexes formed from CH_3OH, H_3O^+ and H_2O were studied in the present work. The H-bond complexes were systematically investigated using quantum chemical methods and BOMD simulations, both in the gas phase and continuum aqueous solution. Since proton transfer reactions could be characterized by vibrational motions of the active protons, vibrational frequencies in H-bonds were computed, categorized and analyzed. Based on the information from quantum chemical calculations and BOMD simulations, elementary reactions and dynamics of proton transfer in the model systems were discussed in comparison with available theoretical and experimental data of the same and similar systems.

Computational methods

Since proton transfer reactions are complicated, care must be exercised in selecting appropriate model systems and theoretical methods. Our experience[27] showed that elementary reactions and dynamics of proton transfer in H-bonds could be studied reasonably well by taking the following three basic steps: (1) searching for all potential precursors and transition state complexes in proton transfer pathways using pair potentials; (2) refinements of the computed structures using an accurate quantum chemical method; (3) BOMD simulations starting from the refined structures. These three steps were also applied in the present work.

Our experience also showed that the inclusion of too many water molecules in the model systems could lead to difficulties in the analyses of proton transfer reactions.[27] Therefore, it was the strategy of the present work to restrict the number of water molecules in the model systems. Since the $CH_3OH_2^+$–CH_3OH complex contributes only 5% to the proton transfer events[14] and the excess proton starts to move away from $CH_3OH_2^+$ when $n = 3$,[20] the CH_3OH–H_3O^+–H_2O $1:1:n$ complexes, $1 \leq n \leq 3$, were chosen in the present study. Some basic structural and dynamic properties of the CH_3OH–H_2O and CH_3OH–H_3O^+ complexes were also investigated.

In order to characterize IR spectra of the transferring proton, as well as their correlations with the probability of proton transfer,[28] O–H stretching frequencies in H-bonds were computed and analyzed, using a quantum chemical method and BOMD simulations. Since the electric field introduced by the polar solvent could determine the potential energy surface on which the active proton moves, a continuum solvent model had to be included in the model calculations. In the present work, the conductor-like screening model (COSMO), with a dielectric constant (ε) of 78, was employed to account for the effects of the extended H-bond networks of water, which were not explicitly included in the model systems. A literature survey showed that COSMO has been applied successfully in various H-bond systems.[29]

Searching for potential precursors and transition state complexes

All the H-bond complexes which could serve as precursors and transition state complexes in proton transfer pathways were

searched, characterized and analyzed. In order to effectively scan the intermolecular potential energy surfaces, test-particle model (T-model) potentials[30–39] were constructed and employed in the calculations of the equilibrium structures and interaction energies of the hydrated complexes. Since the applicability of the T-model had been discussed in details in our previous studies,[30–39] only some important aspects relevant to the geometry optimizations will be briefly summarized using the CH_3OH–H_3O^+–H_2O 1 : 1 : 1 complex as an example.

Experimental geometries of CH_3OH, H_3O^+ and H_2O were employed[40] and kept constant in the geometry optimizations. For the CH_3OH–H_3O^+–H_2O 1 : 1 : 1 complex, a rigid CH_3OH was placed at the origin of the Cartesian coordinate system. The coordinates of H_3O^+ and H_2O were randomly generated in the vicinities of CH_3OH. Based on the T-model potentials, equilibrium structures of the complex were searched using a minimization technique. One hundred starting configurations were generated and employed as starting configurations in the geometry optimizations. The same procedures were applied in the calculations of equilibrium structures and interaction energies of the hydrated complexes considered here.

Structural refinements and vibrational spectra

Since the T-model potentials are based on rigid molecules, in which cooperative effects are not taken into account, structural refinements with full geometry optimizations had to be made using an appropriate quantum chemical method. A literature survey showed that DFT methods have been frequently chosen due to their ability to predict the effects of electron correlations with a reasonable degree of accuracy, especially for similar H-bond systems.[41–46] Since, in the present investigations, the calculations of vibrational spectra and lengthy BOMD simulations had to be performed, it was necessary to compromise between the accuracy of the theoretical method and available computer resources. In order to achieve all the objectives, DFT calculations were performed using the B3LYP hybrid functional[47] and the triple-zeta valence basis sets augmented by polarization functions (TZVP).[48] The performance of B3LYP in the calculations of vibrational spectra of similar systems was examined and discussed in detail in ref. 49 and 50. It was shown that B3LYP/TZVP calculations are sufficient for the systems with and without occupied d-states, and could be applied reasonably well in the calculations of equilibrium structures and interaction energies, as well as vibrational spectra, of such systems.[49]

The absolute and local minimum energy geometries of the H-bond complexes computed from the T-model potentials were employed as starting configurations in B3LYP/TZVP geometry optimizations. In order to ensure that the optimized geometries are at the stationary points of the potential energy surfaces, a tight SCF (self consistent field) energy convergence criterion (less than 10^{-8} au) with a maximum norm of Cartesian gradients of less than 10^{-4} au were adopted in B3LYP/TZVP geometry optimizations. In the present work, B3LYP/TZVP calculations were made using the TURBOMOLE 6.0 software package.[51]

The experiment in ref. 17 showed that the H-bond distance ($R_{O\cdots O}$) in concentrated HCl solutions could be divided into three groups, namely the internal, external and solvation groups. The H-bonds linking directly to proton belong to the internal group, with $R_{O\cdots O}$ in the range of 2.45–2.57 Å, whereas $R_{O\cdots O}$ in the external and solvation groups are in the ranges of 2.60–2.70 Å and longer than 2.70 Å, respectively. The H-bond protons in the internal group are considered to be active in proton transfer. In the present work, an attempt was made to use similar criteria[17] to discuss the tendency of proton transfer in H-bonds. A concept of the "most active" H-bond[52] was tentatively applied to describe the Grothuss mechanism.[53] Within the framework of the most active H-bond, the asymmetric stretching coordinate of a donor (D)–acceptor (A) pair is defined by $\Delta d_{DA} = |d_{A\cdots H} - d_{B\cdots H}|$;[14] $d_{A\cdots H}$ and $d_{B\cdots H}$ are the A–H and B$\cdots$H distances, respectively. A H-bond is considered to be "active" with respect to proton transfer when $\Delta d_{DA} < 0.1$ Å, and "inactive" when $\Delta d_{DA} > 0.4$ Å.[14] Therefore, according to Δd_{DA}, the H-bond in $H_5O_2^+$ is the most active ($\Delta d_{DA} = 0$); the H-bond proton is equally shared by the two water molecules. In the present work, the internal and external H-bonds were classified using plots between Δd_{DA} and $R_{O\cdots O}$; appropriate functions were chosen by the least squares method to represent the relationships in the internal and external groups.

Assuming no coupling between degrees of freedom, harmonic vibrational frequencies were computed in the present work from numerical second derivatives, from which the analyses of normal modes in terms of internal coordinates were made, using NUMFORCE and AOFORCE programs,[51] respectively. Being associated with the dynamics of proton transfer in H-bonds,[54] asymmetric O–H stretching frequencies (ν^{OH}) were of primary interest. It should be noted that vibrational frequencies derived from quantum chemical calculations are generally overestimated compared to experimental values, and a scaling factor which partially accounts for anharmonicities and systematic errors is required. Although the exact O–H stretching frequencies were not the main objective, a scaling factor was applied in the present study; the scaling factor of 0.9614 was proved to be appropriate for B3LYP calculations.[55]

In order to measure the activity of H-bond protons in terms of ν^{OH}, classical interpretations of IR stretching frequencies for concentrated acid solutions[56] were employed as criteria; IR stretching frequencies of H-bond protons were divided into three groups, namely the internal (1300–2200 cm^{-1}), external (2500–3200 cm^{-1}) and outer layer groups (3300–3400 cm^{-1}). In order to correlate the concept of the most active H-bond with the classical interpretations of IR stretching frequencies,[56] the H-bonds in the internal and external groups were distinguished based on the relationship between ν^{OH} and $R_{O\cdots O}$; ν^{OH} and $R_{O\cdots O}$ were plotted and appropriate functions were chosen using the least squares method.

Quantum MD simulations

Dynamics of rapid covalent bond formation and cleavage could be studied reasonably well using quantum MD simulations,[57] among which DFT-MD simulations have been widely used in recent years.[58,59] In the present work, proton transfers in the CH_3OH–H_3O^+ and CH_3OH–H_3O^+–H_2O complexes were investigated using BOMD simulations[60,61]

with canonical ensemble (NVT) at 350 K. Within the framework of BOMD simulations, classical equations of motion of nuclei on the BO (Born–Oppenheimer) surfaces are integrated, whereas forces on nuclei are calculated in each MD step from quantum energy gradients, with the molecular orbitals (MOs) updated by solving Schrödinger equations. BOMD simulations are therefore more accurate, as well as considerably CPU time consuming, compared to conventional classical MD simulations, in which forces on nuclei are determined from predefined empirical or quantum pair potentials. Although the high mobility of protons was initially attributed to quantum mechanical (QM) tunneling,[62,63] the results of BOMD simulations[25] and conductivity measurements[64] showed that mechanisms of proton transfer could be explained reasonably well without assuming proton tunneling to be the important pathways.

In order to ensure that all important dynamics of proton transfer processes in the CH_3OH–H_3O^+–H_2O complexes were taken into account, the equilibrium structures computed in the previous section were used as starting configurations in BOMD simulations. Since proton transfer in aqueous solutions involves dynamic processes with different timescales,[65–67] the complexity of proton transfer reactions could be reduced using various approaches. The observation that the actual proton transfer occurs on a femtosecond (fs) timescale,[67] which is, in general, faster than solvent structure reorganization,[66] made it possible to perform BOMD simulations by focusing on short-lived phenomena taking place before H-bond structure reorganizations. Since, in aqueous solutions, the rapid interconversion between the Zundel and Eigen complexes happens within 100 fs (10^{-13} s),[65] the timestep used in solving dynamic equations was set to about 1 fs (0.968 fs = 40 au). In each BOMD simulations, 4000 timesteps were devoted to equilibration and 10 000 timesteps to property calculations, corresponding to about 10 ps. In order to ensure that, in the course of the BOMD simulations, the active proton is not trapped in a minimum, appropriate temperature fluctuations must be selected, as suggested in ref. 68. This was accomplished in TURBOMOLE 6.0[51] by applying the Nose-Hoover thermostat at every 30 BOMD steps.

In order to search for spectral signatures of transferring protons, IR spectra of H-bonds were computed from Fourier transformations of the velocity autocorrelation function (VACF);[69] the approach is appropriate as it allows various vibrational modes to be computed separately. Since only the H-bond protons involved in structural diffusion were of interest and the reorientation of water molecules takes about 1–2 ps,[70,71] IR spectra were calculated within a short time limit of 1 ps. This choice can be justified by the observation that the average lifetime of the H-bond in CH_3OH–H_2O solutions is approximately 1.2 ps.[14] Only symmetric and asymmetric O–H stretching frequencies (ν^{OH}) of the H-bond protons, as well as the O–O vibrations, were of interest.

The diffusion coefficient (D) of the active proton could be computed from BOMD simulations. The Einstein equation[72–74] was employed in the present work, by which the diffusion coefficient is determined from the slope of the mean square displacement (MSD). Since the calculations of the diffusion coefficient of a single particle (H^+) confined in a short H-bond distance are not straightforward,[73,74] care must be exercised, especially in selecting the time interval over which MSDs were computed; the time interval cannot be too large due to the limitation of the allowed displacement.[74] After several test calculations, linear relationships between MSD and simulation time could be obtained when the time intervals are not larger than 0.5 ps.

Results and discussions

Equilibrium structures and vibrational frequencies

Fig. 1 shows the refined equilibrium structures and interaction energies (ΔE) of the H-bond complexes in the gas phase and continuum aqueous solution, together with characteristic H-bond distances and asymmetric stretching coordinates (Δd_{DA}). Asymmetric O–H stretching frequencies (ν^{OH}) of H-bond protons are given in Fig. 2, together with the frequency shifts ($\Delta\nu^{OH}$) due to the continuum aqueous solvent. The red shifts are designated by negative values of $\Delta\nu^{OH}$. It appeared that the equilibrium structures in the gas phase and continuum aqueous solution are the same and agree well with the theoretical results in ref. 20. Therefore, only Δd_{DA}, ν^{OH} and $\Delta\nu^{OH}$, which could be related to the tendencies of proton transfer in H-bonds, are discussed in details. In order to simplify the discussion, the H-bonds in Fig. 1 and 2 are labeled with numbers in parentheses.

For the CH_3OH–H_2O complex in the gas phase, B3LYP/TZVP calculations predicted the structure, in which a water molecule acts as a proton donor, to be about 1.8 kJ mol^{-1} more stable than the one as proton acceptor (structures (a) and (b) in Fig. 1, respectively). The results are in excellent agreement with microwave[75] and IR measurements.[76] The stabilities of structures (a) and (b) are considerably increased in continuum aqueous solution, with $\Delta E = -73.4$ and -72.8 kJ mol^{-1}, respectively. Δd_{DA} and ν^{OH} do not show a tendency of proton transfer in structures (a) and (b), both in the gas phase and continuum aqueous solution.

Interesting results were obtained for the CH_3OH–H_3O^+ complex (structure (c) in Fig. 1). B3LYP/TZVP calculations revealed that the H-bond proton tends to protonate at CH_3OH, forming $CH_3OH_2^+$. This is in accordance with the observation that CH_3OH in acid solution possesses a higher proton affinity than water.[75] Δd_{DA} shows a slightly higher tendency of proton transfer in the continuum aqueous solution compared to the gas phase (0.24 and 0.32 Å, respectively). The trends of Δd_{DA} are supported by the asymmetric O–H stretching frequencies in Fig. 2. The strong IR absorption peaks at $\nu^{OH} = 2086$ and 1690 cm^{-1} appeared to be the characteristics of the H-bond proton in the CH_3OH–H_3O^+ complex in the gas phase and continuum aqueous solution, respectively, with $\Delta\nu^{OH} = -369$ cm^{-1}. It was reported in ref. 20 that the asymmetric O–H stretching frequencies cannot be measured easily in experiments since the energy provided by a single IR photon is much lower than the minimum energy required to dissociate this complex *via* one-photon excitation processes.

Structures (d) and (e) in Fig. 1 are the two minimum energy geometries of the CH_3OH–H_3O^+–H_2O 1 : 1 : 1 complex. For structure (d), the H-bond between CH_3OH and H_3O^+

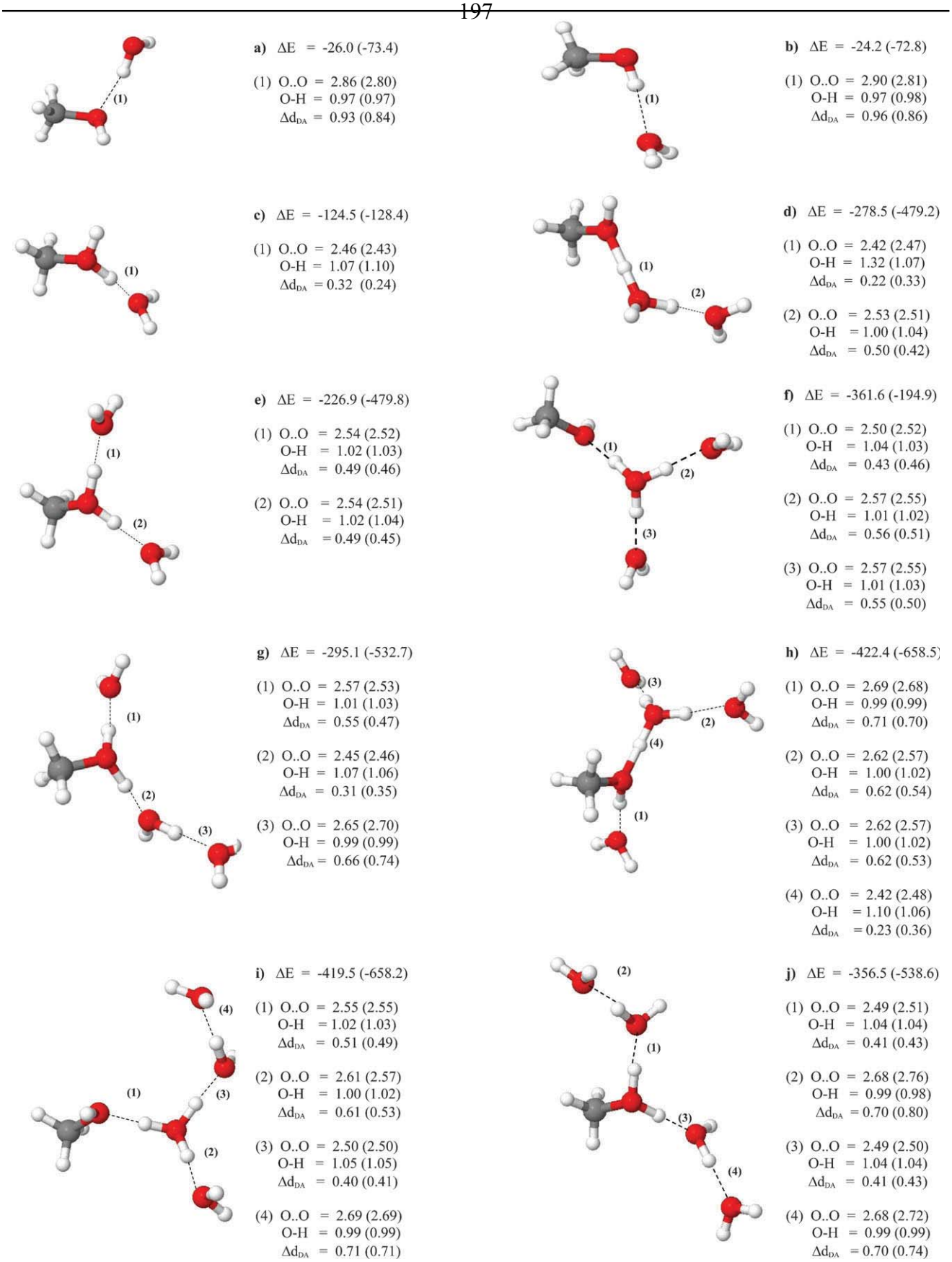

Fig. 1 Refined equilibrium structures, interaction energies (ΔE) and asymmetric stretching coordinates (Δd_{DA}) of the CH_3OH–H_2O, CH_3OH–H_3O^+ and CH_3OH–H_3O^+–H_2O complexes, obtained from B3LYP/TZVP geometry optimizations. H-bond distances are in Å and energies in kJ mol^{-1}. The values in parentheses are the results in continuum aqueous solution. (a)–(b) CH_3OH–H_2O complexes. (c) CH_3OH–H_3O^+ complex. (d)–(e) CH_3OH–H_3O^+–H_2O 1 : 1 : 1 complexes. (f)–(g) CH_3OH–H_3O^+–H_2O 1 : 1 : 2 complexes. (h)–(j) CH_3OH–H_3O^+–H_2O 1 : 1 : 3 complexes.

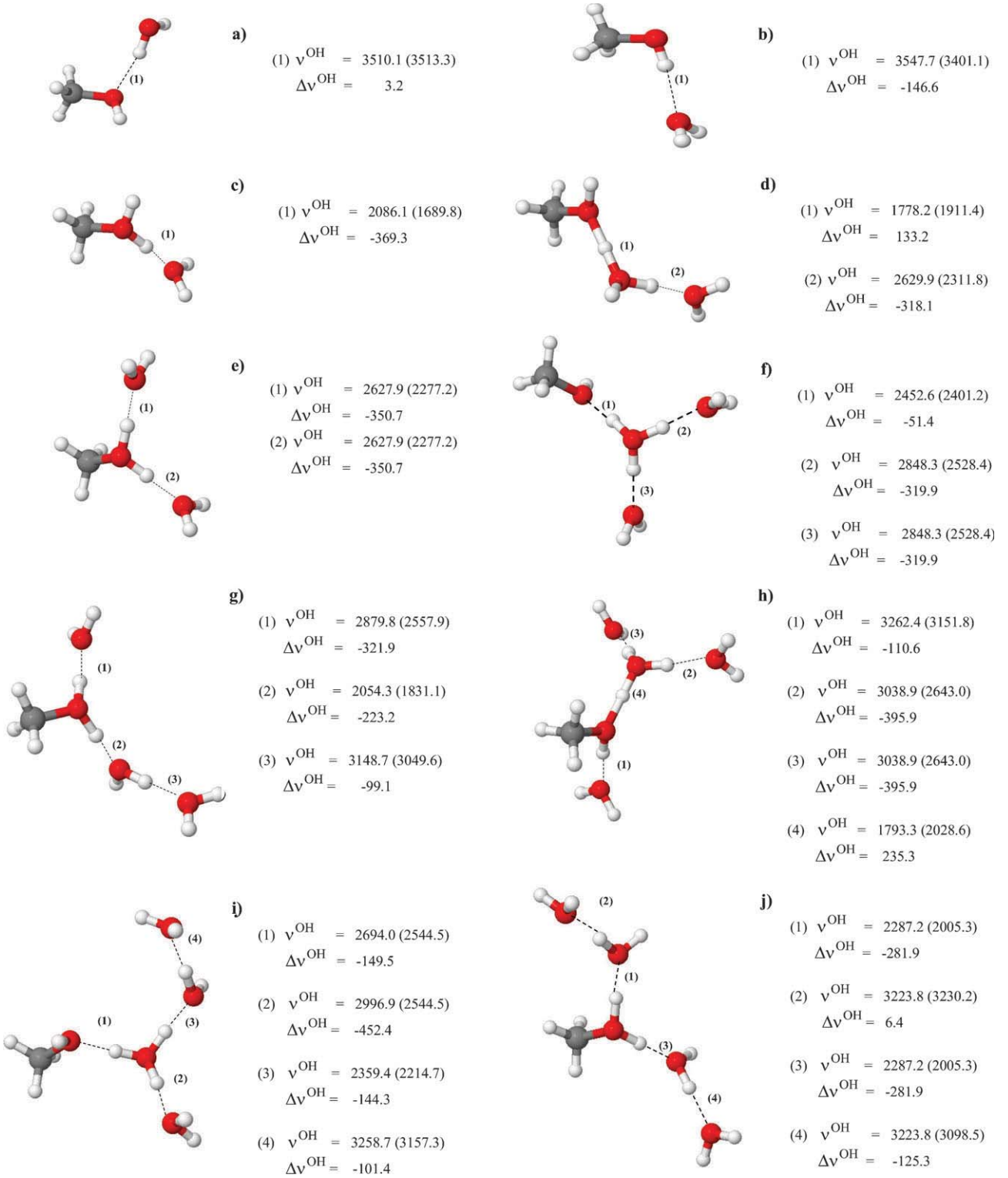

Fig. 2 Asymmetric O–H stretching frequencies (ν^{OH}) of the H-bond protons in the CH_3OH–H_2O, CH_3OH–H_3O^+ and CH_3OH–H_3O^+–H_2O complexes, obtained from B3LYP/TZVP calculations. The values in parentheses are the results in continuum aqueous solution. $\Delta\nu^{OH}$ are the frequency shifts in continuum aqueous solution. ν^{OH} and $\Delta\nu^{OH}$ are in cm^{-1}. (a)–(b) CH_3OH–H_2O complexes. (c) CH_3OH–H_3O^+ complex. (d)–(e) CH_3OH–H_3O^+–H_2O 1 : 1 : 1 complexes. (f)–(g) CH_3OH–H_3O^+–H_2O 1 : 1 : 2 complexes. (h)–(j) CH_3OH–H_3O^+–H_2O 1 : 1 : 3 complexes.

(H-bond (**1**)) shows a higher tendency of proton transfer than H-bond (**2**). In the gas phase and continuum aqueous solution, H-bond (**1**) possesses Δd_{DA} = 0.22 and 0.33 Å, and ν^{OH} = 1778 and 1911 cm^{-1}, respectively. The continuum aqueous solvent leads to a blue shift in H-bond (**1**) and a red shift in H-bond (**2**), with $\Delta\nu^{OH}$ = 133 and −318 cm^{-1},

respectively. The results are different for structure (e), in which $CH_3OH_2^+$ is equally stabilized by two adjacent water molecules, with Δd_{DA} in the gas phase and continuum aqueous solution of 0.49 and 0.46 Å, respectively, and ν^{OH} = 2628 and 2277 cm^{-1}, respectively. These indicated that H-bonds (**1**) and (**2**) in structure (e) are not as active as H-bond (**1**) in structure (d).

Based on the above discussions and the results on the larger hydrated complexes in Fig. 1 and 2, the trends of proton transfer could be anticipated. It appeared that the incomplete water coordination at the charged species, $CH_3OH_2^+$ and H_3O^+ (as in structures (c) and (d), respectively), and the asymmetric H-bond structure at $CH_3OH_2^+$ (as in structures (g) and (h)) could help promote structural diffusion. Therefore, according to Δd_{DA} and the criteria in ref. 14, the H-bond protons in structures (c), (d), (g) and (h) could be active in proton transfer (Δd_{DA} < 0.4 Å), with the tendencies decreasing in the following order:

Gas phase: (d) ≥ (h) > (g) ≥ (c).

Continuum aqueous solution: (c) > (d) ≥ (g) ≥ (h).

Fig. 3a and b show the relationships between the asymmetric stretching coordinate (Δd_{DA}) and the H-bond distance (R_{O-O}), and between ν^{OH} and R_{O-O}, respectively. The trends in Fig. 3a suggest a separation between the internal and external H-bonds at R_{O-O} = 2.55 Å, in good agreement with R_{O-O} = 2.57 Å in ref. 17. The linear relationships for the internal and external H-bonds in the gas phase and continuum aqueous solution could be represented by eqn (1) and (2), respectively.

$$\text{Internal H-bonds: } \Delta d_{DA} = 2.1464R_{O-O} - 4.9559 \quad (1)$$

$$\text{External H-bonds: } \Delta d_{DA} = 1.2936R_{O-O} - 2.7735 \quad (2)$$

Due to the asymptotic behavior at large R_{O-O}, the relationship between ν^{OH} and R_{O-O} in Fig. 3b cannot be approximated by a linear function; at large R_{O-O}, ν^{OH} converges to the asymmetric O–H stretching frequency of a non-H-bonded proton. After several test fittings, an exponential function similar to the integrated rate expression for the first order reaction was found to be the most appropriate. The fitted functions in the gas phase and continuum aqueous solution are shown in eqn (3) and (4), respectively.

$$\text{Gas phase: } \nu^{OH} = -1.17 \times 10^{10}e^{-R_{O-O}/0.1544} + 3526.2 \quad (3)$$

Continuum aqueous solution:

$$\nu^{OH} = -0.71 \times 10^{10}e^{-R_{O-O}/0.1617} + 3583.8 \quad (4)$$

The agreements between ν^{OH} derived from B3LYP/TZVP calculations and the fitted values are included in Fig. 3b.

Based on the results obtained from the static proton transfer potentials (B3LYP/TZVP calculations), one could conclude that, ν^{OH} for the H-bond protons in structures (c), (d), (g) and (h) in the gas phase range from 1778 to 2086 cm^{-1}, and from 1690 to 2029 cm^{-1} in continuum aqueous solution. According to the classical interpretations,[56] the H-bonds in structures (c), (d), (g) and (h) belong to the internal group and could be active in proton transfer reactions. However, these cannot be definitive due to the lack of the IR spectral signatures at ν^{OH} < 1000 cm^{-1}, as in the case of the Zundel complex.[77]

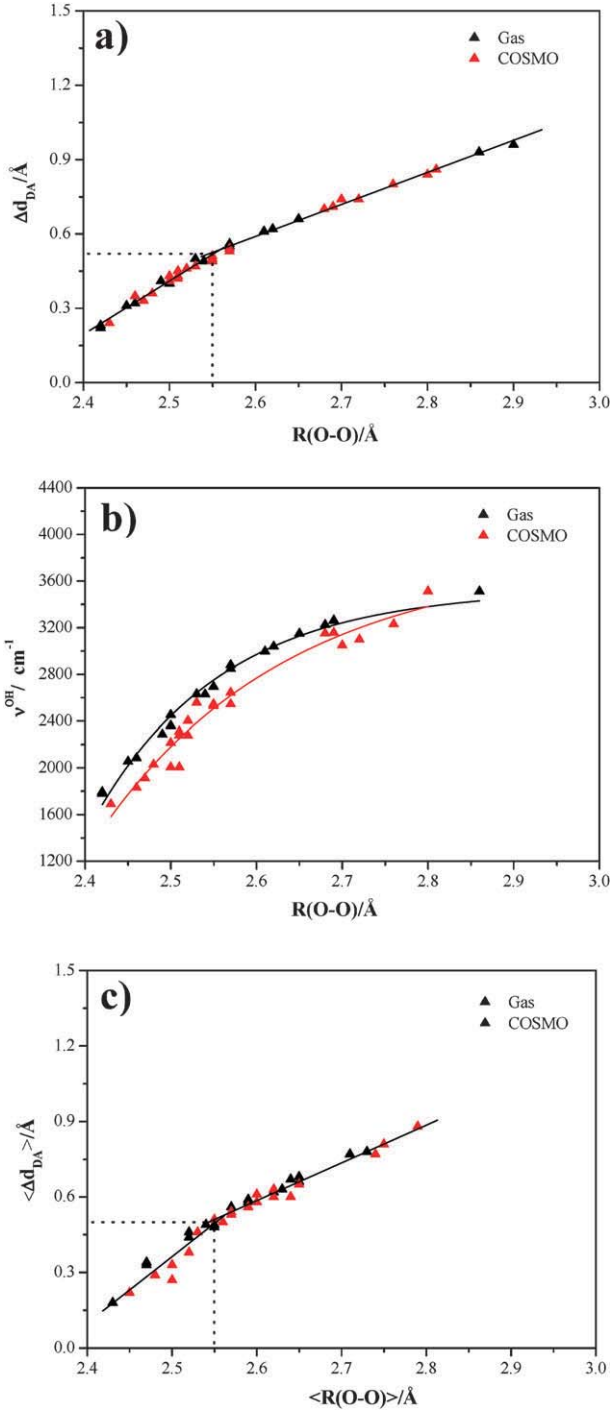

Fig. 3 (a) Plot of asymmetric stretching coordinates (Δd_{DA}) and O–H···O H-bond distances (R_{O-O}), obtained from B3LYP/TZVP calculations. (b) Plot of asymmetric O–H stretching frequencies (ν^{OH}) and O–H···O H-bond distances (R_{O-O}), obtained from B3LYP/TZVP calculations. (c) Plot of average asymmetric stretching coordinates ($\langle\Delta d_{DA}\rangle$) and average O–H···O H-bond distances ($\langle R_{O-O}\rangle$) obtained from BOMD simulations at 350 K.

It should be noted that, using the same approaches, ν^{OH} for the Zundel complex in the gas phase and continuum aqueous solution are 961 and 677 cm^{-1}, respectively.[77] The former is comparable with the theoretical result in ref. 78 of 983 cm^{-1}.

Table 1 Average H-bond distances ($\langle R_{O-O}\rangle$), average asymmetric stretching coordinates ($\langle \Delta d_{DA}\rangle$) and characteristic asymmetric O–H stretching frequencies (ν^{OH}) of the active protons in the transition state complexes. I_A/I_{O-O} are the relative probabilities of proton transfer in the course of the BOMD simulations. Distances and ν^{OH} are in Å and cm^{-1}, respectively

		$\langle R_{O-O}\rangle$	$\langle \Delta d_{DA}\rangle$	ν^{OH} A	ν^{OH} B	I_A/I_{O-O}
c) 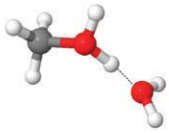	Gas	2.47	0.34	2178.9	2558.8	0.09
	COSMO	2.45	0.22	1138.9	1582.4	0.15
d) 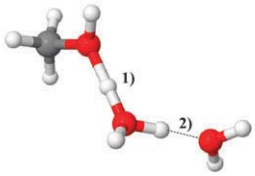	Gas	(1) 2.43	0.18	1115.5	1874.5	0.11
		(2) 2.57	0.54	2305.3	2695.7	0.11
	COSMO	(1) 2.50	0.33	977.7	1716.9	0.41
		(2) 2.57	0.54	2265.7	2680.1	0.13
g) 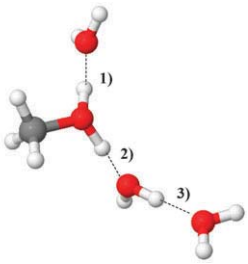	Gas	(1) 2.59	0.59	—	—	—
		(2) 2.47	0.33	1313.5	1613.2	0.03
		(3) 2.71	0.77	—	—	—
	COSMO	(1) 2.60	0.58	—	—	—
		(2) 2.48	0.29	935.0	1590.8	0.08
		(3) 2.75	0.81	—	—	—
h) 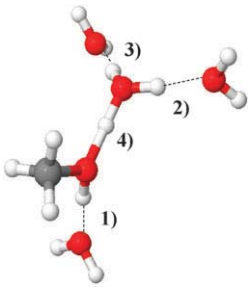	Gas	(1) 2.73	0.78	—	—	—
		(2) 2.65	0.68	—	—	—
		(3) 2.65	0.66	—	—	—
		(4) 2.45	0.22	911.0	1511.3	0.08
	COSMO	(1) 2.74	0.77	—	—	—
		(2) 2.65	0.65	—	—	—
		(3) 2.65	0.65	—	—	—
		(4) 2.50	0.27	979.7	1590.5	0.05

In the gas phase, the experimental O–H stretching frequency of the transferring proton in the Zundel complex was reported to be 1085 cm^{-1}.[79] Therefore, the asymmetric O–H stretching frequencies at $\nu^{OH} \leq 1000\ cm^{-1}$ could be regarded as spectral signatures of proton transfer in H-bonds. In this subsection, one could also conclude that the incomplete water coordination at the central charged species (H_3O^+ and $CH_3OH_2^+$), as well as the electrostatic effects introduced by the continuum aqueous solvent, could directly affect the tendency of proton transfer in H-bonds.

Dynamics and mechanisms of proton transfer reactions

The dynamics and mechanisms of proton transfer reactions in the CH_3OH–H_3O^+ and CH_3OH–H_3O^+–H_2O complexes are discussed in this subsection, with the emphasis on structures (c), (d), (g) and (h). The average H-bond distances ($\langle R_{O-O}\rangle$) and the average asymmetric stretching coordinates ($\langle \Delta d_{DA}\rangle$) obtained from BOMD simulations are listed in Table 1, together with characteristic asymmetric O–H stretching frequencies (ν^{OH}). Similar to the analyses made in the previous subsection, $\langle \Delta d_{DA}\rangle$ and $\langle R_{O-O}\rangle$ were plotted and shown in Fig. 3c. The power spectra of the symmetric and asymmetric O–H stretching modes of the H-bond protons in structures (c) and (d), as well as the O–O stretching modes (ν^{OO}), are given as examples in Fig. 4. The definitions of the three vibrational modes are also included in Fig. 4.

It appeared in Fig. 3c that linear relationships between $\langle \Delta d_{DA}\rangle$ and $\langle R_{O-O}\rangle$ could also be approximated for the internal and external H-bonds, with a separation at $\langle R_{O-O}\rangle$ = 2.55 Å, the same as that from B3LYP/TZVP calculations. The linear functions are shown in eqn (5) and (6), respectively.

$$\text{Internal H-bonds: } \langle \Delta d_{DA}\rangle = 2.6440\langle R_{O-O}\rangle - 6.2468 \quad (5)$$

$$\text{External H-bonds: } \langle \Delta d_{DA}\rangle = 1.4993\langle R_{O-O}\rangle - 3.3128 \quad (6)$$

In order to correlate the probability of proton transfer with ν^{OH} computed from BOMD simulations, the results on the Zundel complex[77] included in Fig. 4 should be discussed. The IR spectra of the H-bond proton in the Zundel complex computed from BOMD simulations at 350 K show two asymmetric O–H stretching bands, labeled **A** and **B** in

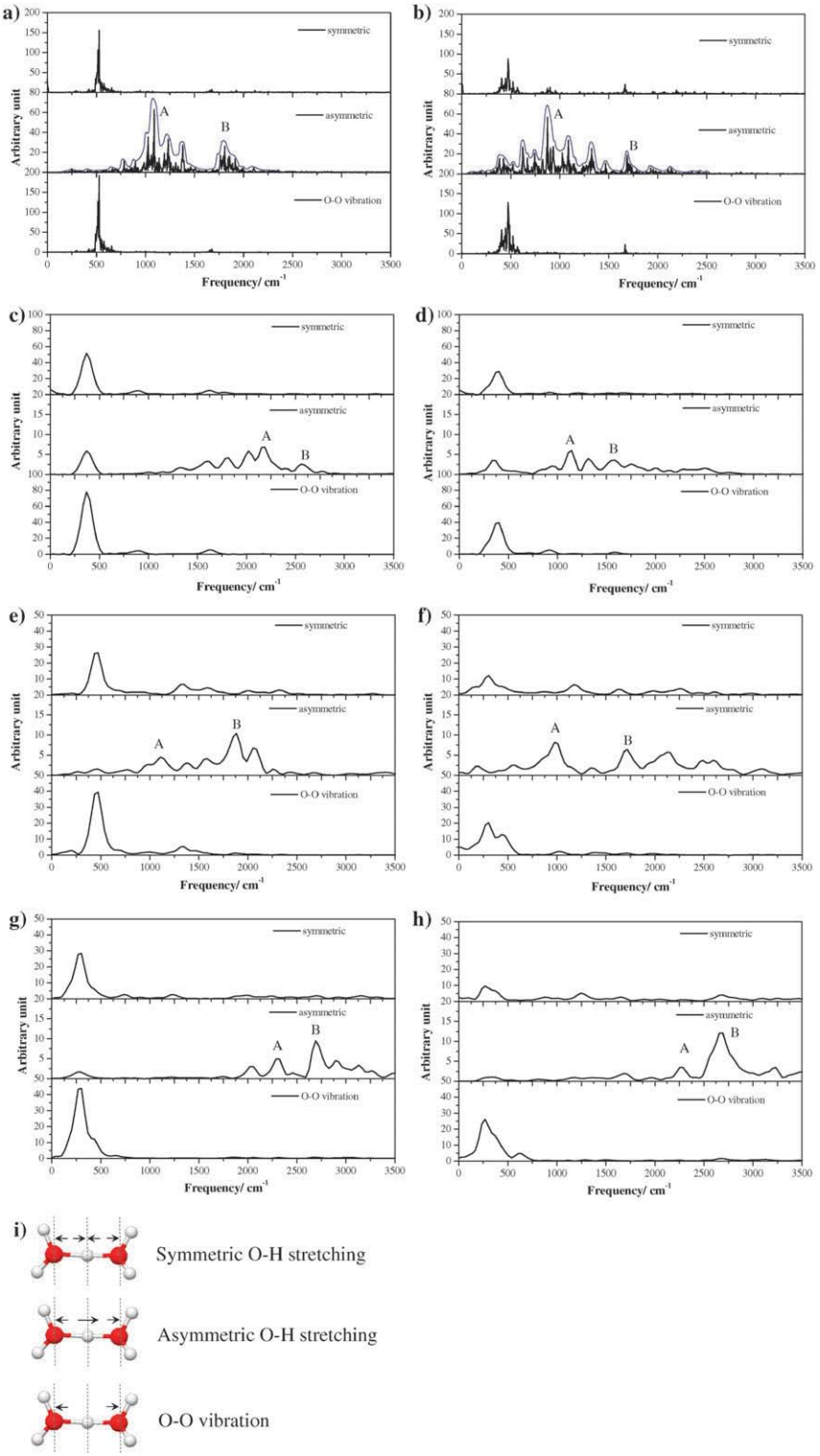

Fig. 4 Symmetric and asymmetric O–H stretching frequencies of the H-bond protons in the $H_5O_2^+$, CH_3OH–H_3O^+ and CH_3OH–H_3O^+–H_2O complexes, together with the O–O stretching frequencies, obtained from BOMD simulations at 350 K. (a) $H_5O_2^+$ in the gas phase. (b) $H_5O_2^+$ in continuum aqueous solution. (c) CH_3OH–H_3O^+ in the gas phase. (d) CH_3OH–H_3O^+ in continuum aqueous solution. (e) CH_3OH–H_3O^+–H_2O 1 : 1 : 1 complex in the gas phase (H-bond (**1**)). (f) CH_3OH–H_3O^+–H_2O 1 : 1 : 1 complex in continuum aqueous solution (H-bond (**1**)). (g) CH_3OH–H_3O^+–H_2O 1 : 1 : 1 complex in the gas phase (H-bond (**2**)). (h) CH_3OH–H_3O^+–H_2O 1 : 1 : 1 complex in continuum aqueous solution (H-bond (**2**)). (i) Definitions of the symmetric and asymmetric O–H stretching modes, as well as the O–O vibration.

Fig. 4a and b; in the gas phase at ν^{OH} = 1090 and 1809 cm^{-1} and in continuum aqueous solution at ν^{OH} = 875 and 1686 cm^{-1}, respectively. The low-frequency bands at **A** are comparable with the characteristic ν^{OH} derived from

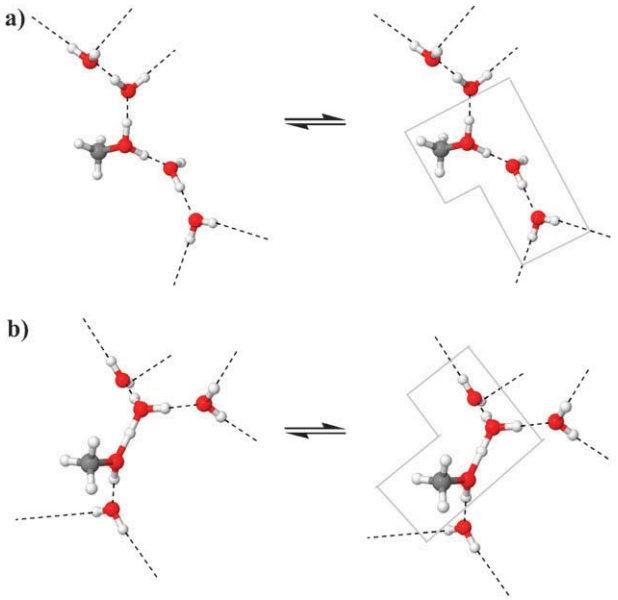

Fig. 5 Elementary reactions consisting of quasi-dynamic equilibriums for the interconversion between the formation and cleavage of the H-bonds linking the transition state complex and water molecules in the second hydration shells. The transition state complex is inside the boundary line. (a) The excess proton transferring in a linear H-bond structure. (b) The excess proton transferring in a fully hydrated transition state complex.

B3LYP/TZVP calculations.[77] They could be associated with the vibration modes, in which a proton shuttles back and forth at the center of the O–H···O H-bond. For the higher-frequency bands at **B**, the centers of vibration are shifted towards an oxygen atom of water. Therefore, ν^{OH} at **A** and **B** could be considered as the IR spectral signatures of the transferring proton in the Zundel complex.

As the proton transfer in the Zundel complex depends strongly on the O–O stretching mode,[27] the relative probability or the extent of proton transfer in BOMD simulations could be estimated from the ratio between the intensity of the asymmetric O–H stretching mode at **A** (I_A) and the intensity of the O–O stretching mode (I_{O-O}); a high I_A/I_{O-O} reflects a high probability of proton transfer in BOMD simulations. For the Zundel complex in the gas phase and continuum aqueous solution at 350 K, I_A/I_{O-O} amounts to 0.33 and 0.44, respectively, indicating a higher probability of proton transfer in continuum aqueous solution. At 298 K, the diffusion coefficient of the transferring proton in the Zundel complex is 5×10^{-5} cm^2 s^{-1},[77] slightly lower than the experimental value of 7×10^{-5} cm^2 s^{-1};[66] the diffusion coefficient of a proton moving across a single water molecule was approximated from the NMR hopping time (τ_p) and the Einstein relation, $D = l^2/6\tau_p$, where l is the hopping length. It should be mentioned that the value of D in ref. 66 was computed by subtracting the water self-diffusion coefficient, 2.3×10^{-5} cm^2 s^{-1}, from the proton diffusion coefficient, 9.3×10^{-5} cm^2 s^{-1}. The discrepancy of about 28% could be partly due to the lack of extensive H-bond networks of water in the model systems. Based on the information on the Zundel complex, one could anticipate proton transfer from the following three spectral evidences: (a) the existence of a threshold frequency at $\nu^{OH} < 1000$ cm^{-1}; (b) the appearance of an additional asymmetric O–H stretching frequency at ν^{OH} between 1600–1800 cm^{-1}; and (c) I_A/I_{O-O} is comparable with the Zundel complex.

For structure (c), the broadening of the asymmetric O–H stretching bands made it difficult to analyze IR spectra. In the gas phase, the appearance of the low- and high-frequency bands at 2179 and 2559 cm^{-1}, respectively, rules out structure (c) from being an active transition state. Similarly, in continuum aqueous solution, $I_A/I_{O-O} = 0.15$ indicates a restricted number of proton transfer events in BOMD simulations. Spectral evidences of proton transfer are clearly seen for structure (d), especially in continuum aqueous solution. Fig. 4f reveals that, H-bond (**1**) possesses an asymmetric O–H stretching frequencies of $\nu^{OH} = 978$ and 1717 cm^{-1}, with $I_A/I_{O-O} = 0.41$; I_A/I_{O-O} is slightly smaller than the Zundel complex.[77] The IR spectra of the active protons in structures (g) and (h) (not shown here) are similar to structure (d), but with I_A/I_{O-O} smaller than 0.1, indicating a small number of proton transfer events in BOMD simulations. Thus, one could conclude that, for the CH_3OH–H_3O^+–H_2O complex, structure (d) is the most active transition state in proton transfer pathways, with a proton diffusion coefficient (D) of 1.95×10^{-5} cm^2 s^{-1}. Since the time interval used in the calculations of MSD was short, the diffusion coefficient could be considered as a pure structural diffusion constant. *Ab initio* MD simulations were employed in the study of proton transfer in CH_3OH–H_2O mixtures at 300 K.[14] It was reported that the diffusion coefficient of an excess proton in the mixture, with a CH_3OH mole fraction of 0.5 (16 H_2O and 16 CH_3OH), is 4.2×10^{-5} cm^2 s^{-1}. Based on the approximation in ref. 66 and the report that the self-diffusion coefficients of $[CH_3OH]_{liq}$ at 298 and 340 K are 2.4×10^{-5} and 4.9×10^{-5} cm^2 s^{-1}, respectively,[80] the proton diffusion coefficient in the present system could be approximated as 4.35×10^{-5} and 6.85×10^{-5} cm^2 s^{-1}, respectively. The values agree well with the theoretical results in ref. 80.

The conclusion that structure (d) is the most active transition state complex is supported by the theoretical results in ref. 14, which showed that the nearest neighbors of the defect oxygen, the oxygen atom attached to an excess proton, consist of two water molecules, independent of whether the defect oxygen is in water or methanol. This corresponds to structure (d) in the present work. Based on the assumption that the thermal energy fluctuations could temporarily break the H-bonds connecting the transition state complex and water molecules in the second hydration shell, two potential elementary reactions of proton transfer could be proposed in Fig. 5: Fig. 5a assumes that the excess proton is transferred in a linear H-bond structure, whereas Fig. 5b assumes a fully hydrated transition state complex. The former was suggested to be more preferential.[13] Finally, as in the case of the Zundel and Eigen complexes,[27] one could further anticipate that the rate-determining steps could be determined from the lifetimes of the quasi-dynamic equilibriums for the interconversion between the formation and cleavage of the H-bonds linking the first and second hydration shells, with structure (d) as the only active transition state complex.

Conclusions

The dynamics and mechanisms of proton transfer in hydrated complexes formed from CH_3OH, H_3O^+ and H_2O were studied using theoretical methods. The investigations began with a search for equilibrium structures at low hydration levels using DFT calculations at the B3LYP/TZVP level. Based on asymmetric stretching coordinates (Δd_{DA}) and asymmetric O–H stretching frequencies (ν^{OH}), four H-bond complexes were identified as transition states, in which the most active unit is represented by an excess proton nearly equally shared between CH_3OH and H_2O. Linear relationships between Δd_{DA} and the H-bond distance (R_{O-O}) could be approximated for both internal and external H-bonds, with a separation at 2.55 Å, whereas the relationship between ν^{OH} and R_{O-O} could be represented by an exponential function similar to the integral rate expression for the first-order reaction. Based on the static proton transfer potentials (B3LYP/TZVP calculations), ν^{OH} for the H-bond protons in the transition state complexes in the gas phase range from 1778 to 2086 cm^{-1}, and from 1690 to 2029 cm^{-1} in continuum aqueous solution. According to the classical interpretations, all the H-bonds in the transition state complexes belong to the internal group, and could be active in proton transfer. These, however, cannot be definitive due to the lack of the IR spectral signatures at $\nu^{OH} \approx 1000$ cm^{-1}; using the same theoretical methods, the Zundel complex possesses $\nu^{OH} = 961$ and 677 cm^{-1}, in the gas phase and continuum aqueous solution, respectively. Therefore, $\nu^{OH} \approx 1000$ cm^{-1} or lower could be considered as an IR spectral signature of the transferring proton in H-bonds.

More definitive results were obtained from BOMD simulations. Based on the three spectral evidences obtained from the Zundel complex, the H-bond structure (structure (d)) with incomplete water coordination at $CH_3OH_2^+$ and H_3O^+ appeared to be the most active transition state in continuum aqueous solution, with a characteristic ν^{OH} of 978 cm^{-1}. This is in accordance with the observation that the excess proton is preferentially taken by CH_3OH in the open chain structures, not the fully hydrated structures. Based on the assumption that the thermal energy fluctuations could temporarily separate or break the H-bonds connecting the transition state complex and the water molecules in the second hydration shell, and the observation that the incomplete water coordination at the charged species could help promote structural diffusion, as in the case of the Zundel and Eigen complex, two elementary reactions of proton transfer were proposed, with structure (d) as the only transition state complex.

The present theoretical results suggested that, due to the coupling among various vibrational modes, the discussions on proton transfer reactions cannot be made based solely on static proton transfer potentials. In order to study proton transfer reactions, thermal energy fluctuations and dynamics must be included in the model calculations. Although the asymmetric O–H stretching frequencies of the transferring protons cannot be measured easily in experiment, due to the limitations of the IR equipment and the difficulties in the assignment of absorption bands, the present theoretical results could provide insights into the vibrational behavior of transferring protons, as well as suggest theoretical methods and criteria to monitor proton transfer reactions in more complex environments. Together with systematic analyses of IR spectra, it has been shown that BOMD simulations are the most appropriate theoretical methods for the investigations of proton transfer reactions.

Acknowledgements

The authors would like to acknowledge the financial supports from the Thailand Research Fund (TRF): the Advanced Research Scholarship, Grant No. BRG5180022 to Prof. Kritsana Sagarik; the Royal Golden Jubilee (RGJ) PhD Program, Grant No. PHD/0071/2547 to Sermsiri Chaiwongwattana and Prof. Kritsana Sagarik. Linux clusters provided by the following organizations are also gratefully acknowledged: School of Mathematics and School of Chemistry, SUT; National Electronics and Computer Technology Center (NECTEC), National Science and Technology Development Agency (NSTDA); the Thai National Grid Center (THAIGRID), Ministry of Information and Communication Technology.

References

1 J. Larminie and A. Dicks, *Fuel Cell Systems Explained*, John Wiley & Sons Ltd, Chichester, 2001.
2 C. A. Vincent and B. Scrosati, *Modern Batteries: An introduction to electrochemical power sources*, John Wiley & Sons Ltd, New York, 1997.
3 M. Cappadonia, J. W. Erning, S. M. S. Niaki and U. Stimming, *Solid State Ionics*, 1995, **77**, 65.
4 J. A. Elliott and S. J. Paddison, *Phys. Chem. Chem. Phys.*, 2007, **9**, 2602.
5 K. D. Kreuer, *Chem. Mater.*, 1996, **8**, 610.
6 K. D. Kreuer, S. J. Paddison, E. Spohr and M. Schuster, *Chem. Rev.*, 2004, **104**, 4637.
7 M. Hachiya, Y. Matsuda, K. Suhara, N. Mikami and A. Fujii, *J. Chem. Phys.*, 2008, **129**, 094306.
8 F. Huisken, S. Mohammad-Pooran and O. Werhahn, *Chem. Phys.*, 1998, **239**, 11.
9 E. E. Fileti, M. A. Castro and S. Canuto, *Chem. Phys. Lett.*, 2008, **452**, 54.
10 S. Urata, J. Irisawa, A. Takada and S. Tsuzuki, *J. Fluorine Chem.*, 2005, **126**, 1312.
11 A. Vishnyakov and A. V. Neimark, *J. Phys. Chem. B*, 2001, **105**, 7830.
12 J. C. Jiang, C. Chaudhuri, Y. T. Lee and H.-C. Chang, *J. Phys. Chem. A*, 2002, **106**, 10937.
13 C.- C. Wu, C. Chaudhuri, J. C. Jiang, Y. T. Lee and H.- C. Chang, *J. Phys. Chem. A*, 2004, **108**, 2859.
14 J. A. Morrone, K. E. Haslinger and M. E. Tuckerman, *J. Phys. Chem. B*, 2006, **110**, 3712.
15 H.-C. Chang, J.-C. Jiang, S. H. Lin, Y. T. Lee and H.-C. Chang, *J. Phys. Chem. A*, 1999, **103**, 2941.
16 J. A. Morrone and M. E. Tuckerman, *J. Chem. Phys.*, 2002, **117**, 4403.
17 R. Buzzoni, S. Bordiga, G. Ricchiardi, G. Spoto and A. Zecchina, *J. Phys. Chem.*, 1995, **99**, 11937.
18 J. B. Asbury, T. Steinel and M. D. Fayer, *J. Lumin.*, 2004, **107**, 271.
19 T. Kabeya, Y. Tamai and H. Tanaka, *J. Phys. Chem. B*, 1998, **102**, 899.
20 C.-C. Wu, J. C. Jiang, D. W. Boo, S. H. Lin, Y. T. Lee and H.-C. Chang, *J. Chem. Phys.*, 2000, **112**, 176.
21 M. Okumura, L. I. Yeh, J. D. Myers and Y. T. Lee, *J. Phys. Chem.*, 1990, **94**, 3416.
22 I. Natkaniec, K. Holderna-Natkaniec, I. Majerz and K. Parlinski, *Chem. Phys.*, 2005, **317**, 171.
23 O. Vendrell, F. Gatti and H.-D. Meyer, *J. Chem. Phys.*, 2007, **127**, 184303.

24 R. Vuilleumier and D. Borgis, *J. Chem. Phys.*, 1999, **111**, 4251.
25 U. W. Schmitt and G. A. Voth, *J. Chem. Phys.*, 1999, **111**, 9361.
26 H.-P. Cheng and J. L. Krause, *J. Chem. Phys.*, 1997, **107**, 8461.
27 K. Sagarik, M. Phonyiem, C. Lao-ngam and S. Chaiwongwattana, *Phys. Chem. Chem.Phys.*, 2008, **10**, 2098.
28 N. Rekik, B. Oujia and M. J. Wójcik, *Chem. Phys.*, 2008, **352**, 65.
29 J. Rejnek, M. Hanus, M. Kabeláč, F. Ryjáček and P. Hobza, *Phys. Chem. Chem. Phys.*, 2005, **7**, 2006.
30 K. P. Sagarik and B. M. Rode, *Chem. Phys.*, 2000, **260**, 159.
31 K. P. Sagarik, S. Chaiwongwattana and P. Sisot, *Chem. Phys.*, 2004, **306**, 1.
32 K. P. Sagarik and S. Dokmaisrijan, *THEOCHEM*, 2005, **718**, 31.
33 K. Sagarik and S. Chaiyapongs, *Biophys. Chem.*, 2005, **117**, 18.
34 N. Deeying and K. Sagarik, *Biophys. Chem.*, 2007, **125**, 72.
35 K. P. Sagarik and R. Ahlrichs, *J. Chem. Phys.*, 1987, **86**, 5117.
36 K. P. Sagarik, V. Pongpituk, S. Chaiyapongs and P. Sisot, *Chem. Phys.*, 1991, **156**, 439.
37 K. P. Sagarik, *THEOCHEM*, 1999, **465**, 141.
38 K. P. Sagarik and E. Spohr, *Chem. Phys.*, 1995, **119**, 73.
39 K. P. Sagarik and P. Asawakun, *Chem. Phys.*, 1997, **219**, 173.
40 *CRC Handbook of Chemistry & Physics, 89th Edition,* CRC Press, 2008–2009, 1476–3508; David W. H. Rankin, *Crystallogr. Rev.*, 2009, **15**(3), 223–224.
41 S. J. Paddison, *Annu. Rev. Mater. Res.*, 2003, **33**, 289.
42 S. J. Paddison and T. Zawodzinski Jr., *Solid State Ionics*, 1998, **113–115**, 333.
43 S. J. Paddison, L. R. Pratt and T. A. Zawodzinski Jr., *J. New Mater. Electrochem. Syst.*, 1999, **2**, 183.
44 S. J. Paddison, L. R. Pratt and T. Zawodzinski Jr., *J. Phys. Chem. A*, 2001, **105**, 6266.
45 S. J. Paddison, *J. New Mater. Electrochem. Syst.*, 2001, **4**, 197.
46 S. J. Paddison and J. A. Elliott, *J. Phys. Chem. A*, 2005, **109**, 7583.
47 R. Dreizler and E. Gross, *Density Functional Theory*, Plenum Press, New York, 1995.
48 A. Schäfer, C. Huber and R. Ahlrichs, *J. Chem. Phys.*, 1994, **100**, 5829.
49 G. Santambrogio, M. Brümmer, L. Wöste, J. Döbler, M. Sierka, J. Sauer, G. Meijer and K. R. Asmis, *Phys. Chem. Chem. Phys.*, 2008, **10**, 3992.
50 R. W. Larsen, P. Zielke and M. A. Suhm, *J. Chem. Phys.*, 2007, **126**, 194307.
51 TURBOMOLE V6.0 2009, a development of University of Karlsruhe and Forschungszentrum Karlsruhe GmbH, 1989–2007, TURBOMOLE GmbH, since 2007; available from http://www.turbomole.com.
52 D. Marx, M. E. Tuckerman, J. Hutter and M. Parrinello, *Nature*, 1999, **397**, 601.
53 C. J. D. von Grotthuss, *Annu. Chim.*, 1806, **58**, 54.
54 N. B. Librovich, V. P. Sakun and N. D. Sokolov, *Chem. Phys.*, 1979, **39**, 351.
55 D. Xenides, B. R. Randolf and B. M. Rode, *J. Chem. Phys.*, 2005, **122**, 174506.
56 G. C. Pimentel and A. L. McClellan, *The Hydrogen Bond*, W. H. Freeman, San Francisco, 1960.
57 P. B. Balbuena and J. M. Seminario, *Theoretical and Computational Chemistry 7, Molecular Dynamics; From Classical to Quantum Methods*, Elsevier, Amsterdam, 1999.
58 C. J. Cramer, *Essentials of Computational Chemistry: Theory and Models*, John Wiley & Sons Ltd, New York, 2002.
59 D. C. Young, *Computational Chemistry: A Practical Guide for Applying Techniques to Real World Problems*, Wiley Interscience, New York, 2001.
60 R. N. Barnett and U. Landman, *Phys. Rev. B: Condens. Matter*, 1993, **48**, 2081.
61 X. Jing, N. Troullier, D. Dean, N. Binggeli, J. R. Chelikowsky, K. Wu and Y. Saad, *Phys. Rev. B: Condens. Matter*, 1994, **50**, 12234.
62 A. R. Leach, *Molecular Modelling: Principles and Applications*, Longman, Edinburgh, 1996.
63 F. Fillaux, A. Cousson and M. Gutmann, *Pure Appl. Chem.*, 2007, **79**, 1023.
64 B. E. Conway, J. O. M. Bockris and H. Linton, *J. Chem. Phys.*, 1956, **24**, 834.
65 K. D. Kreuer, *Solid State Ionics*, 2000, **136–137**, 149.
66 N. Agmon, *Chem. Phys. Lett.*, 1995, **244**, 456.
67 P. A. Giguere, *J. Chem. Educ.*, 1979, **56**, 571.
68 R. R. Sadeghi and H.-P. Cheng, *J. Chem. Phys.*, 1999, **111**, 2086.
69 P. Bopp, *Chem. Phys.*, 1986, **106**, 205.
70 C. J. Montrose, J. A. Bucaro, J. Marshall-Coakley and T. A. Litovitz, *J. Chem. Phys.*, 1974, **60**, 5025.
71 M.-C. Bellissent-Funel and J. Teixeira, *J. Mol. Struct.*, 1991, **250**, 213.
72 M. P. Allen and D. J. Tildesley, *Computer Simulation of Liquids*, Oxford University Press, New York, 1987.
73 J. M. Haile, *Molecular Dynamics Simulations*, John Wiley & Sons Ltd, New York, 1997.
74 D. C. Rapaport, *The Art of Molecular Dynamics Simulation*, Cambridge University Press, London, 1995.
75 A. J. Stace and G. A. Shukla, *J. Am. Chem. Soc.*, 1982, **104**, 5314.
76 J. Crooks, A. J. Stace and B. J. Whitaker, *J. Phys. Chem.*, 1988, **92**, 3554.
77 K. Sagarik and C. Lao-ngam, submitted.
78 L. Ojamäe, I. Shavitt and J. Singer, *Int. J. Quantum Chem.*, 1995, **56**, 657.
79 J. M. Headrick, E. G. Diken, R. S. Walters, N. I. Hammer, R. A. Christie, J. Cui, V. M. Myshakin, M. A. Johnson and K. D. Jordan, *Science*, 2005, **308**, 1765.
80 G. Guevara-Carrion, C. Nieto-Draghi, J. Vrabec and H. Hasse, *J. Phys. Chem. B*, 2008, **112**, 16664.

Chemical Physics 355 (2009) 103–117

Contents lists available at ScienceDirect

Chemical Physics

journal homepage: www.elsevier.com/locate/chemphys

Structures and dynamics of phenol clusters in benzene solutions

Sermsiri Chaiwongwattana, Kritsana Sagarik *

School of Chemistry, Institute of Science, Suranaree University of Technology, 111 University Avenue, Nakhon-Ratchasima 30000, Thailand
National Nanotechnology Center (NANOTEC), National Science and Technology Development Agency (NSTDA), Pathumthani 12120, Thailand

ARTICLE INFO

Article history:
Received 25 December 2007
Accepted 18 November 2008
Available online 27 November 2008

Keywords:
Phenol clusters
Benzene solutions
T-model
Molecular dynamics

ABSTRACT

Structures and dynamics of phenol clusters ($(PhOH)_n$, $n = 1–3$) in benzene (Benz) solutions ($[(PhOH)_n]_{Benz}$) at 298 K were studied using intermolecular potentials derived from the Test-particle model (T-model) and molecular dynamics (MD) simulations. Although Benz molecules interact weakly among themselves and with PhOH, the average three-dimensional structures and interaction energy distributions obtained from MD simulations showed that, they could form well-defined solvent cages in $[(PhOH)_n]_{Benz}$. At infinite dilution, some solvent-separated structures, in which a Benz molecule linked between two PhOH molecules, were observed in $[(PhOH)_2]_{Benz}$, whereas hydrogen bond (H-bond) structures dominated in $[(PhOH)_3]_{Benz}$. Based on the observation that, under thermal equilibrium conditions and at short time, the exchange dynamics between the associated and dissociated forms involved periodic motions of the O–H$\cdots\pi$ H-bond, the lifetimes of the PhOH–Benz 1:1 complex were estimated and in reasonable agreement with 2D-IR vibrational echo experiment. Due to high potential energy barriers on the average potential energy landscapes, solvent exchanges in $[(PhOH)_n]_{Benz}$ could take place through large-amplitude intermolecular vibrations of molecules in the first solvation shell. In order to provide insights into structures and dynamics in $[(PhOH)_n]_{Benz}$, it was shown that, explicit solvent molecules have to be included in the theoretical models.

1. Introduction

Structures and stability of clusters of aromatic compounds in aqueous and non-aqueous solutions are examples of classical problems in the area of molecular associations [1–9]. Molecular clusters formed from aromatic compounds have been of interest, since they represent interactions between π-systems, which are found in DNA and side chains of proteins [10]. Therefore, various experimental and theoretical investigations have been performed in the past two decades to obtain basic information concerning with the driving forces responsible for interactions in aromatic systems, especially among biomolecules [11]. For example, the so-called "π–hydrogen bond" (π–H-bond) has been put forward due to its importance in biological systems, *e.g.* the ability to stabilize α-helix in proteins [12–14].

The presence of π-electrons enables clusters of aromatic compounds, generated in continuous or pulsed supersonic beams, to be examined effectively using modern spectroscopic techniques, such as resonance two photon ionization [15–17], disperse fluorescence [18], cluster ion dip spectroscopy [19,20] and ionization-detected stimulated Raman spectroscopy [21]. Significant advancement in computational chemistry software packages and parallel computer technology [22] has also allowed *ab initio* calculations that include the effects of electron correlations to study large clusters of aromatic compounds with higher accuracy [23]. It has, therefore, become a general practice to apply structural models obtained from *ab initio* calculations for the fitting of spectroscopic observations [24]. Since a large number of review articles on molecular associations have been published, only some important information relevant to the present work will be briefly summarized.

Clusters of benzene ($(Benz)_n$) are considered as prototypes for the $\pi\cdots\pi$ and C–H$\cdots\pi$ interactions. They have been extensively studied by theoretical and experimental methods [25–31]. Theoretical methods [23,32] predicted at least four equilibrium structures of $(Benz)_2$ in the gas phase namely, parallel displaced, T-shaped, parallel staggered and herringbone structures. The parallel displaced structure is stabilized solely by the $\pi\cdots\pi$ interaction, whereas the T-shaped structure mainly by the C–H$\cdots\pi$ interaction. The former was suggested by *ab initio* calculations at the highest level of accuracy [32] to possess the lowest interaction energy and in good agreement with experiment [31], whereas the latter was pointed out to represent a low-energy saddle point for the interconversion between parallel displaced structures.

Fast dynamics of single Benz molecule in the liquid phase ($[Benz]_{liquid}$) was studied in femtosecond heterodyne detected optical Kerr effect (HD-OKE) experiments in a wide temperature range [25]. The results at short times were interpreted by assuming that the basic microscopic system consists of a Benz molecule

* Corresponding author. Tel./fax: +66 44 224635.
E-mail address: kritsana@sut.ac.th (K. Sagarik).

0301-0104/$ - see front matter © 2008 Elsevier B.V. All rights reserved.
doi:10.1016/j.chemphys.2008.11.018

Nomenclature

T-model the Test-particle model
π–H-bond π–hydrogen bond
PD map probability distribution map
π-PD maps solvent probability distribution map
$\langle P^{\pi\text{-PD}}\rangle_{max}$ highest probability at the labeled contour on the π-PD maps
MD-$[(PhOH)_n]^{frozen}_{Benz}$ MD simulations with the structure of $(PhOH)_n$ frozen at the T-model equilibrium geometries
MD-$[(PhOH)_n]^{free}_{Benz}$ MD simulations with all molecules allowed to move, starting from the equilibrated configurations of MD-$[(PhOH)_n]^{frozen}_{Benz}$
$\langle E^{solu-solu}_{Benz}\rangle$ average solute–solute interaction energy
$\langle E^{solu-solv}_{Benz}\rangle$ average solute–solvent interaction energy
$\langle E^{pot}_{Benz}\rangle$ average potential energies of $[(PhOH)_n]_{Benz}$
$\langle E^{T}_{Benz}\rangle$ the average potential energy barriers to the solvent exchange within, as well as between, the first solvation shells
$\langle E^{T}_{Benz}\rangle$ the average potential energy barriers to the solvent exchange between Benz molecules in the first solvation shell and the outside
$g(R)$ atom–atom pair correlation functions
$n(R)$ average running coordination numbers
FFT fast Fourier transformations
I_a associative-interchange scheme
$\tau^{PhOH-Benz}_{O-H\pi}$ lifetime of the PhOH–Benz 1:1 complex
PB-PD the average solute–solvent interaction energy PD maps
BB-PD the average solvent–solvent interaction energy PD maps
PB-BB-PD the average potential energy PD maps
$\langle \Delta E^{PB-PD}_{Benz}\rangle_{min}$ lowest-average interaction energies on the PB-PD map
$\langle \Delta E^{BB-PD}_{Benz}\rangle_{min}$ lowest-average interaction energies on the BB-PD map
$\langle \Delta E^{PB-BB-PD}_{Benz}\rangle_{min}$ lowest-average interaction energies on the PB-BB-PD map

librating and oscillating in a local confinement or solvent "cage". The instantaneous cage structures and dynamics in $[Benz]_{liquid}$ and $[Benz]_{crystal}$ were studied in details by spectroscopic measurements [26], as well as molecular dynamics (MD) [29] and lattice dynamics simulations [28]. It was reported in Ref. [29] that, a reminiscence of crystalline structure was evident in $[Benz]_{liquid}$, although no preferential orientation was observed in the first coordination shell. Moreover, the cages in $[Benz]_{liquid}$ are similar in composition to those in $[Benz]_{crystal}$, and the majority of the cages in $[Benz]_{liquid}$ could live several hundred femtoseconds (fs) or picoseconds (ps), depending upon the radius used to define the cage [29]. Similar solvent cages were observed in our previous theoretical studies [33] to accommodate benzoic acid dimer ($(BA)_2$), as well as BA–H_2O *m*:*n* complexes, *m* and *n* = 1–2, in Benz solutions.

As the simplest aromatic compound which can form O–H···π and O–H···O H-bonds, and a prototype for structurally related subunits in larger biomolecules, such as tyrosine (Tyr) residue in proteins, phenol (PhOH) has been frequently selected as a model molecule in both experimental and theoretical investigations [23,34]. For example, theoretical methods at MP2/6-31G(d) and B3LYP/6-31G(d) levels were employed in the study of structures and stabilities of the O–H···O H-bond in $(PhOH)_n$ and $(H_2O)_n$, n = 1–4, as well as the PhOH–H_2O *m*:*n* complexes, m and n = 1–3, and $m + n \leqslant 4$ [35]. MP2/6-31G(d) results showed that $(PhOH)_n$ and $(H_2O)_n$ possess similar H-bond patterns, and $(PhOH)_n$ are slightly more stable due to the effects of electron correlations. Moreover, it was shown that, the H-bonds in the PhOH–H_2O *m*:*n* complexes are similar to $(H_2O)_n$.

The interplay between electrostatic and dispersion interactions has been frequently studied through the weak interaction between the O–H group in PhOH and the polarizable π-electron clouds in Benz [36,37]. For example, in the gas phase, B3LYP/6-31G(d,p) calculations revealed that, the PhOH–Benz 1:1 complex is stabilized mainly by the O–H···π H-bond, whereas in the 1: 2 complex, the O–H group of PhOH acts simultaneously as proton donor and acceptor towards Benz molecules [37]. It should be noted that, although the density functional theory (DFT) and MP2 have been frequently employed in the calculations of molecular clusters, there have been examples in which both methods could not describe accurately the long-range electron correlation effects; $(Benz)_2$ was predicted to be unstable by almost all standard DFT functionals [32,38], whereas the interaction energy of the PhOH–Benz 1:1 complex was pointed out to be overestimated at the MP2 level [39].

Molecular associations of PhOH in Benz solutions were examined in classical partition experiments, in which distributions of PhOH between Benz and water were studied at 298 K [40]. The measurements of partition coefficients revealed that, in Benz, equilibrium could establish between PhOH and $(PhOH)_3$, whereas in water, PhOH is monomolecular up to at least 0.15 M. It was emphasized in Ref. [40] that, PhOH associates itself in triple molecules and not in double molecules. The existence of the monomer–trimer equilibrium was also suggested from NMR experiment [41], in which the equilibrium constant was determined in CCl_4 by measuring the hydroxyl NMR frequencies as functions of concentrations. However, Philbrick [4] proposed the existence of $(PhOH)_2$ in Benz solutions, by measuring the partition coefficients of PhOH between Benz and water at the concentrations in the water layer below 0.1 M. The results were confirmed by isopiestic experiments in anhydrous solutions [42].

Two-dimensional IR (2D-IR) vibrational echo spectroscopy [39,43–49], an ultrafast vibrational analog of two-dimensional NMR [45], has been developed to study fast chemical exchange in the ground electronic state under thermal equilibrium conditions. For small H-bonded systems, Hochstrasser et al. [48] investigated the H-bond exchange between CH_3OH and the CN of CH_3CN, using 2D-IR heterodyne echo spectroscopy. The activation energy for the exchange from the H-bonded state to the free state was reported to be 6.2 kJ/mol. With the enthalpy of formation of about 17 kJ/mol [12], the association and dissociation of the PhOH–Benz complex in solutions seem too rapid to measure using conventional spectroscopic methods. In Ref. [43], equilibrium dynamics in the PhOH–Benz complex was studied in a mixed solvent of Benz, by measuring in real time the appearance of off-diagonal peaks in the 2D-IR vibrational echo spectra of the PhOH hydroxyl stretching. The high-frequency hydroxyl stretching was assigned to the free PhOH, whereas the low-frequency to the PhOH–Benz complex. According to the analysis of the 2D-IR spectra, the dissociation time of the PhOH–Benz 1:1 complex was estimated to be about 8 ps.

In our previous work, $[PhOH]_{aq}$ [50], $[BA]_{aq}$ and $[(BA)_2]_{aq}$ [51], as well as $[(BA)_2]_{Benz}$ and small microhydrates of BA in Benz [33], were studied using intermolecular potentials derived from the Test-particle model (T-model) and MD simulations at 298 K. It was shown that, in the gas phase and dilute aqueous solutions, the strong cyclic H-bonds in $(BA)_2$ could be disrupted by H-bonding with water. Whereas in Benz, some microhydrates, not particularly associated in the gas phase and dilute aqueous solutions, become quite stable in the course of MD simulations. This reflects

the impact of weak but complicated C–H···π, O–H···π and π···π interactions on structures and stability of H-bond clusters.

In the present study, the effects of weak C–H···π, O–H···π and π···π interactions on structures, energetic and dynamics of H-bond clusters in non-aqueous environment were further examined using $[(PhOH)_n]_{Benz}$, n = 1–3 as model systems. In order to acquire some basic information, equilibrium structures and interaction energies of the PhOH–Benz m:n complexes, m and n = 1–2, in the gas phase, were investigated using the T-model potentials. Then, NVE-MD simulations were performed on $[(PhOH)_n]_{Benz}$ at 298 K. The average three-dimensional structures and interaction energy distributions in $[(PhOH)_n]_{Benz}$ were visualized and analyzed based on solvent probability distribution (PD) maps and average solute–solvent and solvent–solvent interaction energy PD maps, respectively [52–54]. The dynamics in the first solvation shell of $[(PhOH)_n]_{Benz}$ was analyzed and discussed using the average interaction energy PD maps and their cross section plots [52–54], as well as the H-bond and solvent exchange diagrams. The results were discussed in comparison with available theoretical and experimental results of the same and similar systems.

2. Theoretical methods

The theoretical methods employed in the studies of solutions fall into two categories [55]. Microscopic methods consider solvent molecules with solute explicitly, whereas macroscopic methods take into account solvent as a continuum medium characterized by a dielectric constant. Although in principle, *ab initio* calculations, such as the self-consistent reaction field (SCRF) method [56], could provide insights into the stability of clusters of molecules in a continuum solvent, it is inappropriate in the present case, since the average three-dimensional structures and dynamics of solvent molecules were of primary interest.

2.1. The T-model potentials

Intermolecular potentials employed in the present work were constructed based on the T-model. Since the T-model has been explained in details in our previous investigations [33,50–53], only some important aspects will be briefly summarized here. Within the framework of the T-model, the interaction energy ($\Delta E_{T\text{-model}}$) between molecules A and B is written as a sum of the first-order SCF interaction energy (ΔE^1_{SCF}) and a higher-order energy (ΔE^r) [57]

$$\Delta E_{T\text{-model}} = \Delta E^1_{SCF} + \Delta E^r. \quad (1)$$

ΔE^1_{SCF} accounts for the exchange repulsion and electrostatic energies, and takes the following form:

$$\Delta E^1_{SCF} = \sum_{i\in A}\sum_{j\in B}\left[\exp\left[\frac{-R_{ij}+\sigma_i+\sigma_j}{\rho_i+\rho_j}\right]+\frac{q_iq_j}{R_{ij}}\right]. \quad (2)$$

i and j in Eq. (2) label the sites of molecules A and B, respectively. σ_i, ρ_i and q_i are the site parameters. R_{ij} is the site–site distance. The exponential term in Eq. (2) takes into account the sizes and shapes of the interacting molecules A and B. The point charges q_i and q_j are determined to reproduce the electrostatic potentials of the molecules. The higher-order energy, ΔE^r in Eq. (1), represents the dispersion and polarization contributions of the T-model potential. ΔE^r could be determined from both theoretical and experimental data, and takes the following form:

$$\Delta E^r = -\sum_{i\in A}\sum_{j\in B} C^6_{ij}F_{ij}(R_{ij})R^{-6}_{ij}, \quad (3)$$

where

$$F_{ij}(R_{ij}) = \exp\left[-(1.28R^0_{ij}/R_{ij}-1)^2\right], \quad R_{ij} < 1.28R^0_{ij}$$
$$= 1, \quad \text{elsewhere} \quad (4)$$

and

$$C^6_{ij} = C_6\frac{3}{2}\frac{\alpha_i\alpha_j}{(\alpha_i/N_i)^{1/2}+(\alpha_j/N_j)^{1/2}}. \quad (5)$$

R^0_{ij} in Eq. (4) is the sum of the van der Waals radii of the interacting atoms. Eq. (5) is the Slater–Kirkwood relation; α_i and N_i denote the atomic polarizability and the number of valence electrons of the corresponding atom, respectively. $F_{ij}(R_{ij})$ in Eq. (4) is a damping function, introduced to correct the behavior of R^{-6}_{ij} at short R_{ij} distance. Only C_6 in Eq. (5) is unknown. C_6 could be determined by a fit of the incomplete potential, including ΔE^1_{SCF}, to the experimental second-virial coefficients ($B(T)$) [58]. In the present study, α_i, ρ_i, q_i and C_6 for PhOH and Benz were taken from Refs. [33,50]. They were applied successfully in MD simulations of H-bond and aromatic systems, both in aqueous [50] and non-aqueous solutions [33].

2.2. Equilibrium structures in the gas phase

In this subsection, some important aspects of geometry optimization will be briefly summarized, using the PhOH–Benz 1:1 complex as an example. The geometries of PhOH and Benz were taken from Refs. [33,50], respectively. They were kept constant throughout the calculations. The equilibrium structures and interaction energies of the PhOH–Benz 1:1 complex were computed by placing PhOH at the origin of the Cartesian coordinate system. The coordinates of Benz were randomly generated in the vicinities of PhOH. Based on the T-model potentials [33,50], the absolute and local minimum energy geometries of the PhOH–Benz 1:1 complex were searched using a minimization technique [59]. One hundred starting configurations were employed in each geometry optimization. Similar approaches were applied in the calculations of equilibrium structures and interaction energies of the PhOH–Benz m:n complexes, m and n = 1–2. Some characteristic H-bond distances in the PhOH–Benz complexes were computed and used in the discussion of $[(PhOH)_n]_{Benz}$.

2.3. Molecular dynamics simulations

In order to obtain insights into structures, energetic and dynamics in $[(PhOH)_n]_{Benz}$, n = 1–3, NVE-MD simulations were performed at 298 K. MD-$[(PhOH)_n]^{frozen}_{Benz}$ and MD-$[(PhOH)_n]^{free}_{Benz}$ represent two scenarios in $[(PhOH)_n]_{Benz}$. In MD-$[(PhOH)_n]^{frozen}_{Benz}$, the structures of $(PhOH)_n$ were frozen at the T-model equilibrium geometries [50] and only Benz molecules were allowed to move. MD-$[(PhOH)_n]^{frozen}_{Benz}$ was aimed primarily at the average three-dimensional structures and interaction energy distributions of Benz molecules in $[(PhOH)_n]_{Benz}$. MD-$[(PhOH)_n]^{free}_{Benz}$ represents the situation, in which all PhOH and Benz molecules were free to move, starting from the equilibrium configurations of MD-$[(PhOH)_n]^{frozen}_{Benz}$. MD-$[(PhOH)_n]^{free}_{Benz}$ was aimed at the structures and stabilities of solutes, as well as the dynamics in $[(PhOH)_n]_{Benz}$.

In both MD-$[(PhOH)_n]^{frozen}_{Benz}$ and MD-$[(PhOH)_n]^{free}_{Benz}$, $(PhOH)_n$ and five hundred Benz molecules were put in a cubic box subject to periodic boundary conditions. The center of mass of $(PhOH)_n$ was coincident with the center of the simulation box. The density of $[(PhOH)_n]_{Benz}$ was maintained at the liquid density of 0.87 g cm^{-3} [60], corresponding to the box length of about 42 Å. The cut-off radius was half of the box length. The long-range Coulomb interaction was taken into account by means of the Ewald summations. Fifty thousand MD steps of 0.5 fs were devoted to equilibration and one hundred thousand steps to property calculations. The primary energetic results of interest were the average solute–solute ($\langle E^{solu-solu}_{Benz}\rangle$) and solute–solvent ($\langle E^{solu-solv}_{Benz}\rangle$) interaction energies, as well as the average potential energies of $[(PhOH)_n]_{Benz}$ ($\langle E^{pot}_{Benz}\rangle$). $\langle E^{solu-solu}_{Benz}\rangle$ resulted from the average over the number of

MD steps, whereas $\langle E_{Benz}^{solu-solv} \rangle$ over the number of MD steps and solute molecules.

In order to visualize the average three-dimensional structures of solvent molecules in $[(PhOH)_n]_{Benz}$, solvent probability distribution (π-PD) maps were constructed from MD-$[(PhOH)_n]_{Benz}^{frozen}$; the center of mass of Benz is denoted by π and that of PhOH by π_{Ph}. In the calculations of the π-PD maps, molecular plane of a PhOH molecule was assumed to coincide with the *XY* plane of the simulation box ($Z = 0$ Å). The volumes above and below the plane were divided into layers, with the thickness of 1 Å. In each layer, a π-PD map was constructed from 61×61 grid intersections, by following the trajectories of the center of mass of Benz in the course of MD simulations. The π-PD maps were represented by contour lines, computed and displayed using SURFER program [61]. Therefore, the densities of the contour lines could reflect the probability of finding Benz in $[(PhOH)_n]_{Benz}$. For simplicity, the minimum and maximum values of the contour lines, as well as the contour intervals, were chosen to be the same for all π-PD maps. Since the solvent cages in $[(PhOH)_2]_{Benz}$ and $[(PhOH)_3]_{Benz}$ were rather complicated, additional π-PD maps were constructed with respect to *XZ* and *YZ* planes.

Based on similar approaches, the average solute–solvent and solvent–solvent interaction energy PD maps, denoted by the PB–PD and BB–PD maps, respectively, were constructed from MD-$[(PhOH)_n]_{Benz}^{frozen}$. The PB-PD maps were computed from the interaction energies between Benz at the grid intersections and $(PhOH)_n$, whereas BB-PD maps from the interaction energies between Benz at the grid intersections and all other Benz molecules. The average potential energy landscapes in $[(PhOH)_n]_{Benz}$ were represented by the PB-BB-PD maps, computed by combinations of the PB-PD and BB-PD maps. Because the solvent cages tend to bring about stabilization effects in $[(PhOH)_n]_{Benz}$, only negative-energy contour lines were displayed on the PB-PD, BB-PD and PB-BB-PD maps. It should be noted that, since the solvent–solvent interaction energies dominate in $[(PhOH)_n]_{Benz}$, the minimum and maximum values of the contours, as well as the contour intervals, must be assigned differently for the PB-PD, BB-PD and PB-BB-PD maps.

Since the dynamics of PhOH and Benz in the first solvation shell was one of the main objectives, additional MD analyses had to be made. Our experience in aqueous solutions [52–54] showed that, although not straightforward, the dynamics of specific solvent molecules in the first solvation shell could be anticipated at least qualitatively from the structures of the average potential energy landscapes. Therefore, the PB-PD, BB-PD and PB-BB-PD maps computed from MD-$[(PhOH)_n]_{Benz}^{frozen}$ were further analyzed in details. Several cross section plots were generated by taking vertical slices along the predefined profile lines, through the surfaces of the PB-BB-PD maps, as well as the PB-PD and BB-PD maps, using the methods described in Ref. [53]. The cross section plots derived from the longitudinal profile lines could be associated with the average potential energy barriers to solvent exchanges within, as well as between, the first solvation shells ($\langle\langle E_{Benz}^{L} \rangle\rangle$). Whereas those computed from the transverse profile lines are connected to the average potential energy barriers to the solvent exchanges between Benz molecules in the first solvation shell and the outside ($\langle\langle E_{Benz}^{T} \rangle\rangle$).

Solvation structures, stability and dynamics in $[(PhOH)_n]_{Benz}$ were further analyzed based on MD-$[(PhOH)_n]_{Benz}^{free}$. Some atom–atom pair correlation functions ($g(R)$) and the corresponding average running coordination numbers ($n(R)$) related to the $\pi\cdots\pi$ interactions, the C–H$\cdots\pi$, O–H$\cdots\pi$ and O–H$\cdots$O H-bonds were computed and employed in the discussion. $g(R)$ represents basic one-dimensional views on the structures in solutions. Because large-amplitude intermolecular motions, which could lead to solvent structure reorganization, were pointed out to be one of the main reasons for the non-rigidity in aromatic van der Waals clusters [27], they were also investigated in the present study. Since under thermal equilibrium conditions, the PhOH–Benz complexes are repeatedly dissociating and forming, and the O–H$\cdots\pi$ and O–H$\cdots$O H-bonds, as well as $\pi\cdots\pi$ interactions are responsible for the molecular associations in $[(PhOH)_n]_{Benz}$, their periodic motions at short time could be related to the lifetimes of the complexes. In the present case, fast Fourier transformations (FFT) [62] were performed on the O–H$\cdots\pi$ and $\pi\cdots\pi$ distances, from which the large-amplitude intermolecular vibrational frequencies and the lifetimes of the complexes were approximated. Additionally, in the present case, the H-bond exchange diagrams, showing the distance between the oxygen atom of PhOH and the center of mass of a specific Benz molecule as a function of MD simulation time, were constructed.

3. Results and discussion

3.1. The PhOH–Benz m:n complexes

The absolute and some low-lying minimum energy geometries of the PhOH–Benz complexes, obtained from the T-model potentials, are displayed in Figs. 1 and 2. In Fig. 1, the absolute minimum energy geometry of the PhOH–Benz 1:1 complex is represented by structure **a**, in which the O–H group of PhOH acts as proton donor towards the π-electron cloud of Benz, with the interaction energy ($\Delta E_{T\text{-model}}$) of -19.5 kJ/mol and the O–H$\cdots\pi$ and $\pi_{Ph}\cdots\pi$ distances of 3.4 and 5.4 Å, respectively. The structure and interaction energy of structure **a** are in good agreement with the T-shaped structure obtained from *ab initio* calculations [37,39] and the picosecond photofragment spectroscopy [12]. Structures **b** and **c** are two local minimum energy geometries, with $\Delta E_{T\text{-model}}$ of -13.5 and -9.3 kJ/mol, respectively. Structure **b** shows a possibility for the oxygen atom and the π-electron cloud of PhOH to act as proton acceptor towards the C–H groups of Benz, with the C–H$\cdots$O and C–H$\cdots\pi_{Ph}$ H-bond distances of 3.4 and 4.0 Å, respectively. Structure **c** is sta-

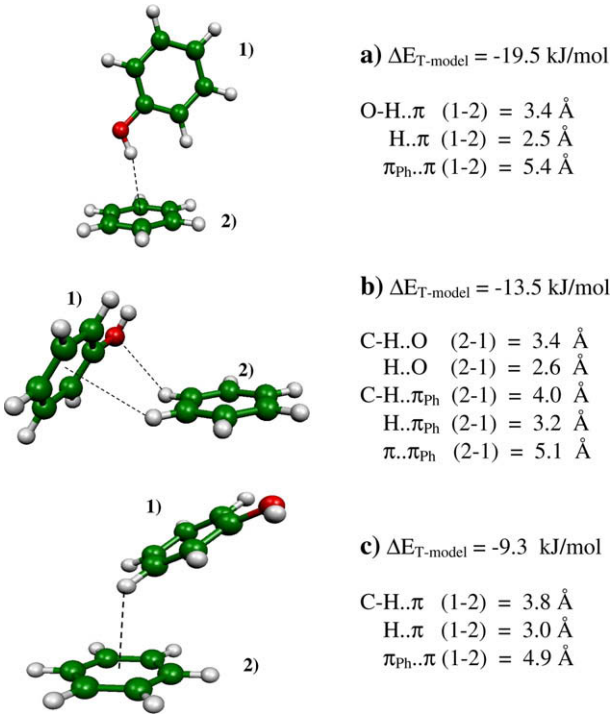

Fig. 1. Equilibrium structures and interaction energies of the PhOH–Benz 1:1 complexes in the gas phase, computed from the T-model potentials.

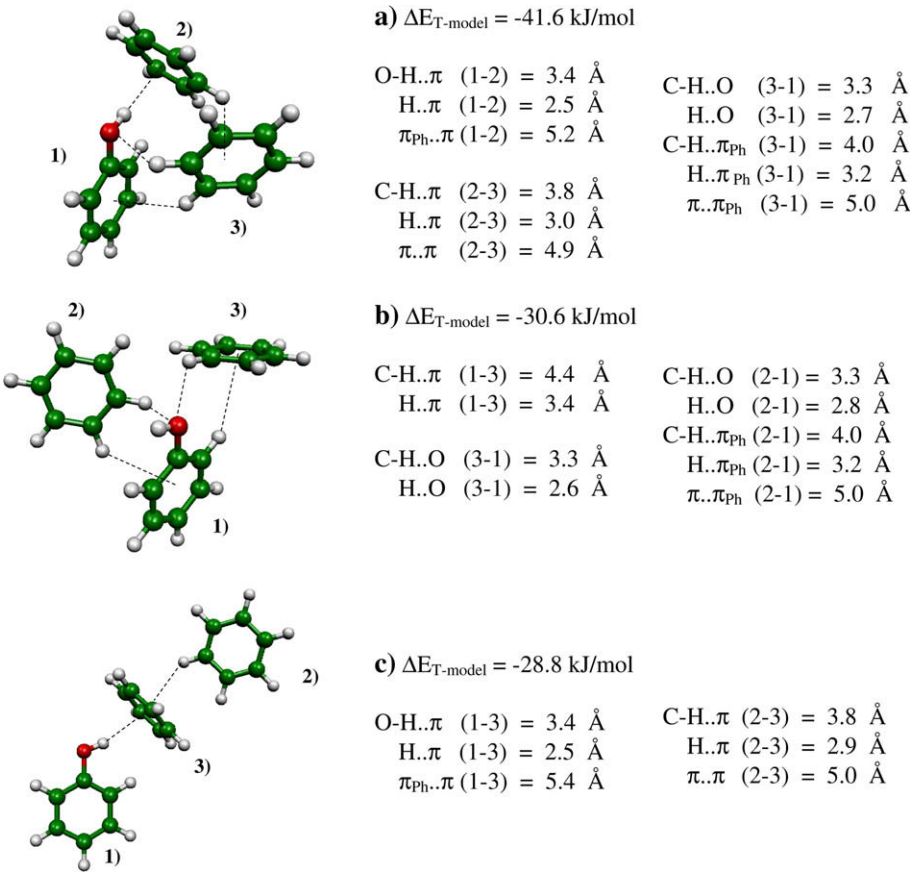

Fig. 2. Equilibrium structures and interaction energies of the PhOH–Benz 1:2 complexes in the gas phase, computed from the T-model potentials.

bilized solely by the C–H···π H-bonds, with the C–H···π and π_{Ph}···π distances of 3.8 and 4.9 Å, respectively.

A compact H-bond cluster formed from the O–H···π, C–H···O, C–H···π and C–H···π_{ph} H-bonds represents the absolute minimum energy geometry of the PhOH–Benz 1:2 complex, structure **a** in Fig. 2. Structure **a** possesses $\Delta E_{T\text{-model}}$ of −41.6 kJ/mol, with the H-bond distances similar to the PhOH–Benz 1:1 complexes. Structure **a** has more C–H···π H-bonds compared to that suggested from supersonic jet spectroscopy [36]. Structure **b** is about 11 kJ/mol less stable than structure **a**. In structure **b**, the oxygen atom of PhOH acts as proton acceptor towards two C–H groups of Benz, with the C–H···O H-bond distances of 3.3 Å. The stability of structure **c** is comparable to structure **b**, with $\Delta E_{T\text{-model}}$ of −28.8 kJ/mol and the O–H···π and C–H···π H-bond distances of 3.4 and 3.8 Å, respectively. The O–H···π H-bond in structure **c** is similar to structure **a** of the PhOH–Benz 1:1 complex, whereas the C–H···π H-bond resembles the T-shaped structure in $(Benz)_2$ [23].

Since H-bonds in the PhOH–Benz 2:1 and 2:2 complexes are not substantially different from the PhOH–Benz 1:1 and 1:2 complexes, in which all characteristic H-bond structures were explained, they are not presented here. Comparison of the results obtained in this subsection with those from experiments [12,36] and *ab initio* calculations [31,45] showed that the T-model potentials [33,50] are accurate enough for further application in MD simulations.

3.2. MD simulations on $[(PhOH)_n]_{Benz}$

The T-model potentials applied in the previous subsection were employed in MD simulations of $[(PhOH)_n]_{Benz}$, n = 1–3, at 298 K. $\langle E^{pot}_{Benz}\rangle$, $\langle E^{solu-solu}_{Benz}\rangle$ and $\langle E^{solu-solv}_{Benz}\rangle$ obtained from MD-$[(PhOH)_n]^{frozen}_{Benz}$ and MD-$[(PhOH)_n]^{free}_{Benz}$ are summarized in Table 1. In order to limit the number of figures, only selected $g(R)$, π-PD, PB-PD and PB-BB-PD maps are displayed. High-density contours on the PD maps are labeled with capital letters.

The average interaction energies in Table 1 show both expected and unexpected trends in $[(PhOH)_n]_{Benz}$. Due to large number of Benz molecules, $\langle E^{pot}_{Benz}\rangle$ are nearly the same for all MD simulations, and since the degree of freedom in MD-$[PhOH]^{free}_{Benz}$ is higher than MD-$[PhOH]^{frozen}_{Benz}$, $\langle E^{solu-solv}_{Benz}\rangle$ is about a factor two higher, −58.1 and −106.0 kJ/mol, respectively. As only one O–H group could act as proton donor towards Benz molecules in both MD-$[(PhOH)_2]^{frozen}_{Benz}$ and MD-$[PhOH]^{frozen}_{Benz}$, $\langle E^{solu-solv}_{Benz}\rangle$ are not substantially different, the former is about 5 kJ/mol higher than the latter. The energetic results seem to be more complicated in MD-$[(PhOH)_2]^{free}_{Benz}$, in which $\langle E^{solu-solv}_{Benz}\rangle$ is about 21 kJ/mol lower than MD-$[(PhOH)_2]^{frozen}_{Benz}$, and $\langle E^{solu-solu}_{Benz}\rangle = -2.3$ kJ/mol. These represent direct evidences for substantial changes in H-bond structures in

Table 1
Energetic results obtained from MD-$[(PhOH)_n]^{frozen}_{Benz}$ and MD-$[(PhOH)_n]^{free}_{Benz}$, n = 1–3. Energies are in kJ/mol.

	$\langle E^{pot}_{Benz}\rangle$	$\langle E^{solu-solu}_{Benz}\rangle$	$\langle E^{solu-solv}_{Benz}\rangle$
MD-$[PhOH]^{frozen}_{Benz}$	−35.4	–	−106.0
MD-$[PhOH]^{free}_{Benz}$	−35.3	–	−58.1
MD-$[(PhOH)_2]^{frozen}_{Benz}$	−35.5	–	−101.0
MD-$[(PhOH)_2]^{free}_{Benz}$	−35.5	−2.3	−123.4
MD-$[(PhOH)_3]^{free}_{Benz}$	−35.4	−51.8	−98.0

$\langle E^{pot}_{Benz}\rangle$ = average potential energy.
$\langle E^{solu-solu}_{Benz}\rangle$ = average solute–solute interaction energy.
$\langle E^{solu-solv}_{Benz}\rangle$ = average solute–solvent interaction energy.

MD-$[(PhOH)_2]^{free}_{Benz}$; an increase in solute–solvent interaction is accompanied by a decrease in solute–solute interaction, leading to some solvent-separated structures. The situations seem to be less complicated in MD-$[(PhOH)_3]^{free}_{Benz}$, in which $\langle E^{solu-solu}_{Benz}\rangle$ is about 64% of $\Delta E_{T\text{-model}}$ of $(PhOH)_3$ in the gas phase [50], and $\langle E^{solu-solv}_{Benz}\rangle = -98.0$ kJ/mol. These indicate that, on average, the three H-bonds in $(PhOH)_3$ did not change substantially in the course of MD-$[(PhOH)_3]^{free}_{Benz}$. The formations of solvent-separated structures in $[(PhOH)_2]_{Benz}$ and close-contact trimers in $[(PhOH)_3]_{Benz}$ will be discussed in detail in the forthcoming sections.

3.2.1. $[PhOH]_{Benz}$

The average three-dimensional structures and interaction energy distributions of solvent molecules obtained from MD-$[PhOH]^{frozen}_{Benz}$ are shown in Fig. 3. The values of the highest probabilities at the labeled contours on the π-PD maps ($\langle P^{\pi\text{-PD}}\rangle_{max}$), together with the corresponding lowest-average interaction energies on the PB-PD, BB-PB and PB-BB-PD maps, denoted by $\langle \Delta E^{PB\text{-}PD}_{Benz}\rangle_{min}$, $\langle \Delta E^{BB\text{-}PD}_{Benz}\rangle_{min}$ and $\langle \Delta E^{PB\text{-}BB\text{-}PD}_{Benz}\rangle_{min}$, respectively, are summarized in Table 2.

The π-PD maps in Fig. 3a and b reveal that, at least three Benz molecules stay in the vicinity the O-H group of PhOH, labeled with **A** (Z = −0.5–0.5 Å), **B** (Z = 2.0–3.0 Å) and **C** (Z = 2.0–3.0 Å). It is obvious that, the π-electron clouds of Benz molecules at **A** and **B** act as proton acceptor towards the O–H and C–H groups of PhOH, respectively, whereas a C–H group of Benz at **C** acts as proton donor towards the oxygen atom of PhOH. Table 2 shows that, Benz molecules at **A**, **B** and **C** possess $\langle \Delta E^{PB\text{-}PD}_{Benz}\rangle_{min}$ of −17.3, −11.7 and −9.8 kJ/mol, respectively. Comparison of $\Delta E_{T\text{-model}}$ in Fig. 1 and $\langle \Delta E^{PB\text{-}PD}_{Benz}\rangle_{min}$ suggests a possibility for a C–H group of Benz at **B** to act as proton donor towards the oxygen atom of PhOH.

The preferential solvation order according to $\langle P^{\pi\text{-}PD}\rangle_{max}$ and the average interaction energy orders based on the absolute values of $\langle \Delta E^{PB\text{-}PD}_{Benz}\rangle_{min}$, $\langle \Delta E^{BB\text{-}PD}_{Benz}\rangle_{min}$ and $\langle \Delta E^{PB\text{-}BB\text{-}PD}_{Benz}\rangle_{min}$ in Table 2 can be written as

$\langle P^{\pi\text{-}PD}\rangle_{max}$: **B** > **A** > **C**
$\langle \Delta E^{PB\text{-}PD}_{Benz}\rangle_{min}$: **A** > **B** > **C**
$\langle \Delta E^{BB\text{-}PD}_{Benz}\rangle_{min}$: **C** > **A** > **B**
$\langle \Delta E^{PB\text{-}BB\text{-}PD}_{Benz}\rangle_{min}$: **A** > **C** > **B**

It should be noted that, the preferential solvation order and the average interaction energy orders in the present case, as well as in many cases [52–54], are different. This is due to the fact that, the π-PD maps show relative probabilities that, a specific "position" in the first solvation shell of PhOH is occupied by Benz molecules, whereas the minima on the average potential energy landscapes, such as $\langle \Delta E^{PB\text{-}BB\text{-}PD}_{Benz}\rangle_{min}$, represent "low-lying interaction energy

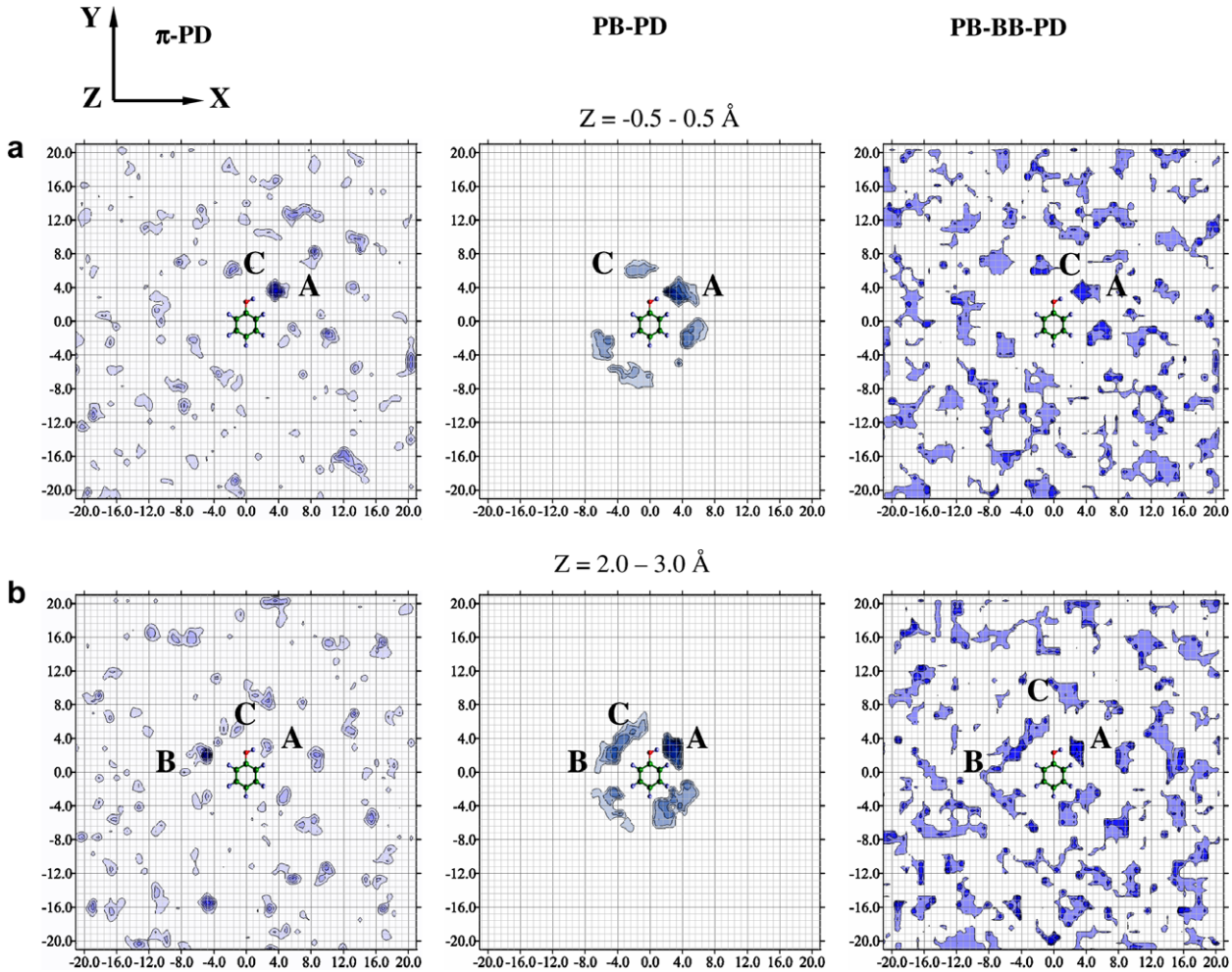

Fig. 3. Structural and energetic results obtained from MD-$[PhOH]^{frozen}_{Benz}$. *X*-, *Y*- and *Z*-axes are in Å, energies in kJ/mol. (a) and (b) The π-PD, PB-PD and PB-BB-PD maps. (c) and (d) Average potential energy landscapes and the cross section plots computed from longitudinal and transverse profile lines. (——) PB-BB-PD cross section plot. (– – – –) PB-PD cross section plot. (– – – –) BB-PD cross section plot. Note: π-PD contour: min = 0.0: max = 0.13: interval = 0.01. PB-PD contour: min = −18.0: max = −3.0: interval = 2.5. PB–BB–PD contour: min = −96.0: max = −75.0: interval = 7.0. (For interpretation of the references in colour in this figure legend, the reader is referred to the web version of this article.)

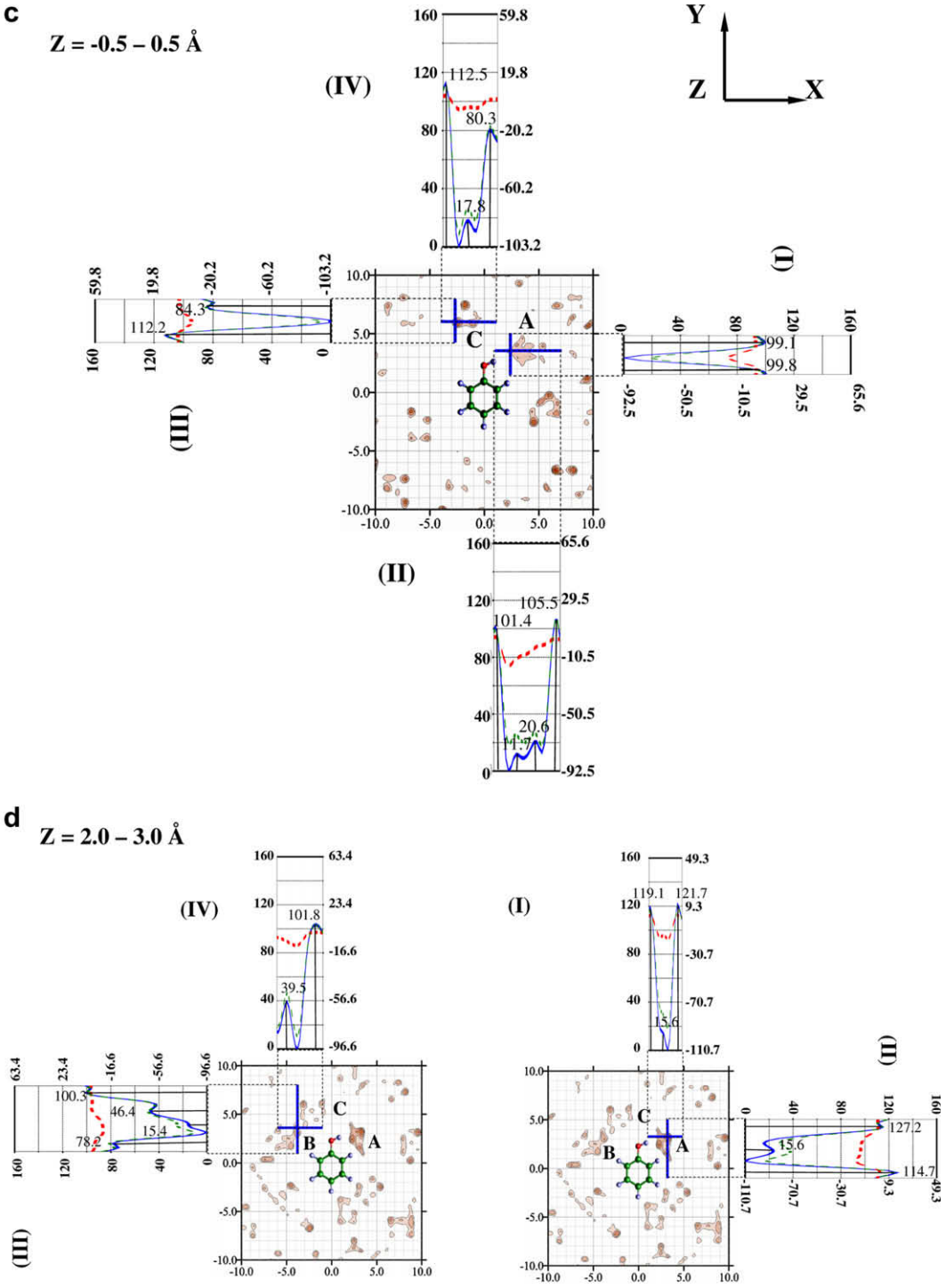

Fig. 3 *(continued)*

states", probed in the course of MD simulations. In other words, Benz molecules at the position with the highest $\langle P^{\pi\text{-PD}}\rangle_{\max}$ need not possess the lowest $\langle \Delta E_{\text{Benz}}^{\text{PB-BB-PD}}\rangle_{\min}$. Since the occupancies of the interaction energy states depend upon dynamics of individual solvent molecules, which could be described by structures of the average potential energy landscapes, it is necessary to include the cross section plots in the discussion of $[(\text{PhOH})_n]_{\text{Benz}}$ [52–54]. They show both the average potential energy barriers interconnecting interaction the energy states and the average potential energy wells, in which solvent molecules are confined. The latter could be related to the "average cage potentials" [26].

Fig. 3c and d shows the examples of the average potential energy landscapes and the cross section plots obtained from MD-$[\text{PhOH}]_{\text{Benz}}^{\text{frozen}}$. The cross section plots indicate that, the average potential energy barriers at **A**, **B** and **C** are quite high, in both longitudinal and transverse directions, *e.g.* about 120 kJ/mol at **A** in Fig. 3d (I) and (II). On the PB-PD and PB-BB-PD maps in Fig. 3b (Z = 2.0–3.0 Å), a possibility for the solvent exchange within the first solvation shell is evident from an interaction energy channel connecting **B** and **C**. All the cross section plots in Fig. 3c and d reveal that, the size and shape of the average potential energy wells are determined nearly exclusively by the average solvent-solvent

Table 2
The highest probabilities at the labeled contours on the π-PD maps ($\langle P^{\pi\text{-PD}}\rangle_{max}$) in Fig. 3, together with the corresponding lowest average interaction energies ($\langle \Delta E^{X}_{Benz}\rangle_{min}$) obtained from MD-$[PhOH]^{frozen}_{Benz}$. Energies are in kJ/mol and X = PB-PD, BB-PD or PB-BB-PD.

	$\langle P^{\pi\text{-PD}}\rangle_{max}$	$\langle \Delta E^{PB-PD}_{Benz}\rangle_{min}$	$\langle \Delta E^{BB-PD}_{Benz}\rangle_{min}$	$\langle \Delta E^{PB-BB-PD}_{Benz}\rangle_{min}$
Z = −0.5 to 0.5 Å				
A	0.104	−17.28	−74.23	−83.65
C	0.042	−7.29	−79.74	−81.41
Z = 0.0–1.0 Å				
A	0.080	−16.10	−78.33	−94.43
C	0.034	−7.53	−77.17	−82.12
Z = 1.0–2.0 Å				
A	0.033	−16.10	−72.97	−83.14
B	0.031	−10.84	−72.94	−82.91
C	0.024	−7.91	−76.35	−88.18
Z = 2.0–3.0 Å				
A	0.036	−9.48	−76.87	−91.47
B	0.114	−11.71	−75.00	−86.06
C	0.027	−9.78	−74.77	−82.46

interactions. These could restrict translational motion of Benz in the first solvation shell of PhOH, especially in the transverse direction. One could, therefore, conclude that, Benz molecules at **A**, **B** and **C** form a part of a quite well-defined local solvent cage at the O–H group of PhOH. Our qualitative interpretation of dynamics of individual solvent molecules in connection to the average potential energy landscapes is similar to Rabani et al. [63]; molecular translation in the liquid phase is characterized by average potential energy landscapes and occurs through jumps between basins separated by high-energy barriers, and the identity of the solvent cage should be more related to the multi-minimum basin itself, rather than to single actual configuration.

It appeared in general that, all structural information obtained from MD-$[PhOH]^{free}_{Benz}$ could be interpreted reasonably well based on the results of the PhOH–Benz 1:1 and 1:2 complexes in Figs. 1 and 2. $g(R_{O-H\cdots\pi})$ in Fig. 4a shows the main peak at $R_{O-H\cdots\pi}$=4.4 Å, with a small shoulder at $R_{O-H\cdots\pi}$ = 3.5 Å, and according to $n(R_{O-H\cdots\pi})$ at the first minimum ($R_{O-H\cdots\pi}$ = 5.5 Å), about five Benz molecules are in the first solvation shell of the O–H group. Since the main peak of $g(R_{C-H\cdots O_{ph}})$ in Fig. 4b is seen at $R_{C-H\cdots O_{ph}}$ = 3.3Å, one could conclude that, the main peak and small shoulder of $g(R_{O-H\cdots\pi})$ correspond to structures **b** and **a** in Fig. 1, respectively. The predominance of the C–H···O_{ph} H-bond in $[PhOH]_{Benz}$ was also suggested based on experiments in Ref. [4]. Additionally in Fig. 4a, $n(R_{O-H\cdots\pi})$ = 2.1 at the first maximum ($R_{O-H\cdots\pi}$ = 4.4 Å) indicates that, in $[PhOH]_{Benz}$, two Benz molecules are in close contact with the O–H group, with the H-bond structures similar to structures **b** and **a** in Fig. 2. These support the three-dimensional structures of solvent obtained from the π-PD maps and the preferential solvation order according to $\langle P^{\pi\text{-PD}}\rangle_{max}$.

Due to deep average potential energy wells, Benz molecules in the inner and outer shells of the O–H group seem not exchange as fast as water solvent [53,54,64]. The H-bond exchange diagram in Fig. 4c demonstrates the exchange of Benz 65 and Benz 423 in the course of MD-$[PhOH]^{free}_{Benz}$. At t_1 = 18.2 ps, Benz 423 entered and shared the first solvation shell with Benz 65, until Benz 65 left at t_2 = 28.3 ps. Therefore, the exchange process, taking place in panel **P1** in Fig. 4c, took about 10 ps. The residence time of Benz 423 could be approximated from the widths of panel **P1** and **P2** to be about 23 ps. The same exchange process repeated again in panel

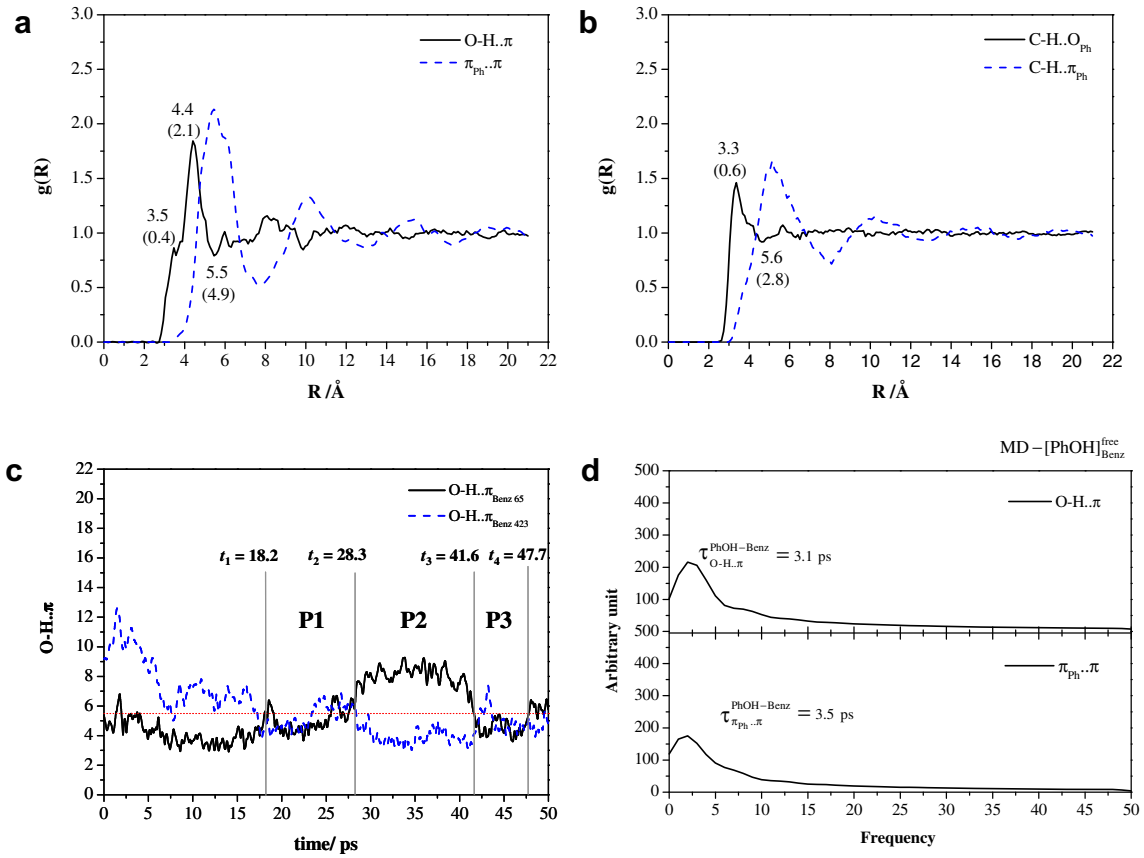

Fig. 4. Structural and dynamic results obtained from MD-$[PhOH]^{free}_{Benz}$. (a) and (b) $g(R)$; characteristic distances given with $n(R)$ in parentheses. (c) Example of H-bond exchange diagram. (d) Fourier transformations of the O–H···π H-bond and $\pi_{ph}\cdots\pi$ distances. Note: $\tau^{PhOH-Benz}_{O-H\cdots\pi}$ = the lifetime of the PhOH–Benz complex computed from FFT of the O–H···π H-bond distance. $\tau^{PhOH-Benz}_{\pi_{Ph}\cdots\pi}$ = the lifetime of the PhOH–Benz complex computed from FFT of the $\pi_{ph}\cdots\pi$ distance.

P3; at t_3 = 41.6 ps, Benz 65 reentered and shared the first solvation shell with Benz 423, etc.

Although the solvent exchange rates and residence times are extremely sensitive to the methods employed, some comparisons could be made using the results on liquid water. Based on MD simulations with the T-model potentials [52], the longest H-bond lifetime at the H atom of water was predicted to be 8.7 ps, whereas that at the O atom was 3.2 ps. These are compared well with the H-bond residence times of water obtained from NMR experiment of about 8 ps [65] and MD simulations of 4.5 ps [66]. Literature survey showed that the mean residence times of water within the first hydration shell of a single water molecule are ranging from 2.5 to 10 ps [67]. Therefore, the residence time of Benz in the first solvation shell of PhOH obtained in the present work is in reasonable agreement with the previous investigations.

Investigations of the H-bond exchange diagrams in details revealed that, Benz molecules at the O–H group of PhOH exchange through large-amplitude intermolecular vibrational motions, which involve periodic displacement of the O–H···π H-bond as discussed in Ref. [27]. According to the five-exchange mechanisms proposed by Langford and Gray [68], the exchanges seem to favor the associative-interchange (I_a) scheme, in which a solvent molecule enters and spends sometime in the first solvation shell before the other leaves.

Analyses of the time evolutions of the cage structures in $[Benz]_{liquid}$ [69,70] showed two relaxation components, which could affect the exchange of Benz molecules constituting the solvent cage; the slow relaxing component is associated with the cage lifetime, whereas the fast relaxing component with the structural rearrangements due to molecular vibrations. Since the average cage potentials or the average potential energy wells are quite low in $[PhOH]_{Benz}$, it was reasonable and possible to investigate the fast component. Based on the assumption that, at short time, the dynamic equilibrium between the associated and dissociated forms could be studied from characteristic intermolecular vibrational frequency [41], the lifetime of the PhOH–Benz 1:1 complex could be approximated. FFT [62] was performed on the O–H···π H-bond distance curve, from which the lifetime of the PhOH–Benz 1:1 complex ($\tau^{PhOH-Benz}_{O-H\cdots\pi}$) was approximated from the characteristic intermolecular vibrational frequency, as half of the association–dissociation dynamic equilibrium cycle time. Examples of FFT obtained from MD-$[PhOH]^{free}_{Benz}$ are shown in Fig. 4d, together with $\tau^{PhOH-Benz}_{O-H\cdots\pi}$. Due to lower degree of freedom, MD-$[PhOH]^{frozen}_{Benz}$ yielded the upper limit of $\tau^{PhOH-Benz}_{O-H\cdots\pi}$ to be 9.2 ps (not shown here), whereas MD-$[PhOH]^{free}_{Benz}$ predicted the lower limit to be 3.1 ps. The values are in reasonable agreement with the 2D-IR vibrational echo spectroscopy of 8 ps [43].

It should be noted that, the present MD simulations estimated $\tau^{PhOH-Benz}_{O-H\cdots\pi}$ directly from the intermolecular vibrational frequencies, whereas the 2D-IR vibrational echo experiment [43] compared the O–H stretching frequencies in the free PhOH with those in the PhOH–Benz 1:1 complex. Although efficient coupling of the O–H stretching with the low-frequency O–H···π H-bond vibrations could be presumed, the excited O–H stretching could live longer than 4 ps [21]. It should be augmented that, MD-$[PhOH]^{free}_{Benz}$ was based on pair-wise additive intermolecular potentials, in which many-body contributions were not taken into account. One could, however, expect that the inclusion of the cooperative effects will lead to slightly more associated PhOH–Benz 1:1 complex and longer $\tau^{PhOH-Benz}_{O-H\cdots\pi}$. In order to obtain a rough estimate of the cooperative effects, *ab initio* geometry optimizations were performed on the PhOH–Benz 1:1 complexes. For this weak O–H···π H-bond, MP2/6-311G(d,p) predicted the upper limit of the cooperative effects to be only about 0.6 kJ/mol, corresponding to the red shift of about 50 cm^{-1}. Therefore, the discrepancy between MD-$[PhOH]^{free}_{Benz}$ and the 2D-IR vibrational echo experiment is reasonable and explainable.

3.2.2. $[(PhOH)_2]_{Benz}$

In order to distinguish H-bonds in $[(PhOH)_2]_{Benz}$, the oxygen atoms were numbered as follow:

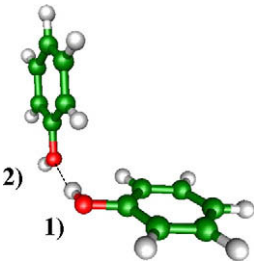

Since the O1–H···O2 H-bond was fixed in MD-$[(PhOH)_2]^{frozen}_{Benz}$, only the O2–H group could act as proton donor towards the π-electron cloud of Benz. Structural and energetic results obtained from MD-$[(PhOH)_2]^{frozen}_{Benz}$ demonstrated that, the solvent cages in $[(PhOH)_2]_{Benz}$ are stronger and more complicated than in $[PhOH]_{Benz}$. The π-PD maps in Fig. 5a–c, show well-defined solvent structures in the vicinities of $(PhOH)_2$; the preferential solvation positions are labeled with **A** to **E**. It is obvious that, Benz molecules prefer to stay at the O2–H group, with the highest probability at **A** (Z = −2.0–1.0 Å) in Fig. 5c and $\langle \Delta E^{PB-BB-PD}_{Benz}\rangle_{min}$ in Table 3 of −86.5 kJ/mol. It appeared that, the C–H···π H-bonds between PhOH and Benz become stronger upon dimer formation. They are labeled with **B**, **C** and **D** on the π-PD maps. The PB-PD and PB-BB-PD maps in Fig. 5b show a larger and more well-defined energy channel in $[(PhOH)_2]_{Benz}$, compared to $[PhOH]_{Benz}$. Therefore, a possibility for the solvent exchange within the first solvation shell of frozen $(PhOH)_2$ could be anticipated at **E**, **D** and **C**.

In $[(PhOH)_2]_{Benz}$, the preferential solvation order according to $\langle P^{\pi\text{-}PD}\rangle_{max}$ and the average interaction energy orders based on the absolute values of $\langle \Delta E^{PB-PD}_{Benz}\rangle_{min}$, $\langle \Delta E^{BB-PD}_{Benz}\rangle_{min}$ and $\langle \Delta E^{PB-BB-PD}_{Benz}\rangle_{min}$ in Table 3 can be written as

$$\langle P^{\pi\text{-}PD}\rangle_{max}: \quad \mathbf{A} > \mathbf{C} > \mathbf{D} > \mathbf{E} > \mathbf{B}$$
$$\langle \Delta E^{PB-PD}_{Benz}\rangle_{min}: \quad \mathbf{D} > \mathbf{E} \geqslant \mathbf{B} > \mathbf{A} > \mathbf{C}$$
$$\langle \Delta E^{BB-PD}_{Benz}\rangle_{min}: \quad \mathbf{C} > \mathbf{E} > \mathbf{A} > \mathbf{B} > \mathbf{D}$$
$$\langle \Delta E^{PB-BB-PD}_{Benz}\rangle_{min}: \quad \mathbf{A} > \mathbf{E} > \mathbf{B} > \mathbf{D} > \mathbf{C}$$

The cross section plots in Fig. 5d and e show high average potential energy barriers for solvent exchanges between the first solvation shell and the outside, up to about 138 kJ/mol at **A** in Fig. 5d (IV). Since the π-PD, PB-PD and PB-BB-PD maps show high-density contours in the vicinity of the O1–H···O2 H-bond, one could anticipate its easy access by Benz molecules, and due to additional entropic effects when $(PhOH)_2$ are free to move, the H-bond dissociation could be expected, as in the cases of $(BA)_2$ [51] and the guanidinium–formate (Gdm^+–FmO^-) complexes in aqueous solutions [52].

Structures and dynamics in $[(PhOH)_2]_{Benz}$ were further examined in MD-$[(PhOH)_2]^{free}_{Benz}$, in which both PhOH and all Benz molecules were free to move. As expected, due to weak solute–solute interaction and the thermal energy fluctuation at 298 K, the O1–H···O2 H-bond was dissociated in MD-$[(PhOH)_2]^{free}_{Benz}$. $g(R_{O1-O2})$ in Fig. 6a shows three well-defined peaks at R_{O1-O2} = 5.7, 8.1 and 9.4 Å, and for $g(R_{\pi_{Ph1}\cdots\pi_{Ph2}})$, two main peaks are seen at $R_{\pi_{Ph1}\cdots\pi_{Ph2}}$ = 6.5 and 9.2 Å. Since the latter is more structured, with two well-defined shoulders at $R_{\pi_{Ph1}\cdots\pi_{Ph2}}$ = 8.1 and 9.8 Å, one could conclude that, the majority of $(PhOH)_2$ in MD-$[(PhOH)_2]^{free}_{Benz}$ took solvent-separated structures. Comparison of $g(R_{O-H\cdots\pi})$ and $g(R_{\pi_{Ph}\cdots\pi})$ in Fig. 6b and c with those obtained

from MD-$[PhOH]^{free}_{Benz}$ in Fig. 4a confirms the dissociation of the O1–H···O2 H-bond and the existence of solvent-separated structures in MD-$[(PhOH)_2]^{free}_{Benz}$. Investigation of structures of $(PhOH)_2$ in the course of MD-$[(PhOH)_2]^{free}_{Benz}$ revealed four examples of close-contact and solvent-separated structures, with $R_{\pi_{Ph1}\cdots\pi_{Ph2}}$ comparable to the positions of the main peaks and shoulders of $g(R_{\pi_{Ph1}\cdots\pi_{Ph2}})$. They are shown in Fig. 6d, and will be used in the discussion of the exchange diagrams in Fig. 6e and f. In structure (**I**), both PhOH molecules are in close contact, with $R_{\pi_{Ph1}\cdots\pi_{Ph2}} = 6.7$ Å. In structures (**II**), (**III**) and (**IV**), Benz 496 separates both PhOH molecules, with $R_{\pi_{Ph1}\cdots\pi_{Ph2}}$ of 8.1, 9.0 and 9.7 Å, respectively.

Fig. 6e and f shows examples of solvent exchange diagrams. In Fig. 6e, the distances between the center of mass of Benz 496 ($\pi_{Benz\ 496}$) and those of PhOH molecules ($R_{\pi_{Ph1}\cdots\pi_{Benz\ 496}}$ and $R_{\pi_{Ph2}\cdots\pi_{Benz\ 496}}$) were plotted as functions of MD simulation time.

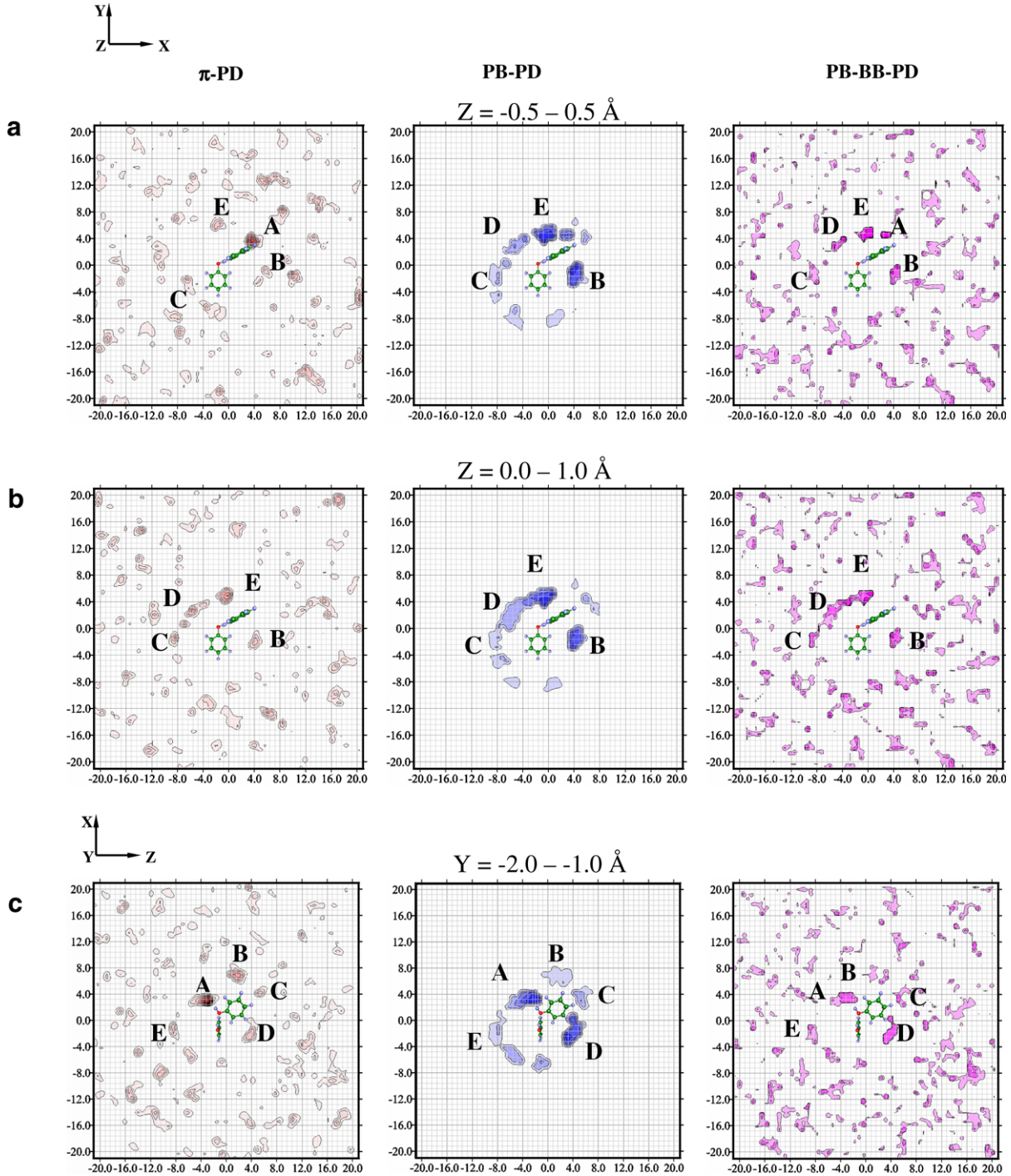

Fig. 5. Structural and energetic results obtained from MD-$[(PhOH)_2]^{frozen}_{Benz}$. *X*-, *Y*- and *Z*-axes are in Å, energies in kJ/mol. (a)–(c) The π-PD, PB-PD and PB-BB-PD maps. (d, e) Average potential energy landscapes and the cross section plots computed from longitudinal and transverse profile lines. (——) PB-BB-PD cross section plot. (- - - - -) PB-PD cross section plot. (- - - - -) BB-PD cross section plot. Note: π-PD contour: min = 0.0: max = 0.13: interval = 0.01. PB-PD contour: min = −30.0: max = −1.0: interval = 4.5. PB–BB–PD contour: min = −99.0: max = −70.0: interval = 7.2. (For interpretation of the references in colour in this figure legend, the reader is referred to the web version of this article.)

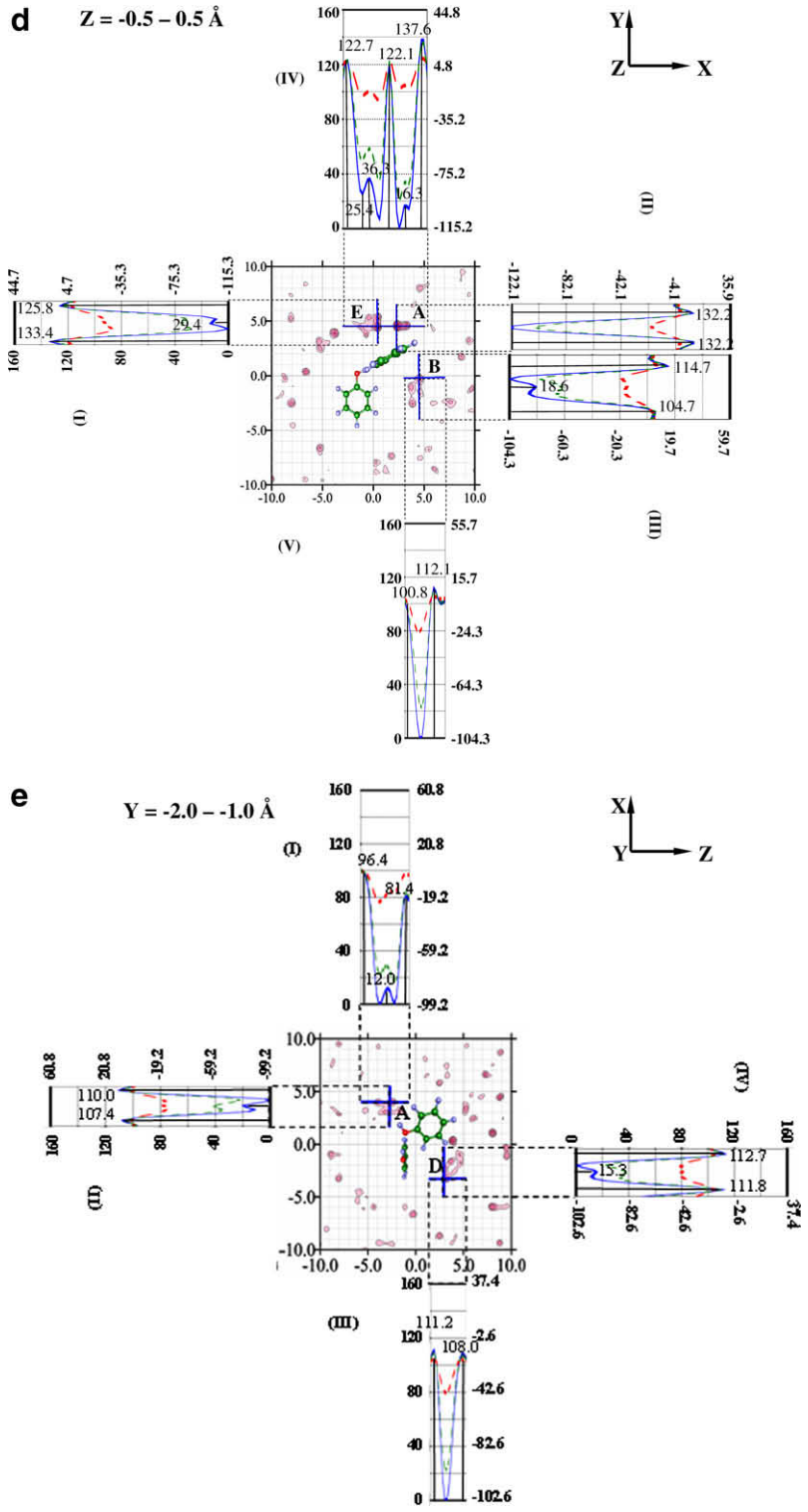

Fig. 5 *(continued)*

Instantaneous solvent-separated structures could be recognized in panels **P1** and $\mathbf{P_3}$, in which Benz 496 stayed between both PhOH molecules, with comparable $R_{\pi_{Ph1}\cdots\pi_{Benz\ 496}}$ and $R_{\pi_{Ph2}\cdots\pi_{Benz\ 496}}$. PhOH2 and PhOH1 could be temporarily separated from Benz 496 in panel $\mathbf{P_2}$ and $\mathbf{P_4}$, respectively. Finally, at $t_5 = 43.6$ ps, Benz 496 moved away from PhOH1, resulting in close-contact structures similar to structure (**I**) in Fig. 6d. Fig. 6f reveals further that, Benz 502 stayed closer to PhOH2 from $t = 15$–33 ps. A similar solvent separated structure was proposed from experiment, in which the association of $(PhOH)_2$ in water saturated CCl_4 was studied [5]; spectroscopic evidence revealed that, the hydrogen atoms of water are not involved in H-bond. It was presumed that, the dimer owes its stability to weak interaction between the hydrogen atoms of the O–H groups of both PhOH molecules and the oxygen atom of water. The so called "hemihydrate dimer" was used to describe this dimer.

Table 3
The highest probabilities at the labeled contours on the π-PD maps ($\langle P^{\pi\text{-PD}}\rangle_{max}$) in Fig. 5, together with the corresponding lowest average interaction energies ($\langle \Delta E^{X}_{Benz}\rangle_{min}$) obtained from MD-$[(PhOH)_2]^{frozen}_{Benz}$ Energies are in kJ/mol and X = PB-PD, BB-PD or PB-BB-PD.

	$\langle P^{\pi\text{-PD}}\rangle_{max}$	$\langle \Delta E^{PB-PD}_{Benz}\rangle_{min}$	$\langle \Delta E^{BB-PD}_{Benz}\rangle_{min}$	$\langle \Delta E^{PB-BB-PD}_{Benz}\rangle_{min}$
Z = −0.5 to 0.5 Å				
A	0.083	−15.11	−79.86	−94.14
B	0.048	−23.67	−65.44	−79.34
C	0.054	−11.66	−76.19	−79.58
E	0.023	−23.89	−71.31	−93.26
Z = 0.0 to 1.0 Å				
B	0.038	−20.32	−70.17	−89.78
C	0.047	−9.06	−79.95	−82.23
D	0.053	−11.79	−73.16	−84.73
E	0.062	−23.91	−71.35	−91.18
Y = −2.0 to −1.0 Å				
A	0.133	−22.14	−73.05	−86.50
B	0.056	−7.10	−74.90	−80.76
C	0.035	−10.94	−81.60	−81.30
D	0.037	−20.85	−70.79	−86.51
E	0.039	−8.33	−80.29	−84.28
X = −1.0 to 0.0 Å				
A	0.047	−13.68	−74.05	−85.53
B	0.043	−18.03	−74.05	−92.08
C	0.106	−9.08	−75.12	−79.62
D	0.091	−26.68	−67.89	−87.73
E	0.040	−15.16	−78.05	−91.64

3.2.3. $[(PhOH)_3]_{Benz}$

Structures and dynamics of $(PhOH)_3$ in Benz solution are discussed based on MD-$[(PhOH)_3]^{free}_{Benz}$. It appeared that, the cyclic O–H···O H-bonds, similar to the water trimer, could be partially opened in the course of MD-$[(PhOH)_3]^{free}_{Benz}$, as follow:

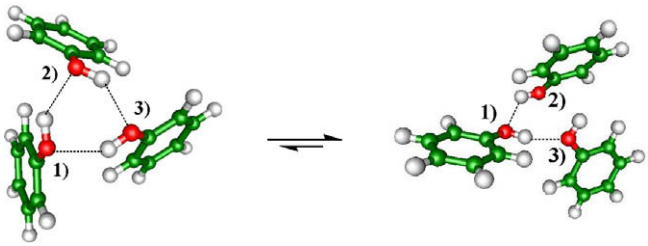

This is evident from $g(R_{O-O})$ in Fig. 7a; $g(R_{O_1-O_2})$ and $g(R_{O_1-O_3})$ are quite similar, with the main peak positions at the average O–H···O H-bond distance of 2.8 Å [50], whereas $g(R_{O_2-O_3})$ possesses different structure, a broad peak with maximum at 4 Å. In Fig. 7b and c, similar trends were observed for $g(R_{O_1\cdots\pi_{Ph2}})$, $g(R_{O_1\cdots\pi_{Ph3}})$ and $g(R_{O_2\cdots\pi_{Ph3}})$, as well as for $g(R_{\pi_{Ph1}\cdots\pi_{Ph2}})$, $g(R_{\pi_{Ph1}\cdots\pi_{Ph3}})$ and $g(R_{\pi_{Ph2}\cdots\pi_{Ph3}})$, respectively. Although the average structure is not as compact as

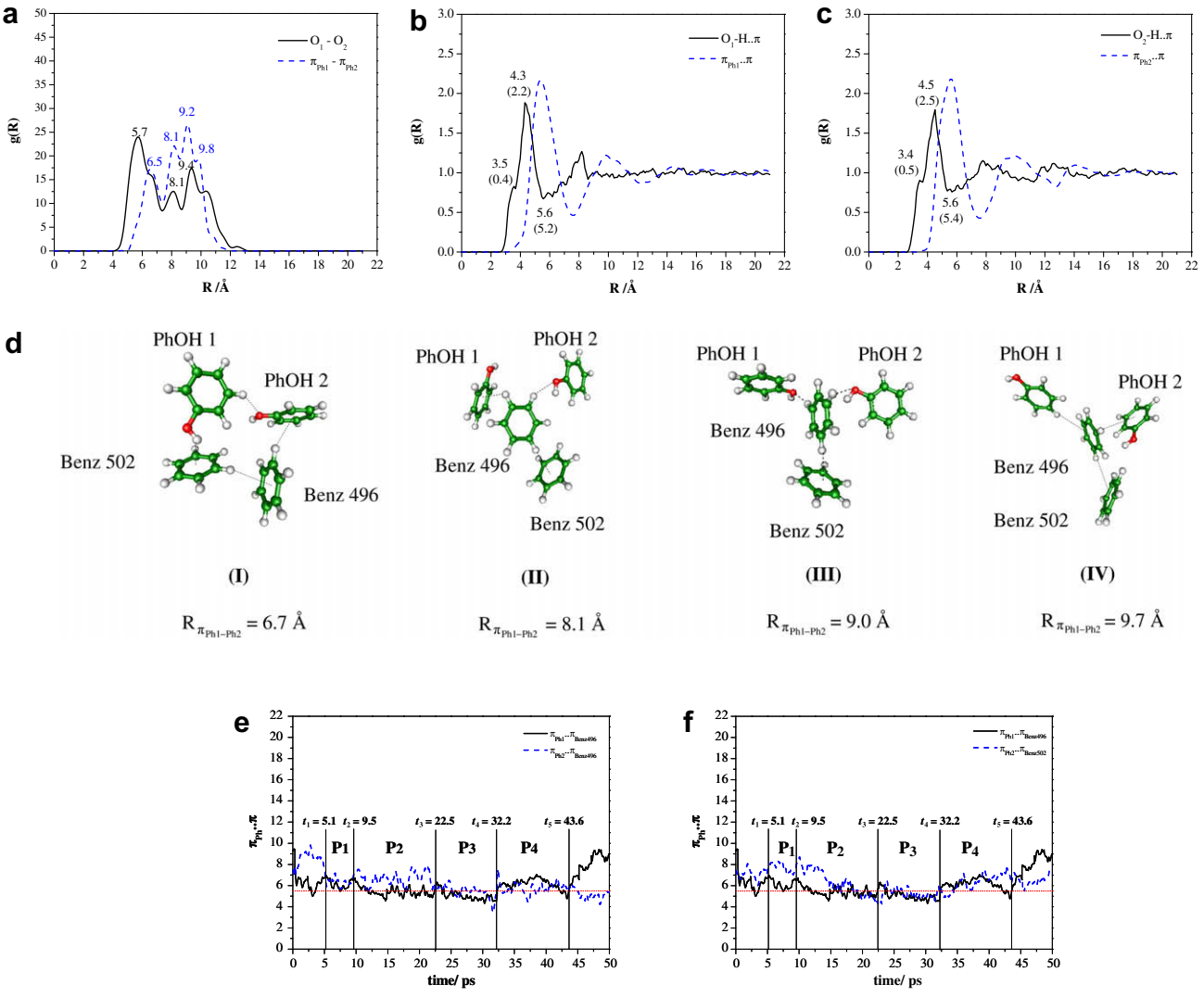

Fig. 6. Structural and dynamic results obtained from MD-$[(PhOH)_2]^{free}_{Benz}$. (a)–(c) $g(R)$; characteristic distances given with $n(R)$ in parentheses. (d) Snapshots of the PhOH–Benz clusters in $[(PhOH)_2]_{Benz}$. (e, f) Example of H-bond exchange diagram.

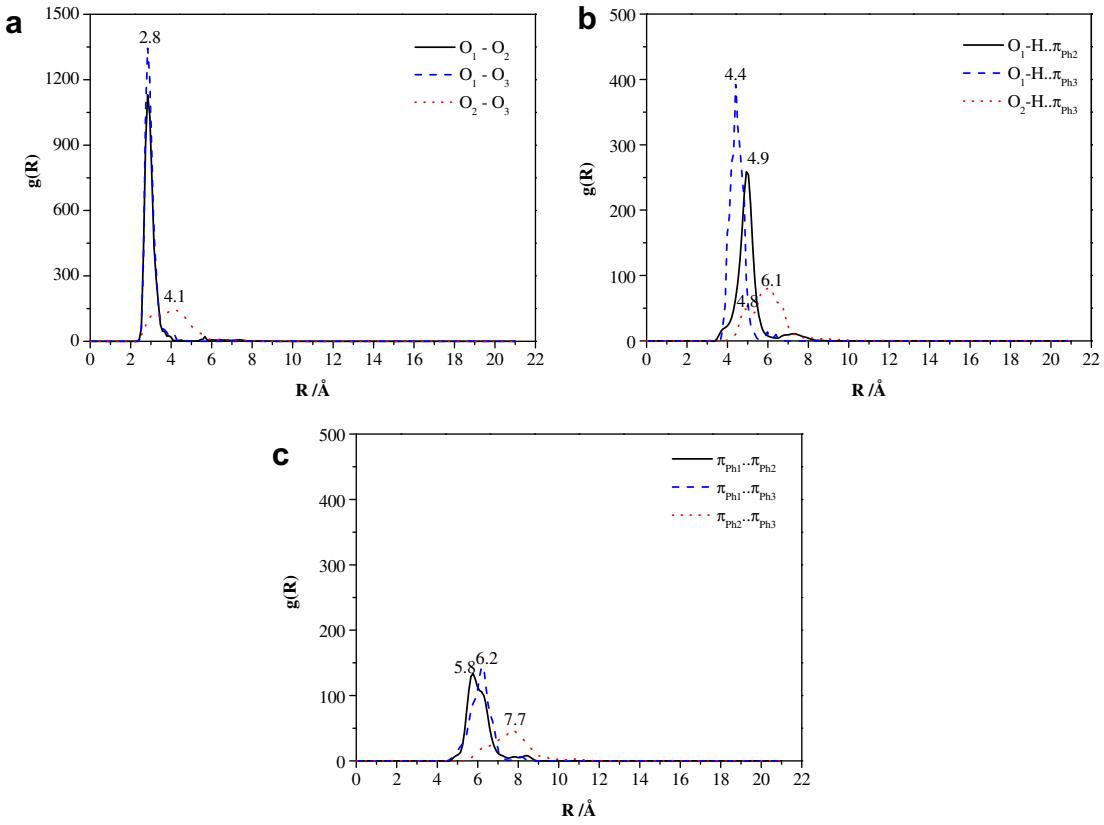

Fig. 7. $g(R)$ obtained from MD-$[(PhOH)_3]^{free}_{Benz}$, together with characteristic distances.

in the gas phase, one could conclude that, $(PhOH)_3$ forms H-bond clusters in $[(PhOH)_3]_{Benz}$. Comparison of the solute structures in the course of MD-$[(PhOH)_2]^{free}_{Benz}$ and MD-$[(PhOH)_3]^{free}_{Benz}$ revealed that, the O–H···O H-bonds in $(PhOH)_3$ are more sterically hindered by the three PhOH molecules, therefore not easily accessible by Benz molecules. Similar steric effects were observed in our previous MD-$[(BA)_2]^{free}_{Benz}$ in Ref. [33], in which cyclic H-bonds in $(BA)_2$ were sterically hindered from Benz molecules, but could be partially opened by small polar molecule such as water.

As mentioned earlier that, molecular associations of aromatic compounds in non-aqueous solvents, such as Benz and CCl_4, represent classical problems in the area of molecular associations, in which partition experiments and various spectroscopic methods have been generally employed in the investigations. For some H-bonded solutes, the associated forms are sufficiently stable to be detected in experiments. However, for PhOH, there have been disagreements as to the most important species in solutions. The majority of the partition experiments seem to point to the existence of the PhOH–$(PhOH)_3$ equilibrium in CCl_4, whereas several spectroscopic results were interpreted in terms of the PhOH–$(PhOH)_2$ equilibrium. At infinite dilution and within ps time scale, the present MD simulations seem to favor instantaneous solvent-separated structures in $[(PhOH)_2]_{Benz}$ and H-bond clusters in $[(PhOH)_3]_{Benz}$. Since it is well accepted that, different experiments could lead to different results, and the advancement of femtosecond laser technology has allowed experiments to probe instantaneous molecular structures and dynamics in weakly associated systems in smaller time scales, it seems unrealistic to rule out possibilities of finding various forms of dimers and trimers, as well as larger clusters in Benz or CCl_4 solutions. Therefore, we anticipate that, no single associated form could be representative in solutions, except in very restricted experimental conditions, such as temperature, concentration and time scale.

4. Conclusions

Structures and dynamics of aromatic clusters have been frequently and extensively studied to demonstrate that, cluster non-rigidity is a general phenomenon in weakly bound systems. In the present study, the effects of weak C–H···π, O–H···π H-bond and π···π interactions on structures and dynamics of H-bond clusters in non-aqueous environment, were studied using $[(PhOH)_n]_{Benz}$, n = 1–3, as model systems. In order to acquire some basic information on equilibrium structures and interaction energies in the gas phase, the PhOH–Benz m:n complexes, m and n = 1–2, were investigated using the T-model potentials. It appeared that, the H-bond structure, in which the O–H group of PhOH acts as proton donor towards the π-electrons of Benz, represents the absolute minimum energy geometry of the PhOH–Benz 1:1 complex. Although the C–H group is not an effective proton donor, various possibilities for the C–H···O and C–H···π H-bond formations were observed from the T-model results on larger PhOH–Benz complexes.

Based on the T-model potentials, a series of NVE-MD simulations was performed on $[(PhOH)_n]_{Benz}$, n = 1–3, at 298 K. Insights on the solvent cage structures and energetic were obtained from $[PhOH]_{Benz}$ and $[(PhOH)_2]_{Benz}$. It was observed from the average three-dimensional structures in $[PhOH]_{Benz}$ that, at least three Benz molecules solvate at the O–H group, and PhOH could act both as proton donor and acceptor towards Benz molecules. The average potential energy landscapes and cross section plots obtained from MD simulations indicated that, the size and shape of the average potential energy wells are determined nearly exclusively by the average solvent–solvent interactions, and the average potential energy barriers to solvent exchanges at the O–H group are quite high. Therefore, Benz molecules at the O–H group could from part of a quite strong local solvent cage. Our interpretation of dynamics of

solvent molecules in connection to the average potential energy landscapes is similar to Rabani et al., by which molecular translation in liquid was proposed to occur through jumps between potential energy wells, separated by high-energy barriers. Investigation on the H-bond exchange diagrams revealed that, Benz molecules at the O–H group could exchange through large-amplitude intermolecular vibrational motions, which involve the periodic displacement of the O–H$\cdots\pi$ H-bond, and the solvent exchanges seem to favor the associative-interchange scheme, in which a solvent molecule enters and spends sometime in the first solvation shell before the other leaves. From the characteristic intermolecular vibrational frequencies of the O–H$\cdots\pi$ H-bond, the lifetimes of the PhOH–Benz 1:1 complex were approximated and in reasonable agreement with 2D-IR vibrational echo experiment.

Due to weak interaction and the thermal energy fluctuation at 298 K, the O–H$\cdots$O H-bond in $(PhOH)_2$ was disrupted in MD simulations. Instantaneous solvent-separated structures, in which a Benz molecule separates both PhOH molecules, were observed in $[(PhOH)_2]_{Benz}$, whereas the cyclic H-bonds in $(PhOH)_3$ were partially opened in $[(PhOH)_3]_{Benz}$. A similar water separated dimer was suggested from experiment, in which spectroscopic evidence revealed that the hemihydrate $(PhOH)_2$ owes its stability to weak interaction between the hydrogen atoms of the O–H groups of both PhOH molecules and the oxygen atom of water. Comparisons of the π-PD maps and the dimer and trimer structures in the course of MD simulations revealed that, the O–H$\cdots$O H-bonds in $(PhOH)_3$ were quite well protected by the three PhOH molecules, therefore not easily accessible by Benz molecules as in the case of $(PhOH)_2$. This suggests that, the competition between solute–solute and solute-solvent interactions could be studied only when explicit solvent molecules are taken into account in the model calculations.

It should be noted finally that, the MD results reported here were based on pair-wise additive scheme, in which many-body effects were not taken into account. Since the interactions among aromatic compounds are not particularly strong, the inclusion of the cooperative effects in our model calculations should not lead to significant change in structures and stability of the complexes considered here; only slightly more associated complexes with longer association times could be anticipated. For organic and biological systems, weak intermolecular interactions could produce complexes that are short-lived. Although short-lived and cannot be detected easily by conventional experimental techniques, the dissociation and association of such complexes can influence chemical processes, especially reactivity and mechanisms in biochemical reactions. Therefore, progress is being made in our laboratory to apply similar theoretical approaches to investigate short-lived phenomena in some biological systems.

Acknowledgements

The authors would like to acknowledge the financial supports from the Thailand Research Fund (TRF): the Royal Golden Jubilee (RGJ) Ph.D. Program, Grant No. PHD/0071/2547 to Sermsiri Chaiwongwattana and Prof. Kritsana Sagarik: the Advanced Research Scholarship, Grant No. BRG51-80022 to Prof. Kritsana Sagarik. Linux clusters provided by the following organizations are also gratefully acknowledged: School of Mathematics and School of Chemistry, SUT; National Electronics and Computer Technology Center (NECTEC) and National Nanotechnology Center (NANOTEC), National Science and Technology Development Agency (NSTDA); the Thai National Grid Center (THAIGRID), Ministry of Information and Communication Technology.

References

[1] E.M. Woolley, L.G. Hepler, J. Phys. Chem. 76 (1972) 3058.
[2] S.H. Weidman, L.E. Swearingen, J. Am. Chem. Soc. 35 (1931) 836.
[3] J.N. Spencer, J.C. Andrefsky, A. Grushow, J. Naghdi, L.M. Patti, J.F. Trader, J. Phys. Chem. 91 (1987) 1673.
[4] F.A. Philbrick, J. Am. Chem. Soc. 56 (1934) 2581.
[5] R.M. Badger, R.C. Greenough, J. Phys. Chem. 65 (1961) 2088.
[6] F.T. Wall, J. Am. Chem. Soc. 64 (1942) 472.
[7] F.T. Wall, P.E. Rouse Jr., J. Am. Chem. Soc. 63 (1941) 3002.
[8] A.K.M. Shamsul Huq, S.A.K. Lodhi, J. Phys. Chem. 70 (1966) 1354.
[9] R. Van Duyne, S.A. Taylor, S.D. Christian, H.E. Affsprung, J. Phys. Chem. 71 (1967) 3427.
[10] K.E. Van Holde, W.C. Johnson, P.S. Ho, Principles of Physical Biochemistry, Prentice-Hall, New Jersey, 1998.
[11] B. Brutschy, Chem. Rev. 100 (2000) 3891.
[12] J.L. Knee, L.R. Khundkar, A.H. Zewail, J. Chem. Phys. 87 (1987) 115.
[13] M.F. Perutz, Philos. Trans. Roy. Soc. London Ser. A 345 (1993) 105.
[14] E.A. Meyer, R.K. Castellano, F. Diederich, Angew. Chem., Int. Ed. Engl. 42 (2003) 1210.
[15] W. Roth, M. Schmitt, C. Jacoby, D. Spangenberg, C. Janzen, K. Kleinerman, Chem. Phys. 239 (1998) 1.
[16] N. Mikami, Bull. Chem. Soc. Jpn. 68 (1995) 683.
[17] R.J. Lipert, S.D. Colson, J. Chem. Phys. 89 (1988) 4579.
[18] Ch. Jacoby, W. Roth, M. Schmitt, Ch. Janzen, D. Spangenberg, K. Kleinermanns, J. Phys. Chem. A 102 (1998) 4471.
[19] T. Sawamura, A. Fujii, S. Sato, T. Ebata, N. Mikami, J. Phys. Chem. 100 (1996) 8131.
[20] K. Ohashi, Y. Inokuchi, N. Nishi, Chem. Phys. Lett. 257 (1996) 137.
[21] G.V. Hartland, B.F. Henson, V.A. Venturo, P.M. Felker, J. Phys. Chem. 96 (1992) 1164.
[22] D.C. Young, Computational Chemistry: A Practical Guide for Applying Techniques to Real-World Problems, Wiley Interscience, New York, 2001.
[23] M.O. Sinnokrot, C.D. Sherrill, J. Am. Chem. Soc. 126 (2004) 7690.
[24] B.M. Rode, C.F. Schwenk, T.S. Hofer, B.R. Randolf, Coord. Chem. Rev. 249 (2005) 2993.
[25] M. Ricci, P. Bartolini, R. Chelli, G. Cardini, S. Califano, R. Righini, Phys. Chem. Chem. Phys. 3 (2001) 2795.
[26] A. Magro, D. Frezzato, A. Polimeno, G.J. Moro, R. Chelli, R. Righini, J. Chem. Phys. 123 (2005) 124511.
[27] S. Sun, E.R. Bernstein, J. Phys. Chem. 100 (1996) 13348.
[28] G.J. Kearley, M.R. Johnson, J. Tomkinson, J. Chem. Phys. 124 (2006) 044514.
[29] R. Chelli, G. Cardini, P. Procacci, R. Righini, S. Califano, A. Albrecht, J. Chem. Phys. 113 (2000) 6851.
[30] L.S. Bartell, F.J. Dulles, J. Phys. Chem. 99 (1995) 17107.
[31] J.R. Grover, E.A. Walters, E.T. Hui, J. Phys. Chem. 91 (1987) 3233.
[32] M.O. Sinnokrot, E.F. Valeev, C.D. Sherrill, J. Am. Chem. Soc. 124 (2002) 10887.
[33] K. Sagarik, S. Chaiwongwattana, P. Sisot, Chem. Phys. 306 (2004) 1.
[34] C.A. Hunter, J. Singh, J.M. Thornton, J. Mol. Biol. 218 (1991) 837.
[35] R. Parthasarathi, V. Subramanian, N. Sathyamurthy, J. Phys. Chem. A 109 (2005) 843.
[36] A. Olkawa, H. Abe, N. Mikami, M. Ito, J. Phys. Chem. 87 (1983) 5083.
[37] R.C. Guedes, K. Coutinho, B.J. Costa Cabral, S. Canuto, C.F. Correia, R.M. Borges dos Santos, J.A. Martinho Simões, J. Phys. Chem. A 107 (2003) 9197.
[38] S. Tsuzuki, K. Honda, T. Uchimaru, M. Mikami, K. Tanabe, J. Am. Chem. Soc. 124 (2002) 104.
[39] K. Kwac, C. Lee, Y. Jung, J. Han, K. Kwak, J. Zheng, M.D. Fayer, M. Cho, J. Chem. Phys. 125 (2006) 244508.
[40] K. Endo, Bull. Chem. Soc. Jpn. 1 (1926) 25.
[41] M. Saunders, J.B. Hyne, J. Chem. Phys. 29 (1958) 1319.
[42] E.N. Lassettre, R.G. Dickinson, J. Am. Chem. Soc. 61 (1939) 54.
[43] J. Zheng, K. Kwak, J. Asbury, X. Chen, I.R. Piletic, M.D. Fayer, Science 309 (2005) 1338.
[44] J. Zheng, K. Kwak, M.D. Fayer, Acc. Chem. Res. 40 (2007) 75.
[45] K. Kwak, J. Zheng, H. Cang, M.D. Fayer, J. Phys. Chem. B 110 (2006) 19998.
[46] J. Zheng, K. Kwak, X. Chen, J.B. Asbury, M.D. Fayer, J. Am. Chem. Soc. 128 (2006) 2977.
[47] I.J. Finkelstein, J. Zheng, H. Ishikawa, S. Kim, K. Kwak, M.D. Fayer, Phys. Chem. Chem. Phys. 9 (2007) 1533.
[48] Y.S. Kim, R.M. Hochstrasser, Proc. Natl. Acad. Sci. 102 (2005) 11185.
[49] R.M. Hochstrasser, Proc. Natl. Acad. Sci. 104 (2007) 14190.
[50] K. Sagarik, P. Asawakun, Chem. Phys. 219 (1997) 173.
[51] K. Sagarik, B.M. Rode, Chem. Phys. 260 (2000) 159.
[52] K. Sagarik, S. Chaiyapongs, Biophys. Chem. 117 (2005) 18.
[53] K. Sagarik, S. Dokmaisrijan, J. Mol. Struct. (Theochem) 718 (2005) 31.
[54] N. Deeying, K. Sagarik, Biophys. Chem. 125 (2006) 14.
[55] M. Orozco, F.J. Luque, Chem. Rev. 100 (2000) 4187.
[56] B.J. Costa Cabral, R.G. Bakker Fonseca, J.A. Martinho Simões, Chem. Phys. Lett. 258 (1996) 436.
[57] H.J. Böhm, R.J. Ahlrichs, J. Chem. Phys. 77 (1982) 2028.
[58] J.H. Dymond, E.B. Smith, The Virial Coefficients of Pure Gases and Mixtures, Clarendon Press, Oxford, 1980.
[59] H.B. Schlegel, J. Comput. Chem. 3 (1982) 214.

[60] Selected Values of Physical and Thermodynamics Properties of Hydrocarbons and Related Compounds, American Petroleum Institute Research Project, vol. 44, Carnegie Press, Pittsburg, 1953.
[61] SURFER for Window, V. 6.04, Golden Software Inc., USA, 1997.
[62] G.J. Borse, Numerical Methods with MATLAB: A Resources for Scientists and Engineers, PWS Publishing, Boston, 1997.
[63] J.D. Gezelter, E. Rabani, B.J. Berne, J. Chem. Phys. 107 (1997) 4618.
[64] S. Chaiwongwattana, K. Sagarik, in preparation.
[65] H.G. Hertz, in: F. Franks (Ed.), Water, A Comprehensive Treatise, vol. 3, Plenum Press, New York, 1973.
[66] R.W. Impey, P.A. Madden, I.R. McDonald, J. Phys. Chem. 87 (1983) 5071.
[67] F. Brugé, E. Parisi, S.L. Fornili, Chem. Phys. Lett. 250 (1996) 443.
[68] C.H. Langford, H.B. Gray, Ligand Substitution Processes, W.A. Benjain, New York, 1966.
[69] E. Rabani, J.D. Gezelter, B.J. Berne, J. Chem. Phys. 107 (1997) 6867.
[70] J.D. Gezelter, E. Rabani, B.J. Berne, J. Chem. Phys. 110 (1999) 3444.